SCUOLA DI DOTTORATO
UNIVERSITÀ DEGLI STUDI *MEDITERRANEA* DI REGGIO CALABRIA

DIPARTIMENTO DI INGEGNERIA CIVILE, DELL'ENERGIA, DELL'AMBIENTE E DEI MATERIALI

DOTTORATO DI RICERCA IN INGEGNERIA CIVILE, AMBIENTALE E DELLA SICUREZZA
S.S.D. ICAR/08
XXXI CICLO

A GENERALISED FUNCTION APPROACH TO THE DYNAMIC ANALYSIS OF COUPLED CONTINUOUS-DISCRETE SYSTEMS UNDER DETERMINISTIC AND STOCHASTIC LOADS

PHD STUDENT:
Andrea Burlon

SUPERVISORS:
Prof. Giuseppe Failla
Prof. Felice Arena

COORDINATOR:
Prof. Felice Arena

REGGIO CALABRIA, FEBBRAIO 2019

Contents

List of Figures

List of Tables

Preface

This thesis is the summary of the research activity carried out at the Department of Civil, Environmental, Energy and Materials Engineering, University Mediterranea of Reggio Calabria (Reggio Calabria), and at Department of Civil Engineering and Engineering Mechanics, Columbia University (New York).

The main topic concerns the dynamics of continuous systems coupled with discrete ones. The first step of the research activity involves modelling real dynamic systems as coupled continuous-discrete ones. The second step involves finding innovative and efficient solutions for evaluating the deterministic and stochastic response of these systems.

To address these problems, a well known mathematical tool is employed: the theory of generalised functions. Specifically, generalised functions, as the impulse function, allow formulating and solving the dynamic problem of coupled continuous-discrete systems in a very simple and efficient way. To perform dynamic analysis, the classical tools of deterministic and stochastic dynamics are developed, extended and suited for the present problems.

Chapter 1

Introduction

1.1 Aims and motivations

Looking closely at every day life experience, we can realize that many daily engineering devices, structures and applications can be modelled as coupled continuous-discrete systems (CCDS). For CCDS we mean systems made up of a well identified continuous primary structure/system endowed with various elements interrupting its continuity in some sense.

As for purely mechanical and civil applications, several number of elements as supports, dampers, additional masses, control devices, transversal ribs can be found coupled with a primary structure/system. These elements most of the time play important and crucial roles as stiffening and protecting the primary structure/system, controlling and reducing vibrations, avoiding resonance problems and consequently catastrophic events.

Since last decades a great challenge for engineers has been to design devices to be coupled with structures or mechanical systems, as some of the aforementioned elements, which are able to ensure absolute safety against wind, earthquake actions and any external excitations. Indeed, structures and mechanical systems are generally subjected to random actions whose frequency energy content can vary greatly, and it is not an easy task at all to design devices able to completely control their dynamics for every external

input. For instance, well established devices for vibration mitigation of structures are the tuned mass dampers (TMDs), which are subsystems tuned such to move away the main resonance frequency of the primary structure from a troubling excitation frequency. A TMD is usually modelled as a lumped mass attached to a structure element by a spring and in general a viscous dashpot in parallel. In general, elements as mass-spring subsystems are involved not only in vibration control but they are used to model machineries, engines and in general secondary structures whose motion is coupled with that of the primary one. Furthermore, in combination with beams, mass-spring subsystem are employed to model human-structure interaction.

Sometimes, some elements can be found as part of the primary structure/system itself; this is the case of additional attached masses, or internal local cracks/damages; the last as well as bolted or welded joints with flexibility and damping caused by imperfections, since reducing the local rigidity of the structure, are usually modelled as concentrated rotational/translational springs or dampers. Then, they fully cover the role of local elements within the continuous primary structure/system. It is well-known that damages are able to completely change the normal dynamic response of the primary structure/system and for this reason the problem of detecting, locating and quantifying the damage is another great challenge nowadays for researchers. Not by chance Structural health monitoring is probably the branch in dynamics of structures that has received greatest attention in the last decades, since it is born to maintain safety and integrity of the structure avoiding monetary loss or in the worst case loss of human life. Certainly, a better understanding of the complicated damage-identification problems can come from the analysis of the direct problem, that means estimating the effects of damages in the dynamics of the studied structures.

Other possible combination of primary structures with local elements could involve wings equipped with external stores as fuel tanks, tip winglets and engines, or ships with additional masses and transversal ribs. The last, within the previous ones, are just some examples of CCDS, and all of them

demonstrate how local elements are able to completely change the normal behavior of a primary continuous structure/system. For all the aforementioned reasons, in the last decades a great amount of works was dedicated to deep understanding the behavior of CCDS, and a lot of researchers have spent their time and energy in developing efficient techniques to investigate their dynamics. Indeed, it is important not only to develop techniques able to simulate the real dynamics of these systems, but what is mostly required from these techniques is that they are computationally efficient and low time consuming, since they can be used for optimization and inverse problems. Moreover, nowadays the scientific progress in all fields of science is measured in relation to the speed of execution of the algorithms and to their computational efficiencies.

In this sense, this thesis is an attempt to give a little contribution, developing a very simple and at the same time computationally efficient technique to exactly evaluate the deterministic and stochastic response of CCDS with particular attention to structural and mechanical systems.

1.2 Mathematical and modelling tools

As briefly discussed above, in this thesis an innovative approach is proposed to evaluate the deterministic and stochastic response of CCDS. Specifically, attention is focused on structural and mechanical systems. Indeed, the primary systems which are taken in consideration are mono-dimensional elements as beams and their 2-D assembly, i.e. plane frames. The structural dynamic problem is formulated applying continuum mechanics principles; consequently the equations governing the motion of the mono-dimensional elements are partial differential equations (PDEs) whose order is determined according to the structural model and theory adopted.

The elements considered, to be coupled with the primary structure/system, are control devices as dampers, tuned mass dampers, spring-mass-systems;

stiffeners as springs/supports, transversal ribs; additional attached masses; rotational/translational springs or dampers modeling a crack or a damage. All these elements are modelled as discrete elements, which means that the actions that they exercise on the primary structure/system are concentrated (concentrated forces, moments, etc...). These actions determine some discontinuities in the response variables of the primary structure/system. For instance, due to the reaction exerted by external rotational and translational supports/dampers on EB beams, discontinuities in the bending moment and shear force arise respectively. A discrete element can determine a contemporary presence of a double discontinuity, as the case of an attached mass with inertial properties, determining a discontinuity in the shear force and bending moment. Deflection and rotation discontinuities can arise also, due to for example to internal translational and rotational springs, usually used to model damaged cross sections. For all these reasons, beams which are coupled with discrete elements are usually called discontinuous beams.

All the concentrated actions and discontinuities in the response variables of the primary system are modelled via generalized functions, whose pertinent theory and principles will be presented in Chapter 2. The most common and known generalized function is probably the impulse function, better known as Dirac's delta function because of its frequent employment by Dirac in quantum mechanics [1]. This function is generally used to describe a singularity in the distribution of any variable in its pertinent domain. For this reason impulse function within other generalized functions results in perfect tools to model non-smooth functions and to take into account discontinuity in the response variables of the primary system induced by the discrete elements.

It is underlined that the mainly proposed technique applies for a linear behavior of both the structure (small displacements and linear elasticity) and discrete elements. Specifically, the constitutive law adopted to generally model dampers is a Kelvin-Voigt viscoelastic model, including linear elasticity and viscous damping. Only in the last Chapter some source of non-linearity are introduced and an innovative solution method is developed

to solve the associated non-linear dynamic problems.

Further, since the proposed technique handles closed form expressions for the dynamic response variables of CCDS, the pertinent algorithms are mainly implemented using the symbolic package Mathematica 8.0 [2].

Before introducing the proposed method, a review of the existing method to evaluate the dynamic response of CCDS follows in order to have a deeper insight into the topic of the thesis.

1.3 Dynamics of coupled continuous-discrete systems

Evaluate the dynamic response of CCDS means to predict the displacement/rotations and stress resultants of any part of the primary structure and every discrete elements, when subjected to any external dynamic input.

A lot of information regarding the dynamics of a CCDS are given by the frequency analysis. This consists, firstly, in investigating the free vibrations, i.e. to find the natural frequencies and associated mode shapes of the primary structure and the influence of the discrete elements on the eigen-properties. As second step, the frequency response function, which provides the steady state response of CCDS to harmonically varying excitations, have to be computed. Frequency response and free vibration data are essential for control design, system identification and damage detection.

Finally, a fully and more complete description of the dynamic behavior of CCDS is given computing the response to time varying input conditions, both deterministic and random.

The innovative approach proposed in this thesis is based on the theory of generalized functions, and is able to efficiently and exactly determine the frequency and time domain response of CCDS. The proposed method shows several advantages, which will be discussed through the thesis, over other approaches which already exists in literature. At this regard, in this Section

a review of the existing methods investigating the dynamics of CCDS follows, starting from the most classical approach. Successively, more details are given regarding methods which makes use of generalised functions. Short hints are then given regarding alternative approaches. Finally, the features of the proposed approach are summarized.

1.3.1 Classical approach

The most classical approach to evaluate the dynamic response of CCDS is based on the subdivision of the primary structural domain in subdomain between two discrete elements; the procedure requires studying independently each part and subsequently introducing the matching conditions between adjacent parts. This approach is able to exactly solve the dynamics of CCDS, but becomes very disadvantageous when the number of discrete elements increases.

An example of the application of this method is here reported for a simple case of CCDS: the bending deflection of an Euler-Bernoulli (EB) beam with n cracks at locations x_i along the beam axis x, with $0 < x_1 < x_2 < \dots x_i < \dots x_n < L$, being L the beam length.

It is well known that the free vibration problem of the j-th segment of the beam between the i-th and $(i+1)$-th crack locations is governed by the following 4-th order differential equation:

$$EI\frac{d^4V_n^{(j)}(x)}{dx^4} + m\omega_n^2 V_n^{(j)}(x) = 0 \tag{1.1}$$

being EI the flexural rigidity, m the mass per unit length, ω_n the n-th natural frequency and $V_n^{(j)}(x)$ the deflection of the j-th beam segment in frequency domain, corresponding to the n-th mode shape of the beam. The n-th crack is modeled as an internal rotational spring with flexibility α_n, determined making use of the principles of fracture mechanics.

According to the classical approach a $(n+1)$ number of 4-th order differential equation as Eq.(1.1) has to be written, one for each segment. Every

solution of the 4-th order differential equation is expressed in a trigonometric form as function of 4 integration constants c_i, with i=1, 2, 3, 4. Then, $4(n+1)$ unknowns have to be computed to solve the free vibration problem. A number of 4 equations can be written imposing the Boundary Conditions (B.C.) of the problem and the remaining $(4n)$ equations are derived from the continuity and compatibility conditions at each crack location. Being $V_n^{(j-1)}(x_i)$ and $V_n^{(j)}(x_i)$ the deflection at the left and right ends of the i-th crack, the continuity and compatibility conditions can be written as follows

$$\begin{aligned} V_n^{(j-1)}(x_i) &= V_n^{(j)}(x_i) \\ \frac{dV_n^{(j)}(x_i)}{dx} - \frac{dV_n^{(j-1)}(x_i)}{dx} &= \alpha_n \frac{d^2V_n^{(j)}(x_i)}{dx^2} \\ \frac{d^2V_n^{(j-1)}(x_i)}{dx^2} &= \frac{d^2V_n^{(j)}(x_i)}{dx^2} \\ \frac{d^3V_n^{(j-1)}(x_i)}{dx^3} &= \frac{d^3V_n^{(j)}(x_i)}{dx^3} \end{aligned} \tag{1.2}$$

where the second equation in Eq.(1.2) is obtained by imposing equilibrium between transmitted bending moment and rotation of the spring representing the crack.

The characteristic equation of the EB beam with n cracks, useful to find the natural frequencies and mode shapes of the CCDS, is then obtained as the determinant of a $4(n+1) \times 4(n+1)$ matrix. When the number n increases, inevitably the matrix increases and the algorithm used to search the roots of the characteristic equation becomes too much time consuming. Furthermore, the matrix shall be updated whenever positions of discontinuity location changes.

The same approach can be used to obtain the dynamic Green's function (DGF), which provides the beam responses to a harmonically varying unit point load at an arbitrary position on the beam. The steady-state response over every uniform beam segment between two consecutive springs/point load locations is again expressed in a trigonometric form with 4 unknown integration constants; these are computed by enforcing the B.C. and a set of

matching conditions between the responses over adjacent beam segments, at the locations of the springs (as previously done) and additional conditions for harmonic point load of amplitude P at location x_0, given as:

$$\begin{aligned} V^{(k-1)}(x_0) &= V^{(k)}(x_0) \\ \frac{dV^{(k-1)}(x_0)}{dx} &- \frac{dV^{(k)}(x_0)}{dx} \\ \frac{d^2V^{(k-1)}(x_0)}{dx^2} &= \frac{d^2V^{(k)}(x_0)}{dx^2} \\ \frac{d^3V^{(k-1)}(x_0)}{dx^3} &- \frac{d^3V^{(k)}(x_0)}{dx^3} = \frac{P}{EI} \end{aligned} \tag{1.3}$$

where $V^{(k-1)}$, $V^{(k)}$ are the deflection in the frequency domain of the $(k-1)$-th and k-th segments respectively at the right and left ends of the location of the applied load P. The size of the coefficient matrix associated with the equations to be solved, will inevitably increase with the number of springs/point loads, as for the free vibration problem. Further, the coefficient matrix associated has to be numerically reinverted for any forcing frequency of interest and has to be updated whenever the springs/point load locations change along the axis. Even when a distributed load is applied on a beam portion, the procedure requires to divide the beam in portion such that the load is continuous in each part.

Obviously, the same procedure can be applied in the presence of multiple discontinuities as well as to solve the axial and torsional vibrations of beams with multiple discontinuities.

Due to the excessive computational effort required by the classical approach, even prohibitive in some cases, it was necessary to develop more efficient methods to solve the above problems. Indeed, the methods that were successively developed, focused on reducing the order of the matrix associated to the free/forced vibration problem.

However, it is remarked that the classical approach is an exact method and can be used to compare and validate the alternative methods.

Regarding CCDS made up of frames, the only available approach to ob-

tain exact evaluation of eigen-properties, is based on the use of the dynamic stiffness matrix of the single beam/column between two consecutive discrete elements. The dynamic stiffness matrices of all elements, which are those matrices relating the harmonic nodal displacements and nodal forces of each element, are subsequent assembled to obtain the global dynamic stiffness matrix; from the latter, the eigen-properties of the frame can be obtained. This approach, suffers from the same drawbacks of the classical approach used for beams. Indeed, this implies an increase of the order of the global matrix as the number of discontinuity increases.

1.3.2 Generalised function approaches

One of the possible alternative approach to evaluate the dynamic response of CCDS consists in reformulating the vibration problem in the space of generalized functions. Indeed, generalised functions are perfect tools to treat discontinuity in some functions, as beam response variables of the primary system/structure in presence of concentrated elements along the domain.

The first attempt to use generalised functions in civil engineering has been for static problems. Similarly to the dynamic problem, the solution of the static beam bending problem with multiple discontinuities can be searched using the classical approach; this suffers from the same drawbacks previously discussed for the dynamic problem. One of the first significative contribution to simplify the static beam bending problem is represented by the singularity function method developed by Macaulay in ref.[3], where for the first time point loads are treated as continuous ones via the use of appropriate generalised functions (the so called "Macaulay's brackets"). Specifically, Macaulay wrote a single differential equation governing the bending moment of a beam with concentrated loads and with a number of r supports. Then, he obtained a single solution equation involving only 2 integration constants and r unknowns reactions at each support to be determined imposing 2 static equilibrium equations, for vertical forces and moments, and r conditions at every support location. Macaulay's method was successfully generalized

by Brungaber [4] to the case of beams with other kind of discontinuities due to along-axis essential and natural constraints. Specifically Brungaber has shown that each discontinuity can be modeled as an equivalent load, expressed as an appropriate generalised function involving an unknown response variable at the discontinuity location. If the number of discontinuity is r, the response generalized function is expressed in terms of $(4+r)$ unknowns, which are 4 integration constants and r response variable, determined imposing the 4 boundary conditions and r conditions at the discontinuous points.

Later, the generalised functions approach was extended to discontinuous beams with flexural stiffness jumps by Kanwal [5]. Although he formulated the problem in the space of generalised functions, the solution procedure is sought in the space of classical functions not offering advantages in terms of computational effort as compared to the classical approach.

Some steps forward were done by Yavari [6] who proposed an innovative method, formulated with generalized function, to compute the solution of the problems with multiple discontinuitities involving external loads, cross section, transversal displacement, rotation function. This method, named auxiliary beam method, can be seen as an improvement of the Kanwal's method; indeed the solution is still searched in the space of classical function, but offers a great advantage with respect to the classical approach in terms of computational effort. For example, for one point of discontinuity, the method requires solving one differential equation with 6 boundary and continuity conditions instead of solving 2 differential equations for the 2 segments and applying 8 B.C. and continuity conditions as required by the classical approach. Next, Yavari extended his method to columns with discontinuities and to EB beams with jump discontinuities in discontinuous foundation.

Later, a significative contribution was given by Falsone [7] who clarified with a novel perspective some aspects related to beam bending problem in presence of multiple discontinuities. His study is substantially a revision of Macaulay and Brungaber's works, and at the same time an extension to the

case in which discontinuities are given for displacement and rotations, and in which natural and essential constraints are presented. The approach has the same advantage of that of Macaulay, that is reducing to one the differential equation to be solved in order to find the displacement law.

Although the methods previously described have been able to express the beam bending problem with a single equation, the associated solution requires to calculate several unknown parameters by imposing the B.C. within a number of additional conditions at the discontinuity points. All the strategies and techniques that were developed later focused on implicitly satisfying the B.C. or the internal conditions at the discontinuity locations. At this regard, it has to be mentioned the contribution by Biondi and Caddemi [8, 9] who developed an efficient approach for beams with multiple cracks. The solution implicitly satisfies a number of internal conditions and depends on 4 integration constants only, computed imposing 4 B.C, with a great computational effort with respect to the other methods. The approach by Biondi and Caddemi [8, 9] was later reviewed by Palmeri and Cicirello [10] who in developing a very similar approach to Biondi and Caddem, corrected a physical inconsistency of their work. In addition, they proposed an integration of the governing differential equation via Laplace transform method. Another efficient approach was developed by Failla [11], who thought an analytical technique for arbitrary mixed-type discontinuous beams. The solution is sought implicitly satisfying the B.C. and depends only on the unknown parameters to be computed by appropriate conditions at the discontinuity locations. The key tool was to compute the beam response in terms of the Green's function of a uniform reference beam. In this way, only the equations at the discontinuity locations shall be solved with a reduction of the computational effort compared to alternative methods.

The generalized function approaches used for static bending problem have been subsequently exported by different authors to dynamic problems. One the first attempt to solve the dynamics of Euler-Bernoulli beam with a number of n cracks was done by Shifrnin and Ruotolo [12]. They elaborated

a method based on generalized functions, named smooth function method, able to reduce the order of the determinant involved in the calculation of the natural frequencies from $4(n+1)$ to $(n+2)$. Although it was possible to reduce the computer time needed to calculate natural frequencies, the order of the determinant was always dependent on the number of crack locations.

A great improvement in terms of the dynamics of beams with any types of discontinuity was given by Wand and Qiao [13]. They expressed the flexural vibrating problem of beams with arbitrary discontinuitites in terms of a single equation via a generalised function approach. Applying the Laplace transform they obtained the modal displacement function as a single function which results as the superposition of basic modal displacement functions introduced, at a discontinuous location, for each discontinuity; the modal displacement, containing the unknown discontinuity values, is then expressed in the form of a recurrence expression as function only of the boundary conditions at the right/left end of the beam. In this way the characteristic equation is obtained solving a second-order determinant regardless of the number of discontinuities along the beam.

Failla and Santini [14] proposed a solution method for Euler-Bernoulli vibrating discontinuous beams. Specifically, they formulated the eigenvalue problem for stepped beams with internal translational and rotational springs employing a lumped-mass methods involving exact influence coefficients. To this aim pertinent exact closed form Green's function giving the response of the discontinuous beam to static unit force are derived. The method consists of a generalization to discontinuous beams of the lumped-mass methods employing exact influence coefficients for shafts and beams [15, 16], showing several computational advantages to compute the eigenvalues.

Later, Caddemi and Caliò [17] provided exact closed form expressions for the mode shapes of the vibrating Euler-Bernoulli beam with multiple concentrated cracks. The cracks, likewise the approach in Biondi and Caddemi [8, 9], are represented as a sequence of Dirac's delta function in the expression of the flexural stiffness. It is shown that this representation is equivalent

to have internal hinges with rotational linear-elastic springs. An integration procedure is applied to obtain the mode shapes as functions of 4 integration constants, only dependent on the boundary conditions, and then showing the same analytical framework of the undamaged structure. Based on the availability of the exact closed form solution of the vibration modes of the multi cracked beam, Caddemi and Caliò [18] derived closed expressions for the exact dynamic stiffness matrix in the presence of an arbitrary number of cracks. The knowledge of the exact dynamic stiffness matrix allowed the evaluation of the exact global dynamic stiffness matrix of damage frame structures by an assembling procedure similar to that of Finite Element Method (FEM). Once built this global matrix, the application of the Wittrick-Williams [19] algorithm allowing the direct evaluation of the eigenfrequencies and vibration modes. The great advantage of the proposed approach is that the degrees of freedom of the overall damage structure are exactly the same as those of the equivalent undamaged structure regardless of the number of damages. This is a great advantage in terms of computational cost and implementation effort and makes more simple the numerical investigation of the inverse problem, i.e. the damage identification problem.

Recently, an innovative approach has been developed by Failla [20] for EB beams with an arbitrary number of Kelvin-Voigt viscoelastic rotational joints, translational supports and attached lumped masses. Using the theory of generalised functions, he solved the free vibration problem upon deriving closed form eigenfunctions that inherently fulfill the required conditions at the discontinuity points; the characteristic equation is obtained as determinant of 4×4 matrix regardless of the number of discontinuities. Next, he solved the forced vibration problem in frequency and time domain by complex modal superposition, upon deriving pertinent orthogonality conditions for the discontinuous modes. On the basis of the same analytical framework, Failla in refs.[21] and [22] computed the frequency response of plane frames with viscoelastic and fractional dampers; specifically, he built the exact global frequency response matrix and load vector with size depending

only on the number of beam-to-column nodes, for any number of dampers and point/polynomial loads along the frame members. Further, in ref.[23] novel exact modal analysis approach is presented for vibration analysis (time and frequency) of plane continuous structures, which are coupled with discrete mass-spring sub-systems.

In this thesis, part of the works in refs.[20, 21, 22, 23] is summarized, being the starting point from which developing efficient solutions to different dynamic problems. For example, all the previous cited studies were limited only to the bending or axial vibration of discontinuous beams with symmetric cross section. While, in this thesis discontinuous beams with mono symmetric cross section are taken in consideration also. These beams have the peculiarity, due to the asymmetry of the cross section, to exhibiting coupled bending torsion phenomena and they require novel modeling tools to be studied.

Since alternative methods to the classical approach are not limited to the use of generalized functions, in the next Section short hints are given regarding other existing methods.

1.3.3 Alternative approaches

Generally, if we have to solve a dynamic problem involving a structure endowed with concentrated elements, we surely think to adopt a simulation software based on Finite Element Method (FEM). Probably, for very large primary structures, FEM remains the most suitable method to solve the dynamics of CCDS. For primary structures made up of beams, or frames as 2-D beams assembly it is no longer the case. Indeed, using FEM to determine, for instance, the free vibrations of a CCDS brings to an approximate solution; specifically it involves a linear eigenvalue problem solvable by well-establised algorithms. In addition, FEM is based on domain decomposition, the size of which depends on the number of discontinuity locations; then it also suffers from increasing computational effort as the number of discontinuity locations increases.

In general, methods to solve the eigenvalue problem of discontinuous beams may be either exact or approximate and they differ for type of discontinuity addressed and computational efficiency achieved, availability of orthogonality conditions for the eigenfunction and applicability to forced-vibration problems. In principle exact solutions are always preferred. As an alternative to exact eigensolution, approximate ones have been sought. Several authors developed methods for beams with multiple cracks, focused on reducing the order of the determinant giving the characteristic equation. An innovative and efficient approach was the transfer matrix method by Kiem and Lien [25], able to drastically reduce the order of the matrix leading to the characteristic equation. This method was able to relate the state variable at the end of each sub-beam with the values at the first end; the fulfilling of continuity conditions at the cracked cross-sections allowed the authors to relate the state variables at both ends of the entire beam; then the characteristic equation is found by solving a determinant of order 4. Ruotolo and Surace [24] extended the method previously proposed to evaluate the longitudinal natural frequencies of vibrating bars with any number of cracks. Li [26] proposed a recurrence method, exploiting the fundamental solutions for each sub-beam and obtained the characteristic equation as determinant of order 2. The expressions of the mode shapes are provided for each sub beam, and since they are dependent on the preceding values they are given by means of recurrence formula.

The above studies are limited to the case of free vibrations of beams with transverse cracks modeled as a rotational spring, which is only one element which can be found coupled with a primary system. Indeed, a primary system can be endowed with other elements like attached masses, external or internal supports, spring-mass-systems, grounded translational dampers (TDs), rotational dampers (RDs), tuned mass dampers (TMDs), axial dampers (Ads) transversal ribs etc...which can determine different discontinuities in response variables of the primary system.

For example, in literature several studies have addressed the frequency

response of beams with dampers. Frequency response analysis is of great importance since provides the steady state response to harmonically varying excitations. Particular attention has been focused on the DGF which provide the response to harmonic varying point load at an arbitrary position along the beam and led to the Frequency response simply by spatial integration over the beam axis. In principle, as seen in the previous Section the DGFs can be built by a classical approach. Therefore, as beams carrying multiple TDs, TMDs, RDs, ADs are encountered in many engineering applications [4-15], alternative methods to compute the DGFs and FRFs, which may overcome the inherent limitations of the classical approach, have been actively sought in several studies, for both bending and axial vibrations. For Example, Sorrentino et al. [27, 28] following a transfer matrix approach obtained the characteristic equation of the free vibration problem as the determinant of 4×4 matrix regardless of the number of dampers, and demostrating the orthogonality conditions for the eigenfunctions, they derived the exact DGFs by complex modal superposition method. The DGFs for Timoshenko has been obtained by Hong and Kim [29] using the dynamic stiffness matrix approach in conjunction with a Laplace transformation of the beam governing equation of motion. For an EB simply-supported beam carrying a TMD subjected to a harmonic excitation, Tang et al.[30] derived exact DGFs using the recurrence method.

Other authors have built approximate but accurate techniques by a modal representation using the eigenfunctions of the bare beam. Examples may be found in the studies of Wu and Chen [31] for an EB beam with an arbitrary number of TMDs, Gürgöze and Erol [32] for an EB beam with an intermediate viscous TD, an intermediate fixed support and a tip mass. Gürgöze and Erol [33] later applied the method to derive the DGFs of a cantilever with an end viscous damper and subjected to external distributed damping.

It is underlined that the literature concerning the dynamic of CCDS is very wide, and in this Section only short hints have been reported. In the next Section, the features of the proposed approach are given.

1.3.4 Proposed approach

The proposed method [34, 35, 36, 37, 38, 39, 40] is a generalization and an extension of the already existing approaches in literature which make use of generalised functions. Indeed, not only CCDS made up of beams with symmetric cross section are dealt with, but beams with mono symmetric, asymmetric cross section and composite beams are taken in consideration.

Firstly, it is shown that the dynamic Green's functions of the bare beam, i.e. the beam without discrete elements, can be used and combined to build exact closed form expressions of the frequency response of coupled beams-discrete systems to point/polynomial load. This involves 2 or 4 or 6 or 8 or 10 or 12 integration constants (it depends on the kind of beam and vibration problem considered) only, regardless of the number of discrete elements. Specifically, the discrete elements considered are Kelvin-Voigt translational/rotational and internal/external dampers, supports, attached masses and tuned mass dampers (TMD). The closed form expressions of the frequency response are the basis to obtain:

- For a single beam, the exact FRF once enforcing the B.C., and the exact dynamic stiffness matrix (DSM) and Load vector (LV).

- For a plane frame made up of beams with symmetric cross section, the exact global DSM and LV by a finite element assembling procedure and the corresponding exact FRF by inverting the global DSM; from the nodal displacement solution, exact FRFs are derived in every frame member in a closed form. The size of the FRF and LV depends only on the number of beam-to-columns nodes, regardless of the number of point/polynomial loads and dampers along the frame members.

Next, since for generality the damping in beams is not proportional due to the presence of concentrated dampers, a complex modal analysis approach is led to obtain the modal frequency response functions of coupled beams-discrete systems. This is possible upon introducing pertinent orthogonality conditions for the modes. Within this framework, modal impulse response functions

are also derived, to be readily used for time domain analysis. Finally, the response to random loads of CCDS is computed. Specifically

- The exact stationary response using the exact FRF for a single discontinuous beam, and the exact frequency response matrix (FRM) and LV for a discontinuous plane frame.
- The response to non-stationary loads for discontinuous beams and frames, obtained by an efficient Monte Carlo simulation which relies on the closed analytical expressions for the impulse response functions.
- Via a novel statistical linearization approach, an approximate stationary response for beams with symmetric cross section carrying non-linear in-span supports. In addition, a distributed non-linearity is considered due to the assumption of moderately large beam displacement.

It is underlined that when structures are not coupled with concentrated dampers, a proportional distributed damping is added along every structural member to compute the frequency response. Alternatively, when performing time domain analysis via modal superposition, the equation for the generic oscillator can be modified assuming proportional viscous damping due to the linearity of the problem.

The method has several advantages over other approaches and is feasible for optimization problem. For example, all the closed form expressions are inherently able to satisfy all the required condition at the discrete elements and point loads locations, capturing jump and slope discontinuities of response variables; further, the analytical form is easy to implement in any symbolic package, and can readily be computed for any frequency of interest, parameters of dampers (location, stiffness, damping), position of the loads, regardless of the number of dampers and positions of the dampers relative to the loads.

Other general features of the proposed approach are discussed in Section 1.2. While all the advantages will be specifically discussed in the next Chapters.

1.4 Organization of the thesis

The thesis is organized as follows. In Chapter 2, the theory of generalised functions is introduced, representing the key mathematical tool of the proposed method. In Chapter 3, the proposed approach is introduced and developed for the deterministic response of coupled beams-discrete systems; different kind of beams and pertinent theories are considered: beams with symmetric cross section, beams with mono-symmetric and asymmetric cross section, and composite beams. In Chapter 4, the proposed approach is extended to coupled plane frames-discrete systems made up of beams with symmetric cross section. The stochastic analysis of CCDS is performed in Chapter 5 where both stationary and non-stationary response are computed; furthermore, a novel statistical linearization technique is developed to deal non-linear problems, for non-linearity arising in both the primary structure and discrete elements. Finally, conclusions are drawn in Chapter 6.

Chapter 2

Generalised functions

In this Chapter, short hints are given regarding the theory of distributions which rigorously define the concept of generalised functions. Then, a less formal approach to describe generalized functions and their properties is presented according to the engineering spirit of the thesis.

2.1 Theory of distributions

A rigorous description and interpretation of generalized functions is undoubtedly attributed to Laurent Schwartz, who was awarded for his work a Fields Medal at the 1950 International Congress of Mathematicians. He systematically generalized the concept of a function developing the so called Theory of Distributions, which provides rigorous basis for operations with singularity functions. The most famous and known among these functions is probably the impulse function, denoted as $\delta(x)$, alternatively called Dirac's delta function because it became well-known by frequent employment by Dirac in quantum mechanics [1].

The key concept introduced by Schwartz has been to define "generalized functions" as kernels of continuous linear functionals, called distributions. Every distribution assigns a real number to every generalized function whether it is a classically differentiable function or a singularity function.

The apparently complex definition of distribution to extend the concept of a function (including that of singularity function), as remarked by Pilkey [41], hides a very simple method to employ the singularity functions, that is as they were point functions; this interpretation can be carried out provided that their use can be justified by recourse of their functional representation. Indeed, their meaning need have no significance independent of the functional representation, except for the impulse function whose meaning can be easily found. For example, this can be seen as a function representing a singularity in the mass distribution of a system. The mass distribution represented by the impulse function $\delta(x - x_0)$ represent a mass distribution along the x-axis with zero density everywhere except $x = x_0$, where a unit mass is located. The total mass in a segment excluding the point $x = x_0$ is zero, while in a segment including the point $x = x_0$ is one. Hence the term "distribution" introduced by Schwartz to denote the generalization of the mass density introduced by a function. In general, the impulse function can be used to describe a singularity in the distribution of any variable in its pertinent domain, and in this sense it will be used in the following chapters.

Below, some definitions are given to formally introduce the concept of generalized functions.

2.1.1 Unit Step function

Firstly, the Unit Step function is introduced. It is defined as follows:

$$H(x - x_0) = \begin{cases} 0 & \text{for } x < x_0 \\ 1 & \text{for } x > x_0 \end{cases} \tag{2.1}$$

As can be seen from Eq.(2.1), the Unit Step function has a jump discontinuity at the point $x = x_0$, then resulting a non-classical differentiable function. This function is very useful in many problems involving variables with jump discontinuities; indeed, any function $f(x)$ which has a jump discontinuity at

the point $x = x_0$ and is continuous elsewhere, defined as

$$f(x) = \begin{cases} f(x_1) & \text{for } x < x_0 \\ f(x_2) & \text{for } x > x_0 \end{cases} \tag{2.2}$$

can be expressed as follows:

$$f(x) = f_1(x) + (f_2(x) - f_1(x))H(x - x_0) \tag{2.3}$$

It is possible to extend the concept of differentiability to functions with jump discontinuities, as the Unit Step function or the function $f(x)$ in Eq.(2.3), substituting the concept of classical function with that of generalised function. To do this aim test functions and distributions have to be introduced.

2.1.2 Distributions and Generalised functions

A test function $\phi(x)$ is a real valued function, satisfying two conditions:

- $\phi(x)$ is infinitely smooth, i.e. it has classical derivative of any order or alternatively $\phi(x) \in C^{\infty}$.
- $\phi(x)$ has a compact support, i.e. $\phi(x)$ is zero outside a finite interval.

The space generated by all the test functions is denoted as D.

A distribution (or generalised functions) is a continuous linear functional on the space D of the test functions. The space created by all distribution is denoted as D'. The latter space is linear and forms a generalizations of the class of locally integrable function since it contains also functions which are not locally integrable.

A classical differentiable function $f(x)$ generates a *regular* distribution, denoted as $< f, \phi >$, by means of the following formula

$$< f, \phi >= \int_{-\infty}^{\infty} f(x)\phi(x)dx \tag{2.4}$$

The distribution created by non-classically differentiable functions are called *singular distributions*.

For example, the Dirac's delta function $\delta(x)$ generates a singular distribution defined as

$$< \delta(x - x_0), \phi(x) >= \int_{-\infty}^{\infty} \delta(x - x_0)\phi(x)dx = \phi(x_0) \tag{2.5}$$

Once introduced the concept of distribution, the n-th distributional derivative of a generalised function $g(x)$ is defined as

$$< g^{(n)}(x), \phi(x) >=< g(x), (-1)^n \phi^{(n)}(x) > \quad \forall \phi \in D \tag{2.6}$$

Consequently, the n-th distributional derivative of the Dirac's delta function is

$$< \delta^{(n)}(x), \phi(x) >=< \delta(x), (-1)^n \phi^{(n)}(x) > \tag{2.7}$$

From the above relations, it can be shown that the Dirac's delta function is the first distributional derivative of the Heaviside function. Indeed it can be written that

$$\begin{aligned} < H^{(1)}(x - x_0), \phi(x) > =< H(x - x_0), -\phi^{(1)}(x) >= -\int_{x_0}^{+\infty} \phi^{(1)}dx = \\ = \phi(x_0) =< \delta(x - x_0), \phi(x) > \end{aligned} \tag{2.8}$$

or in alternative form

$$\frac{\bar{d}}{dx} H(x - x_0) = \delta(x - x_0) \tag{2.9}$$

where a bar over the distributional differentiation symbol indicates distributional or formal derivative to make a distinction with the classical derivative.

2.2 Alternative definition of Generalised functions

In order to simply deal with generalised functions, without necessarily resorting to their functional representations, an alternative and intuitive definition of singularity functions is introduced.

Consider the function $f(x) = R(x - x_0)$ defined in this way

$$R(x - x_0) = \begin{cases} 0 & \text{for } x < x_0 - \tau/2 \\ 1/\tau & \text{for } x_0 - \tau/2 < x < x_0 + \tau/2 \\ 0 & \text{for } x > x_0 + \tau/2 \end{cases} \tag{2.10}$$

This function is known as the rectangle function centered at the abscissa $x = x_0$ with height τ^{-1} and base τ.

An alternative definition of the Dirac's delta function can be obtained, thinking that it can be represented as the limit of the rectangle function for $\tau \to 0$. In this way, it is allowed to apply any integral or differential operator on the Dirac delta function if it is applied before on the rectangle function and then the limit is performed.

On this basis, the fundamental relationship between the Dirac's delta function $\delta(x - x_0)$ and the Unit Step function $H(x - x_0)$ placed at the abscissa $x = x_0$ follows

$$\int_{-\infty}^{x} \delta(x - x_0)dx = H(x - x_0) \tag{2.11}$$

Alternatively, the fundamental relationship in Eq.(2.11) can be expressed in the inverse form

$$\delta(x - x_0) = \frac{\bar{d}}{dx} H(x - x_0) \tag{2.12}$$

that is the same relation obtained in the previous Section. Again the bar does not refer to derivative in a strict analytical sense but in a generalised (or formal) sense. In this sense, hereinafter, we can say that the Dirac delta function is the derivative of the Unit Step function and that the Unit Step

function is integral of the Dirac's delta function.

In the same sense, the generalized derivative of the Dirac's delta function can be performed. The result is a doublet, indicated as $\delta'(x - x_0)$, that is a generalized function consisting of a coupled of second-order Dirac delta with opposite sign and both placed at the abscissa x_0. Generalizing this concept, it can be shown that the n-th formal derivative of a Dirac's delta function gives a generalised function made of 2^n alternate order Dirac delta function placed at the abscissa $x = x_0$. This function is called double-n function, is indicated as $\delta^{(n)}(x - x_0)$ and the following properties can be verified for it:

$$\begin{aligned} &\int_{-\infty}^{\infty} \delta^{(n)}(x - x_0)dx = 0 \\ &\int_{-\infty}^{\infty} \delta^{(n)}(x - x_0)f(x)dx = (-1)^n f^{(n)}(x_0) = (-1)^n \left[\frac{d^n f(x)}{dx^n}\right]_{x=x_0} \end{aligned} \tag{2.13}$$

Properties in Eq.(2.13) are called sampling properties, and are in agreement with the formal definitions given in the previous Section.

Similarly the formal integral of the Unit Step function $H(x - x_0)$ can be performed. This gives the unit 0-th order ramp function $R_0(x - x_0)$, i.e.

$$R_0(x - x_0) = \int_{-\infty}^{x} H(x - x_0) = \begin{cases} 0 & x < x_0 \\ x - x_0 & x > x_0 \end{cases} \tag{2.14}$$

Consequently the inverse formal relationship can be written

$$\frac{\bar{d}}{dx} R(x - x_0) = H(x - x_0) \tag{2.15}$$

In turn the ramp function $R_0(x-x_0)$ can be seen as the generalized derivative of the parabolic ramp function (or 1-th order), named as R_1, defined as follows

$$R_0(x - x_0) = \int_{-\infty}^{x} R_1(x - x_0) = \begin{cases} 0 & x < x_0 \\ \frac{1}{2}(x - x_0)^2 & x > x_0 \end{cases} \tag{2.16}$$

The above definitions can be extended to the n-th order formal integral of the Unit Step function, obtaining the n-th order ramp function

$$R_{n-1}(x-x_0) = \int_{-\infty}^{x} R_n(x-x_0) = \begin{cases} 0 & x < x_0 \\ \frac{1}{n!}(x-x_0)^n & x > x_0 \end{cases} \tag{2.17}$$

As seen at the beginning of the Section, the n-th order ramp function can be alternatively expressed also as

$$R_n(x-x_0) = H(x-x_0)\frac{1}{n!}(x-x_0)^n \qquad \forall x \tag{2.18}$$

Next, differential equations involving generalised functions will be introduced within a method to solve them, based on the Laplace transform.

2.3 Differential equations with Generalised functions

It is well known that the Laplace transform is a very effective tool to solve differential equations, since in the Laplace domain some differential equations are transformed in algebraic ones and then the result is easily anti-transformed in the original domain. When singularity functions are involved in differential equation, Laplace transform becomes even more beneficial due to their sampling properties of singularity functions.

For a function $f(x)$. differentiable in generalized sense in the domain $[0, \infty)$, the Laplace transform is defined as

$$L\{f\} = F(s) = \int_0^{\infty} f(t)e^{-st}dt \tag{2.19}$$

being s a complex number.

While the inverse Laplace transform is defined as follows

$$L^{-1}\{F(s)\} = f(t) = \frac{1}{2\pi}\lim_{t\to\infty}\int_{\gamma-iT}^{\gamma-iT} e^{st}F(s)ds \tag{2.20}$$

Applying Eq.(2.19) to the Dirac's delta function, that is $f(x) = \delta(x - x_0)$, it is obtained

$$L\{\delta\} = F(s) = \int_0^\infty \delta(t - x_0)e^{-st}dt = e^{-sx_0} \tag{2.21}$$

Generalized functions have been introduced in the previous section because they will be exploited to model concentrated actions on structural continuous elements, as beams and frames, due to the presence of external loads or discrete elements along the structural domain. The resulting governing equations are differential equations involving generalized functions.

For example it is well known that the differential equation governing the bending static deflection of an Euler-Bernoulli beam subjected to a concentrated force of amplitude P located at a certain point $x = x_0$ of the beam domain, has the following form:

$$EIV''''(x) = P\delta(x - x_0) \tag{2.22}$$

under the assumption that the flexural stiffness EI in constant along the whole domain, being $V(x)$ the beam displacement.

Applying the Laplace Transform to Eq.(2.22) it is obtained:

$$EI(s^4V(s) - s^3V(0) - s^2V'(0) - sV''(0) - V'''(0)) - \beta V(s) - Pe^{-sx_0} = 0 \tag{2.23}$$

Then it follows

$$V(s) = \frac{1}{s}V(0) + \frac{1}{s^2}V'(0) + \frac{1}{s^3}V''(0) + \frac{1}{s^4}V'''(0) + \frac{P}{EI}\frac{1}{s^4}e^{-sx_0} \tag{2.24}$$

Applying the Inverse Laplace Transform yields

$$v(x) = \frac{P}{EI}\frac{1}{6}(x - x_0)^3H(x - x_0) + V(0) + xV'(0) + \frac{x^2}{2}V''(0) + \frac{x^3}{6}V'''(0) \tag{2.25}$$

Redefining the integration constants $V(0), V'(0), V''(0), V'''(0)$ as function of another set of constants c_j, with $j = 1, 2, 3, 4$, it is possible to express $V(x)$ in this way

$$V(x) = \frac{P}{EI} R_3(x - x_0) + \sum_{j=1}^{4} c_j R_{4-j}(x) \tag{2.26}$$

where c_j are determined by imposing the boundary conditions of the problem.

Notice that the same solution (Eq.(2.26)) could be found performing directly the integral in the generalized sense up to obtaining the bending deflection $V(x)$:

The problems that will be dealt with in the next Section are more complex since they involve the dynamic behavior of beams; moreover different kind of beams are taken in consideration, not only with symmetric cross section, but also with mono symmetric or asymmetric ones and composite beams. Studying the dynamics of these beams require increasingly complex differential equations which become hard to solve. For these equations, the direct integration in generalized sense is not possible, then the Laplace Transform will be used within the help of a symbolic calculus package as Mathematica [2].

In this Section, the solutions to several differential equations involving generalized functions are given, in order to make the reading of the following Chapters more fluid. All the differential equations involved are non-homogeneous differential equation of a single variable, where only odd derivatives of the variable are involved; these equations are non-homogeneous due to the presence of a Dirac's delta function.

Fro instance, consider the following differential equation:

$$\alpha \frac{d^4 V(x)}{dx^4} - \beta V(x) - \rho \delta(x - x_0) = 0 \tag{2.27}$$

with α and β constants and ρ not depending on the variable x.

Applying the Laplace Transform to the differential equation (Eq.2.27)

yields

$$\alpha(s^4V(s)-s^3V(0)-s^2V'(0)-sV''(0)-V'''(0))-\beta V(s)-\rho e^{-sx_0}=0 \quad (2.28)$$

Then, it follows that

$$\begin{aligned} V(s) = &\frac{\alpha s^3}{\alpha s^4-\beta}V(0)+\frac{\alpha s^2}{\alpha s^4-\beta}V'(0)+\frac{\alpha s}{\alpha s^4-\beta}V''(0)+\frac{\alpha}{\alpha s^4-\beta}V'''(0) \\ &+\rho\frac{e^{sx_0}}{\alpha s^4-\beta} \end{aligned} \quad (2.29)$$

Denoting $\gamma=(\beta/\alpha)^{1/4}$, and applying the inverse Laplace transform

$$\begin{aligned} V(x) = &\frac{1}{2}(\cos(x\gamma)+\cosh(x\gamma))V(0)+\frac{1}{2\gamma}(\sin(x\gamma)+\sinh(x\gamma))V'(0)+ \\ &+\frac{1}{2\gamma^2}(\text{-}\cos(x\gamma)+\cosh(x\gamma))V(0)+\frac{1}{2\gamma^3}(\text{-}\sin(x\gamma)+\sinh(x\gamma))V'(0)+ \\ &+\frac{\rho\left(-\sin\left[\frac{(x-x0)\beta^{1/4}}{\alpha^{1/4}}\right]+\sinh\left[\frac{(x-x0)\beta^{1/4}}{\alpha^{1/4}}\right]\right)}{2\alpha^{1/4}\beta^{3/4}}\mathrm{H}(x-x0) \end{aligned} \quad (2.30)$$

Redefining the integration constants $V(0), V'(0), V''(0), V'''(0)$ as function of another set of constant c_1, c_2, c_3, c_4 it is possible to express $V(x)$ in this way

$$\begin{aligned} V(x) = &e^{-x\gamma}c_2+e^{x\gamma}c_4+\cos(x\gamma)c_1+\sin(x\gamma)c_3 \\ &+\frac{\rho\left(-\sin\left[\frac{(x-x0)\beta^{1/4}}{\alpha^{1/4}}\right]+\sinh\left[\frac{(x-x0)\beta^{1/4}}{\alpha^{1/4}}\right]\right)}{2\alpha^{1/4}\beta^{3/4}}\mathrm{H}(x-x0) \end{aligned} \quad (2.31)$$

Generally, given a differential equation of n-th order, with n odd, and where only odd derivatives are involved, "forced" by a Dirac delta function

$$\alpha_n\frac{d^nV}{dx^n}+\alpha_{n-2}\frac{d^{n-2}V}{dx^{n-2}}+\cdots+\alpha_4\frac{d^4V}{dx^4}+\alpha_2\frac{d^2V}{dx^2}+\alpha_0V-\rho\delta(x-x_0)=0 \quad (2.32)$$

The general solution, called fundamental solution, is obtained as follows:

$$V(x) = \sum_{j=1}^{n/2}(c_j e^{R_j x} + c_{j+n/2} e^{-R_j x}) + \sum_{j=1}^{n/2} \frac{\sinh(R_j(x - x_0))}{\alpha_n \prod_{i=1}^{n/2}(R_j - R_i)} \quad \text{for } i \neq j \tag{2.33}$$

where R_j are the j-th solution of the following polynomial equation associated to the differential equation

$$\alpha_n R^{n/2} + \alpha_{n-2} R^{(n-2)/2} + \cdots + \alpha_4 R^2 + \alpha_2 R + \alpha_0 = 0 \tag{2.34}$$

In the next Chapter, taking advantage of the theory of generalized functions, the proposed approach is introduced and developed to investigate the deterministic dynamics of coupled beams-discrete systems.

Chapter 3

Proposed approach to the dynamic analysis of coupled beams-discrete systems: Deterministic analysis

In this Chapter, an exact and efficient method, based on generalised functions, is proposed to solve the deterministic dynamics of coupled beams-discrete systems. The method is developed for different types of beams and pertinent models, starting from the simplest problems involving beams with symmetric cross section and proceeding to increasingly complex problems involving beams with mono symmetric/asymmetric cross section and composite beams. It is underlined that all beams are considered uniform, i.e. their physical properties do not change in space and time.

3.1 Flexural vibrations of discontinuous beams with symmetric cross section

This Section focuses on discontinuous beams with symmetric cross section, carrying an arbitrary number of external and internal dampers. Translational, as well as rotational dampers with Kelvin-Voigt viscoelastic behavior are considered. On using the theory of generalised functions, novel exact expressions of the frequency response are derived in closed analytical form, which hold for harmonically-varying point/polynomial loads arbitrarily placed along the beam, and any number of dampers. On the basis of the same analytical framework, free vibration analysis is led. Specifically, exact natural frequencies and closed-form eigenfunctions will be calculated from a characteristic equation built as determinant of a 4×4 matrix, for any number of dampers. The final step is a complex modal analysis approach to obtain the modal frequency response functions of the beam, upon introducing pertinent orthogonality conditions for the modes. Within this framework, modal impulse response functions are also derived, to be readily used for time domain analysis.

The Section is organized as follows. Firstly, the equations governing the problem under study are formulated. Secondly, frequency response is derived. On this basis and upon deriving orthogonality conditions for complex modes, modal impulse response functions are obtained for time domain analysis.

3.1.1 Description of the problem

Consider the beam with doubly symmetric cross section in Figure 3.1 referred to a right handed coordinate system (x, y, z), where x is the longitudinal axis, y the transverse axis. Let EI be the flexural rigidity, and m the mass per unit length; denote as $v(x,t)$ and $\theta(x,t)$, the flexural deflection and bending rotation of the cross section; while with $s(x,t)$ and $m(x,t)$ the shear force and bending moment(positive sign conventions are shown in Figure 3.1.

Euler-Bernoulli beam theory is adopted to compute flexural vibrations. The beam carries an arbitrary number n of external and internal dampers at the abscissa x_j. Spring stiffness and damper parameters are denoted as follows:

- External translational dampers (ETDs): k_{G_j}, c_{G_j} for grounded dampers; k_{M_j}, c_{M_j} for tuned mass dampers, with M_j denoting the pertinent mass.
- Internal rotational dampers (ITDs): $k_{\Delta V_j^+}$, $c_{\Delta V_j^+}$, $k_{\Delta V_j^-}$, $c_{\Delta V_j^-}$ for right and left dampers.
- External rotational dampers (ERDs): k_{W_j}, c_{W_j} for grounded dampers.
- Internal rotational dampers (IRDs): $k_{\Delta\Theta_j^+}$, $c_{\Delta\Theta_j^+}$, $k_{\Delta\Theta_j^-}$, $c_{\Delta\Theta_j^-}$ for right and left dampers.

Single viscous damper and single spring can be trivially obtained as particular cases of the previous ones. For example, and external translational viscous damper can be simply obtained setting $k_{G_j} = 0$, and an external translational spring setting $c_{G_j} = 0$. The case of an attached mass can be simply obtained , but it will be discussed later.

For generality, governing equations will be written for translational and rotational dampers occurring simultaneously at the same location. As shown later in the text, however, changes are straightforward to consider a single damper at a given location.

According to Euler-Bernoulli beam theory and using the theory of generalized functions (see Chapter 2), the flexural displacement due to an external time and space varying vertical force $f(x,t)$ is governed by the following partial differential equation:

$$EI\frac{\bar{\partial}^4 v(x,t)}{\partial x^4} + m\frac{\partial^2 v(x,t)}{\partial t^2} + r_{ext}(t) + r_{int}(t) + f(x,t) = 0 \qquad (3.1)$$

where bar means generalised derivative (see Chapter 2), while $r_{ext}(t)$ and $r_{int}(t)$ are concentrated actions on the beam, due to the presence of external and internal dampers respectively. The external time and space varying vertical force $f(x,t)$ will be represented in the separable form $f(x,t) = f(x)f(t)$.

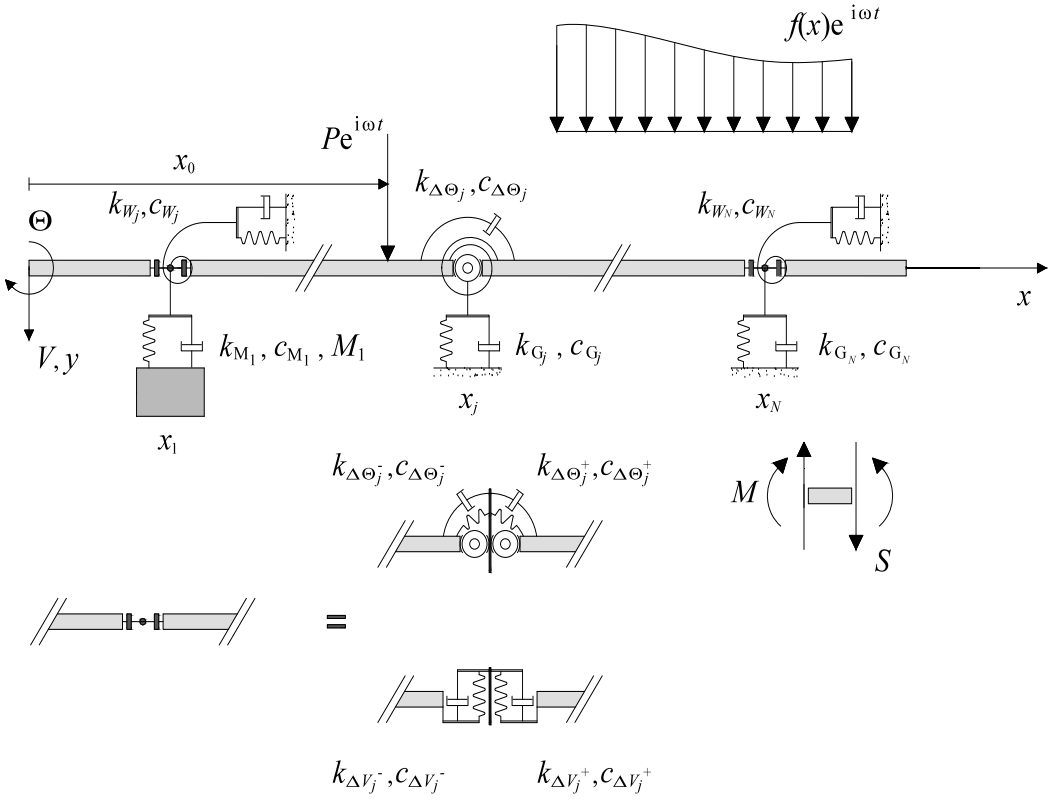

Figure 3.1: Beam with symmetric cross section carrying an arbitrary number of KV dampers (bending problem).

Firstly, an exact frequency analysis is led, including free vibrations and frequency response functions. Next, a complex modal analysis follows to compute time domain response.

3.1.2 Direct Frequency analysis

Assume that the vibration response of the system in Figure 3.1 can be represented in the form

$$\mathbf{y} = \mathbf{Y}e^{i\omega t} \tag{3.2}$$

where $\mathbf{y} = \{v\ \theta\ m\ s\}$ and $\mathbf{Y} = \{V\ \Theta\ M\ S\}$ collect the response variable of the beam. Eq.(3.2) is a general form to represent:

1. The frequency response function, that is the steady state response under an harmonic load $f(x,t) = f(x)e^{i\omega t}$ with any frequency ω, i.e. $\mathbf{Y} = \mathbf{Y}(x,\omega)$.

2. Free vibration response setting $f(x,t) = 0$, and being $\omega = \omega_n$ an eigenvalue and $\mathbf{Y} = \mathbf{Y}_n(x)$ the corresponding vectors of eigenfunctions; in general, the damping in the system is not proportional, then eigenvalues and eigenfunctions will be complex.

Using Eq.(3.2) in equation of motion Eq.(3.1), one obtains

$$EI\frac{\bar{d}^4}{dx^4}V(x) - m\omega^2 V(x) + R_{ext}(\omega) + \Delta_{int}(\omega) + f(x) = 0 \tag{3.3}$$

where bar means generalized derivative (see Chapter 2), $R_{ext}(\omega)$ and $\Delta_{int}(\omega)$ are the counterparts of terms in Eq.(3.1) and are generalized functions given as

$$R_{ext}(\omega) = -\sum_{j=1}^{n} P_j(\omega)\delta(x - x_j) + \sum_{j=1}^{n} W_j(\omega)\delta^{(1)}(x - x_j) \tag{3.4}$$

$$\Delta_{int}(\omega) = -\sum_{j=1}^{n} EI\Delta\Theta_j(\omega)\delta^{(2)}(x - x_j) - \sum_{j=1}^{n} EI\Delta V_j(\omega)\delta^{(3)}(x - x_j) \tag{3.5}$$

where $\delta^{(k)}(x - x_0)$ is the k-th formal derivative of the Dirac's delta function at $x = x_0$, as shown in Chapter 2.

Now, let analyze the terms associated to the discontinuities in Eq.(3.4) and in Eq.(3.5). The quantity P_j is the reaction of the j-th ETDs, whose expression is given as

$$P_j(\omega) = -\kappa_{P_j}(\omega)V(x_j) \tag{3.6}$$

where $V(x_j)$ is the deflection at $x = x_j$, and $\kappa_{P_j}(\omega)$ is a frequency dependent term. Assuming the most general case of a grounded and a tuned-mass-damper both applied at $x = x_j$, κ_{P_j} can be written as $\kappa_{P_j}(\omega) = k_{G_j}(\omega) +$

$k_{M_j}(\omega)$ with

$$k_{G_j}(\omega) = k_{G_j} + i\omega c_{G_j} \tag{3.7}$$

$$k_{M_j}(\omega) = \frac{(k_{M_j} + i\omega c_{M_j})M_j\omega^2}{M_j\omega^2 - (k_{M_j} + i\omega c_{M_j})} \tag{3.8}$$

The reaction $P_j(\omega)$ is related to the shear forces $S(x_j^+)$, $S(x_j^-)$ computed at the right and left of the abscissa $x = x_j$

$$P_j(\omega) + S(x_j^+) = S(x_j^-) \tag{3.9}$$

Similarly, $W_j(\omega)$ in Eq.(3.4) is the reaction of the j-th ERD

$$W_j(\omega) = -\kappa_{W_j}(\omega)\Theta(x_j) \tag{3.10}$$

where $\Theta(x_j)$ is the rotation at $x = x_j$, with $\kappa_{W_j}(\omega)$ denoting a frequency-dependent term given as follows

$$\kappa_{W_j}(\omega) = k_{W_j} + i\omega c_{W_j} \tag{3.11}$$

The reaction $W_j(\omega)$ is related to the bending moments $M(x_j^+)$, $M(x_j^-)$ computed at the right and left of the abscissa $x = x_j$ by the equilibrium equation

$$W_j(\omega) + M(x_j^-) = M(x_j^+) \tag{3.12}$$

While due to the presence of ITDs, the relative deflection between the cross sections at $x = x_j^+$ and $x = x_j^-$ takes the form

$$\Delta V_j(\omega) = V(x_j^+) - V(x_j^-) = \frac{S(x_j^+)}{k_{\Delta V^+(\omega)}} + \frac{S(x_j^-)}{k_{\Delta V^-(\omega)}} \tag{3.13}$$

Eq.(3.13) can be written by considering that

$$\Delta V_j(\omega) = V(x_j^+) - V(x_j) + V(x_j) - V(x_j^-) \tag{3.14}$$

where using the constitutive laws of the ITDs in the frequency domain,

$$\begin{aligned}
&\Delta V_j^+(\omega) = V(x_j^+) - V(x_j) = \frac{S(x_j^+)}{\kappa_{\Delta V_j^+}(\omega)} \\
&\kappa_{\Delta V_j^+} = k_{\Delta V_j^+} + i\omega c_{\Delta V_j^+} \\
&\Delta V_j^-(\omega) = V(x_j) - V(x_j^-) = \frac{S(x_j^-)}{\kappa_{\Delta V_j^-}(\omega)} \\
&\kappa_{\Delta V} = k_{\Delta V_j^-} + i\omega c_{\Delta V_j^-}
\end{aligned} \tag{3.15}$$

Similarly, for the IRDs, the relative rotation between cross sections $x = x_j^+$ and $x = x_j^-$ can be expressed as

$$\Delta\Theta_j(\omega) = \Theta(x_j^+) - \Theta(x_j^-) = -\frac{M(x_j^+)}{\kappa_{\Delta\Theta_j^+}(\omega)} - \frac{M(x_j^-)}{\kappa_{\Delta\Theta_j^-}(\omega)} \tag{3.16}$$

where

$$\Delta\Theta_j(\omega) = \Theta(x_j^+) - \Theta(x_j) + \Theta(x_j) - \Theta(x_j^-) \tag{3.17}$$

being for the constitutive equations of the IRDs in the frequency domain

$$\begin{aligned}
&\Delta\Theta_j^+(\omega) = \Theta(x_j^+) - \Theta(x_j) = -\frac{M(x_j^+)}{\kappa_{\Delta\Theta_j^+}(\omega)} \\
&\kappa_{\Delta\Theta_j^+}(\omega) = k_{\Delta\Theta_j^+} + i\omega c_{\Delta_\Theta^+} \\
&\Delta\Theta_j^-(\omega) = \Theta(x_j) - \Theta(x_j^-) = -\frac{M(x_j^-)}{\kappa_{\Delta\Theta_j^-}(\omega)} \\
&\kappa_{\Delta\Theta_j^-}(\omega) = k_{\Delta\Theta_j^-} + i\omega c_{\Delta\Theta_j^-}
\end{aligned} \tag{3.18}$$

All previous equations tell us that, in frequency domain any dampers is mechanically equivalent to a spring with a frequency dependent stiffness. Further, a lumped mass along the beam can be modeled as an ETD with $k_{M_j} = \infty$ in Eq.(3.8).

Notice that the frequency dependence of the response variables $V(x)$, $\Theta(x)$, $M(x)$, $S(x)$ has been omitted in the above equations for brevity.

Next, the exact dynamic Green's function of the bare beam, i.e. the beam without any dampers, will be computed being the basis to determine the exact frequency response functions and free vibrations of the beam with dampers.

Dynamic Green's function of the bare beam

The first step to compute the frequency response of the beam in Figure 3.1 is to find the Dynamic Green's function of the bare beam, that is the stationary response to harmonically varying unit force, moment, relative rotation, and relative deflection at a generic abscissa x_0, with $0 < x_0 < L$. These functions are the solutions of the following equations:

$$EI\frac{\bar{d}^4 G_V^{(P)}(x,x_0)}{dx^4} - m\omega^2 G_V^{(P)}(x,x_0) - P\delta(x-x_0) = 0, \quad P = 1 \tag{3.19}$$

$$EI\frac{\bar{d}^4 G_V^{(W)}(x,x_0)}{dx^4} - m\omega^2 G_V^{(W)}(x,x_0) + W\delta^{(1)}(x-x_0) = 0, \quad W = 1 \tag{3.20}$$

$$EI\frac{\bar{d}^4 G_V^{(\Delta\Theta)}(x,x_0)}{dx^4} - m\omega^2 G_V^{(\Delta\Theta)}(x,x_0) - EI\Delta\Theta\delta^{(2)}(x-x_0) = 0, \quad \Delta\Theta = 1 \tag{3.21}$$

$$EI\frac{\bar{d}^4 G_V^{(\Delta V)}(x,x_0)}{dx^4} - m\omega^2 G_V^{(\Delta V)}(x,x_0) - EI\Delta V\delta^{(3)}(x-x_0) = 0, \quad \Delta V = 1 \tag{3.22}$$

where superscripts in "G" indicates if the the dynamics Green's function is due to a unit force $P = 1$, a unit moment $W = 1$, a unit relative rotation $\Delta\Theta = 1$ or a unit relative deflection $\Delta V = 1$; while subscripts indicate the response variable which the Green's function is related to. For example, $G_V^{(P)}$ denote the Green's function of the deflection due to a unit point load.

Now, collect all the Dynamic Green's functions in the vector $\mathbf{G}^{(r)}(x,x_0) =$

$[G_V^{(r)}\ G_{\Delta\Theta}^{(r)}\ G_M^{(r)}\ G_S^{(r)}]$ for $r = P, W, \Delta\Theta, \Delta V$. Then, vector $\mathbf{G}^{(r)}(x, x_0)$ can be expressed as

$$\mathbf{G}^{(r)}(x, x_0) = \mathbf{\Omega}(x)\mathbf{c} + \mathbf{J}^{(r)}(x, x_0) \qquad r = P, W, \Delta\Theta, \Delta V \tag{3.23}$$

where $\mathbf{\Omega}(x)\mathbf{c}$ are the solutions of the homogeneous equations associated with Eqs.(3.19)-(3.22), and given as:

$$\mathbf{\Omega}(x)\mathbf{c} = \begin{bmatrix} \Omega_{V1} & \Omega_{V2} & \Omega_{V3} & \Omega_{V4} \\ \Omega_{\Theta 1} & \Omega_{\Theta 2} & \Omega_{\Theta 3} & \Omega_{\Theta 4} \\ \Omega_{M1} & \Omega_{M2} & \Omega_{M3} & \Omega_{M4} \\ \Omega_{S1} & \Omega_{S2} & \Omega_{S3} & \Omega_{S4} \end{bmatrix} \begin{bmatrix} c_1 \\ c_2 \\ c_3 \\ c_4 \end{bmatrix} \tag{3.24}$$

where $\mathbf{c}_j = [c_1\ c_2\ c_3\ c_4]^T$ is a vector collecting all the integration constants, while the vector $\mathbf{J}^{(r)}(x, x_0)$ collects the particular integrals

$$\mathbf{J}^{(r)}(x, x_0) = [J_V^{(r)}\ J_\Theta^{(r)}\ J_M^{(r)}\ J_S^{(r)}] \qquad r = P, W, \Delta\Theta, \Delta V \tag{3.25}$$

The solutions $\mathbf{\Omega}(x)\mathbf{c}$ applies for every kind of external input, i.e. for $r = P, W, \Delta\Theta, \Delta V$, because the same homogeneous equation is associated with Eqs.(3.19)-(3.22). Solutions collected in Eq.(3.23) can be derived based on two simple considerations.

1. The first is that the the following relations hold among the particular integrals $\mathbf{J}^{(r)}(x, x_0)$:

$$J_V^{(W)}(x, x_0) = -\int_0^L J_V^{(P)}(x, \xi)\delta^{(1)}(\xi - x_0)d\xi = \frac{\bar{d}J_V^{(P)}(x, x_0)}{dx_0} \tag{3.26}$$

$$J_V^{(\Delta\Theta)}(x, x_0) = EI\int_0^L J_V^{(P)}(x, \xi)\delta^{(2)}(\xi - x_0)d\xi = EI\frac{\bar{d}^2 J_V^{(P)}(x, x_0)}{dx_0^2} \tag{3.27}$$

$$J_V^{(\Delta V)}(x,x_0) = EI\int_0^L J_V^{(P)}(x,\xi)\delta^{(3)}(\xi-x_0)d\xi = -EI\frac{\bar{d}^3 J_V^{(P)}(x,x_0)}{dx_0^3} \tag{3.28}$$

2. The second consideration is that, due to EB beam theory, the following relations connect all the response variables:

$$\frac{\bar{d}G_V^{(r)}}{dx} = G_\Theta^{(r)} \quad r = P, W, \Delta\Theta \tag{3.29}$$

$$\frac{\bar{d}G_V^{(\Delta V)}}{dx} = G_\Theta^{(\Delta V)} + \Delta V\delta(x-x_0) \qquad r = \Delta V = 1 \tag{3.30}$$

$$\frac{\bar{d}G_\Theta^{(r)}}{dx} = -\frac{G_M^{(r)}}{EI} \qquad \text{for } r = P, W, \Delta V \tag{3.31}$$

$$\frac{\bar{d}G_\Theta^{(\Delta\Theta)}}{dx} = -\frac{G_M^{(\Delta\Theta)}}{EI} + \Delta\Theta\delta(x-x_0) \qquad \text{for } \Delta\Theta = 1 \tag{3.32}$$

$$\frac{\bar{d}G_M^{(r)}}{dx} = G_S^{(r)} \qquad \text{for } r = P, \Delta\Theta, \Delta V \tag{3.33}$$

$$\frac{\bar{d}G_M^{(W)}}{dx} = G_S^{(W)} + W\delta(x-x_0) \qquad \text{for } W = 1 \tag{3.34}$$

$$\frac{\bar{d}G_S^{(r)}}{dx} = -m\omega^2 G_V^{(r)} \qquad \text{for } r = W, \Delta\Theta, \Delta V \tag{3.35}$$

$$\frac{\bar{d}G_S^{(P)}}{dx} = -m\omega^2 G_V^{(P)} - P\delta(x-x_0) \qquad \text{for } P = 1 \tag{3.36}$$

Eqs.(3.29-3.36) express the concept that the full set of Green's functions collected in $\mathbf{G}^{(r)}(x,x_0)$ (for $r = P, W, \Delta\Theta, \Delta V$) can be derived just

knowing the Green's function of the deflection $G_V^{(P)}(x, x_0)$ due to a unit point load P. The latter, solution of Eq.(3.19) is available in the following closed form [13] (obtained via Laplace Transform in Chapter 2):

$$G_V^{(P)}(x, x_0) = \sum_{j=1}^{4} \Omega_{V_j}(x) c_j + J_V^{(P)}(x, x_0) \tag{3.37}$$

where

$$\Omega_{V_1}(x) = e^{-\beta x} \quad \Omega_{V_2}(x) = e^{\beta x} \quad \Omega_{V_3}(x) = \cos(\beta x) \quad \Omega_{V_4}(x) = \sin(\beta x) \tag{3.38}$$

for $\beta = \beta(\omega) = EI^{-1/4} m^{1/4} \omega^{1/2}$ and

$$J_V^{(P)}(x, x_0) = \alpha\{\sinh(\beta(x - x_0)) - \sin(\beta(x - x_0))\} H(x - x_0) \tag{3.39}$$

for $\alpha = \alpha(\omega) = 2^{-1} EI^{-1/4} m^{-3/4} \omega^{-3/2}$, being $H(x - x_0)$ the unit step function (defined in Chapter 2), i.e. $H(x - x_0) = 0$ for $x < x_0$ and $H(x - x_0) = 1$ for $x > x_0$. Hence, starting from Eq.(3.37) for $G_V^{(P)}(x, x_0)$, and using Eqs.(3.29)-(3.36), the vector $\mathbf{G}^{(P)}(x, x_0) = \mathbf{\Omega}(x)\mathbf{c} + \mathbf{J}^{(P)}(x, x_0)$ can be built. The vectors $\mathbf{G}^{(r)}(x, x_0)$ can be derived for $r = W, \Delta\Theta, \Delta V$, using Eqs.(3.26)-(3.36). The full set of Green's functions is given in Appendix A.

Exact Frequency response of beam with dampers

The closed form expressions derived for the Dynamic Green's functions of the bare beam can be used to build the exact frequency response function of the beam with dampers.

For this purpose, consider the beam represented in Figure 3.1 acted upon by an arbitrary transverse harmonic load $f(x, t) = f(x)e^{i\omega t}$ on the interval (a, b). Due to the linearity of the problem, the vector collecting the FRFs of all response variable $\mathbf{Y}(x, \omega)$, defined at the beginning of the present Section,

can be obtained applying the linear superposition principle as follows

$$\mathbf{Y}(x,\omega) = \mathbf{\Omega}(x)\mathbf{c} + \sum_{j=1}^{n} \mathbf{J}(x,x_j)\mathbf{\Lambda}_j + \mathbf{Y}^{(f)}(x) \tag{3.40}$$

where the vector $\mathbf{Y}^{(f)}(x,\omega)$ is the particular integral associated to the distributed load $f(x)$, obtained via the following convolution integral

$$\mathbf{Y}^{(f)}(x) = \int_a^b \mathbf{J}^{(P)}(x,\xi) f(\xi) d\xi \tag{3.41}$$

The vector $\mathbf{\Lambda}_j$ in Eq.(3.40) collects the unknown reaction force $P_j(\omega)$, reaction moment $W_j(\omega)$, relative deflection $\Delta V_j(\omega)$ and relative rotation $\Delta\Theta_j$ at the damper location x_j. While, $\mathbf{J}(x,x_j)$ is a 4×4 matrix collecting the particular integrals related to the response discontinuities at the damper location:

$$\mathbf{\Lambda_j} = [P_j \;\; \Delta V_j \;\; W_j \;\; \Delta\Theta_j]^T \quad \text{for } j = 1,2,\ldots,n \tag{3.42}$$

$$\mathbf{J}(x,x_j) = \begin{bmatrix} J_V^{(P)} & J_V^{(\Delta V)} & J_V^{(W)} & J_V^{(\Delta\Theta)} \\ J_\Theta^{(P)} & J_\Theta^{(\Delta V)} & J_\Theta^{(W)} & J_\Theta^{(\Delta\Theta)} \\ J_M^{(P)} & J_M^{(\Delta V)} & J_M^{(W)} & J_M^{(\Delta\Theta)} \\ J_S^{(P)} & J_S^{(\Delta V)} & J_S^{(W)} & J_S^{(\Delta\Theta)} \end{bmatrix} \quad \text{for} j = 1,2,\ldots n \tag{3.43}$$

Notice that on the right hand side of Eq.(3.40) frequency dependence is omitted for brevity.

The key step to obtain the exact FRF $\mathbf{Y}(x,\omega)$ is to express the unknowns $\mathbf{\Lambda}_j$ in Eq.(3.40) as functions of the integration constants only. For this purpose, using Eqs.(3.6)-(3.18) the following 4 condition involving P_j, ΔV_j, W_j, $\Delta\Theta_j$ are established at every discontinuous location x_j:

$$P_j = -\kappa_{P_j}(\omega)V(x_j) = -\kappa_{P_j}(\omega)[V(x_j^-) + \frac{S(x_j^-)}{\kappa_{\Delta V_j^-}(\omega)}] \tag{3.44}$$

$$\Delta V_j = \frac{S(x_j^-)}{\kappa_{\Delta V_j^-}(\omega)} + \frac{S(x_j^+)}{\kappa_{\Delta V_j^+}(\omega)} = S(x_j^-)[\frac{1}{\kappa_{\Delta V_j^-}(\omega)} + \frac{1}{\kappa_{\Delta V_j^+}(\omega)}] - \frac{P_j}{\kappa_{\Delta V_j^+}(\omega)}$$
$$= S(x_j^-)[\frac{1}{\kappa_{\Delta V_j^-}(\omega)} + \frac{1}{\kappa_{\Delta V_j^+}(\omega)}] + \frac{\kappa_{P_j}}{\kappa_{\Delta V_j^+}(\omega)}[V(x_j^-) + \frac{S(x_j^-)}{\kappa_{\Delta V_j^-}(\omega)}] \tag{3.45}$$

$$W_j = -\kappa_{W_j}(\omega)\Theta(x_j) = -\kappa_{W_j}(\omega)[\Theta(x_j^-) - \frac{M(x_j^-)}{\kappa_{\Delta\Theta_j^-}(\omega)}] \tag{3.46}$$

$$\Delta\Theta_j = -\frac{M(x_j^-)}{\kappa_{\Delta\Theta_j^-}(\omega)} - \frac{M(x_j^+)}{\kappa_{\Delta\Theta_j^+}(\omega)} = -M(x_j^-)[\frac{1}{\kappa_{\Delta\Theta_j^-}(\omega)} + \frac{1}{\kappa_{\Delta\Theta_j^+}(\omega)}] - \frac{W_j}{\kappa_{\Delta\Theta_j^+}(\omega)}$$
$$= -M(x_j^-)[\frac{1}{\kappa_{\Delta\Theta_j^-}(\omega)} + \frac{1}{\kappa_{\Delta\Theta_j^+}(\omega)}] + \frac{\kappa_{W_j}}{\kappa_{\Delta\Theta_j^+}(\omega)}[\Theta(x_j^-) - \frac{M(x_j^-)}{\kappa_{\Delta V_j^-}(\omega)}] \tag{3.47}$$

Next, replacing Eq.(3.40) written for $V(x)$, $\Theta(x)$, $M(x)$, $S(x)$, on the RHS of Eqs.(3.44), (3.45), (3.46), (3.47), it is noticed that the unit-step-functions $H(x - x_j)$ involved in $\mathbf{J}(x, x_j)$ are not zero only when computed as $x < x_j$. This makes it possible to cast vector $\mathbf{\Lambda}_1$ at the first damper location x_1 and vectors $\mathbf{\Lambda}_j$ at damper location x_j, for $j = 2, \ldots, n$ as follows:

$$\mathbf{\Lambda}_1 = \mathbf{\Phi_\Omega}(x_1)\mathbf{c} + \mathbf{\Phi}^{(f)}(x_1) \tag{3.48}$$

$$\mathbf{\Lambda}_j = \mathbf{\Phi_\Omega}(x_j)\mathbf{c} + \sum_{k=1}^{j-1} \mathbf{\Phi_J}(x_j^-, x_k)\mathbf{\Lambda}_k + \mathbf{\Phi}^{(f)}(x_j) \quad \text{for} \quad j = 2, \ldots, n \tag{3.49}$$

In Eqs.(3.48), (3.49) $\mathbf{\Phi_\Omega}(x_j)$ is a 4×4 matrix given as:

$$\mathbf{\Phi_\Omega}(x_j)=\begin{bmatrix} -\kappa_{P_j}(\omega)(\mathbf{\Omega}_1(x_j)+\frac{\mathbf{\Omega}_4(x_j)}{\kappa_{\Delta V_j^-}(\omega)}) \\ \mathbf{\Omega}_4(x_j)(\frac{1}{\kappa_{\Delta V_j^-}(\omega)}+\frac{1}{\kappa_{\Delta V_j^+}(\omega)})+\frac{\kappa_{P_j}(\omega)}{\kappa_{\Delta V_j^+}(\omega)}(\mathbf{\Omega}_1(x_j)+\frac{\mathbf{\Omega}_4(x_j)}{\kappa_{\Delta V_j^-}(\omega)}) \\ -\kappa_{W_j}(\omega)(\mathbf{\Omega}_2(x_j)-\frac{\mathbf{\Omega}_3(x_j)}{\kappa_{\Delta\Theta_j^-}(\omega)}) \\ -\mathbf{\Omega}_3(x_j)(\frac{1}{\kappa_{\Delta\Theta_j^-}(\omega)}+\frac{1}{\kappa_{\Delta\Theta_j^+}(\omega)}]+\frac{\kappa_{W_j}(\omega)}{\kappa_{\Delta\Theta_j^+}(\omega)}[\mathbf{\Omega}_2(x_j)-\frac{\mathbf{\Omega}_2(x_j)}{\kappa_{\Delta V_j^-}(\omega)}] \end{bmatrix} \tag{3.50}$$

being $\mathbf{\Omega}_i$ the row vectors coinciding with the ith row of matrix $\mathbf{\Omega}(x)$. Then, $\mathbf{\Phi_J}(x_j^-,x_k)$ is the following 4×4 matrix:

$$\mathbf{\Phi_J}(x_j^-,x_k)=\begin{bmatrix} -\kappa_{P_j}(\omega)(\mathbf{J}_1(x_j^-,x_k)+\frac{\mathbf{J}_4(x_j^-,x_k)}{\kappa_{\Delta V_j^-}(\omega)}) \\ \mathbf{J}_4(x_j^-,x_k)(\frac{1}{\kappa_{\Delta V_j^-}(\omega)}+\frac{1}{\kappa_{\Delta V_j^+}(\omega)})+\frac{\kappa_{P_j}(\omega)}{\kappa_{\Delta V_j^+}(\omega)}(\mathbf{J}_1(x_j^-,x_k)+\frac{\mathbf{J}_4(x_j^-,x_k)}{\kappa_{\Delta V_j^-}(\omega)}) \\ -\kappa_{W_j}(\omega)(\mathbf{J}_2(x_j^-,x_k)-\frac{\mathbf{J}_3(x_j^-,x_k)}{\kappa_{\Delta\Theta_j^-}(\omega)}) \\ -\mathbf{J}_3(x_j^-,x_k)(\frac{1}{\kappa_{\Delta\Theta_j^-}(\omega)}+\frac{1}{\kappa_{\Delta\Theta_j^+}(\omega)}]+\frac{\kappa_{W_j}(\omega)}{\kappa_{\Delta\Theta_j^+}(\omega)}[\mathbf{J}_2(x_j^-,x_k)-\frac{\mathbf{J}_2(x_j^-,x_k)}{\kappa_{\Delta V_j^-}(\omega)}] \end{bmatrix} \tag{3.51}$$

where $\mathbf{J}_i(x_j,x_k)$ is the row vector coinciding with the ith row of matrix $\mathbf{J}(x,x_j)$. Finally $\mathbf{\Phi}^{(f)}(x_j)$ is the 4×1 vector

$$\mathbf{\Phi}^{(f)}(x_j)=\begin{bmatrix} -\kappa_{P_j}(\omega)(Y_1^{(f)}(x_j)+\frac{Y_4^{(f)}(x_j)}{\kappa_{\Delta V_j^-}(\omega)}) \\ Y_4^{(f)}(x_j)(\frac{1}{\kappa_{\Delta V_j^-}(\omega)}+\frac{1}{\kappa_{\Delta V_j^+}(\omega)})+\frac{\kappa_{P_j}(\omega)}{\kappa_{\Delta V_j^+}(\omega)}(Y_1^{(f)}(x_j)+\frac{Y_4^{(f)}(x_j)}{\kappa_{\Delta V_j^-}(\omega)}) \\ -\kappa_{W_j}(\omega)(Y_2^{(f)}(x_j)-\frac{Y_3^{(f)}(x_j)}{\kappa_{\Delta\Theta_j^-}(\omega)}) \\ -Y_3^{(f)}(x_j)(\frac{1}{\kappa_{\Delta\Theta_j^-}(\omega)}+\frac{1}{\kappa_{\Delta\Theta_j^+}(\omega)}]+\frac{\kappa_{W_j}(\omega)}{\kappa_{\Delta\Theta_j^+}(\omega)}[Y_2^{(f)}(x_j)-\frac{Y_2^{(f)}(x_j)}{\kappa_{\Delta V_j^-}(\omega)}] \end{bmatrix} \tag{3.52}$$

where $Y_i^{(f)}$ are the elements of vector $\mathbf{Y}^{(f)}$. Notice the formal corrispondence between the rows of $\mathbf{\Phi_\Omega}(x_j)$, $\mathbf{\Phi_J}(x_j,x_k)$, $\mathbf{\Phi}^{(f)}(x_j)$ and Eqs.(3.44)-(3.47).

Eqs.(3.48-3.49) for $\mathbf{\Lambda}_j$ is the basis to obtain $\mathbf{\Lambda}_j$ as function of the vector of integration constants $\mathbf{c}$ only. Indeed, starting from Eq.(3.48) for $\mathbf{\Lambda}_1$, Eq.

(3.49) leads to the following general form of $\mathbf{\Lambda}_j$

$$\begin{aligned}\mathbf{\Lambda}_j = \mathbf{\Phi_\Omega}(x_j)\mathbf{c} + \mathbf{\Phi}^{(f)}(x_j) + \sum_{(j,m)\in N_2^{(j)}} \mathbf{\Phi_J}(x_j^-, x_m)(\mathbf{\Phi_\Omega}(x_m)\mathbf{c} + \mathbf{\Phi}^{(f)}(x_m)) + \\ + \sum_{2<q\leq j} \sum_{(j,m,n,\ldots,r,s)\in N_q^{(j)}} \mathbf{\Phi_J}(x_j^-, x_m)\mathbf{\Phi_J}(x_m^-, x_n)\ldots\mathbf{\Phi_J}(x_r^-, x_s)(\mathbf{\Phi_\Omega}(x_s)\mathbf{c} \\ + \mathbf{\Phi}^{(f)}(x_s))\end{aligned} \tag{3.53}$$

where $N_q^{(j)} = \Big\{(j,m,n,\ldots,r,s) : j > m > n > \cdots > r > s; m,n,\ldots,r,s = 1,2,\ldots,(j-1)]\Big\}$ is the set including all possible q-ples of indexes $(j,m,n,\ldots,r,s)$ such that $j > m > n > \cdots > r > s$, being $2 \leq q \leq j$. For instance, with $n = 4$ damper locations the following sets shall be considered in Eq.(3.53):

for $j = 2:\ N_2^{(2)} = \{(2,1)\}$
for $j = 3:\ N_2^{(3)} = \{(3,1),(3,2)\}; N_3^{(3)} = \{(3,2,1)\}$
for $j = 4:\ N_2^{(4)} = \{(4,1),(4,2),(4,3)\}; N_3^{(4)} = \{(4,3,2),(4,3,1),(4,2,1)\};$
$N_4^{(4)} = \{(4,3,2,1)\}$

Hence, on replacing Eq.(3.53) for $\mathbf{\Lambda}_j$ in Eq.(3.40), the following relation is derived for the exact frequency response $\mathbf{Y}(x)$

$$\mathbf{Y}(x) = \tilde{\mathbf{Y}}(x)\mathbf{c} + \tilde{\mathbf{Y}}^{(f)}(x) \tag{3.54}$$

where the only unknown is the vector of integration constants $\mathbf{c}$, while $\tilde{\mathbf{Y}}(x)$ and $\tilde{\mathbf{Y}}^{(f)}(x)$ are given as:

$$\begin{aligned}\tilde{\mathbf{Y}}(x) = \mathbf{\Omega}(x) + \sum_{j=1}^{N} \mathbf{J}(x,x_j)\mathbf{\Phi_\Omega}(x_j) + \sum_{j=1}^{N} \mathbf{J}(x,x_j)\Bigg\{ \sum_{(j,m)\in N_2^{(j)}} \mathbf{\Phi_J}(x_j^-, x_m)\mathbf{\Phi_\Omega}(x_m) + \\ + \sum_{2<q\leq j} \sum_{(j,m,n,\ldots,r,s)\in N_q^{(j)}} \mathbf{\Phi_J}(x_j^-, x_m)\mathbf{\Phi_J}(x_m^-, x_n)\ldots\mathbf{\Phi_J}(x_r^-, x_s)\mathbf{\Phi_\Omega}(x_s)\Bigg\}\end{aligned} \tag{3.55}$$

$$\tilde{\mathbf{Y}}^{(f)}(x) = \mathbf{Y}^{(f)}(x) + \sum_{j=1}^{N} \mathbf{J}(x, x_j)\boldsymbol{\Phi}^{(f)}(x_j) + \sum_{j=1}^{N} \mathbf{J}(x, x_j)\Bigg\{ \sum_{(j,m)\in N_2^{(j)}} \boldsymbol{\Phi}_{\mathbf{J}}(x_j^-, x_m)\boldsymbol{\Phi}^{(f)}(x_m) + + \sum_{2<q\leq j} \sum_{(j,m,n,\ldots,r,s)\in N_q^{(j)}} \boldsymbol{\Phi}_{\mathbf{J}}(x_j^-, x_m)\boldsymbol{\Phi}_{\mathbf{J}}(x_m^-, x_n)\ldots\boldsymbol{\Phi}_{\mathbf{J}}(x_r^-, x_s)\boldsymbol{\Phi}^{(f)}(x_s)\Bigg\} \tag{3.56}$$

In Eq.(3.55), the matrix $\tilde{\mathbf{Y}}(x)$ depends on the beam parameters only, through matrices $\boldsymbol{\Omega}(x)$ and $\mathbf{J}(x, x_j)$, while $\tilde{\mathbf{Y}}^{(f)}(x)$ depends on the beam parameters and the applied load, as includes the particular integral $\mathbf{Y}^{(f)}(x)$ and the load-dependent vector $\boldsymbol{\Phi}^{(f)}(x)$.

At this point, in order to derive closed-form expressions for the exact frequency response $\mathbf{Y}(x)$ in Eq.(3.54), two further steps only have to be pursued:

1. Firstly, consider the vector of integration constants $\mathbf{c}$ in Eq.(3.54). Enforcing the B.C. of the beam leads to 4 equations, regardless of the number of dampers, with general form

$$\mathbf{Bc} = \mathbf{r} \rightarrow \mathbf{c} = (\mathbf{B})^{-1}\mathbf{r} \tag{3.57}$$

   where vector $\mathbf{r}$ involves the load-dependent terms $\tilde{\mathbf{Y}}^{(f)}(x)$ in Eq.(3.56), as computed at the beam ends. Due to the limited size (4×4), the coefficient matrix $\mathbf{B}$ can readily be inverted in a symbolic form, as shown in Appendix B. Therefore, from Eq.(3.57) closed-form expressions can be derived for $\mathbf{c}$, to be replaced in Eq.(3.54).

2. Secondly, consider Eq.(3.41) for the particular integrals $\mathbf{Y}^{(f)}(x)$ related to the applied load. In view of the analytical expressions of $\mathbf{J}^{(P)}(x, \xi)$, (see Appendix A), it is immediate to recognize that every integral in

Eq.(3.41) can be reverted to the general form $\int_a^b g(\xi)H(x-\xi)d\xi$, with $g(\xi)$ given by the product of the loading function and certain trigonometric/hyperbolic functions. For instance, in view of Eq.(3.39) for $J_V^{(P)}$, computing $\mathbf{Y}^{(f)}(x)$ will involve, among others, the integral

$$\int_a^b J_V^{(P)}(x,\xi)f(\xi)d\xi = \int_a^b g(\xi)H(x-\xi)d\xi \tag{3.58}$$

with $g(\xi) = f(\xi)[\sinh(\beta_1(x-\xi))\gamma_1+\sinh(\beta_2(x-\xi))\gamma_2]$. Using the theory of generalized functions, integrals $\int_a^b g(\xi)H(x-\xi)d\xi$ can be computed as:

$$\begin{aligned}\int_a^b g(\xi)H(x-\xi)d\xi &= [H(x-\xi)(g^{[1]}(\xi)-g^{[1]}(x))]_a^b \\ &= H(x-b)(g^{[1]}(b)-g^{[1]}(x)) \\ &- H(x-a)(g^{[1]}(a)-g^{[1]}(x))\end{aligned} \tag{3.59}$$

where $g^{[1]}$ denotes the first-order primitive function of $g(\xi)$. It is noticed that, for polynomial loads $f(x)$ typically encountered in engineering applications, the first order primitive $g^{[1]}$ can be obtained in a closed form by any symbolic package [2]. This means that, upon deriving closed-form expressions of $\mathbf{c}$ from Eq.(3.57), Eq.(3.54) provides exact closed-form expressions for the frequency response functions of the beam with an arbitrary number of dampers, due to a polynomial load $f(x)e^{\mathrm{i}\omega t}$, for all the response variables.

Eq.(3.54) can be used for both homogeneous and non-homogeneous B.C., the latter as associated with end dampers. In fact, the B.C. can still be considered as homogeneous, while the end dampers are modeled as internal dampers located at $x_1 = 0^+$ and $x_n = L^-$.

Eq.(3.54) for $\mathbf{Y}(x)$ has been derived for the most general case of translational and rotational dampers occurring simultaneously at the same location $x = x_j$. Changes for single dampers occurring at a given location are immediate, as explained in the following.

If no ETD occurs at $x = x_j$, $\kappa_{P_j}(\omega) = 0$ shall be set at $x = x_j$. This will automatically set equal to zero all terms in the 1^{st} row of matrices $\mathbf{\Phi_\Omega}(x_j), \mathbf{\Phi_J}(x_j, x_k)$ and $\mathbf{\Phi}^{(f)}(x_j)$. In addition, being $P_j = 0$ at $x = x_j$, terms in the 1^{st} column of matrix $\mathbf{\Phi_J}(x_m, x_j)$ shall be set equal to zero for all $x_m > x_j$. Obviously, if at $x = x_j$ there is no ETD, but there is a ITD, $S(x_j^-) = S(x_j^+)$ and, $\kappa_{\Delta V_j^+}(\omega) = \kappa_{\Delta V_j^-}(\omega) = \kappa_{\Delta V_j}(\omega)/2$, with $\kappa_{\Delta V_j}(\omega)$ the frequency dependent stiffness of the ITD located at $x = x_j$.

Changes to be made if no ERD or IRD occurs at $x = x_j$ mirror those explained above for translational dampers, and are not report for brevity. A final consideration concerns the case in which the applied load is a point force $P\delta(x - x_0)$ located at $x = x_0$. in this case, Eq.(3.41) gives $\mathbf{Y}^{(f)} = P\mathbf{J}^{(P)}(x, x_0)$; if in particular the pint load is applied at a damper location x_j, i.e. $x_0 = x_j$ Eq.(3.9) will be written as $P + P_j(\omega) + S(x_j^+) = S(x_j^-)$ and consequently and additional term $-P/\kappa_{\Delta V_j^+}(\omega)$ shall be considered on the RHS of Eq.(3.15) and in the second entry of vector $\mathbf{\Phi}^{(f)}(x_j)$, where in the case $Y_4^{(f)}(x)$ will be computed at $x = x_j^-$.

Free vibrations

Due to the presence of concentrated dampers, the damping in the primary system is not proportional and consequently the eigenvalues ω_n and the associated eigenfunctions $V_n(y)$ are complex. The eigenvalues are computed as a root of the characteristic equation built as $\det(\mathbf{B}) = 0$. This is obtained from Eq.(3.57) with $\mathbf{r} = \mathbf{0}$, that means imposing $f(x, t) = 0$: on computing every eigenvalue and calculating the corresponding matrix $\mathbf{B}$, the associated eigenfunction is given by Eq.(3.54) with $\mathbf{c}$ = non-trivial solution of $\mathbf{Bc} = \mathbf{0}$ and $\tilde{\mathbf{Y}}^{(f)} = \mathbf{0}$.

Now, consider that along the beam there are TMD, TD and IRD only.

Then, the following orthogonality conditions among the modes are derived:

$$m(\omega_m^2 - \omega_n^2)\int_0^L V_n V_m dy + \sum_{j=1}^{N}\Bigg\{(\kappa_{P_j}(\omega_n) - \kappa_{P_j}(\omega_m))V_m(x_j)V_n(x_j) + ((\kappa_{\Delta\theta_j})^{-1} - (\kappa_{\Delta\theta_j})^{-1})M_m(x_j)M_n(x_j)\Bigg\} = 0 \tag{3.60}$$

$$\begin{aligned}&(\omega_m - \omega_n)EI\int_0^L V_n'' V_m'' dy + m(\omega_m - \omega_n)\omega_m\omega_n\int_0^L V_m V_n dy \\ &+ \sum_{j=1}^{N}\Bigg\{(\omega_m\kappa_{P_j}(\omega_n) - \omega_n\kappa_{P_j}(\omega_m))V_m(x_j)V_n(x_j) \\ &[\omega_n(\kappa_{\Delta\theta_j}(\omega_m))^{-1} - \omega_m(\kappa_{\Delta\theta_j}(\omega_n))^{-1}]M_m(x_j)M_n(x_j) \\ &+ (k_{\Delta\theta_j}(\omega_m))^{-1}(k_{\Delta\theta_j}(\omega_n))^{-1}M_m(x_j)\int_0^L M_n(x_j)\delta(x - x_j)\delta(x - x_j)dx\Bigg\} = 0\end{aligned} \tag{3.61}$$

where ω_n and ω_m are the n-th and m-th complex eigenvalues, while $V_n(y)$, $M_n(y)$ and $V_m(y)$, and $M_m(y)$ denote the corresponding complex eigenfunctions.

Notice that Eq.(3.60) and Eq.(3.61) are derived from the governing equation of motion Eq.(3.3) written in free vibrations, i.e. for $f(y) = 0$. Eq.(3.60) is obtained as the difference of two equations: the first equation is built writing the equation of motion for the n-th mode, multiplied by $V_m(y)$ and integrated over $[0, L]$ taking into account the beam B.C.; the second equation mirrors the first one, i.e. is built writing the equation of motion for the m-th mode, multiplied by $V_n(y)$ and, integrated over $[0, L]$ using the beam B.C. Eq.(3.61) is obtained as the difference of the same two equations, upon multiplying the first by ω_m and the second by ω_n.

3.1.3 Complex modal analysis and time domain response

Here, in order to perform an exact time domain analysis and obtain a complete description of the frequency response of beam with dampers/masses in Figure 3.1, a pertinent complex modal analysis approach is devised. The approach generalizes to the beams with dampers/masses the approach introduced by Oliveto et al. in ref. [42] for beams in pure bending with viscous dampers at the ends.

Consider the bending equations of motion of the beam under a space-dependent impulsive force $f(x)f(t) = f(x)\delta(t)$, i.e.

$$EI\frac{\bar{\partial}^4 v_{RF}}{dx^4} + m\frac{\partial^2 v_{RF}}{\partial t^2} - \sum_{j=1}^{N} g_j(x,t) - f(x)\delta(t) = 0 \tag{3.62}$$

where $g_j(x,t) = r_j(t)\delta(x-x_j) + \Delta\theta_j(t)\delta^{(2)}(x-x_j)$, with $r_j(t)$ and $\Delta\theta_j(t)$ time-domain counterparts of terms in Eq.(3.3), i.e.: $r_j(t) = r_{G_j}(t) + r_{M_j}(t)$, for $r_{G_j}(t) = -k_{G_j}v(x_j,t) - c_{G_j}\dot{v}(x_j,t)$ and $r_{M_j}(t) = k_{M_j}(z_{M_j}(t) - v(x_j,t)) + c_{M_j}(\dot{z}_{M_j}(t) - \dot{v}(x_j,t)) = -M_j\ddot{z}_{M_j}(t)$, being $z_{M_j}(t)$ the displacement of the jth TMD; $\mu(x_j,t) = -k_{\Delta\theta_j}(t) - c_{\Delta\theta_j}(t)\Delta\dot{\theta}_j(t)$.

The response variables obtained from Eqs.(3.62), here collected in vector $\mathbf{I}_{RF}(y,t) = [h_{RF}\ \ \theta_{RF}\ \ m_{RF}\ \ s_{RF}]^T$, are the impulse response functions of the beam. Using the mode superposition principle, they can be represented as

$$\mathbf{I}_{RF}(y,t) = \sum_{k=1}^{\infty}\mathbf{I}_{RF,k}(y,t) = \sum_{k=1}^{\infty} b_k(t)\mathbf{Y}_k(y) = \sum_{k=1}^{\infty}\tilde{b}_k e^{i\omega_k t}\mathbf{Y}_k(y) \tag{3.63}$$

where $\mathbf{I}_{RF,k}(y,t)$ is the vector of modal impulse response functions associated with the k-th mode, $\mathbf{Y}_k(y) = [V_k\ \ \Theta_k\ \ M_k\ \ S_k]^T$ is the vector of k-th complex eigenfuctions and $\tilde{b}_k$ are complex coefficients. In Eq.(3.63), notice that $b_k(t) = \tilde{b}_k e^{i\omega_k t}$ in view of the impulsive nature of the load [42, 43]. Then, further manipulations are: use Eq.(3.63) for the response variables in Eqs.(3.62), multiply Eq.(3.62) by $V_m(y)$, integrate over $[0, L]$ considering the

beam B.C.; finally, using the orthogonality conditions (3.60)-(3.61) leads to the following equations for $\tilde{b}_k$:

$$\tilde{b}_k = \frac{L_k}{i\omega_k \Gamma_k} \tag{3.64}$$

$$L_k = \int_0^L V_k(x) f(x) dx \tag{3.65}$$

$$\Gamma_k = 2m \int_0^L V_k^2 dx + \sum_{j=1}^{N} \Big\{ \frac{M_j[2(\kappa_{M_j}(\omega_k))^2 - ic_{M_j} M_j \omega_k^3]]}{[\kappa_{M_j}(\omega_k) - M_j \omega_k^2]^2} - \frac{ic_{G_j}}{\omega_k} \Big\} (V_k(x_j))^2 - \sum_{j=1}^{N} \frac{ic_{\Delta\theta_j}}{\omega_k} \Big(\frac{M_k(x_j)}{\kappa_{\Delta\theta_j}(\omega_k)} \Big)^2 \tag{3.66}$$

On replacing Eq.(3.64) for $\tilde{b}_k$ in Eq.(3.63), the impulse response $\mathbf{I}_{RF}(y,t)$ is obtained, as well as the corresponding modal impulse responses $\mathbf{I}_{RF,k}(y,t)$.

Now it is observed that, for the damping levels generally encountered in engineering applications, the complex modes contributing to the structural response occur in complex-conjugate pairs [43, 42]. Correspondingly, a pair of complex-conjugate modal impulse responses $\mathbf{I}_{RF,k}(y,t)$ is indeed associated with the k-th mode; their sum provides the following real form for the vector of modal impulse response functions of the k-th mode, to be used in Eq.(3.63)

$$\mathbf{I}^r_{RF,k}(y,t) = \boldsymbol{\alpha}_k(y)|\omega_k| z_k(t) + \boldsymbol{\beta}_k(y) \dot{z}_k(t) \tag{3.67}$$

with

$$\begin{aligned} &\boldsymbol{\alpha}_k(y) = \xi_k \boldsymbol{\beta}_k(y) - \sqrt{(1-\xi_k^2)} \boldsymbol{\lambda}_k(y) \ ; \ \ \boldsymbol{\beta}_k(y) = 2\mathrm{Re}[\tilde{b}_k \mathbf{Y}_k(y)] \ ; \\ &\boldsymbol{\lambda}_k(y) = 2\mathrm{Im}[\tilde{b}_k \mathbf{Y}_k(y)] \end{aligned} \tag{3.68}$$

$$z_k(t) = \frac{1}{\omega_{D_k}} e^{-\xi_k |\omega_k| t} \sin(\omega_{D_k} t) \ ; \ \ \omega_{D_k} = |\omega_k| (\sqrt{1-\xi_k^2}) \tag{3.69}$$

being $\xi_k = \mathrm{Im}[\omega_k]/|\omega_k|$ the modal damping ratio of the k-th mode [42]. In

the frequency domain, each vector $\mathbf{I}^r_{RF,k}$ is associated with a vector $\hat{\mathbf{R}}_k(y) = [\hat{V}_k \;\; \hat{\Theta}_k \;\; \hat{M}_k \;\; \hat{S}_k]^{\mathrm{T}}$, which contains the modal frequency response functions of the k-th mode and is given by (frequency dependence is omitted for brevity):

$$\hat{\mathbf{R}}_k(y) = \boldsymbol{\alpha}_k(y)|\omega_k|Z_k + \boldsymbol{\beta}_k(y)\dot{Z}_k \tag{3.70}$$

where

$$Z_k(\omega) = \frac{1}{|\omega_k|^2 - \omega^2 + 2i\xi_k|\omega_k|\omega} \;\; ; \;\; \dot{Z}_k(\omega) = \frac{i\omega}{|\omega_k|^2 - \omega^2 + 2i\xi_k|\omega_k|\omega} \tag{3.71}$$

Using the mode superposition principle with a finite number of modes M, the approximate frequency response $\hat{\mathbf{Y}} = [\hat{V} \;\; \hat{\Theta} \;\; \hat{M} \;\; \hat{S}]^{\mathrm{T}}$ can be built as

$$\mathbf{Y}(y) \approx \hat{\mathbf{Y}}(y) = \sum_{k=1}^{M} \hat{\mathbf{R}}_k(y) \tag{3.72}$$

Eq.(3.72) approximates the exact frequency response $\mathbf{Y}(y)$ given by Eq.(3.54) in Section 3, providing an insight into the contribution of every mode. Eq.(3.72) for the frequency response and Eq.(3.63) for the impulse response are obtained in a closed analytical form. Obviously, Eq.(3.63) can be used to calculate the time-domain response to an arbitrary force $p(x,t) = f(x)w(t)$ by a standard Duhamel convolution integral

$$\mathbf{y}(x,t) = \int_0^t \mathbf{I}_{RF}(x, t-\tau)w(\tau)d\tau \tag{3.73}$$

where $\mathbf{y}(x,t) = [v \;\; \theta \;\; m \;\; s]^T$ is the vector collecting the time-dependent response variables of the beam. In Eq.(3.169), notice that the impulse response $\mathbf{I}_{RF}(x, t-\tau)$ includes the space-dependent functions of the applied load, i.e. $f(x)$, see Eqs.(3.64).

3.1.4 Advantages and remarks

Now, advantages of the proposed approach are discussed. Firstly, the exact analytical frequency response functions (3.54) is compared with the alternative exact expressions obtainable by a classical procedure. This consists in dividing the beam in uniform segments, each between two consecutive application points of dampers/masses/point loads or under a distributed load, where the frequency response can be expressed using the solution to the homogeneous equations of motion, and including a particular integral for the segments where a distributed load is applied. For n segments, $4 \times n$ integration constants should be computed by enforcing the B.C. at beam ends and matching conditions among the solutions over adjacent segments. By using this approach, even with a low number of dampers/masses/loads, the coefficient matrix associated with the equations to be solved shall be re-inverted numerically for any forcing frequency of interest, and updated whenever dampers/masses/load change positions (as discussed in Chapter 1). Over this classical procedure, the proposed exact expression (3.54) has the following advantages:

- It is inherently able to satisfy all the required conditions at the dampers and point load locations, capturing jump and slope discontinuities of the response variables.
- The analytical form is easy to implement in any symbolic package, and can readily be computed for any frequency of interest, parameters of dampers (location, stiffness, damping), position of the loads, regardless of the number of dampers and positions of the dampers relative to the loads.

These two characteristics make Eq.(3.54) particularly suitable for optimization problems, where several solutions shall be built and compared for changing position and parameters of dampers/masses/loads.

Next, it is remarked that the characteristic equation $\det(\mathbf{B}) = 0$ is obtained from matrix $\mathbf{B}$ in Eq.(3.57), which holds the same size 4×4 for any

number of dampers. Once the natural frequencies are calculated, Eq.(3.54) provides the exact eigenfunctions of all response variables $\mathbf{Y}(y)$ in a closed form inherently fulfilling the required conditions at the applications points of supports/masses. Then, all the advantages previously presented for the frequency response functions, holds for the free vibration response too and are consequently conveyed to the impulse response functions.

In the next Section, an application of the proposed method to an axially loaded Euler-Bernoulli beam will be shown. Specifically, a frequency response analysis will be led, showing through some numerical examples that the method is exact and suitable for optimization problems.

3.2 Flexural vibrations of discontinuous axially loaded beams with symmetric cross section

3.2.1 Description of the problem

Figure 3.2 shows an axially-loaded EB beam carrying an arbitrary number of Kelvin-Voigt viscoelastic ETDs and IRDs, and subjected to harmonic transverse loads. The axial load is constant and is assumed to remain along the x-axis during motion. For generality, beam, load and damper parameters in Figure 3.2 are in dimensionless form. Corresponding dimensional parameters are given in Table 3.1, being L, EI and m_0 length, flexural stiffness and mass per unit length of the beam ("$\hat{}$" denote dimensional parameters). Figure 3.2 shows positive sign conventions. Specifically, positive shear forces are reported on an elementary beam segment in the undeformed beam configuration. For this problem, the shear force will always indicate the stress resultant acting on the plane of the rotated cross section, i.e. orthogonal to the deformed beam axis.

Being x_j the dimensionless abscissa of a damper application point, $0 <$

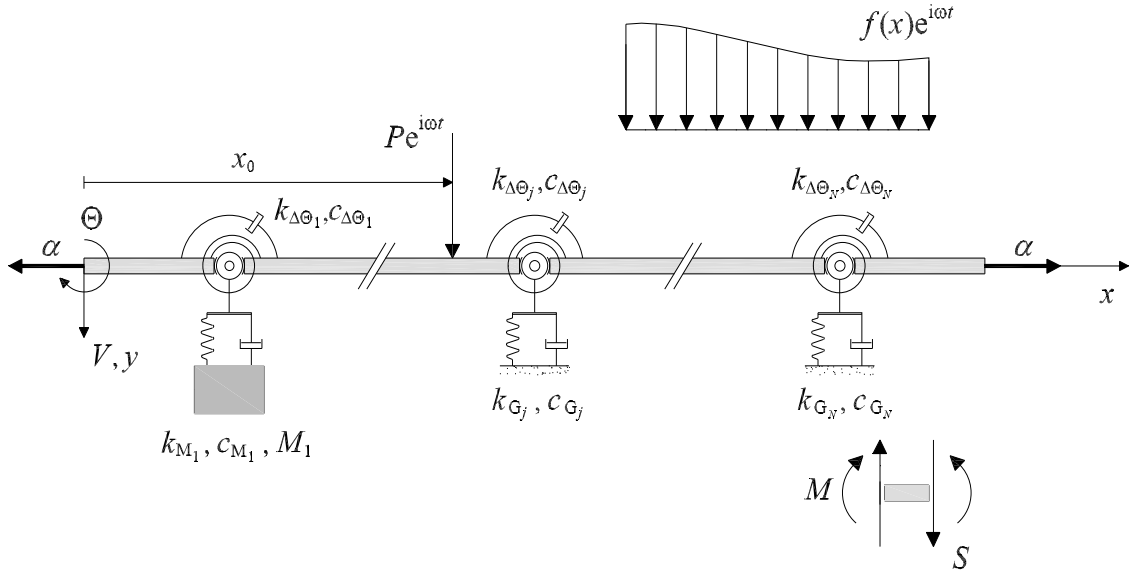

Figure 3.2: Axially-loaded Euler-Bernoulli beam carrying an arbitrary number of Kelvin-Voigt viscoelastic translational and rotational dampers. Positive sign conventions are reported.

$x_1 < \cdots < x_j < \cdots < x_N < 1$, for $j = 1, 2, \ldots, N$, dimensionless stiffness and damping parameters are denoted as follows:

1. ETDs: k_{G_j}, c_{G_j} for grounded dampers; k_{M_j}, c_{M_j} for mass dampers, with M_j indicating the pertinent mass.

2. ITDs: $k_{\Delta\Theta_j}, c_{\Delta\Theta_j}$.

For this problem, closed form expressions of the frequency response function are derived and a couple of numerical examples are given showing the powerful of the technique. Again, governing equations will be written for translational and rotational dampers occurring simultaneously at the same location.

3.2.2 Direct Frequency analysis

Next, assume that the beam is loaded by a harmonic transverse distributed load $f(x)e^{i\omega t}$ on the interval (a, b), with $0 \leq a \leq b \leq 1$. Let

$v(x,\omega,t) = V(x,\omega)e^{\mathrm{i}\omega t}, \theta(x,\omega,t) = \Theta(x,\omega)e^{\mathrm{i}\omega t}, m(x,\omega,t) = M(x,\omega)e^{\mathrm{i}\omega t}$ and $s(x,\omega,t) = S(x,\omega)e^{\mathrm{i}\omega t}$ be the steady-state response variables. By using the theory of generalized functions, the following dimensionless steady-state motion equation is derived:

$$\frac{\bar{d}^4 V(x)}{dx^4} - \alpha\frac{\bar{d}^2 V(x)}{dx^2} - \omega^2 V(x) + R_{ext}(x) + \Delta_{int}(x) - f(x) = 0 \tag{3.74}$$

where frequency dependence in $V(x)$, $R_{ext}(x)$ and $\Delta_{int}(x)$ is omitted for brevity. In Eq.(3.74) $R_{ext}(x)$ and $\Delta_{int}(x)$ are generalized functions given as:

$$R_{ext}(x) = -\sum_{j=1}^{N} P_j \delta(x - x_j) \tag{3.75}$$

$$\Delta_{int}(x) = -\sum_{j=1}^{N} \Delta\Theta_j \delta^{(2)}(x - x_j) \tag{3.76}$$

In Eq.(3.75), P_j is the reaction of the jth ETD, given as:

$$P_j = -\kappa_{P_j}(\omega) V(x_j) \tag{3.77}$$

where $V(x_j)$ is the deflection at $x = x_j$, while $\kappa_{P_j}(\omega)$ is a frequency-dependent term.

In Eq.(3.76), $\Delta\Theta_j$ is the relative rotation between cross sections at $x = x_j^+$ and $x = x_j^-$ of the jth internal rotational damper, given as:

$$\Delta\Theta_j = \Theta(x_j^+) - \Theta(x_j^-) = -(\kappa_{\Delta\Theta_j}(\omega))^{-1} M(x_j) \tag{3.78}$$

where $M(x_j)$ is the bending moment at $x = x_j$, and $\kappa_{\Delta\Theta_j}(\omega)$ is a frequency-dependent term.

It is worth remarking that both rotation and shear force are discontinuous at the location x_j of a rotational damper [44]. Indeed, due the continuity of the vertical stress resultant $Q = S + \alpha \cdot \Theta$ and in view of Eq.(3.78), it can be

written that [44]

$$S(x_j^+)+\alpha\cdot\Theta(x_j^+) = S(x_j^-)+\alpha\cdot\Theta(x_j^-) \rightarrow S(x_j^+) \neq S(x_j^-) \text{ being } \Theta(x_j^+) \neq \Theta(x_j^-) \tag{3.79}$$

Eq.(3.79) shows that a discontinuity in rotation implies a discontinuity in shear force.

Dimensional parameters	Dimensionless parameters
$\hat{x}$	$x = \hat{x}/L$
$\hat{V}$	$V = \hat{V}/L$
$\hat{H}$	$\alpha = \hat{H}\frac{L^2}{EI}$
$\hat{\omega}$	$\omega = \hat{\omega}L^2(\frac{m_0}{EI})^{-1/2}$
$\hat{M}_j$	$M_j = \hat{M}_j(m_0 L)^{-1}$
$\hat{S}$	$S = \hat{S}\frac{L^2}{EI}$
$\hat{k}_{\Delta\Theta_j}$	$k_{\Delta\Theta_j} = \hat{k}_{\Delta\Theta_j}\frac{L}{EI}$
$\hat{c}_{\Delta\Theta_j}$	$c_{\Delta\Theta_j} = \hat{c}_{\Delta\Theta_j}(m_0 EI L^2)^{-1/2}$
$\hat{k}_{G_j}$	$k_{G_j} = \hat{k}_{G_j}\frac{L^2}{EI}$
$\hat{c}_{G_j}$	$c_{G_j} = \hat{c}_{G_j}(\frac{m_o EI}{L^2})^{-1/2}$
$\hat{M}$	$M = \hat{M}\frac{L}{EI}$
$\hat{\Theta}$	$\Theta = \hat{\Theta}$
$\hat{P}$	$P = \hat{P}\frac{L^2}{EI}$
$\hat{f}$	$f = \frac{\hat{f}L^3}{EI}$

Table 3.1: Dimensional and respective dimensionless parameters.

Dynamic Green's functions of the bare beam

In order to compute the exact frequency response of the beam in Figure 3.2, the dimensionless dynamic Green's functions of the axially-loaded bare

beam, subjected to harmonic unit transverse point load and unit relative rotation at a given abscissa $x = x_0, 0 < x_0 < 1$, will be used. They are solutions of the following steady-state equations, respectively:

$$\frac{\bar{d}^4 G_V^{(P)}(x,x_0)}{dx^4} - \alpha \frac{\bar{d}^2 G_V^{(P)}(x,x_0)}{dx^2} - \omega^2 G_V^{(P)}(x,x_0) - P\delta(x-x_0) = 0, \qquad P = 1 \tag{3.80}$$

$$\begin{aligned} \frac{\bar{d}^4 G_V^{(\Delta\Theta)}(x,x_0)}{dx^4} - \alpha \frac{\bar{d}^2 G_V^{(\Delta\Theta)}(x,x_0)}{dx^2} - \omega^2 G_V^{(\Delta\Theta)}(x,x_0) \\ - \Delta\Theta\delta^{(2)}(x-x_0) = 0, \quad \Delta\Theta = 1 \end{aligned} \tag{3.81}$$

where meaning of the superscripts and subscripts In Eqs.(3.80)-(3.81), are the same of the previous Section. Based on the governing equation of EB beam theory, the dimensionless relations can be written for rotation, bending-moment and shear-force dynamic Green's functions similarly to the previous Section.

Next, be $\mathbf{G}^{(r)}(x,x_0) = [G_V^{(r)}\ G_\Theta^{(r)}\ G_M^{(r)}\ G_S^{(r)}]$, for $r = P, \Delta\Theta$, the vector collecting the dynamic Green's functions of all response variables. Again, it can readily be seen that the general form of $\mathbf{G}^{(r)}(x,x_0)$ is:

$$\mathbf{G}^{(r)}(x,x_0) = \mathbf{\Omega}(x)\mathbf{c} + \mathbf{J}^{(r)}(x,x_0) \qquad r = P, \Delta\Theta \tag{3.82}$$

In Eq.(3.82), $\mathbf{\Omega}(x)\mathbf{c}$ contains the solution of the homogeneous equation associated with Eqs.(3.80),(3.81) and successive derivatives according to the relation between the response variables given by EB beam theory.

$$\mathbf{\Omega}(x)\mathbf{c} = \begin{bmatrix} \Omega_{V1} & \Omega_{V2} & \Omega_{V3} & \Omega_{V4} \\ \Omega_{\Theta 1} & \Omega_{\Theta 2} & \Omega_{\Theta 3} & \Omega_{\Theta 4} \\ \Omega_{M1} & \Omega_{M2} & \Omega_{M3} & \Omega_{M4} \\ \Omega_{S1} & \Omega_{S2} & \Omega_{S3} & \Omega_{S4} \end{bmatrix} \begin{bmatrix} c_1 \\ c_2 \\ c_3 \\ c_4 \end{bmatrix} \tag{3.83}$$

with $\mathbf{c} = [c_1\ c_2\ c_3\ c_4]^{\mathrm{T}}$ vector of integration constants, while $\mathbf{J}^{(\cdot)}$ collects the

particular integrals

$$\mathbf{J}^{(r)}(x,x_0)=\left[J_V^{(r)}\ J_\Theta^{(r)}\ J_M^{(r)}\ J_S^{(r)}\right] \qquad r=P,\Delta\Theta \tag{3.84}$$

All terms in Eq.(3.82) can be derived as follows, basing on the same considerations done in the previous Section.

Regarding the vector of dynamic Green's functions $\mathbf{G}^{(P)}(x,x_0)$ due to a point load $P=1$ at $x=x_0$, it is noticed, first, that the deflection dynamic Green's function $G_V^{(P)}(x,x_0)$ is available in the following closed form (see Chapter 2):

$$G_V^{(P)}(x,x_0)=\sum_{j=1}^{4}\Omega_{Vj}(x)c_j+J_V^{(P)}(x,x_0) \tag{3.85}$$

where

$$\Omega_{V1}(x)=e^{\beta_1 x}\ ;\ \Omega_{V2}(x)=e^{-\beta_1 x}\ ;\ \Omega_{V3}(x)=e^{\beta_2 x}\ ;\ \Omega_{V4}(x)=e^{-\beta_2 x}\ ; \tag{3.86a-d}$$

$$J_V^{(P)}(x,x_0)=[\sinh(\beta_1(x-x_0))\gamma_1+\sinh(\beta_2(x-x_0))\gamma_2]\cdot H(x-x_0) \tag{3.87}$$

for $\beta_1=\beta_1(\omega)=\sqrt{(\alpha-\sqrt{\alpha^2+4\omega^2})/2}$, $\beta_2=\beta_2(\omega)=\sqrt{(\alpha+\sqrt{\alpha^2+4\omega^2})/2}$, $\gamma_1=\gamma_1(\omega)=-(\beta_1\sqrt{\alpha^2+4\omega^2})^{-1}$,
$\gamma_2=\gamma_2(\omega)=(\beta_2\sqrt{\alpha^2+4\omega^2})^{-1}$, being $H(x-x_0)$ the unit step function. Hence, starting from Eq.(3.85) for $G_V^{(P)}$, and using the beam governing equations for $r=P$ to derive $G_\Theta^{(P)}$, $G_M^{(P)}$, $G_S^{(P)}$, the vector of dynamic Green's functions $\mathbf{G}^{(P)}(x,x_0)=\mathbf{\Omega}(x)\mathbf{c}+\mathbf{J}^{(P)}(x,x_0)$, due to a point load $P=1$ at $x=x_0$, can be constructed. It is remarked that the solution in Eq.(3.85) is obtained exploiting the general closed form expressions obtained in Chapter 2 and after some algebraic manipulations.

As for the vector of dynamic Green's functions $\mathbf{G}^{(\Delta\Theta)}(x,x_0)$, it is seen,

first, that $G_V^{(\Delta\Theta)}(x, x_0)$ takes the form

$$G_V^{(\Delta\Theta)}(x, x_0) = \sum_{j=1}^{4} \Omega_{Vj}(x) c_j + J_V^{(\Delta\Theta)}(x, x_0) \tag{3.88}$$

In Eq.(3.88) Ω_{V_j} are given by Eqs.(3.86a-d), as indeed the homogenous equations associated with Eq.(3.80) for $G_V^{(P)}$ and Eq.(3.81) for $G_V^{(\Delta\Theta)}$ are the same. Also, $J_V^{(\Delta\Theta)}$, can be derived from the particular integral $J_V^{(P)}$ of Eq.(3.80), using the following relation among the particular integrals of Eq.(3.80) and Eq.(3.81):

$$\begin{aligned} J_V^{(\Delta\Theta)}(x, x_0) &= \frac{\bar{d}^2 J_V^{(P)}(x, x_0)}{dx^2} \\ &= [\beta_1^2 \sinh(\beta_1(x - x_0))\gamma_1 + \beta_2^2 \sinh(\beta_2(x - x_0))\gamma_2] \cdot H(x - x_0) \end{aligned} \tag{3.89}$$

Again, starting from Eq.(3.88) for $G_V^{(\Delta\Theta)}$ and using the beam governing equations lead to the vector of dynamic Green's functions $\mathbf{G}^{(\Delta\Theta)}(x, x_0) = \mathbf{\Omega}(x)\mathbf{c} + \mathbf{J}^{(\Delta\Theta)}(x, x_0)$ due to a relative rotation $\Delta\Theta = 1$ at $x = x_0$. For brevity, the full set of dynamic Green's functions $\mathbf{G}^{(r)}(x, x_0)$ is reported in Appendix A, for $r = P, \Delta\Theta$.

Frequency response of the beam with dampers

The exact frequency response of the axially-loaded beam with an arbitrary number of dampers, shown in Figure 3.2, can be built based on the dynamic Green's functions of the bare beam computed before.

Be $\mathbf{Y}(x) = [V\ \Theta\ M\ S]^T$ the vector collecting the frequency response functions of all response variables (again, frequency dependence is omitted for brevity). Based on Eq.(3.82) and applying the linear superposition principle, $\mathbf{Y}(x)$ can be written as

$$\mathbf{Y}(x) = \mathbf{\Omega}(x)\mathbf{c} + \sum_{j=1}^{N} \mathbf{J}(x, x_j)\mathbf{\Lambda}_j + \mathbf{Y}^{(f)}(x) \tag{3.90}$$

In Eq.(3.90), $\mathbf{Y}^{(f)}(x)$ is the particular integral related to load $f(x)$, given as

$$\mathbf{Y}^{(f)}(x) = \int_a^b \mathbf{J}^{(P)}(x,\xi) f(\xi) d\xi \tag{3.91}$$

Vector $\mathbf{\Lambda}_j$ collects the unknown reaction force $P_j(\omega)$ and relative rotation $\Delta\Theta_j(\omega)$ at the damper location x_j, while $\mathbf{J}(x, x_j)$is a 4×2 matrix collecting the particular integrals related to response discontinuities at the damper locations, i.e.

$$\mathbf{\Lambda}_j = [P_j \ \Delta\Theta_j]^T \quad \text{for } j = 1, 2, \ldots, N. \tag{3.92}$$

$$\mathbf{J}(x, x_j) = \begin{bmatrix} J_V^{(P)} & J_V^{(\Delta\Theta)} \\ J_\Theta^{(P)} & J_\Theta^{(\Delta\Theta)} \\ J_M^{(P)} & J_M^{(\Delta\Theta)} \\ J_S^{(P)} & J_S^{(\Delta\Theta)} \end{bmatrix} \quad \text{for} j = 1, 2, \ldots N \tag{3.93}$$

The first step to build the exact frequency response $\mathbf{Y}(x)$ of the beam is to obtain the unknowns $\mathbf{\Lambda}_j$ in Eq.(3.90), as functions of the vector of integration constants $\mathbf{c}$ only. Due to the equations Eq.(3.77) for P_j, and Eq.(3.78) for $\Delta\Theta_j$, using Eq.(3.90) for $V(x)$ and $M(x)$ and exploiting the properties of the Unit Step function it is possible to cast vector $\mathbf{\Lambda}_1$ at the damper location x_1 and vectors $\mathbf{\Lambda}_j$ at damper locations x_j, for $j = 2, \ldots, N$ in the following forms:

$$\mathbf{\Lambda}_1 = \mathbf{\Phi}_{\mathbf{\Omega}}(x_1)\mathbf{c} + \mathbf{\Phi}^{(f)}(x_1) \tag{3.94}$$

$$\mathbf{\Lambda}_j = \mathbf{\Phi}_{\mathbf{\Omega}}(x_j)\mathbf{c} + \sum_{k=1}^{j-1} \mathbf{\Phi}_{\mathbf{J}}(x_j, x_k)\mathbf{\Lambda}_k + \mathbf{\Phi}^{(f)}(x_j) \quad for \ \ j = 2, \ldots, N \tag{3.95}$$

In Eqs.(3.94,3.95) $\mathbf{\Phi}_{\mathbf{\Omega}}(x_j)$ is a 2 x 4 matrix given as:

$$\mathbf{\Phi}_{\mathbf{\Omega}}(x_j) = \begin{bmatrix} -\kappa_{P_j}(\omega)\mathbf{\Omega}_1(x_j) \\ (-\kappa_{\Delta\Theta_j}(\omega))^{-1}\mathbf{\Omega}_3(x_j) \end{bmatrix} \tag{3.96}$$

being $\mathbf{\Omega}_i$ the row vector coinciding with the ith row of matrix $\mathbf{\Omega}(x)$. Further, $\mathbf{\Phi_J}(x_j, x_k)$ is the 2×2 matrix:

$$\mathbf{\Phi_J}(x_j, x_k) = \begin{bmatrix} -\kappa_{P_j}(\omega)\mathbf{J}_1(x_j, x_k) \\ (-\kappa_{\Delta\Theta_j}(\omega))^{-1}\mathbf{J}_3(x_j) \end{bmatrix} \tag{3.97}$$

where $\mathbf{J}_i(x_j, x_k)$ is the row vector coinciding with the ith row of matrix $\mathbf{J}(x, x_j)$, and $\mathbf{\Phi}^{(f)}(x_j)$ is the 2×1 vector

$$\mathbf{\Phi}^{(f)}(x_j) = \begin{bmatrix} -\kappa_{P_j}(\omega)Y_1^{(f)}(x_j) \\ (-\kappa_{\Delta\Theta_j}(\omega))^{-1}Y_3^{(f)}(x_j) \end{bmatrix} \tag{3.98}$$

where $Y_i^{(f)}$ are the elements of vector $\mathbf{Y}^{(f)}$.

Eqs.(3.94-3.95) for $\mathbf{\Lambda}_j$ serve as a basis to obtain $\mathbf{\Lambda}_j$ as function of the vector of integration constants $\mathbf{c}$ only. Indeed, starting from Eq.(3.94) for $\mathbf{\Lambda}_1$, Eq. (3.95) leads to the following general form of $\mathbf{\Lambda}_j$

$$\begin{aligned} \mathbf{\Lambda}_j = \mathbf{\Phi_\Omega}(x_j)\mathbf{c} + \mathbf{\Phi}^{(f)}(x_j) + \sum_{(j,m)\in N_2^{(j)}} \mathbf{\Phi_J}(x_j, x_m)(\mathbf{\Phi_\Omega}(x_m)\mathbf{c} + \mathbf{\Phi}^{(f)}(x_m)) + \\ + \sum_{2<q\leq j} \sum_{(j,m,n,\ldots,r,s)\in N_q^{(j)}} \mathbf{\Phi_J}(x_j, x_m)\mathbf{\Phi_J}(x_m, x_n)\ldots\mathbf{\Phi_J}(x_r, x_s)(\mathbf{\Phi_\Omega}(x_s)\mathbf{c} \\ + \mathbf{\Phi}^{(f)}(x_s)) \end{aligned} \tag{3.99}$$

where $N_q^{(j)}$ assumes the same meaning given in the previous Section.

Hence, on replacing Eq.(3.99) for $\mathbf{\Lambda}_j$ in Eq.(3.90), the following relation is derived for the exact frequency response $\mathbf{Y}(x)$

$$\mathbf{Y}(x) = \tilde{\mathbf{Y}}(x)\mathbf{c} + \tilde{\mathbf{Y}}^{(f)}(x) \tag{3.100}$$

where the only unknown is the vector of integration constants $\mathbf{c}$, while $\tilde{\mathbf{Y}}(x)$

and $\tilde{\mathbf{Y}}^{(f)}(x)$ are given as:

$$\tilde{\mathbf{Y}}(x) = \mathbf{\Omega}(x) + \sum_{j=1}^{N} \mathbf{J}(x, x_j)\mathbf{\Phi}_{\mathbf{\Omega}}(x_j) + \sum_{j=1}^{N} \mathbf{J}(x, x_j)\Bigg\{ \sum_{(j,m)\in N_2^{(j)}} \mathbf{\Phi}_{\mathbf{J}}(x_j, x_m)\mathbf{\Phi}_{\mathbf{\Omega}}(x_m) + \\ + \sum_{2<q\leq j} \sum_{(j,m,n,\ldots,r,s)\in N_q^{(j)}} \mathbf{\Phi}_{\mathbf{J}}(x_j, x_m)\mathbf{\Phi}_{\mathbf{J}}(x_m, x_n)\ldots\mathbf{\Phi}_{\mathbf{J}}(x_r, x_s)\mathbf{\Phi}_{\mathbf{\Omega}}(x_s)\Bigg\} \tag{3.101}$$

$$\tilde{\mathbf{Y}}^{(f)}(x) = \mathbf{Y}^{(f)}(x) + \sum_{j=1}^{N} \mathbf{J}(x, x_j)\mathbf{\Phi}^{(f)}(x_j) \\ + \sum_{j=1}^{N} \mathbf{J}(x, x_j)\Bigg\{ \sum_{(j,m)\in N_2^{(j)}} \mathbf{\Phi}_{\mathbf{J}}(x_j, x_m)\mathbf{\Phi}^{(f)}(x_m) + \\ + \sum_{2<q\leq j} \sum_{(j,m,n,\ldots,r,s)\in N_q^{(j)}} \mathbf{\Phi}_{\mathbf{J}}(x_j, x_m)\mathbf{\Phi}_{\mathbf{J}}(x_m, x_n)\ldots\mathbf{\Phi}_{\mathbf{J}}(x_r, x_s)\mathbf{\Phi}^{(f)}(x_s)\Bigg\} \tag{3.102}$$

In Eq.(3.101), $\tilde{\mathbf{Y}}(x)$ depends on the beam parameters only, through matrices $\mathbf{\Omega}(x)$ and $\mathbf{J}(x, x_j)$, while $\tilde{\mathbf{Y}}^{(f)}(x)$ depends on the beam parameters and the applied load, as includes the particular integral $\mathbf{Y}^{(f)}(x)$ and the load-dependent vectors $\mathbf{\Phi}^{(f)}(x)$.

At this point, closed-form expressions for the exact frequency response $\mathbf{Y}(x)$ in Eq.(3.100) can be derived according to the two further steps shown in the previous Section. Here only the first is reported. Consider the vector of integration constants $\mathbf{c}$ in Eq.(3.100). Enforcing the B.C. of the beam leads to 4 equations, regardless of the number of dampers, with general form

$$\mathbf{Bc} = \mathbf{r} \rightarrow \mathbf{c} = (\mathbf{B})^{-1}\mathbf{r} \tag{3.103}$$

where vector $\mathbf{r}$ involves the load-dependent terms $\tilde{\mathbf{Y}}^{(f)}(x)$ in Eq.(3.100), as computed at the beam ends. Due to the limited size (4×4), the coefficient matrix $\mathbf{B}$ can readily be inverted in a symbolic form, as shown in Appendix

B. Therefore, from Eq.(3.103) closed-form expressions can be derived for $\mathbf{c}$, to be replaced in Eq.(3.100).

3.2.3 Numerical examples

Two numerical applications are presented, to show the potential of the proposed method.

Example A

Consider the axially-loaded beam in Figure 3.3, featuring two elastic translational supports, two attached mass dampers and three rotational dampers. Dimensionless parameters are reported in Table 3.2 (a set of corresponding dimensional parameters may be found in ref.[21]).

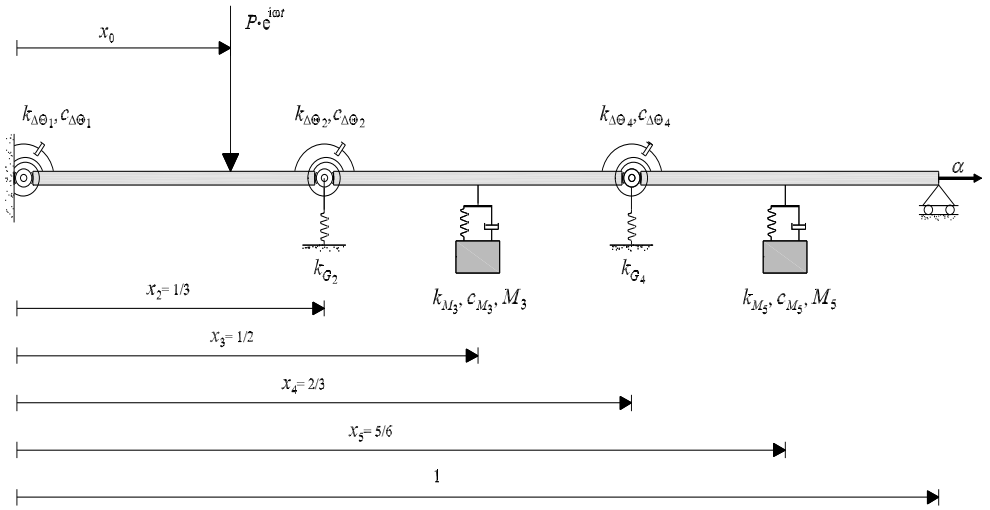

Figure 3.3: Axially-loaded Euler-Bernoulli beam with elastic translational supports, Kelvin-Voigt viscoelastic mass dampers and rotational dampers, subjected to harmonic transverse point load.

The proposed method is applied to investigate the frequency response under harmonic transverse point loads, as shown in Figure 3.3. It is implemented treating the left-end damper as an internal damper at $x = 0^+ =$

10^{-10}, that is $N = 5$ damper positions are considered. For comparison, solutions are built by the classical approach, i.e. representing the vibration response in terms of 4 unknown integration constants over every beam segment between two consecutive damper/load positions, computed by internal matching conditions between the responses over adjacent segments, along with the B.C. Both proposed and classical methods provide the exact frequency response. However, the proposed method provides the frequency response in a closed form, because closed-form expressions can be obtained for the integration constants $\mathbf{c}$ in Eq.(3.100), using formulae in Appendix B for symbolic inversion of the 4×4 coefficient matrix $\mathbf{B}$ associated with the B.C. in Eq.(3.103). In contrast, the classical method requires computing $6 \times 4 = 24$ integration constants for an arbitrarily placed point load (or $5 \times 4 = 20$ integration constants if the point load is applied, in particular, at a damper location), by inverting the coefficient matrix associated with the internal conditions + 4 B.C. Due to the large size, in this case matrix inversion is performed numerically, and the inverse matrix shall be re-computed for any forcing frequency of interest.

For a first insight, free vibrations are investigated. The characteristic equation of the proposed method is built as determinant of matrix $\mathbf{B}$ in Eq.(3.103), for $\mathbf{r} = \mathbf{0}$. Tables 3.3-3.4 report the eigenvalues of the first 4 modes, computed by proposed and classical methods using Mathematica [2]. Specifically, Table 3.3 shows dimensionless eigenvalues of the undamped beam, i.e. assuming zero damping in the rotational dampers and mass dampers. In this case the eigenvalues are real, and decrease or increase with decreasing or increasing axial load parameter α. This is consistent with the fact that decreasing values of α correspond to increasing axial compression, i.e. to a progressive reduction of bending stiffness, while increasing values of α correspond to increasing axial tension, i.e. to a progressive increase of bending stiffness. The dimensionless complex eigenvalues of the damped beam, i.e. when damping in Table 3.2 is considered in the rotational dampers and mass dampers, are reported in Table 3.4. Consistently with the results in Table 3.3, Table 3.4

shows that the axial load parameter α greatly affects also the eigenvalues of the damped beam. Finally, notice that there is an excellent agreement among the eigenvalues computed by proposed and classical methods, up to the first three digits, in both Tables 3.3 and 3.4.

Next, consider the damped beam under different harmonically-varying transverse point loads. Figure 3.4 shows the frequency response functions of all response variables, for a transverse point load $P = 1.36 \cdot 10^{-5}$with frequency $\omega = 9.8$ applied at $x_0 = 0.5$ and axial load parameter $\alpha = -10$, as computed by proposed and classical methods. Real and imaginary parts of the two solutions are in perfect agreement. The response variables built by the proposed method inherently satisfy all the required discontinuity conditions at the damper locations, i.e. the rotation is discontinuous at the locations of rotational dampers where, correspondingly, the deflection is not differentiable; also, the shear force is discontinuous at the locations of translational supports, mass dampers and point load, where, in turn, the bending moment is not differentiable. Notice that the shear-force discontinuity at $x_2 = 1/3$ and $x_4 = 2/3$ is due to the reaction of the translational support and the rotation discontinuity caused by the rotational damper [44].

Figure 3.5 shows the deflection frequency response function at $x = 1/3$, for a transverse point load $P = 1.36 \cdot 10^{-5}$ with varying excitation frequency ω and position x_0 along the beam, and axial load parameter $\alpha = -10$, as computed by the proposed method. It can be noted that the contribution of the various modes to the frequency response amplitude at $x = 1/3$ varies depending on the position of the transverse point load, with a generally dominating contribution from the first mode. In order to compare the results obtained by proposed and classical methods, Figure 3.6 shows cross sections of the deflection frequency response function at $x = 1/3$ shown in Figure 3.5, for a few fixed positions x_0 of the transverse point load. Again, an excellent agreement is found between the two solutions. It is worth noticing that the proposed method proves particularly efficient for building the results in Figures 3.5-3.6, since Eq.(3.222) for the frequency response holds, in a closed

form, for any load position and forcing frequency. In contrast, the classical approach requires re-building the set of equations to be solved depending on the load position relative to damper/support locations; in addition, the coefficient matrix involved in the classical method has to be inverted numerically, for any load position and forcing frequency.

Next, Figure 3.7 illustrates the deflection frequency response function at $x = 1/3$, for a transverse point load $P = 1.36 \cdot 10^{-5}$ applied at $x_0 = 0.5$, for varying excitation frequency ω and axial load parameter α, as computed by the proposed method. It is observed that the peaks shift towards lower frequency values as the axial load parameter α decreases, i.e. as a result of the bending stiffness reduction due to increasing axial compression. For a comparison between proposed method and classical method, see Figure 3.8 reporting cross sections of the deflection frequency response function at $x = 1/3$ shown in Figure 3.7, for various axial load parameters α. Again, the agreement between the two solutions is very satisfactory.

x_j	$k_{\Delta\Theta_j}$	$c_{\Delta\Theta_j}$	k_{G_j}	c_{G_j}	M_j
x_1	6	0.0036	-	-	-
x_2	6	0.0036	16.38	-	-
x_3	-	-	163.8	0.525	3.36
x_4	6	0.0036	16.38	-	-
x_5	-	-	163.8	0.525	3.36

Table 3.2: Beam in Figure 3.3: dimensionless parameters of elastic supports and dampers.

	$\alpha = 0$		$\alpha = 1$		$\alpha = 10$	
Mode	C. M.	P. M.	C.M.	P.M.	C.M.	P.M.
1	3.641937	3.641929	3.720185	3.720169	4.27651	4.27649
2	6.308792	6.308741	6.321693	6.321674	6.41531	6.41539
3	24.92631	24.92615	25.11917	25.11928	26.8023	26.8023
4	39.20693	39.20671	39.74475	39.74467	44.2766	44.2765

	$\alpha = 0$		$\alpha = -1$		$\alpha = -10$	
Mode	C. M.	P. M.	C.M.	P.M.	C.M.	P.M.
1	3.641937	3.641929	3.559254	3.559243	2.499723	2.499731
2	6.308792	6.308741	6.295246	6.295258	6.131294	6.131263
3	24.92631	24.92615	24.73227	24.73249	22.92794	22.92766
4	39.20693	39.20671	38.66144	38.66158	33.33327	33.33348

Table 3.3: Beam in Figure 3.3: eigenvalues of the undamped beam calculated through classical method (C.M.) and proposed method (P.M.).

	$\alpha = 0$		$\alpha = 1$	
Mode	C. M.	P. M.	C.M.	P.M.
1	3.641972+0.006251i	3.641964+0.006242i	3.720221+0.006723i	3.720214+0.006746i
2	6.308764+0.052247i	6.308736+0.052258i	6.321667+0.052654i	6.321679+0.052673i
3	24.91828+0.717221i	24.91841+0.717253i	25.11113+0.717014i	25.11105+0.717012i
4	39.20397+0.501993i	39.20363+0.501958i	39.74175+0.501667i	39.74146+0.501683i

	$\alpha = 1$		$\alpha = 10$	
Mode	C. M.	P. M.	C.M.	P.M.
1	3.720221+0.006723i	3.720214+0.006746i	4.276586+0.011123i	4.276559+0.011114i
2	6.321667+0.052654i	6.321679+0.052673i	6.415247+0.055772i	6.415259+0.055761i
3	25.11113+0.717014i	25.11105+0.717012i	26.79458+0.499376i	26.79423+0.499361i
4	39.74175+0.501667i	39.74146+0.50183i	44.27454+0.499367i	44.27422+0.499382i

	$\alpha = 0$		$\alpha = -1$	
Mode	C. M.	P. M.	C.M.	P.M.
1	3.641972+0.006251i	3.641964+0.006242i	3.559213+0.005794i	3.559237+0.005761i
2	6.308764+0.052247i	6.308736+0.052258i	6.295476+0.051811i	6.295493+0.051801i
3	24.91828+0.717221i	24.91841+0.717253i	24.72412+0.717436i	24.72443+0.717487i
4	39.20397+0.501993i	39.20363+0.501958i	38.65826+0.502365i	38.65893+0.502684i

	$\alpha = -1$		$\alpha = -10$	
Mode	C. M.	P. M.	C.M.	P.M.
1	3.559213+0.005794i	3.559237+0.005761i	2.499735+0.002368i	2.499716+0.002379i
2	6.295476+0.051811i	6.295493+0.051801i	6.131314+0.046901i	6.131196+0.046917i
3	24.72412+0.717436i	24.72443+0.717487i	22.91974+0.718134i	22.91992+0.718196i
4	38.65826+0.502365i	38.65893+0.502684i	33.32858+0.507027i	33.32831+0.507456i

Table 3.4: Beam in Figure 3.3: eigenvalues of the damped beam calculated through classical method (C.M.) and proposed method (P.M.).

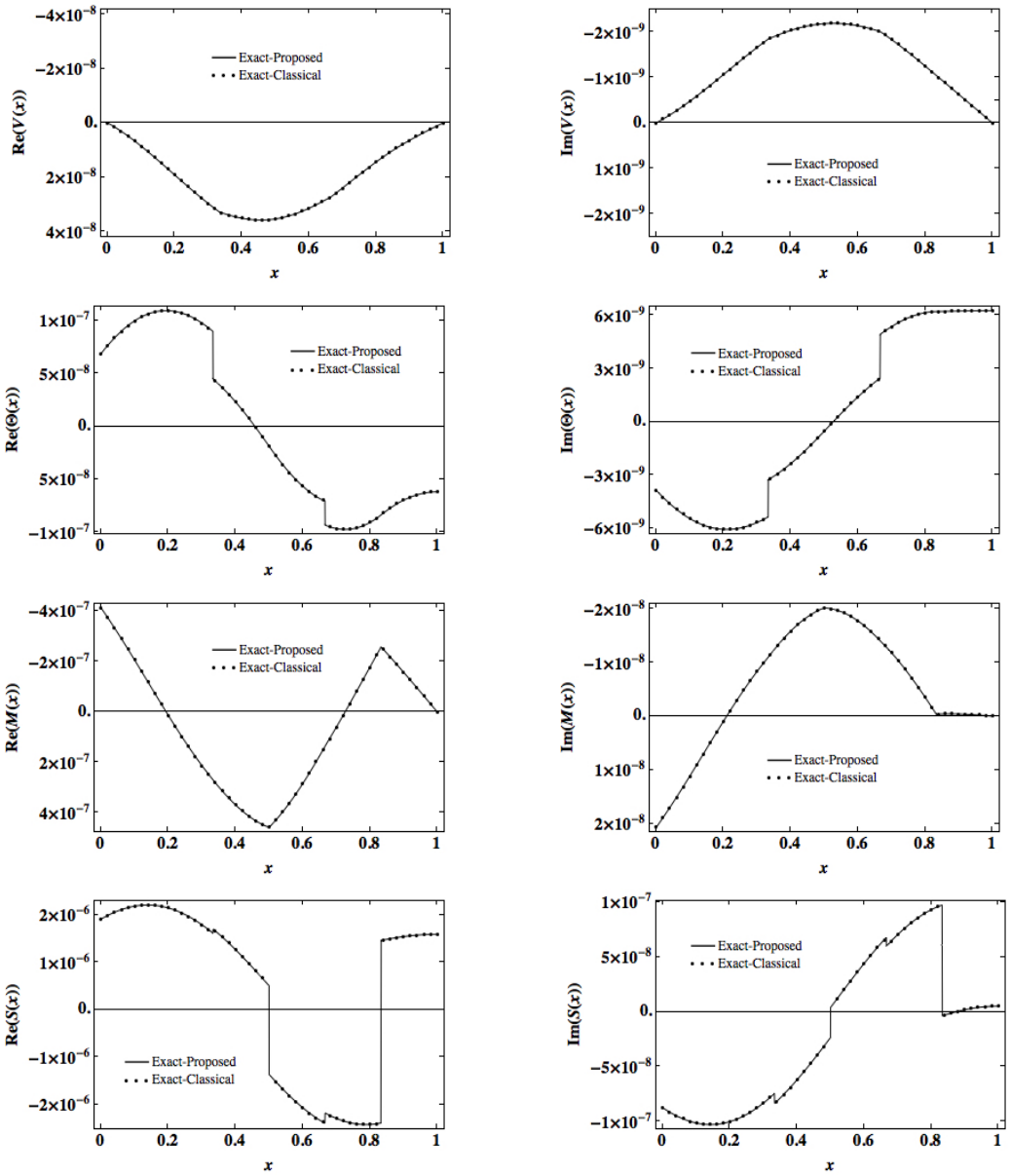

Figure 3.4: Beam in Figure 3.3: frequency response functions due to a transverse point load $P = 1.36 \cdot 10^{-5}$ with frequency $\omega = 9.8$ applied at $x_0 = 0.5$, and axial load parameter $\alpha = -10$, as computed by proposed and classical methods. Left column: real part; right column: imaginary part.

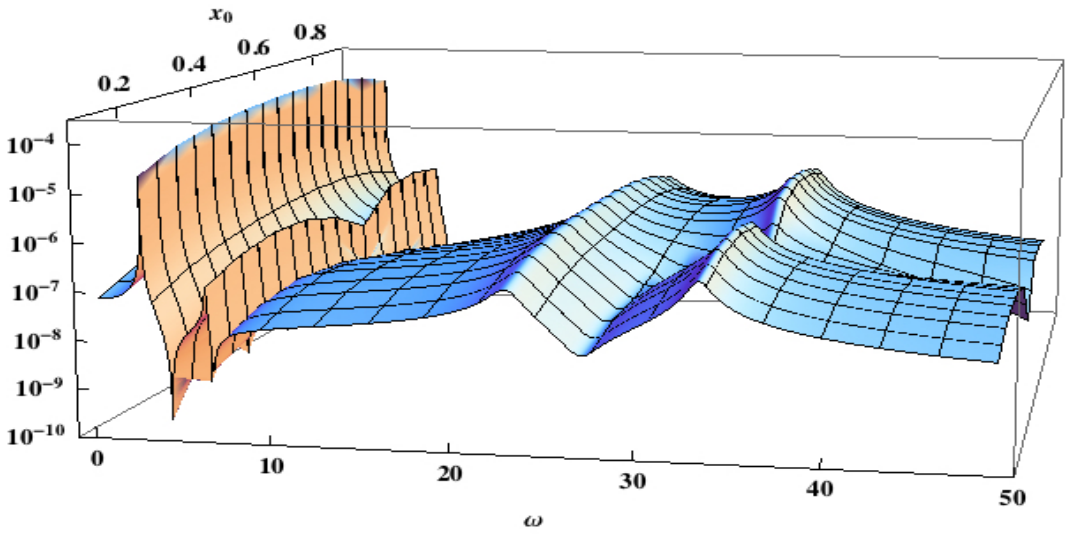

Figure 3.5: Beam in Figure 3.3: deflection frequency response function at $x = 1/3$, due to a transverse point load $P = 1.36{\cdot}10^{-5}$ with varying frequency ω applied at positions $0 < x_0 < 1$, for axial load parameter $\alpha = -10$, as computed by proposed method.

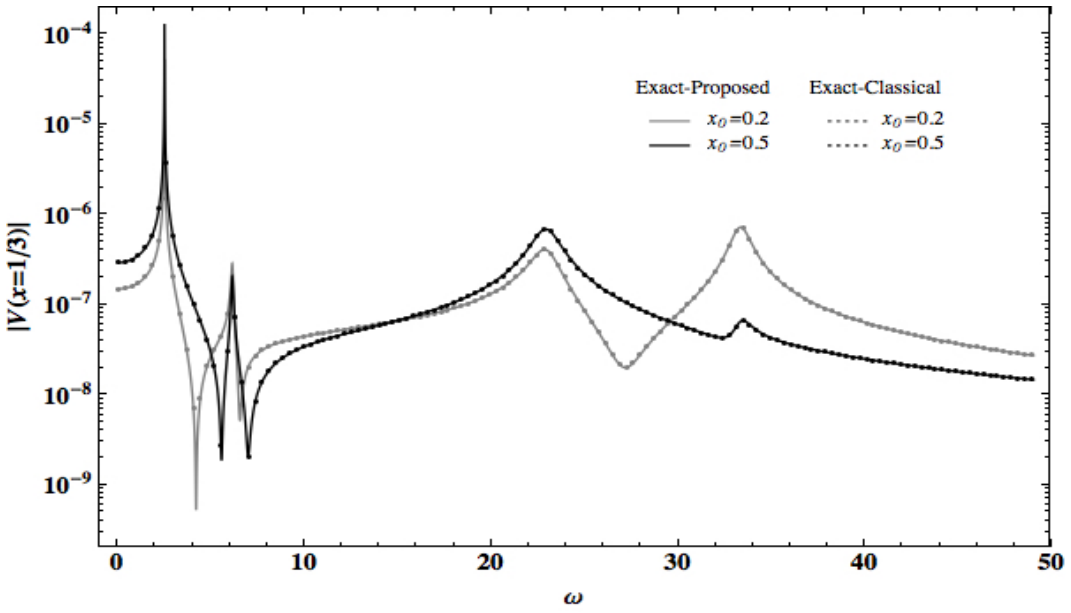

Figure 3.6: Beam in Figure 3.3: deflection frequency response function at $x = 1/3$, due to a transverse point load $P = 1.36{\cdot}10^{-5}$ with varying frequency ω applied at two positions x_0, for axial load parameter $\alpha = -10$, as computed by proposed and classical methods.

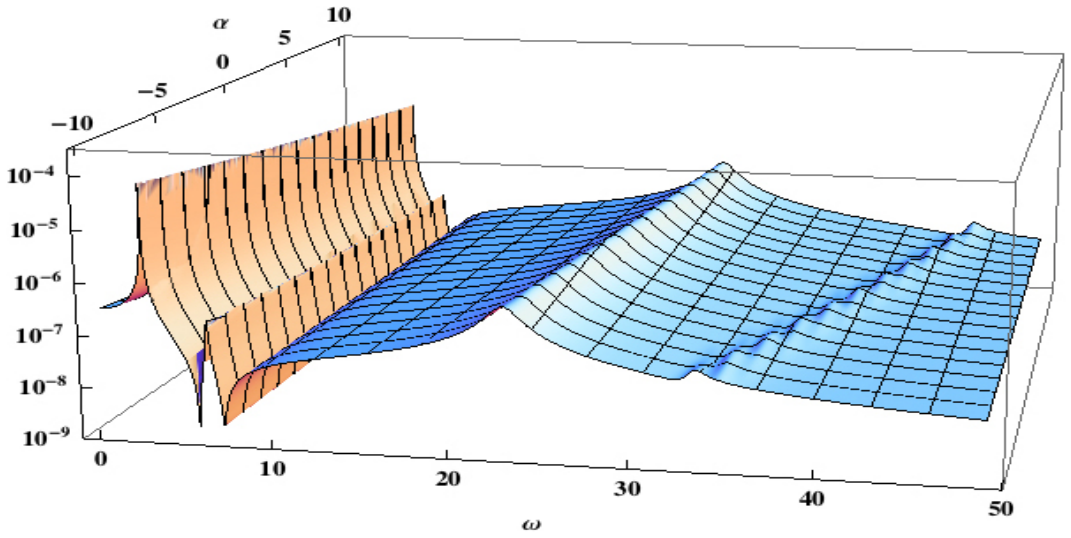

Figure 3.7: Beam in Figure 3.3: deflection frequency response function at $x = 1/3$, due to a transverse point load $P = 1.36{\cdot}10^{-5}$ with varying frequency ω applied at $x_0 = 0.5$, for varying axial load parameters α, as computed by proposed method.

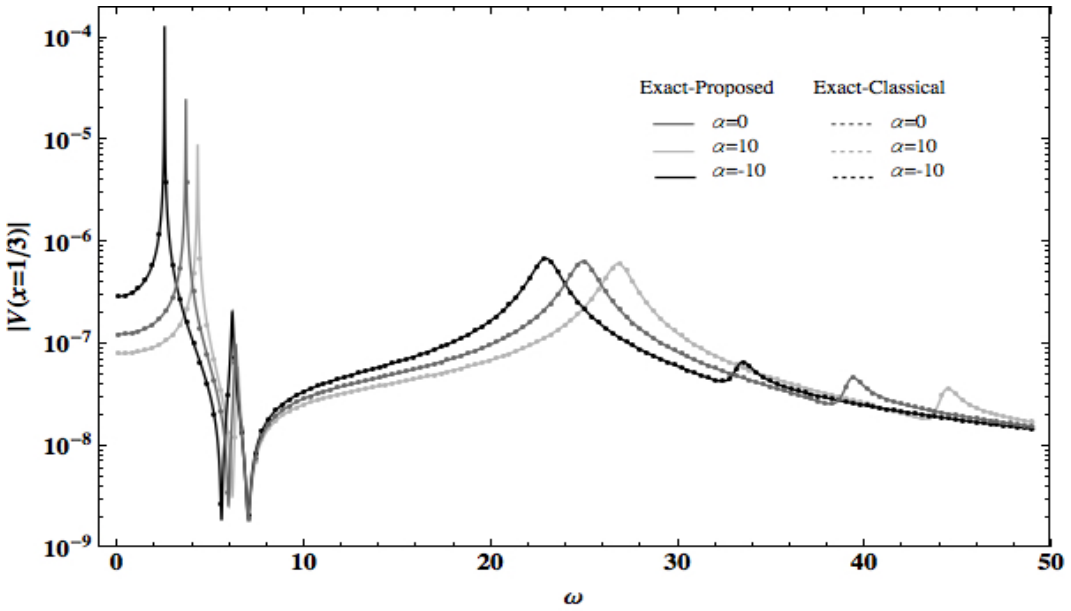

Figure 3.8: Beam in Figure 3.3: deflection frequency response function at $x = 1/3$, due to a transverse point load $P = 1.36{\cdot}10^{-5}$ with varying frequency ω applied at $x_0 = 0.5$, for three axial load parameters α, as computed by proposed and classical methods.

Example B

Consider the axially-loaded beam in Figure 3.9, with two lumped dimensionless masses $M_1 = 3.36$ and $M_2 = 3.36$ attached at $x_1 = 0.25$ and $x_3 = 0.75$, an elastic translational support at $x_2 = 0.5$ and a viscous translational damper. For convenience, position and damping coefficient of the viscous damper are indicated as "η" and "ζ", respectively. The frequency response of the beam is studied in two different configurations: (a) undamped beam, i.e. without the viscous damper; (b) damped beam, with the viscous damper applied at various locations $x = \eta$.

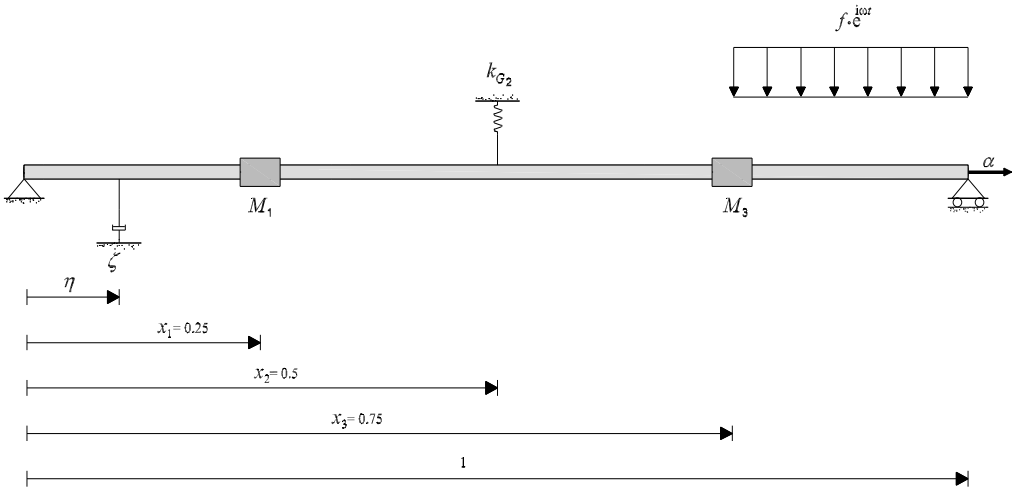

Figure 3.9: Axially-loaded Euler-Bernoulli beam with attached masses, elastic translational support and viscous translational damper, subjected to a harmonic transverse load uniformly-distributed over (0.75,1). Two distinct configurations are studied: (a) beam without damper; (b) beam with damper.

First, consider the undamped beam. Table 3.5 shows the eigenvalues of the first 2 modes, for different values of the axial load parameter α, as computed by exact proposed and classical methods. Results obtained by the two methods are in a very good agreement, up to the first three digits. All eigenvalues are real, since in this case the beam is undamped. The corresponding real eigenfunctions are shown in Figure 3.10, for the axial load parameter

$\alpha = 0$ (denoting with $\Psi_V(x)$, $\Psi_\Theta(x)$, $\Psi_M(x)$, $\Psi_S(x)$, the eigenfunctions of the deflection, rotation, moment and shear force, respectively) . As expected, the shear force is discontinuous at the mass locations x_1,x_3 and the translational support location x_2, while all other response variables are continuous through the whole domain. Again, an excellent agreement is encountered between the exact solutions built by proposed and classical methods.

Then, assume that the undamped beam is acted upon by a harmonic transverse load $f = 1.63{\cdot}10^{-4}$ with frequency $\omega = 6.15$, uniformly distributed over $0.75 \leq x \leq 1$, as shown in Figure 3.9. In this case, the exact frequency response (3.222) of the proposed method can be computed, in a closed form, using Eq.(3.59). Notice that the forcing frequency $\omega = 6.15$ is very close to the first mode resonance frequency of the undamped beam without axial load (see Table 3.5 for $\alpha = 0$). Figure 3.11 shows the deflection frequency response function over the whole beam, as computed by the proposed method for different values of the axial load parameter α. It is apparent that the frequency response is dominated by the first mode for $\alpha = 0$, i.e. without axial load, but becomes progressively dominated by the second mode as α decreases, i.e. as the axial compression increases. This behavior is consistent with results in Table 3.5, showing that the natural frequency of the second mode progressively decreases with decreasing α, shifting towards the forcing frequency $\omega = 6.15$ of the transverse load. Results in Figure 3.11 suggest that the axial load greatly affects the frequency response, shifting the dominating mode from the first to the second, as axial compression increases.

Next, consider the damped beam, with the viscous damper applied at $x = \eta$. Let the forcing frequency of the transverse load in Figure 3.9 be $\omega = 6.15$. It is now of interest to assess whether the presence of the axial load shall be taken into account, and to which extent, when searching for an optimal position of the damper. Here, the optimal position will be considered as the one for which the maximum deflection amplitude along the beam attains a minimum value, for a given damping coefficient "ζ" of the damper.

For a preliminary insight, it is worth evaluating whether the shift of dom-

inating modes caused by increasing axial compression occurs also in presence of the damper. For this purpose, Figures 3.12-3.13 show the deflection frequency response function (3.100) over the whole beam as α decreases, for two damper positions, $\eta = 0.25$ in Figure 3.12 and $\eta = 0.35$ in Figure 3.13 and damping coefficient of the damper $\zeta = 5.24$. It is evident that the shift of dominating modes in the damped beam, shown by Figures 3.12-3.13, mirrors the shift of dominating modes in the undamped beam, previously shown by Figure 3.11. The same behavior is encountered for different positions η and damping coefficients ζ of the damper, and pertinent results are not reported for brevity.

In order to estimate the optimal position of the damper, the maximum deflection amplitude along the beam, $V_{max} = max\Big\{|V(x)|, 0 < x < 1\Big\}$, has been computed by Eq.(3.100), considering a discrete grid of potential damper positions (grid steps= 0.01). Specifically, the maximum deflection amplitude along the beam has been computed for any potential damper position in the grid, various axial load parameters α in the interval (-25.55,0), and two different damping coefficients of the damper, $\zeta = 5.24$ and $\zeta = 2.62$. To illustrate the results, the maximum deflection amplitudes along the beam, obtained for the damper positions $\eta = 0.35$, 0.5, 0.75, 0.85, $\alpha \in (-25.55, 0)$, $\zeta = 5.24$ and $\zeta = 2.62$, are reported in Figures 3.14-3.15. It is worth noticing that all other damper positions in the grid do not provide maxima deflection amplitudes smaller than those in Figures 3.14-3.15 and, for this, pertinent curves have not been reported for brevity. In addition, Figures 3.14-3.15 include the maximum deflection amplitude when no damper is applied.

The first relevant comment on Figures 3.14-3.15 concerns the response when no damper is applied. In this case it is evident that the maximum deflection amplitudes become significantly larger as $\alpha \to 0$ and $\alpha \to -25.55$. These results are consistent with the shift of dominating modes caused by increasing axial compression, shown for the undamped beam in Figure 3.11: in fact, the forcing frequency $\omega = 6.15$ becomes closer to the first mode resonance frequency as $\alpha \to 0$, and closer to the second mode resonance

frequency as $\alpha \to -25.55$, see Table 3.5 for the undamped beam. Then, regarding the response when the damper is applied, Figures 3.14-3.15 clearly show that, for relatively low values of the axial load parameter α, the optimal damper position is $\eta = 0.5$, which provides the minimum value among the maxima deflection amplitudes obtained for the various damper positions. However, as α decreases, a damper applied at $\eta = 0.5$ becomes ineffective, as in fact the corresponding maximum deflection amplitude (gray-continuous curve) coincides with the one for no damper (black-dotted curve). It is evident that, as $\alpha \to -25.55$, the optimal damper position becomes $\eta = 0.75$. Again, these results correspond to the shift of dominating modes caused by increasing axial compression, as shown for the damped beam in Figures 3.12-3.13.

A further important observation on Figures 3.14-3.15 is that, for certain intervals of axial load parameter α, approximately (-21,-13) in Figure 3.14 and (-23,-7) in Figure 3.15, the maximum deflection amplitude along the beam is not affected by the presence of the damper. For further insight into this result, two different values of α within the interval (-21, -13) shown in Figure 3.14 are considered, specifically $\alpha = -13.5$ and $\alpha = -18.5$. Considering that the maximum deflection amplitude V_{max} is attained at $x = 0.32$ for $\alpha = -13.5$ and $x = 0.285$ for $\alpha = -18.5$, Figures 3.16-3.17 show the frequency response functions of the deflection $V(x)$ at $x = 0.32$ and $x = 0.285$, respectively, computed for no damper, and for the damper applied at the four positions $\eta = 0.35, 0.5, 0.75, 0.85$ indicated in Figure 3.14. The results in Figures 3.16-3.17 are consistent with those in Figure 3.14: indeed, at the forcing frequency $\omega = 6.15$ considered in Figure 3.14, the frequency response function of the beam without damper does coincide with the frequency response functions of the beam with the damper at positions $\eta = 0.35, 0.5, 0.75, 0.85$ indicated in Figure 3.14. Analogous results are obtained for all values of α within the interval (-21,-13) in Figure 3.14 and (-23,-7) in Figure 3.15, and are omitted for coinciseness. Based on Figures 3.14-3.17, it can be argued that the axial compression level may greatly affect the damper performances,

to the extent that benefits in terms of maximum amplitude may be negligible, for certain values of axial compression.

A final remark is in order. All results obtained by the exact proposed method, shown in Figure 3.11 through Figure 3.17, have been compared with those obtained by the exact classical method, and a perfect agreement has been always encountered. For brevity and clarity of presentation, results obtained by the classical method have not been included. It is noted, however, that the proposed method appears particularly suitable for constructing results as in Figure 3.14-3.15 or Figures 3.16-3.17, as Eq.(3.222) for the frequency response function holds, in a closed form, for any position of the damper relative to the positions of masses, translational support and distributed load, with significant advantages in terms of implementation and computational effort.

	$\alpha = 0$		$\alpha = -10$		$\alpha = -25.55$	
Mode	C. M.	P. M.	C.M.	P.M.	C.M.	P.M.
1	6.153071	6.153082	5.109113	5.109132	2.770184	2.770169
2	10.31764	10.31772	8.928753	8.928934	6.152586	6.152462

Table 3.5: Beam in Figure 3.9 without damper: eigenvalues of the beam calculated through classical method (C.M.) and proposed method (P.M.).

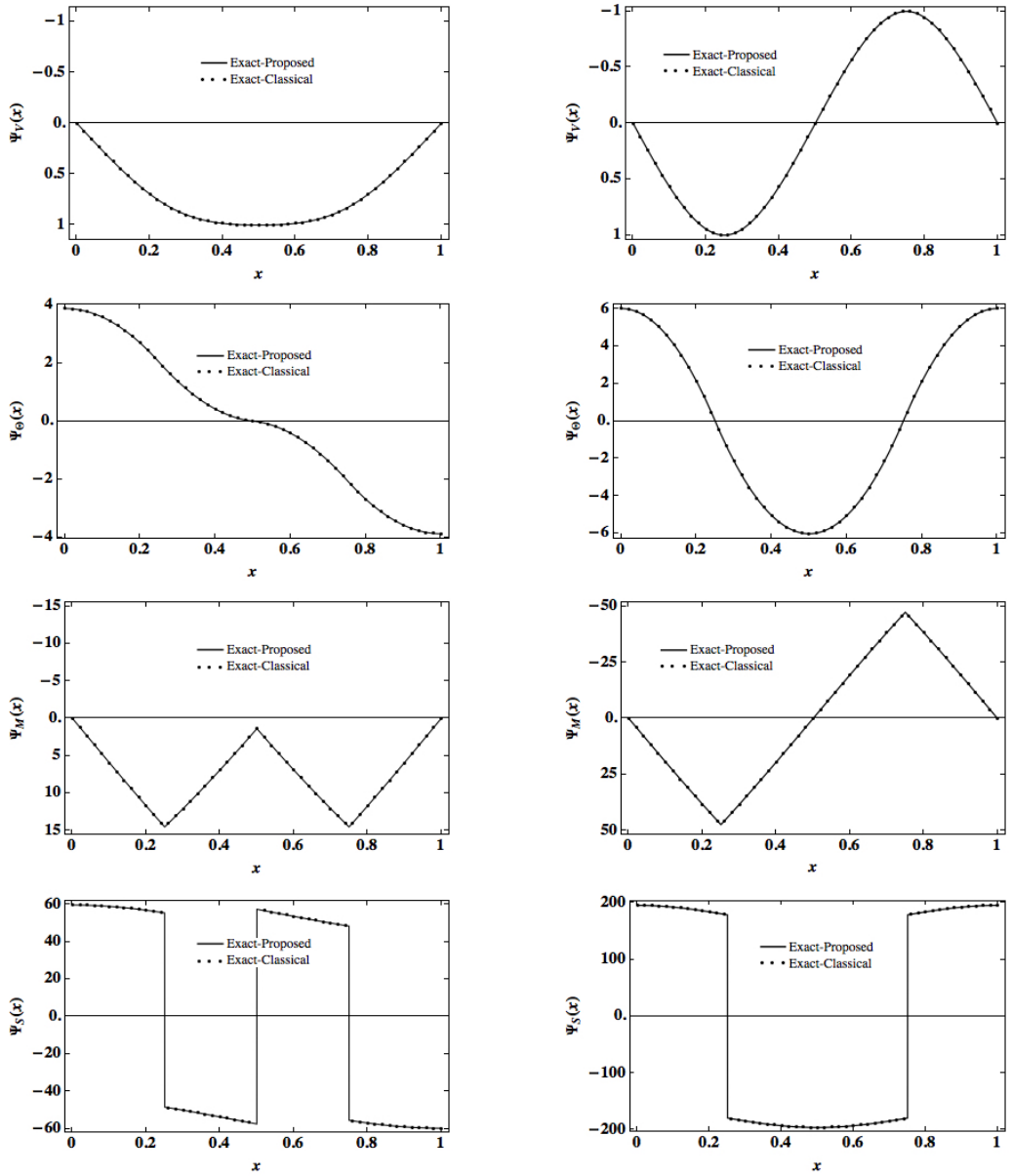

Figure 3.10: Beam in Figure 3.9 without damper: eigenfunctions of all response variables, for axial load parameter $\alpha = 0$, as computed by proposed and classical methods. Left column: real part, right column: imaginary part.

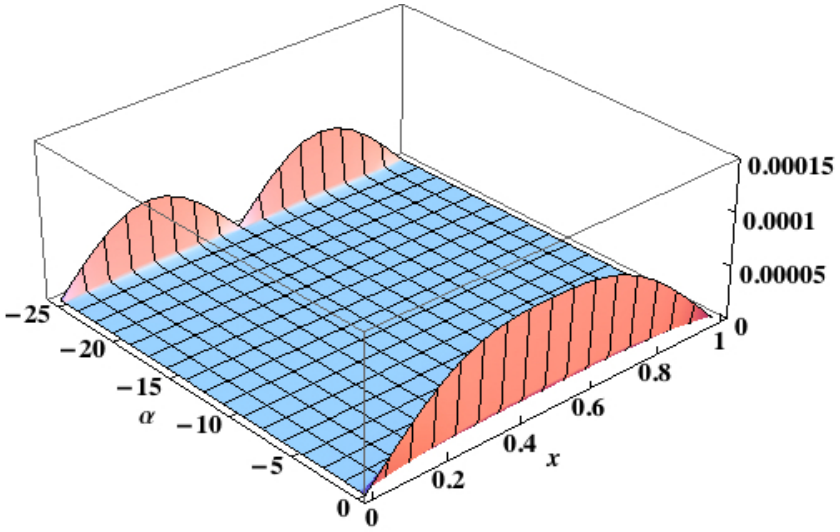

Figure 3.11: Beam in Figure 3.9 without damper: deflection frequency response function over the whole beam axis, due to a transverse load with frequency $\omega = 6.15$ uniformly-distributed over (0.75,1), for varying axial load parameter α, as computed by proposed method.

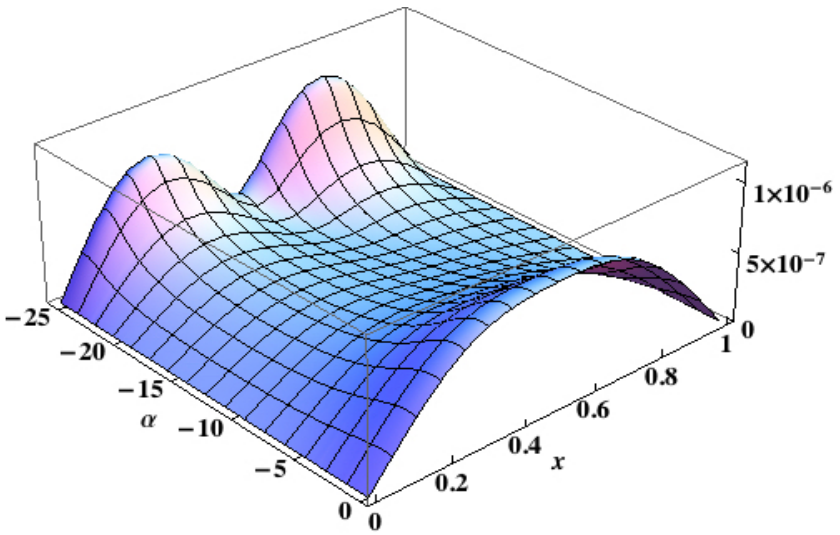

Figure 3.12: Beam in Figure 3.9, with damper applied at $\eta = 0.25$, for a damping coefficient $\zeta = 5.24$: deflection frequency response function over the whole beam axis, due to a transverse load with frequency $\omega = 6.5$ uniformly-distributed over (0.75,1), for varying axial load parameter α, as computed by proposed method.

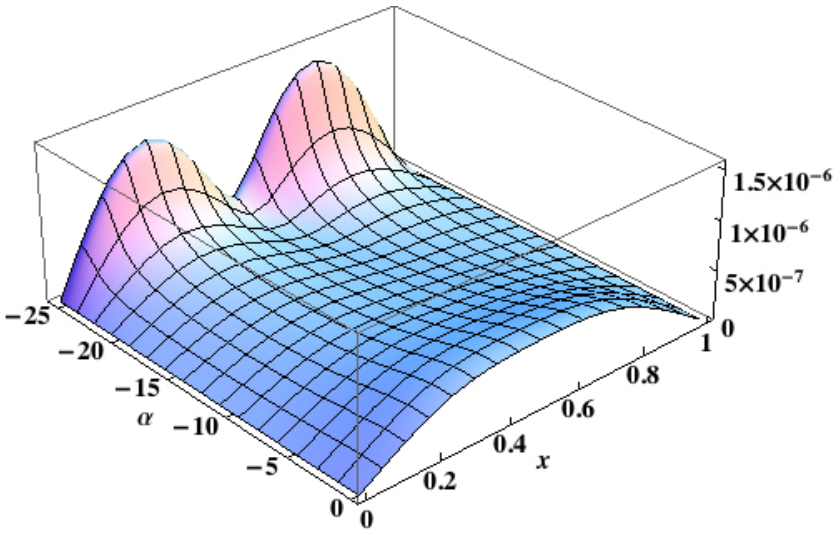

Figure 3.13: Beam in Figure 3.9, with damper applied at $\eta = 0.35$, for a damping coefficient $\zeta = 5.24$: deflection frequency response function over the whole beam axis, due to a transverse load with frequency $\omega = 6.15$ uniformly-distributed over (0.75,1), for varying axial load parameter α, as computed by proposed method.

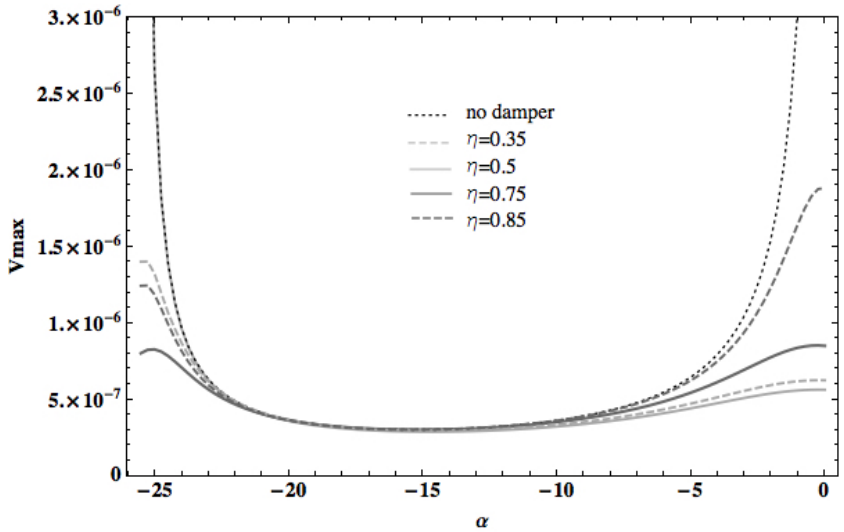

Figure 3.14: Beam in Figure 3.9, (a) without damper and (b) with damper applied at different positions η, for a damping coefficient $\zeta = 5.24$: maximum deflection amplitude along the beam due to a transverse load with frequency $\omega = 6.15$ uniformly-distributed over (0.75,1), for various axial load parameters α, as computed by proposed method.

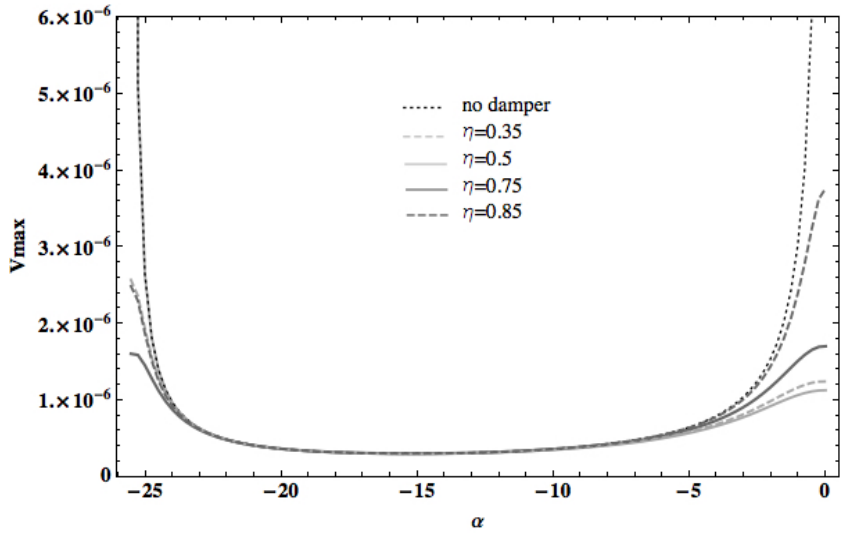

Figure 3.15: Beam in Figure 3.9, (a) without damper and (b) with damper applied at different positions η, for a damping coefficient $\zeta = 2.62$: maximum deflection amplitude along the beam due to a transverse load with frequency $\omega = 6.15$ uniformly-distributed over (0.75,1), for various axial load parameters α, as computed by proposed method.

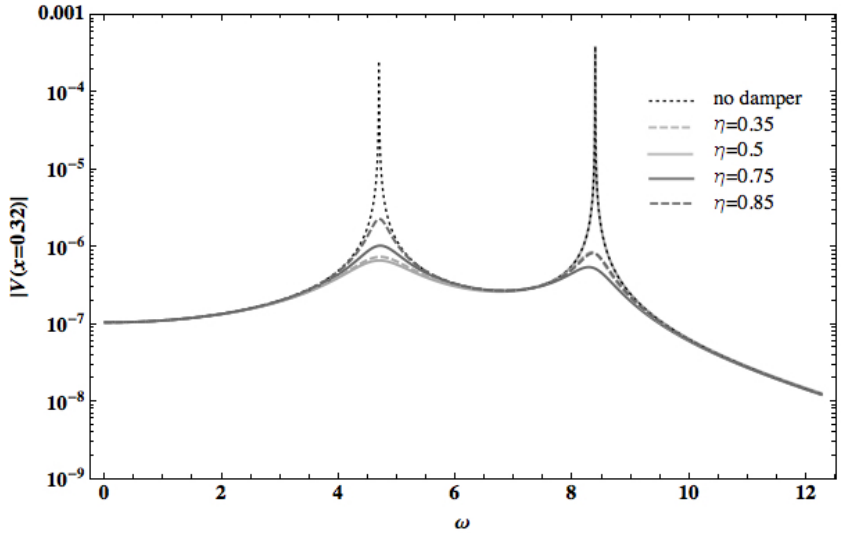

Figure 3.16: Beam in Figure 3.9, (a) without damper and (b) with damper applied at different positions η, for a damping coefficient $\zeta = 5.24$: frequency response function of deflection $V(x)$ at $x = 0.32$, due to a transverse load with frequency $\omega = 6.15$ uniformly-distributed over (0.75,1), for axial load parameter $\alpha = -13.5$, as computed by proposed method.

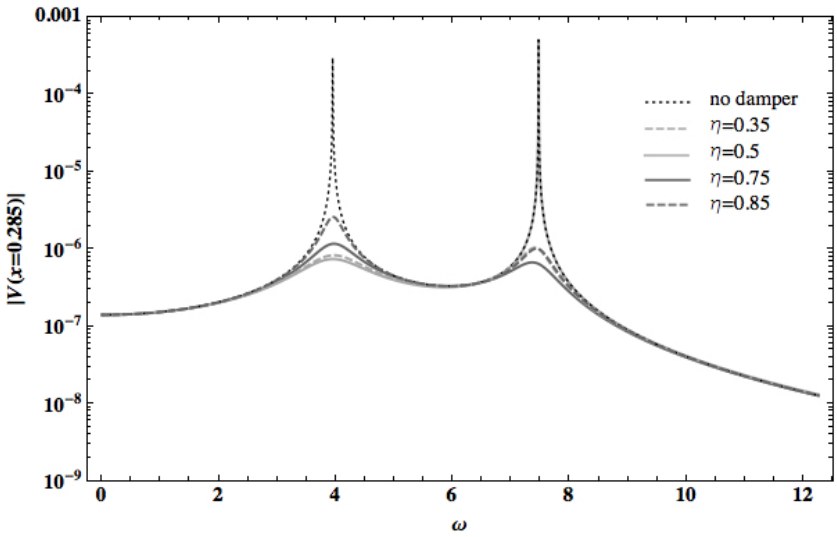

Figure 3.17: Beam in Figure 3.9, (a) without damper and (b) with damper applied at different positions η, for a damping coefficient $\zeta = 5.24$: frequency response function of deflection $V(x)$ at $x = 0.285$, due to a transverse load with frequency $\omega = 6.15$ uniformly-distributed over (0.75,1), for axial load parameter $\alpha = -18.5$, as computed by proposed method.

3.3 Axial vibrations of discontinuous beams with symmetric cross section

The axial vibrations of discontinuous beams with symmetric cross sections can be dealt with an approach similar to the one adopted for bending vibrations. At this regard, short hints are given regarding the derivation of the dynamics Green's functions and frequency response functions.

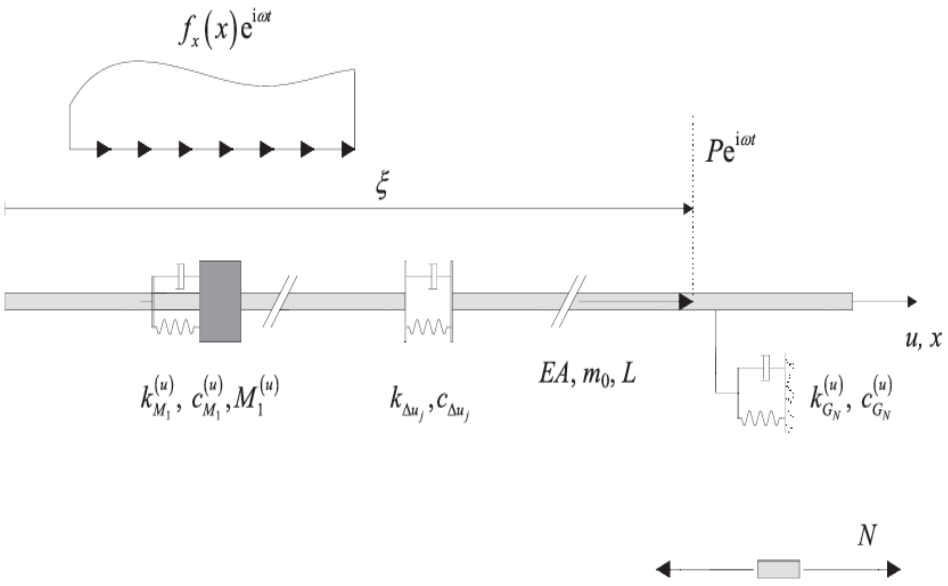

Figure 3.18: Beam with symmetric cross section carrying an arbitrary number of KV dampers (axial problem).

Assume that the beam in Figure 3.18 is loaded by an axial harmonically varying point load at $x = x_0$, denoted as $Pe^{i\omega t}$. Using the theory of generalised functions and representing the steady-state axial displacement and axial force as $u = U(x, x_0, \omega)e^{i\omega t}$ and $n = N(x, x_0, \omega)e^{i\omega t}$ respectively, the following steady-state motion equation is derived

$$EA\frac{\bar{d}U(x,\xi)}{dx^2} + m\omega^2 U(x,\omega) + \sum_{j=1}^{N} G_j(x) + P\delta(x - x_0) = 0 \qquad (3.104)$$

where in Eq.(3.104) EA is the axial rigidity of the beam, frequency dependence in $U(x,\omega)$ is omitted for brevity; while $G_j(x)$ is a generalised function given as

$$G_j(x) = R_j\delta(x-x_j) - EA\Delta U\delta^{(1)}(x-x_j) \tag{3.105}$$

In Eq.(3.105) is the reaction of the j-th TD/TMD in x-direction, ΔU_j is the relative axial displacement between adjacent sections at the j-th AD, given as

$$R_j = -[k_{Geq_j}(\omega) + k_{Meq_j}(\omega)]U(x_j,x_0) \tag{3.106}$$

$$\Delta U_j = (k_{\Delta ueq_j}(\omega))^{(-1)}N(x_j,x_0) \tag{3.107}$$

where $k_{Geq_j}(\omega)$, $k_{Meq_j}(\omega)$, $k_{\Delta ueq_j}(\omega)$ are frequency dependent parameters

$$k_{Geq_j}(\omega) = k_{G_j} + i\omega c_{G_j};\quad k_{Meq_j}(\omega) = \frac{(k_{M_j}+i\omega c_{M_j})M_j\omega^2}{M_j\omega^2 - (k_{M_j}+i\omega c_{M_j})} \tag{3.108}$$

$$k_{\Delta ueq_j}(\omega) = k_{\Delta u_j} + i\omega c_{\Delta u_j} \tag{3.109}$$

Eq. (3.108) shows again that in the frequency domain TMDs can be treated as TDs, i.e. the (steady-state) reaction force of a TMD depends on the displacement of the attachment point only through a pertinent frequency-dependent term, involving stiffness/damping/mass of the TMD. Also, notice that a lumped mass along the beam can be modeled as TMD with $k_{M_j} = \infty$ Eq. (3.108).

Next, to build the vector $\mathbf{Z} = [U\ N]$ of the steady-state response variables, the linear superposition principle can be applied:

$$\mathbf{Z}(x,\xi) = \mathbf{Z}_{HM}(x)\mathbf{c} + \sum_{j=1}^{N}\mathbf{Z}_{\Lambda}(x,x_j)\mathbf{\Lambda}_j + P\mathbf{Z}_P(x,\xi) \tag{3.110}$$

where $\mathbf{Z}_{HM}(x)\mathbf{c}$ is the solution to the homogeneous equation associated with Eq.(3.104); $\mathbf{Z}_{\Lambda}(x,x_j)\mathbf{\Lambda}_j$ are the particular integrals associated with reactions

R_j and relative displacements ΔU_j at x_j, with $\mathbf{\Lambda}_j$ the unknown reactions; $\mathbf{Z}_P(x,\xi)$ are the particular integral associated with the axial harmonic load.

According to approach shown in the previous Section, the vectors $\mathbf{\Lambda}_j$ can be expressed with a recursive procedure as functions of integrations constants $\mathbf{c}$ only. Then, enforcing the B.C. will lead to 2 equations regardless of the number of dampers. The frequency response vectors can be similarly obtained simply exploiting the relationship between the particular integral due to a unit point load and that to a distributed load. For brevity further details are omitted.

It is underlined that the proposed method can be applied and extended to pure torsional vibrations too.

With this Section, the deterministic analysis of discontinuous beams with symmetric cross section ends.

Now, attention will be focused on beams with asymmetric cross sections and composited beams. Despite these beams are involved in a lot of practical applications and are of great engineering interest, the literature concerning the dynamics of CCDS involving these beams is very poor. In the next Section, a contribution in this sense in given, extending the method presented for beams with symmetric cross section to beams with asymmetric cross section and composite beams.

3.4 Coupled bending-torsional vibrations of discontinuous beams with mono symmetric cross sections (warping effects neglected)

The proposed method is now formulated for another kind of mono-dimensional element, a uniform beam with mono-symmetric cross section. These beams are of great engineering interest since they are involved in several applications. For these beams shear center (SC) and mass center (MC) of the cross

section do not coincide, and consequently bending and torsion vibrations are inherently coupled. Indeed, on one hand, the inertial forces developing along the mass axis (the loci of the MCs of the beam cross sections) will cause twisting about the elastic axis (the loci of the SCs of the cross sections) while, on the other hand, the inertial forces will depend on both bending and twisting effects.

Existing studies regarding the more general case of beams with various attachments as supports, dampers and masses, generally consider pure bending vibration and, therefore, related solutions are applicable only when the cross section is doubly-symmetric, i.e. when SC and MC coincide. EB theory for bending is not more sufficient to describe the dynamics of beams with non symmetric cross section and to capture the coupling phenomena. For this reason, alternative theories will be adopted to take into account coupling effects. Firstly the elementary coupled bending torsion theory will be taken into account, i.e. warping rigidity is neglected in the torsion equation of motion, as well as shear deformation and rotatory inertia. In the next Section, warping effects will be taken into account.

Short hints are now given regarding past studies on coupled bending torsional vibrations and on CCDS where beams with mono symmetric cross section are involved.

Many studies have been devoted to the challenging task of solving coupled bending-torsion motion equations. Friberg [45] built a dynamic stiffness matrix for coupled bending-torsional beams, computing natural frequencies and mode shapes for specific boundary conditions (B.C.). Exact mode shapes were then obtained by Dokumaci [46] and Hallauer [47] in a closed analytical form, for any B.C. Later, Banerjee derived the exact analytical expressions of a coupled bending-torsional dynamic stiffness matrix [48], as well as the exact characteristic equation and mode shapes of a coupled bending-torsional beam with cantilever end condition [49]. Hashemi and Richard [50] built a dynamic stiffness matrix of coupled bending-torsional beams, using the exact solutions of the corresponding uncoupled equations of motion in conjunction with the

principle of virtual work. Based on the concept of generalized mass, in ref. [51] Eslymy and Banerjee introduced an original approach for the interpretation of coupled bending-torsion modes, and studied the response to concentrated random forces and twisting moments. The response to deterministic and random loads was also investigated in ref. [52] by using the normal mode method. In ref. [45, 46, 47, 48, 49, 50, 51, 52], equations were derived based on the elementary coupled bending-torsion theory, i.e. neglecting warping rigidity in the torsion equation of motion, as well as shear deformation and rotatory inertia. Further studies considered these effects, as well as those induced by an axial load [53, 54, 55, 56, 57, 58, 59, 60, 61, 62, 63, 64, 65, 66, 67]. Specifically, warping effects on dynamics of beams with mono-symmetric cross section will be discussed in the next Section.

Works in ref. [53]-[67] concerned the dynamics of uniform beams, with no attachments along the span. On the other hand, coupled bending-torsional beams with attachments were investigated in few studies focusing, in particular, on attached masses. Specifically, Oguamanam [68] studied the coupled bending-torsional free vibrations of a Euler-Bernoulli beam with doubly-symmetric cross section, carrying a tip mass; in this case, coupling between bending and torsion arises because the tip mass is applied on the beam axis and its gravity center does not coincide with the application point. Gokdag and Kopmaz [69] proposed a method to analyze free and forced vibrations of a beam with mono-symmetric cross section, carrying in-span distributed masses, a mass and an elastic support at the tip. Further, several studies were devoted to wings equipped with external stores as fuel tanks, tip winglets or engines. In this context, structural models with different degrees of complexity were proposed for the wing-stores system: e.g. a rigid wing coupled with a tip mass by a piecewise-linear stiffness [70], an anisotropic laminated composite plate incorporating transverse shear flexibility and warping effects, which carries rigidly-connected masses [71], a homogeneous and isotropic beam [72] and a non-linear composite beam accounting for large deflections [73, 74], both carrying rigidly-connected masses acted upon by force vec-

tors modelling engine thrust [72, 73, 74]. In these studies, the structural models were coupled with different aeroelastic models, with the aim of investigating the effects of the stores on aeroelasticity and flutter phenomena [70, 71, 72, 73, 74].

This Section focuses on generalization of the method proposed in the previous section and developed for discontinuous beams with symmetric cross section to coupled bending-torsional beams with mono-symmetric cross section, carrying an arbitrary number of external dampers/masses. Translational, as well as bending-rotational and torsional-rotational dampers with Kelvin-Voigt viscoelastic behavior are considered. Likewise the previous Section, on using the theory of generalized functions, novel exact expressions of the frequency response are derived in closed analytical form, which hold for harmonically-varying point/polynomial loads arbitrarily placed along the beam, and any number of dampers and attached masses. On the basis of the same analytical framework free vibration analysis is led. Specifically, exact natural frequencies and closed-form eigenfunctions will be calculated from a characteristic equation built as determinant of a 6×6 matrix, for any number of supports/masses. The final step is a complex modal analysis approach to obtain the modal frequency response functions of the beam, upon introducing pertinent orthogonality conditions for the modes. Within this framework, modal impulse response functions are also derived, to be readily used for time domain analysis.

The Section is organized as follows. Firstly, the equations governing the problem under study are formulated. Secondly, frequency response is derived. On this basis, and upon deriving orthogonality conditions for complex modes, modal impulse response functions are obtained for time domain analysis. For completeness, the proportional damping case is also dealt with. Finally, two numerical applications are shown.

3.4.1 Problem statement

Figure 3.19 shows the problem under study, i.e. a uniform straight beam of length L, referred to a right handed coordinate system, carrying an arbitrary number of external Kelvin-Voigt dampers and attached masses.

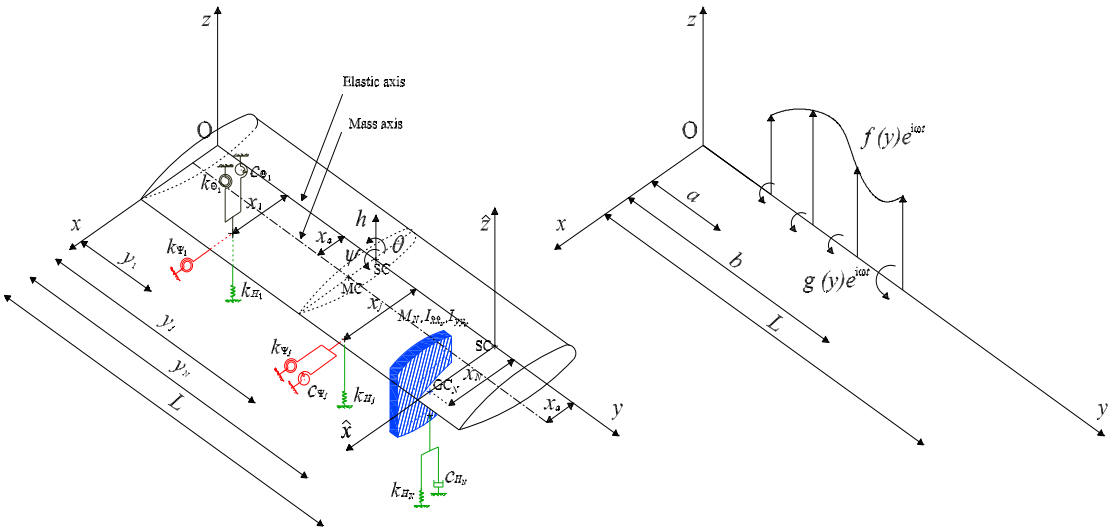

Figure 3.19: Beam with mono-symmetric cross section carrying an arbitrary number of Kelvin-Voigt dampers and attached masses, subjected to harmonically-varying distributed loads.

The beam cross section is assumed to be mono-symmetric, being x the symmetry axis. The loci of the SCs and MCs of the beam cross sections are respectively the elastic axis and mass axis; the first coincides with the y-axis, while the second is at distance x_a from the y-axis. The bending deflection in the z-direction, the bending rotation about the x-axis and the torsional rotation about the y-axis of the SCs are denoted respectively by $h(y,t)$, $\theta(y,t)$ and $\psi(y,t)$, while bending moment, shear force and torque are denoted respectively by $\mu(y,t)$, $s(y,t)$ and $\tau(y,t)$, where t is the time.

The dampers and attached masses are applied at y_j, with $0 < y_1 < \cdots < y_j < \cdots < L$; stiffness and damping parameters of the j-th damper and properties of the j-th mass are denoted as follows:

- k_{H_j}, c_{H_j} for translational dampers, k_{Ψ_j}, c_{Ψ_j} for torsional-rotational

dampers and k_{Θ_j}, c_{Θ_j} for bending-rotational dampers.

- M_j is the mass, $I_{\hat{x}\hat{x}_j}$ and I_{yy_j} the components of the mass inertia tensor about axes $\hat{x}$ and y in Figure 3.38, where $\hat{x}$ is a principal centroidal axis of the mass, assumed to be parallel to the x axis.

Further, it is assumed that the gravity center (GC_j) of the j-th attached mass is at distance $z_j = 0$ from the elastic axis, and that its principal centroidal axes are parallel to those of the beam cross section. These assumptions ensure that twisting is coupled with bending in z-direction only, as in ref. [46, 47, 48, 49, 51, 52, 53, 54, 55, 57, 58, 59, 61, 62, 63, 64]. For simplicity, it is also assumed that the j-th damper and gravity center GC_j of the j-th mass are both applied at distance x_j from the elastic axis.

It is remarked that in this section bending and torsional vibrations are studied within the elementary coupled bending-torsion theory, i.e. neglecting warping rigidity in the torsion equation of motion, shear deformation and rotatory inertia.

According to this theory and using the theory of generalized functions (see Chapter 2), the flexural and torsional displacement due to an external time-space varying force $f(y,t)$ acting in z-direction along the y-axis and twisting moment $g(y,t)$ about the y-axis the following set of six equations can be written the set of six equations is given as:

$$\theta(y,t) = \frac{\bar{\partial} h(y,t)}{\partial y} \tag{3.111}$$

$$\mu(y,t) = EI \frac{\bar{\partial}\theta(y,t)}{\partial y} \tag{3.112}$$

$$s(y,t) = -\frac{\bar{\partial}\mu(y)}{\partial y} - \sum_{j=1}^{N} m f_j(t)\, \delta(y - y_j) \tag{3.113}$$

$$\frac{\bar{d}s(y,t)}{dy} = \frac{\partial^2 h(y,t)}{\partial t^2} - x_a \frac{\partial^2 \psi(y,t)}{\partial t^2} - \sum_{j=1}^{N} p_j(t)\delta(y-y_j) - f(y,t) \tag{3.114}$$

$$\tau(y,t) = GJ\frac{\bar{\partial}\psi(y,t)}{\partial y} \tag{3.115}$$

$$\begin{aligned}\frac{\bar{\partial}\tau(y,t)}{dy} &= I_\alpha \frac{\partial^2 \psi(y,t)}{\partial t^2} - m x_a \frac{\partial^2 h(y,t)}{\partial t^2} + \sum_{J=1}^{N} p_j(t) x_j \delta(y-y_j) \\ &\quad - \sum_{j=1}^{N} m t(t)_j\, \delta(y-y_j) - g(y)\end{aligned} \tag{3.116}$$

Inserting Eqs.(3.111)-(3.112)-(3.113) into Eq.(3.114), the governing equation for the flexural problem (3.117) is obtained, while the governing equation for the torsional problem (3.118) is derived inserting Eq.(3.115) into Eq.(3.116), which are given as follows:

$$\begin{aligned}EI\frac{\bar{\partial}^4 h}{dy^4} + m\frac{\partial^2 h}{\partial t^2} - m x_a \frac{\partial^2 \psi}{\partial t^2} - \sum_{j=1}^{N}(p_j(t)\delta(y-y_j) - m f_j(t)\delta^{(1)}(y-y_j)) \\ - f(y,t) = 0\end{aligned} \tag{3.117}$$

$$\begin{aligned}GJ\frac{\bar{\partial}^2 \psi}{\partial y^2} - I_\alpha \frac{\partial^2 \psi}{\partial t^2} + m x_a \frac{\partial^2 h}{\partial t^2} - \sum_{j=1}^{N}(p_j(t) x_j \delta(y-y_j) - m t_j(t)\delta(y-y_j)) \\ + g(y,t) = 0\end{aligned} \tag{3.118}$$

where EI and GJ are respectively bending and torsional rigidities, m is the mass per unit length, I_α is the polar moment of inertia per unit length about the elastic axis, while $p_j(t)$, $mf_j(t)$ and $mt_j(t)$ are concentrated forces, bending moments and twisting moments on the beam, due to the presence

of external dampers and attached masses. The external time-space varying vertical force $f(y,t)$ and twisting moment will be represented in the separable form $f(y,t) = f(y)f(t)$ and $g(y,t) = g(y)g(t)$ and for generality, it is assumed that $f(y)$ and $g(y)$ are arbitrary polynomial functions.

Firstly, an exact frequency analysis is led, including free vibrations and frequency response functions. Next, a complex modal analysis follows to compute time domain response.

3.4.2 Direct Frequency analysis

Assume that the vibration response of the system in Figure 3.19 can be represented in the form

$$\mathbf{v} = \mathbf{Y}e^{i\omega t} \tag{3.119}$$

where $\mathbf{v} = \{h\ \theta\ m\ s\ \phi\ t_0\}$ and $\mathbf{Y} = \{H\ \Theta\ M\ S\ \Phi\ T\}$ collect the response variable of the beam. Eq.(3.2) is a general form to represent:

1. The frequency response function, that is the steady state response under an harmonic force $f(y,t) = f(y)e^{i\omega t}$ and twisting moment $g(y,t) = g(y)e^{i\omega t}$ with any frequency ω, i.e. $\mathbf{Y} = \mathbf{Y}(x,\omega)$

2. Free vibration response setting $f(y,t) = g(y,t) = 0$, and being $\omega = \omega_n$ an eigenvalue and $\mathbf{Y} = \mathbf{Y}_n(x)$ the corresponding vectors of eigenfunctions; in general, the damping in the system is not proportional, then eigenvalues and eigenfunctions will be complex.

Using Eq.(3.119) in equations of motions, it is obtained:

$$EI\frac{\bar{d}^4 H}{dy^4} - m\omega^2 H + mx_a\omega^2\Psi - \sum_{j=1}^{N} P_j\delta(y-y_j) + \sum_{j=1}^{N} Mf_j\delta^{(1)}(y-y_j) - f(y) = 0 \tag{3.120}$$

$$GJ\frac{\bar{d}^2\Psi}{dy^2} + I_\alpha\omega^2\Psi - m\omega^2 x_a H - \sum_{j=1}^{N} P_j x_j \delta(y-y_j) + \sum_{j=1}^{N} Mt_j \delta(y-y_j) + g(y) = 0 \tag{3.121}$$

In Eqs.(3.120)-(3.121) P_j, Mt_j and Mf_j are the counterparts of terms in Eqs.(3.117)-(3.118) and are concentrated force, twisting moment and bending moment associated with dampers and attached mass at y_j, given as

$$P_j = -\kappa_{P_j}(\omega)\left[H(y_j) - x_j\Psi(y_j)\right] \tag{3.122}$$

$$Mt_j = -\kappa_{T_j}(\omega)\Psi(y_j) \tag{3.123}$$

$$Mf_j = -\kappa_{M_j}(\omega)\Theta(y_j) \tag{3.124}$$

being $H(y_j)$, $\Psi(y_j)$ and $\Theta(y_j)$ the deflection, torsional and bending rotation at $y = y_j$, and $\kappa_{P_j}(\omega)$, $\kappa_{T_j}(\omega)$, $\kappa_{M_j}(\omega)$ frequency-dependent terms given as

$$\kappa_{P_j}(\omega) = k_{H_j} + i\omega c_{H_j} - M_j\omega^2 \tag{3.125}$$

$$\kappa_{T_j}(\omega) = k_{\Psi_j} + i\omega c_{\Psi_j} - (I_{yy_j} - M_j x_j^2)\omega^2 \tag{3.126}$$

$$\kappa_{M_j}(\omega) = k_{\Theta_j} + i\omega c_{\Theta_j} - I_{\hat{x}\hat{x}_j}\omega^2 \tag{3.127}$$

Notice that Eq.(3.120) and Eq.(3.121) (as well as Eqs.(3.117)-(3.118)) have been written for a general case of dampers and masses occurring simultaneously at every location y_j. Removing this assumption produces simple changes in the derived solutions as similarly shown in the previous Section.

Eqs.(3.120)-(3.121) can be combined, by eliminating either H or Ψ, to obtain two 6-th order differential equations for deflection and torsional rotation

$$\alpha\frac{\bar{d}^6H}{dy^6}+\beta\frac{\bar{d}^4H}{dy^4}-\gamma\frac{\bar{d}^2H}{dy^2}+\eta H-\frac{I_a\omega^2}{mx_a\omega^2}f(y)-\frac{GJ}{mx_a\omega^2}f^{(2)}(y)-g(y)+R_{H_{ext}}(y)=0 \tag{3.128}$$

$$\alpha\frac{\bar{d}^6\Psi}{dy^6}+\beta\frac{\bar{d}^4\Psi}{dy^4}-\gamma\frac{\bar{d}^2\Psi}{dy^2}+\eta\Psi-f(y)+\frac{EI}{mx_a\omega^2}g^{(4)}(y)-\frac{m\omega^2}{mx_a\omega^2}g(y)+R_{\Psi_{ext}}(y)=0 \tag{3.129}$$

where $R_{H_{ext}}(y), R_{\Psi_{ext}}(y)$ are the following generalized functions:

$$\begin{aligned}R_{H_{ext}}(y)=&-\sum_{j=1}^{N}P_j\left[(\frac{I_a}{mx_a}-x_j)\delta(y-y_j)+\frac{GJ}{mx_a\omega^2}\delta^{(2)}(y-y_j)\right]\\&-\sum_{j=1}^{N}Mt_j\delta(y-y_j)\\&+\sum_{j=1}^{N}Mf_j\left[\frac{I_a}{mx_a}\delta^{(1)}(y-y_j)+\frac{GJ}{mx_a\omega^2}\delta^{(3)}(y-y_j)\right]\end{aligned} \tag{3.130}$$

$$\begin{aligned}R_{\Psi_{ext}}(y)=&-\sum_{j=1}^{N}P_j\left[\frac{EIx_j}{mx_a\omega^2}\delta^{(4)}(y-y_j)-\frac{x_j-x_a}{x_a}\delta(y-y_j)\right]\\&+\sum_{j=1}^{N}Mt_j\left[\frac{EI}{mx_a\omega^2}\cdot\delta^{(4)}(y-y_j)-\frac{1}{x_a}\cdot\delta(y-y_j)\right]\\&+\sum_{j=1}^{N}Mf_j\delta^{(1)}(y-y_j)\end{aligned} \tag{3.131}$$

while α, β, γ and η are given as

$$\alpha=\frac{GJEI}{mx_a\omega^2};\ \ \beta=\frac{EII_\alpha}{mx_a};\ \ \gamma=\frac{GJ}{x_a};\ \ \eta=(mx_a\omega^2-\frac{\omega^2I_\alpha}{x_a}) \tag{3.132}$$

Further, in Eqs.(3.128)-(3.129) $f^{(k)}(y)$ and $g^{(k)}(y)$ denote the k-th derivative of $f(y)$ and $g(y)$ with respect to y.

Next, the exact frequency response functions and free vibrations response of the coupled bending torsion beam with dampers in Figure 3.19 will be derived.

Exact frequency response functions

Pursuing the primary purpose of obtaining the frequency response, assume that the beam carrying dampers/masses is loaded on the interval (a, b), with $0 \leq a, b \leq L$, by a harmonic distributed force $f(y)e^{i\omega t}$ and a harmonic distributed twisting moment $g(y)e^{i\omega t}$, as shown in Figure 3.19

By applying the linear superposition principle, the vector of the steady state response variables $\mathbf{Y}(y) = [H\ \Theta\ M\ S\ \Psi\ T]^{\mathrm{T}}$ can be written as (again, frequency dependence is omitted for conciseness)

$$\mathbf{Y}(y) = \mathbf{\Omega}(y)\mathbf{c} + \sum_{j=1}^{N} \mathbf{J}(y, y_j)\mathbf{\Lambda}_j + \mathbf{Y}^{(f)}(y) + \mathbf{Y}^{(g)}(y) \tag{3.133}$$

where vector $\mathbf{\Lambda}_j = [P_j\ Mt_j\ Mf_j]^{\mathrm{T}}$ collects the unknown reaction force P_j, twisting moment Mt_j and bending moment Mf_j at location y_j, see Eqs.(3.122)-(3.123)-(3.124). Further, $\mathbf{c} = [c_1\ c_2\ c_3\ c_4\ c_5\ c_6]^{\mathrm{T}}$ is a vector of integration constants, $\mathbf{\Omega}(y)$, $\mathbf{J}(y, y_j)$, $\mathbf{Y}^{(f)}(y)$ and $\mathbf{Y}^{(g)}(y)$ are given as

$$\mathbf{\Omega}(y) = \begin{bmatrix} \Omega_{H1} & \Omega_{H2} & \Omega_{H3} & \Omega_{H4} & \Omega_{H5} & \Omega_{H6} \\ \Omega_{\Theta 1} & \Omega_{\Theta 2} & \Omega_{\Theta 3} & \Omega_{\Theta 4} & \Omega_{\Theta 5} & \Omega_{\Theta 6} \\ \Omega_{M1} & \Omega_{M2} & \Omega_{M3} & \Omega_{M4} & \Omega_{M5} & \Omega_{M6} \\ \Omega_{S1} & \Omega_{S2} & \Omega_{S3} & \Omega_{S4} & \Omega_{S5} & \Omega_{S6} \\ \Omega_{\Psi 1} & \Omega_{\Psi 2} & \Omega_{\Psi 3} & \Omega_{\Psi 4} & \Omega_{\Psi 5} & \Omega_{\Psi 6} \\ \Omega_{T1} & \Omega_{T2} & \Omega_{T3} & \Omega_{T4} & \Omega_{T5} & \Omega_{T6} \end{bmatrix} \tag{3.134}$$

$$\mathbf{J}(y, y_j) = [\mathbf{J}^{(P)} \ \ \mathbf{J}^{(Mt)} \ \ \mathbf{J}^{(Mf)}] = \begin{bmatrix} J_H^{(P)} & J_H^{(Mt)} & J_H^{(Mf)} \\ J_\Theta^{(P)} & J_\Theta^{(Mt)} & J_\Theta^{(Mf)} \\ J_M^{(P)} & J_M^{(Mt)} & J_M^{(Mf)} \\ J_S^{(P)} & J_S^{(Mt)} & J_S^{(Mf)} \\ J_\Psi^{(P)} & J_\Psi^{(Mt)} & J_\Psi^{(Mf)} \\ J_T^{(P)} & J_T^{(Mt)} & J_T^{(Mf)} \end{bmatrix} \quad \text{for } \ j = 1, 2, \ldots N \tag{3.135}$$

$$\mathbf{Y}^{(f)}(y) = \int_a^b \mathbf{J}^{(P)}(y, \xi) f(\xi) d\xi \tag{3.136}$$

$$\mathbf{Y}^{(g)}(y) = \int_a^b \mathbf{J}^{(Mt)}(y, \xi) g(\xi) d\xi \tag{3.137}$$

Simple closed analytical expressions for $\mathbf{\Omega}(y)$ may be derived from the solutions to the homogeneous equations associated with Eq.(3.128) and Eq.(3.129); for $\mathbf{J}(y, y_j)$ from particular integrals of Eq.(3.128) and Eq.(3.129) associated with a unit point force $P = 1$, unit bending moment $Mf = 1$ and unit twisting moment $Mt = 1$ applied at y_j; for $\mathbf{Y}^{(f)}(y)$ and $\mathbf{Y}^{(g)}(y)$ from particular integrals of Eq.(3.128) and Eq.(3.129) associated with the external load. Specifically, the analytical expressions can readily be obtained based on the theory of generalized functions (see Chapter 2) in conjunction with the standard equations of the elementary coupled bending-torsion theory, as detailed in Appendix A for brevity. Here, it is only reported the fundamental solution from which all the closed form solutions are derived. The fundamental solution is the solution of the following equation:

$$\alpha \frac{\bar{d}^6 X}{dy^6} + \beta \frac{\bar{d}^4 X}{dy^4} - \gamma \frac{\bar{d}^2 X}{dy^2} + \eta X - \delta(y - y_0) = 0 \tag{3.138}$$

where y_0 is an arbitrary location along the y-axis. It may be seen that the

solution X takes the form

$$X(y, y_0) = \sum_{j=1}^{6} \Omega_j(y) c_j + J^{(*)}(y, y_0) \tag{3.139}$$

where Ω_j denotes terms of the solution to the associated homogeneous equation

$$\begin{aligned} &\Omega_1 = \cosh(\sqrt{r_1}y) \ ; \ \Omega_2 = \sinh(\sqrt{r_1}y) \ ; \ \Omega_3 = \cos(\sqrt{r_2}y) \ ; \\ &\Omega_4 = \sin(\sqrt{r_2}y) \ ; \ \Omega_5 = \cos(\sqrt{r_3}y) \ ; \ \Omega_6 = \sin(\sqrt{r_3}y) \end{aligned} \tag{3.140}$$

while the particular integral $J^{(*)}$ is obtained by Laplace transform (see Chapter 2), after some manipulations, in the following form:

$$\begin{aligned} J^{(*)}(y, y_0) = D\,[&\sinh(\sqrt{r_1}(y - y_0))\sqrt{r_2}\sqrt{r_3}(r_3 - r_2) - \sin(\sqrt{r_2}(y - y_0)) \\ &\sqrt{r_1}\sqrt{r_3}(r_1 + r_3) + \sin(\sqrt{r_3}(y - y_0))\sqrt{r_1}\sqrt{r_2}(r_1 + r_2)\,] \cdot U(y - y_0) \end{aligned} \tag{3.141}$$

In Eq.(3.141), $U(\cdot)$ is the Unit-Step function (notice that a change of notation is needed, since the symbol "H" denote herein the bending deflection), $D = -d(r_1 + r_2)(r_1 + r_3)(r_3 - r_2)/(\sqrt{r_1}\sqrt{r_2}\sqrt{r_3})$, $d = \alpha^3/(4\eta\beta^3 + 4\gamma^3\alpha + 27\alpha^2\eta^2 - \gamma^2\beta^2 - 18\alpha\beta\gamma\eta)$ while r_1, $-r_2$, $-r_3$ ($r_1 > 0$, $r_2 > 0$, $r3 > 0$) [49] are the three solutions of the following 3-rd order polynomial equation:

$$\alpha \cdot r^3 + \beta \cdot r^2 - \gamma r + \eta = 0 \tag{3.142}$$

Next, focus on Eqs.(3.122)-(3.123)-(3.124) for P_j, Mt_j and Mf_j. Using Eq.(3.133), it is noticed that $H(y_j)$, $\Psi(y_j)$ and $\Theta(y_j)$ on the right hand sides of Eqs.(3.122)-(3.123)-(3.124) involve unknowns $\mathbf{\Lambda}_k$ for $k < j$ only, as indeed the particular integrals in $\mathbf{J}(y_j, y_k)$ are not zero only for $y_j > y_k$ and vanish for $y_j \leq y_k$ (see Appendix A). Based on this observation, the approach introduced for beams with symmetric cross sections can readily be generalized to obtain the frequency response $\mathbf{Y}(y)$ as closed-form function of

the vector of integration constants $\mathbf{c}$ only, as follows:

$$\mathbf{Y}(y) = \tilde{\mathbf{Y}}(y)\mathbf{c} + \tilde{\mathbf{Y}}^{(f)}(y) + \tilde{\mathbf{Y}}^{(g)}(y) \tag{3.143}$$

where

$$\tilde{\mathbf{Y}}(y) = \mathbf{\Omega}(y) + \sum_{j=1}^{N} \mathbf{J}(y, y_j)\mathbf{\Phi}_{\mathbf{\Omega}}(y_j) + \sum_{j=1}^{N} \mathbf{J}(y, y_j)\Bigg\{ \sum_{(j,m)\in N_2^{(j)}} \mathbf{\Phi}_{\mathbf{J}}(y_j, y_m)\mathbf{\Phi}_{\mathbf{\Omega}}(y_m) + \sum_{2<q\leq j} \sum_{(j,m,n,\ldots,r,s)\in N_q^{(j)}} \mathbf{\Phi}_{\mathbf{J}}(y_j, y_m)\mathbf{\Phi}_{\mathbf{J}}(y_m, y_n)\ldots\mathbf{\Phi}_{\mathbf{J}}(y_r, y_s)\mathbf{\Phi}_{\mathbf{\Omega}}(y_s)\Bigg\} \tag{3.144}$$

$$\tilde{\mathbf{Y}}^{(f)}(x) = \mathbf{Y}^{(f)}(y) + \sum_{j=1}^{N} \mathbf{J}(y, y_j)\mathbf{\Phi}^{(f)}(y_j) + \sum_{j=1}^{N} \mathbf{J}(y, y_j)\Bigg\{ \sum_{(j,m)\in N_2^{(j)}} \mathbf{\Phi}_{\mathbf{J}}(y_j, y_m)\mathbf{\Phi}^{(f)}(y_m) + \sum_{2<q\leq j} \sum_{(j,m,n,\ldots,r,s)\in N_q^{(j)}} \mathbf{\Phi}_{\mathbf{J}}(y_j, y_m)\mathbf{\Phi}_{\mathbf{J}}(y_m, y_n)\ldots\mathbf{\Phi}_{\mathbf{J}}(y_r, y_s)\mathbf{\Phi}^{(f)}(y_s)\Bigg\} \tag{3.145}$$

$$\tilde{\mathbf{Y}}^{(g)}(y) = \mathbf{Y}^{(g)}(y) + \sum_{j=1}^{N} \mathbf{J}(y, y_j)\mathbf{\Phi}^{(g)}(y_j) + \sum_{j=1}^{N} \mathbf{J}(y, y_j)\Bigg\{ \sum_{(j,m)\in N_2^{(j)}} \mathbf{\Phi}_{\mathbf{J}}(y_j, y_m)\mathbf{\Phi}^{(g)}(y_m) + \sum_{2<q\leq j} \sum_{(j,m,n,\ldots,r,s)\in N_q^{(j)}} \mathbf{\Phi}_{\mathbf{J}}(y_j, y_m)\mathbf{\Phi}_{\mathbf{J}}(y_m, y_n)\ldots\mathbf{\Phi}_{\mathbf{J}}(y_r, y_s)\mathbf{\Phi}^{(g)}(y_s)\Bigg\} \tag{3.146}$$

In Eqs.(3.144)-(3.145)-(3.146), $\mathbf{\Phi_\Omega}(y_j)$ is a 3×6 matrix given as

$$\mathbf{\Phi_\Omega}(y_j) = \begin{bmatrix} -\kappa_{P_j}(\omega)(\mathbf{\Omega}_1(y_j) - x_j\mathbf{\Omega}_5(y_j)) \\ -\kappa_{T_j}(\omega)\mathbf{\Omega}_5(y_j) \\ -\kappa_{M_j}(\omega)\mathbf{\Omega}_2(y_j) \end{bmatrix} \tag{3.147}$$

being $\mathbf{\Omega}_i(y_j)$ the row vector coinciding with the i-th row of matrix $\mathbf{\Omega}(y_j)$, while $\mathbf{\Phi_J}(y_j, y_k)$ is the 3×3 matrix

$$\mathbf{\Phi_J}(y_j, y_k) = \begin{bmatrix} -\kappa_{P_j}(\omega)(\mathbf{J}_1(y_j, y_k) - x_j\mathbf{J}_5(y_j, y_k)) \\ -\kappa_{T_j}(\omega)\mathbf{J}_5(y_j, y_k) \\ -\kappa_{M_j}(\omega)\mathbf{J}_2(y_j, y_k) \end{bmatrix} \tag{3.148}$$

where $\mathbf{J}_i(y_j, y_k)$ is the row vector coinciding with the i-th row of matrix $\mathbf{J}(y_j, y_k)$; further, $\mathbf{\Phi}^{(f)}(y_j)$ and $\mathbf{\Phi}^{(g)}(y_j)$ are the 3×1 vectors

$$\mathbf{\Phi}^{(f)}(y_j) = \begin{bmatrix} -k_{P_j}(\omega)(Y_1^{(f)}(y_j) - x_j Y_5^{(f)}(y_j)) \\ -k_{T_j}(\omega)Y_5^{(f)}(y_j) \\ -k_{M_j}(\omega)Y_2^{(f)}(y_j) \end{bmatrix} \tag{3.149}$$

$$\mathbf{\Phi}^{(g)}(y_j) = \begin{bmatrix} -k_{P_j}(\omega)(Y_1^{(g)}(y_j) - x_j Y_5^{(g)}(y_j)) \\ -k_{T_j}(\omega)Y_5^{(g)}(y_j) \\ -k_{M_j}(\omega)Y_2^{(g)}(y_j) \end{bmatrix} \tag{3.150}$$

being $Y_i^{(f)}(y_j)$ and $Y_i^{(g)}(y_j)$ the i-th components of vectors $\mathbf{Y}^{(f)}(y_j)$ and $\mathbf{Y}^{(g)}(y_j)$. Also, in Eqs.(3.144)-(3.145)-(3.146) $N_q^{(j)}$ assumes the same meaning of the previous Sections. All terms in Eq.(3.143) through Eq.(3.150) are available in closed analytical form, using the expressions reported in Appendix A.

Next, the final step to derive the exact frequency response $\mathbf{Y}(y)$ is to enforce the B.C. of the beam. This leads to 6 equations with general form

$$\mathbf{Bc} = \mathbf{r} \rightarrow \mathbf{c} = (\mathbf{B})^{-1}\mathbf{r} \tag{3.151}$$

where vector $\mathbf{r}$ involves the load-dependent terms $\tilde{\mathbf{Y}}^{(f)}(y)$, $\tilde{\mathbf{Y}}^{(g)}(y)$ in Eqs.(3.145)-(3.146), as computed at the beam ends. Remarkably, the coefficient matrix $\mathbf{B}$ has size 6×6 regardless of the number of dampers/masses, and can readily be inverted in closed form by any symbolic package [2], as shown in Appendix B. This means that, upon deriving $\mathbf{c}$ from Eq.(3.151), Eq.(3.143) provides exact closed-form expressions for the frequency response $\mathbf{Y}(y)$ of the coupled bending-torsional beam with an arbitrary number of dampers/masses, under distributed polynomial loads $f(y)e^{i\omega t}$ and $g(y)e^{i\omega t}$. The closed-form expressions are available for all response variables in $\mathbf{Y}(y)$. Obviously, they hold also for point loads applied at any y_0 along the y-axis, with $\mathbf{Y}^{(f)}(y) = \mathbf{J}^{(P)}(y, y_0)$ in Eq.(3.136) and $\mathbf{Y}^{(g)}(y) = \mathbf{J}^{(Mt)}(y, y_0)$ in Eq.(3.137).

Finally, notice that Eq.(3.143) can be used also for non-homogenous B.C., e.g. for end dampers or tip masses. Indeed, the end dampers or tip masses can be modeled as located at $y_1 = 0^+$ and $y_N = L^-$, and the B.C. can still be considered as homogeneous.

Free vibrations

Due to the presence of concentrated dampers, the damping in the primary system is not proportional and consequently the eigenvalues ω_n and the associated eigenfunctions $H_n(y)$, $\Psi_n(y)$ are complex. The eigenvalues are computed as a root of the characteristic equation $\det(\mathbf{B}) = 0$ obtained from Eq.(3.151) with $\mathbf{r} = \mathbf{0}$: on computing every eigenvalue and calculating the corresponding matrix $\mathbf{B}$, the associated eigenfunction is given by Eq.(3.143) with $\mathbf{c}$ = non-trivial solution of $\mathbf{Bc} = \mathbf{0}$ and $\tilde{\mathbf{Y}}^{(g)} = \tilde{\mathbf{Y}}^{(f)} = \mathbf{0}$.

The eigenfunctions satisfy the following orthogonality conditions

$$
\begin{aligned}
0 = & -m(\omega_n^2-\omega_m^2)\int_0^L H_nH_m dy - I_\alpha(\omega_n^2-\omega_m^2)\int_0^L \Psi_m\Psi_n dy \\
& + mx_a(\omega_n^2-\omega_m^2)\int_0^L (H_n\Psi_m dy + H_m\Psi_n)dy \\
& + \sum_{j=1}^{N}\Bigg\{ - M_j(\omega_n^2-\omega_m^2)H_n(y_j)H_m(y_j) + M_jx_j(\omega_n^2-\omega_m^2)(H_n(y_j)\Psi_m(y_j) \\
& + H_m(y_j)\Psi_n(y_j)) - I_{yy_j}(\omega_n^2-\omega_m^2)\Psi_n(y_j)\Psi_m(y_j) + I_{xx_j}(\omega_n^2-\omega_m^2)\Theta_n(y_j)\Theta_m(y_j) \\
& + ic_{H_j}(\omega_n-\omega_m)\Big(H_n(y_j)H_m(y_j) - H_n(y_j)\Psi_m(y_j)x_j - H_m(y_j)\Psi_n(y_j)x_j \\
& + \Psi_m(y_j)\Psi_n(y_j)\Big) + ic_{\Psi_j}(\omega_n-\omega_m)\Big(\Psi_n(y_j)\Psi_m(y_j)\Big) \\
& - ic_{\theta_j}(\omega_n-\omega_m)\Theta_n(y_j)\Theta_m(y_j)\Bigg\}
\end{aligned}
\tag{3.152}
$$

$$
\begin{aligned}
& EI\int_0^L H_n''H_m''dy + GJ\int_0^L \Psi'_m\Psi'_n dy = -m\omega_m\omega_n\int_0^L H_mH_n dy \\
& - I_\alpha\omega_m\omega_n\int_0^L \Psi_n\Psi_m dy + mx_a\omega_m\omega_n\Bigg(\int_0^L H_n\Psi_m + \int_0^L H_m\Psi_n dy\Bigg) \\
& + \sum_{j=1}^{N}\Bigg\{ - M_j\omega_m\omega_n H_m(y_j)H_n(y_j) \\
& + M_jx_j\Bigg(H_n(y_j)\Psi_m(y_j) + H_m(y_j)\Psi_n(y_j)\Bigg) - I_{yy_j}\omega_m\omega_n\Psi_n(y_j)\Psi_m(y_j) \\
& + I_{xx_j}\omega_m\omega_n\Theta_n(y_j)\Theta_m(y_j) - \frac{k_{H_j}(\omega_m-\omega_n)}{\omega_m-\omega_n}\Big(H_m(y_j)H_n(y_j) - H_n(y_j)\Psi_m(y_j)x_j \\
& - H_m(y_j)\Psi_n(y_j)x_j + \Psi_m(y_j)\Psi_n(y_j)x_j^2\Big) - \frac{k_{\Psi_j}(\omega_m-\omega_n)}{\omega_m-\omega_n}\Big(\Psi_m(y_j)\Psi_n(y_j)\Big) + \\
& \frac{k_{\Theta_j}(\omega_m-\omega_n)}{\omega_m-\omega_n}\Big(\Theta_m(y_j)\Theta_n(y_j)\Big)\Bigg\}
\end{aligned}
\tag{3.153}
$$

where ω_n and ω_m are complex eigenvalues, while $H_n(y)$, $\Psi_n(y)$, $\Theta_n(y)$ and $H_m(y)$, $\Psi_m(y)$ and $\Theta_m(y)$ denote the corresponding complex eigenfunctions.

Notice that Eq.(3.152) and Eq.(3.153) are derived from Eq.(3.120) and Eq.(3.121) written in free vibrations, i.e. for $f(y) = g(y) = 0$. Eq.(3.152)

is obtained as the difference of two equations: the first equation is built subtracting Eq.(3.121) from Eq.(3.120) for the n-th mode, where Eq.(3.120) is multiplied by $H_m(y)$ and Eq.(3.121) multiplied by $\Psi_m(y)$, and both are integrated over $[0, L]$ taking into account the beam B.C.; the second equation mirrors the first one, i.e. is built subtracting Eq.(3.120) from Eq.(3.121) for the m-th mode, where Eq.(3.120) is multiplied by $H_n(y)$ and Eq.(3.121) is multiplied by $\Psi_n(y)$ and, again, both are integrated over $[0, L]$ using the beam B.C. Eq.(3.153) is obtained as the difference of the same two equations, upon multiplying the first by ω_m and the second by ω_n

3.4.3 Complex modal analysis and time domain response

Here, in order to perform a time domain analysis and to obtain a complete description of the frequency response of the coupled bending-torsional beam with dampers/masses in Figure 3.38, a pertinent complex modal analysis approach is devised. The approach generalizes to the coupled bending-torsional beam with dampers/masses the approach introduced by Oliveto et al. in ref.[42] for beams in pure bending with viscous dampers at the ends. In both cases, damping is not proportional.

Next, consider the coupled bending-torsion equations of motion of the beam under a space-dependent impulsive force $f(y)\delta(t)$ and torque $g(y)\delta(t)$, i.e.

$$EI\frac{\bar{\partial}^4 h_{RF}}{dy^4} + m\frac{\partial^2 h_{RF}}{\partial t^2} - mx_a\frac{\partial^2 \psi_{RF}}{\partial t^2} - \sum_{j=1}^{N}(p_j(t)\delta(y-y_j) - mf_j(t)\delta^{(1)}(y-y_j)) - f(y)\delta(t) = 0 \tag{3.154}$$

$$GJ\frac{\bar{\partial}^2\psi_{RF}}{\partial y^2} - I_\alpha\frac{\partial^2\psi_{RF}}{\partial t^2} + mx_a\frac{\partial^2 h_{RF}}{\partial t^2} - \sum_{j=1}^{N}(p_j(t)x_j\delta(y-y_j) - mt_j(t)\delta(y-y_j)) + g(y)\delta(t) = 0 \tag{3.155}$$

where $p_j(t)$, $mf_j(t)$, $mt_j(t)$ are time-domain counterparts of terms in Eqs.(1)-(2). The response variables obtained from Eqs.(3.154)-(3.155), here collected in vector $\mathbf{I}_{RF}(y,t) = [h_{RF}\ \ \theta_{RF}\ \ m_{RF}\ \ s_{RF}\ \ \psi_{RF}\ \ t_{RF}]^T$, are the impulse response functions of the beam. Using the mode superposition principle, they can be represented as

$$\mathbf{I}_{RF}(y,t) = \sum_{k=1}^{\infty}\mathbf{I}_{RF,k}(y,t) = \sum_{k=1}^{\infty} b_k(t)\mathbf{Y}_k(y) = \sum_{k=1}^{\infty}\tilde{b}_k e^{i\omega_k t}\mathbf{Y}_k(y) \tag{3.156}$$

where $\mathbf{I}_{RF,k}(y,t)$ is the vector of modal impulse response functions associated with the k-th mode, $\mathbf{Y}_k(y) = [H_k\ \ \Theta_k\ \ M_k\ \ S_k\ \ \Psi_k\ \ T_k]^T$ is the vector of k-th complex eigenfuctions and $\tilde{b}_k$ are complex coefficients. In Eq.(3.156), notice that $b_k(t) = \tilde{b}_k e^{i\omega_k t}$ in view of the impulsive nature of the load [42, 43]. Then, further manipulations are: use Eq.(3.156) for the response variables in Eqs.(3.154)-(3.155), multiply Eq.(3.154) by $H_m(y)$ and Eq.(3.155) by $\Psi_m(y)$, integrate over $[0, L]$ considering the beam B.C.; sum up Eq.(3.154) and Eq.(3.155) and, finally, use the orthogonality conditions (3.152)-(3.153). In this manner, the following equation is obtained for every time-dependent function $b_k(t)$:

$$\mu_k\ddot{b}_k + \sum_{j=1}^{N}\left\{(C_{k,j}^{(h)} + C_{k,j}^{(\psi)} + C_{k,j}^{(\theta)})\right\}\dot{b}_k = \left(\int_0^L \Psi_k g(y)dy - \int_0^L H_k f(y)dy\right)\delta(t) = L_k\delta(t) \tag{3.157}$$

being

$$\mu_k = 2\int_0^L mH_k^2 dy + 2I_\alpha \int_0^L \Psi_k^2 dy - 4mx_a \int_0^L H_k \Psi_k dy + \sum_{j=1}^{N} \left\{ 2M_j H_k^2(y_j) + 2I_{yy_j} \Psi_k^2(y_j) - 4M_j x_j H_k(y_j)\Psi_k(y_j) + 2I_{xx_j}\Theta_k^2(y_j) \right\} \tag{3.158}$$

$$C_{k,j}^{(h)} = c_{H_k}\left(H_k^2(y_j) - 2H_k(y_j)\Psi_k(y_j)x_j + \Psi_k^2(y_j)x_j^2 \right) \tag{3.159}$$

$$C_{k,j}^{(\psi)} = -c_{\Psi_k}\Psi_k^2(y_j) \tag{3.160}$$

$$C_{k,j}^{(\theta)} = -c_{\Theta_k}\Theta_k^2(y_j) \tag{3.161}$$

Integrating Eq.(3.157) over $[0^-, 0^+]$ [42] leads to the following expression for the complex coefficients $\tilde{b}_k$:

$$\tilde{b}_k = \frac{L_k}{\mu_k i\omega_k + \sum_{j=1}^{N}\left\{ C_{k,j}^{(h)} + C_{k,j}^{(\psi)} + C_{k,j}^{(\theta)} \right\}} \tag{3.162}$$

On replacing Eq.(3.162) for $\tilde{b}_k$ in Eq.(3.156), the impulse response $\mathbf{I}_{RF}(y,t)$ is obtained, as well as the corresponding modal impulse responses $\mathbf{I}_{RF,k}(y,t)$.

Now it is observed that, for the damping levels generally encountered in engineering applications, the complex modes contributing to the structural response occur in complex-conjugate pairs [43, 42]. Correspondingly, a pair of complex-conjugate modal impulse responses $\mathbf{I}_{RF,k}(y,t)$ is indeed associated with the k-th mode; their sum provides the following real form for the vector of modal impulse response functions of the k-th mode, to be used in Eq.(3.156)

$$\mathbf{I}_{RF,k}^r(y,t) = \boldsymbol{\alpha}_k(y)|\omega_k| z_k(t) + \boldsymbol{\beta}_k(y)\dot{z}_k(t) \tag{3.163}$$

with

$$\begin{aligned}&\boldsymbol{\alpha}_k(y) = \xi_k\boldsymbol{\beta}_k(y) - \sqrt{(1-\xi_k^2)}\boldsymbol{\lambda}_k(y);\ \boldsymbol{\beta}_k(y) = 2\mathrm{Re}[\tilde{b}_k\mathbf{Y}_k(y)];\\&\boldsymbol{\lambda}_k(y) = 2\mathrm{Im}[\tilde{b}_k\mathbf{Y}_k(y)]\end{aligned} \tag{3.164}$$

$$z_k(t) = \frac{1}{\omega_{D_k}}e^{-\xi_k|\omega_k|t}\sin(\omega_{D_k}t);\ \omega_{D_k} = |\omega_k|(\sqrt{1-\xi_k^2}) \tag{3.165}$$

being $\xi_k = \mathrm{Im}[\omega_k]/|\omega_k|$ the modal damping ratio of the k-th mode [42]. In the frequency domain, each vector $\mathbf{I}^r_{RF,k}$ is associated with a vector $\hat{\mathbf{R}}_k(y) = [\hat{H}_k\ \hat{\Theta}_k\ \hat{M}_k\ \hat{S}_k\ \hat{\Psi}_k\ \hat{T}_k]^{\mathrm{T}}$, which contains the modal frequency response functions of the k-th mode and is given by (frequency dependence is omitted for brevity):

$$\hat{\mathbf{R}}_k(y) = \boldsymbol{\alpha}_k(y)|\omega_k|Z_k + \boldsymbol{\beta}_k(y)\dot{Z}_k \tag{3.166}$$

where

$$Z_k(\omega) = \frac{1}{|\omega_k|^2 - \omega^2 + 2i\xi_k|\omega_k|\omega}\ ;\ \dot{Z}_k(\omega) = \frac{i\omega}{|\omega_k|^2 - \omega^2 + 2i\xi_k|\omega_k|\omega} \tag{3.167}$$

Using the mode superposition principle with a finite number of modes M, the approximate frequency response $\hat{\mathbf{Y}} = [\hat{H}\ \hat{\Theta}\ \hat{M}\ \ \hat{S}\ \hat{\Psi}\ \hat{T}]^{\mathrm{T}}$ can be built as

$$\mathbf{Y}(y) \approx \hat{\mathbf{Y}}(y) = \sum_{k=1}^{M}\hat{\mathbf{R}}_k(y) \tag{3.168}$$

Eq.(3.168) approximates the exact frequency response $\mathbf{Y}(y)$ given by Eq.(3.143) in Section 3, providing an insight into the contribution of every mode. Eq.(3.168) for the frequency response and Eq.(3.156) for the impulse response are obtained in a closed analytical form. Obviously, Eq.(3.156) can be used to calculate the time-domain response to an arbitrary force $p(y,t) = f(y)w(t)$ and torque $q(y,t) = g(y)w(t)$ by a standard Duhamel convolution integral

$$\mathbf{v}(y,t) = \int_0^t \mathbf{I}_{RF}(y, t-\tau)w(\tau)d\tau \tag{3.169}$$

where $\mathbf{v}(y,t) = [h\ \ \theta\ \ m\ \ s\ \ \psi\ \ t]^T$ is the vector collecting the time-dependent

response variables of the beam. In Eq.(3.169), notice that the impulse response $\mathbf{I}_{RF}(y, t-\tau)$ includes the space-dependent functions of the applied load, i.e. $f(y)$ and $g(y)$, see Eqs.(3.162)-(3.163). Whereas force and torque are given as $p(y,t) = f(y)w_1(t)$ and $q(y,t) = g(y)w_2(t)$, with $w_1(t) \neq w_2(t)$, the response can be built as the sum of separate responses, one to $p(y,t)$ and the other to $q(y,t)$ only, both calculated by Eq.(3.169).

3.4.4 Classical modal analysis and time domain response

Now, assume that along the beam domain there are no concentrated dampers. Then, assume that the only source of damping is a proportional viscous damping, which can be directly taken into account in the equation of the generic modal oscillator due to the linearity of the problem.

The formulation presented in the previous subsections may serve as a basis to build the beam response with proportional damping via the normal mode method. For this purpose, notice that the free-vibration undamped response can be represented as

$$\mathbf{Y}(y) = \tilde{\mathbf{Y}}(y)\mathbf{c} \tag{3.170}$$

using Eq.(3.143) with no load-dependent terms and zero viscous damping coefficients $c_{h_j} = c_{\psi_j} = c_{\theta_j} = 0$. Again, constants $\mathbf{c}$ are determined from the non-trivial solutions of the following equations built on setting the beam B.C.:

$$\mathbf{B}\mathbf{c} = \mathbf{0} \tag{3.171}$$

where $\mathbf{B}$ is the 6×6 matrix in Eqs.(3.151). Upon computing the n-th modal frequency as root of the characteristic equation associated with Eq.(3.171), the corresponding exact vector of eigenfunctions $\mathbf{Y}_n(y) = [H_n\ \Theta_n\ M_n\ S_n\ \Psi_n\ T_n]$ is derived, in a closed analytical form, from Eq.(3.170).

Being H_n and Ψ_n the eigenfunctions of deflection and torsional rotation,

respectively, the orthogonality condition in Eq.(3.152) modified as follows:

$$\begin{aligned}
&\int_0^L \left[mx_a(\Psi_n H_m + H_n\Psi_m) - (mH_nH_m + I_\alpha\Psi_n\Psi_m)\right] dy \\
&+ \sum_{j=1}^{N}\Big\{-I_{yy_j}\Psi_n(y_j)\Psi_m(y_j) - MH_n(y_j)H_m(y_j) + M_jx_j\Psi_n(y_j)H_m(y_j) \\
&+ MH_n(y_j)\Psi_m(y_j)x_j - M_j\Psi_n(y_j)\Psi_m(y_j)x_j^2 \\
&+ I_{xx_j}\Theta_n(y_j)\Theta_m(y_j)\Big\} = \mu_{nm}
\end{aligned} \tag{3.172}$$

where again μ_{nm} is a real number defined as follows:

$$\begin{cases} \mu_{nm} = 0 & if\ n \neq m \\ \mu_{nm} \neq 0 & if\ n = m \end{cases}$$

Being $h(y,t)$, $\theta(y,t)$, $\mu(y,t)$, $s(y,t)$, $\psi(y,t)$ and $\tau(y,t)$ the time domain bending deflection, bending rotation, bending moment, shear force, torsional rotation and torque, vector $\mathbf{u}(y,t) = [h(y,t)\ \theta(y,t)\ \mu(y,t)\ s(y,t)\ \psi(y,t)\ \tau(y,t)]$ is obtained via superposition principle as follows:

$$\mathbf{u}(y,t) = \mathbf{u}^{(f)}(y,t) + \mathbf{u}^{(g)}(y,t) \tag{3.173}$$

where $\mathbf{u}^{(f)}(y,t)$, $\mathbf{u}^{(g)}(y,t)$ are:

$$\mathbf{u}^{(f)}(y,t) = \sum_{n=1}^{\infty} q_n^{(f)}\mathbf{Y}_n(y) \tag{3.174}$$

$$\mathbf{u}^{(g)}(y,t) = \sum_{n=1}^{\infty} q_n^{(g)}\mathbf{Y}_n(y) \tag{3.175}$$

being $q_n^{(f)}(t)$ and $q_n^{(g)}(t)$ time-dependent modulating functions for the n-th mode. Substituting Eqs.(3.174)-(3.175) into equations (3.120)-(3.121), and making use of the orthogonality conditions (3.172), the following pair of

differential equations is obtained:

$$\ddot{q}_n^{(f)}(t) + \omega_n^2 q_n^{(f)}(t) = \frac{1}{\mu_{nn}} \int_0^L H_n f(y,t) dy \tag{3.176}$$

$$\ddot{q}_n^{(g)}(t) + \omega_n^2 q_n^{(g)}(t) = \frac{1}{\mu_{nn}} \int_0^L \Psi_n g(y,t) dy \tag{3.177}$$

Assuming proportional viscous damping, with ξ_n the n-th modal damping coefficient, Eqs.(3.176)-(3.177) modify as follows

$$\ddot{q}_n^{(f)}(t) + 2\xi_n\omega_n\dot{q}_n^{(f)}(t) + \omega_n^2 q_n^{(f)}(t) = \frac{1}{\mu_{nn}} \int_0^L H_n f(y,t) dy \tag{3.178}$$

$$\ddot{q}_n^{(g)}(t) + 2\xi_n\omega_n\dot{q}_n^{(g)}(t) + \omega_n^2 q_n^{(g)}(t) = \frac{1}{\mu_{nn}} \int_0^L \Psi_n g(y,t) dy \tag{3.179}$$

The solution to equations (3.176)-(3.177) can be obtained by using Duhamel's integral. Obviously, time-domain expressions for any response variable can be obtained in the form (3.174)-(3.175), using the pertinent eigenfunction from vector $\mathbf{Y}_n(y)$.

From the exact undamped modes, exact expressions for the frequency response functions, alternative to Eqs.(3.143), can be built as

$$\mathbf{Y}_{(f)}(y,\omega) = \sum_{n=1}^{\infty} Q_n^{(f)}(\omega)\mathbf{Y}_n(y) \tag{3.180}$$

$$\mathbf{Y}_{(g)}(y,\omega) = \sum_{n=1}^{\infty} Q_n^{(g)}(\omega)\mathbf{Y}_n(y) \tag{3.181}$$

where $Q_n^{(f)}(\omega)$ and $Q_n^{(g)}(\omega)$ denote the modal frequency response of the n-th mode to the loads $f(y)e^{i\omega t}$ and $g(y)e^{i\omega t}$ respectively:

$$Q_n^{(f)}(\omega) = \frac{\int_0^L f(y)[H_n(y)]dy}{\mu_n(\omega_n^2 - \omega^2 + 2i\xi_n\omega_n\omega)} \tag{3.182}$$

$$Q_n^{(g)}(\omega) = \frac{\int_0^L g(y)[\Psi_n(y)]dy}{\mu_n(\omega_n^2 - \omega^2 + 2i\xi_n\omega_n\omega)} \tag{3.183}$$

Eqs.(3.182)-(3.183) provide an insight into the contributions of every mode to the frequency response of the beam, which is highly desirable for design purposes.

Notice that the frequency response function, in the case of proportional damping, can be computed without resorting to the modal superposition. For this purpose, the equations of motion Eqs.(3.120)-(3.121) (as well as Eqs.(3.117)-(3.118)) have to be modified. Specifically, additional terms taking into account of distributed proportional damping have to be added [34], according with Eqs.(3.178)-(3.179)

3.4.5 Advantages and remarks

Now, advantages of the proposed approach are discussed. Firstly, the exact analytical frequency response functions (3.143) is compared with the alternative exact expressions obtainable by a classical procedure. This consists in dividing the beam in uniform segments, each between two consecutive application points of dampers/masses/point loads or under a distributed load, where the frequency response can be expressed using the solution to the homogeneous equations of motion, and including a particular integral for the segments where a distributed load is applied. For n segments, $6 \times n$ integration constants should be computed by enforcing the B.C. at beam ends and matching conditions among the solutions over adjacent segments. By using this approach, even with a low number of dampers/masses/loads, the coefficient matrix associated with the equations to be solved shall be re-inverted numerically for any forcing frequency of interest, and updated whenever dampers/masses/load change positions (as discussed in Chapter 1 for beams with symmetric cross section). Over this classical procedure, the proposed exact expression (3.143) has the following advantages:

- It is inherently able to satisfy all the required conditions at the dampers and point load locations, capturing jump and slope discontinuities of the response variables.

- The analytical form is easy to implement in any symbolic package, and can readily be computed for any frequency of interest, parameters of dampers (location, stiffness, damping), position of the loads, regardless of the number of dampers and positions of the dampers relative to the loads.

These two characteristics make Eq.(3.143) particularly suitable for optimization problems, where several solutions shall be built and compared for changing position and parameters of dampers/masses/loads.

Next, it is remarked that the characteristic equation $\det(\mathbf{B}) = 0$ is obtained from matrix $\mathbf{B}$ in Eq.(3.151), which holds the same size 6×6 for any number of dampers. Once the natural frequencies are calculated, Eq.(3.143) provides the exact eigenfunctions of all response variables $\mathbf{Y}(y)$ in a closed form inherently fulfilling the required conditions at the applications points of supports/masses. Then, all the advantages previously presented for the frequency response functions, holds for the free vibration response too and are consequently conveyed to the impulse response functions.

3.4.6 Numerical examples

In this Section two numerical examples are reported. Two different beams are considered, with angular and "Tee" cross section respectively, for which warping rigidity is generally neglected in the torsion equation of motion. Frequency responses are obtained making use of the exact solutions derived in the previous subsections and are compared with those calculated by the exact classical method, that is dividing the beam in uniform segments, which are adjacent to damper/mass/point-load locations or are subjected to a distributed load, where the vibration response is represented in terms of 6 unknown integration constants totalling $6 \times n$ constants for n segments, to be determined enforcing the B.C. along with matching conditions between solutions over adjacent segments. In addition, a comparison will be made to the frequency response built by the complex mode superposition approach.

In Example A, frequency response functions are built for different loadings, and terms of the dynamic stiffness and load vector are given for two values of frequency ω.

In Example B, thanks to the closed-form expressions derived in the previous subsections, a parametric analysis is led for different positions of a viscous damper along the beam, and results for the adopted coupled bending-torsion beam model are compared with those obtained by considering the pure bending Euler-Bernoulli beam model. The aim is to point out the different predictions of the two models and show that, if the pure bending Euler-Bernoulli theory was erroneously adopted to address the dynamics of the beam with mono-symmetric cross section under study, where SC and MC do not coincide, significantly wrong results would be obtained when searching for the optimal position of the damper.

Example A

Consider the cantilever beam with an angular cross section depicted in Figure 3.20, whose properties are chosen as follows: $I = 1.0174 \cdot 10^{-5}\mathrm{m}^4$, $J = 9.6666 \times 10^{-8}\mathrm{m}^4$, $I_\alpha = 0.0549\,\mathrm{kg}\cdot\mathrm{m}$, $x_a = 0.0512\,\mathrm{m}$, $L = 3\,\mathrm{m}$, $m = 7.83\,\mathrm{kg}\cdot\mathrm{m}^{-1}$, $E = 70 \times 10^9\mathrm{N}\cdot\mathrm{m}^{-2}$, $G = 26.3158 \times 10^9\mathrm{N}\cdot\mathrm{m}^{-2}$, $b = 0.15$ m, $t = 0.01$ m.

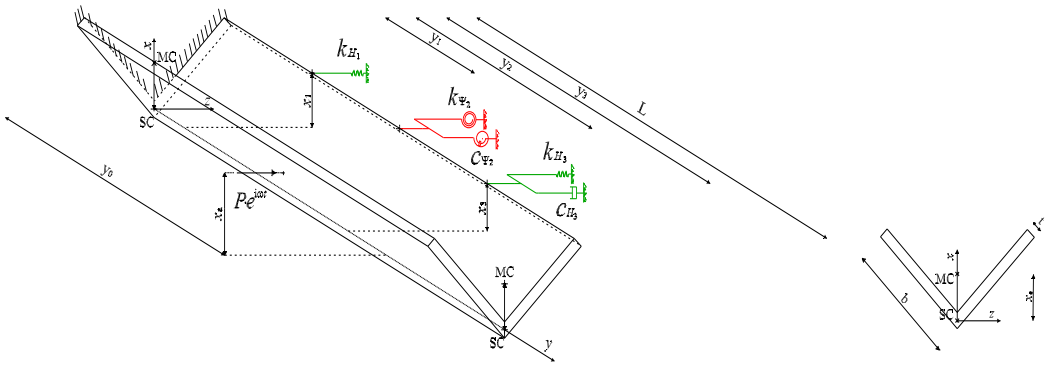

Figure 3.20: Cantilever beam with angular cross section carrying a translational elastic support, translational and torsional-rotational Kelvin-Voigt dampers, subjected to a harmonically-varying transverse point force.

The beam carries a translational elastic support at $y_1 = 0.25 \cdot L$ and a translational damper at $y_3 = 0.75 \cdot L$, both applied at distance $x_1 = x_3 = 0.1025$ from the SC of the beam cross section, as well as a torsional-rotational damper at $y_2 = 0.5 \cdot L$; it is assumed that $k_{H_1} = k_{H_3} = 10^5\,\mathrm{N \cdot m^{-1}}$, $k_{\Psi_2} = 10^4\,\mathrm{N \cdot m}$, $c_{\Psi_2} = 10\,\mathrm{N \cdot s \cdot m}$, $c_{H_3} = 10^2\,\mathrm{N \cdot s \cdot m^{-1}}$.

Since the MC is eccentric with the respect to the SC along the x-axis, as shown in Figure 3.20, the beam response in the $y - z$ plane is investigated considering coupling effects between bending vibrations in z-direction and torsional vibrations about the elastic axis (i.e. the y-axis). The coupled response will be studied under harmonically-varying, transverse point and distributed forces applied at various positions y along the beam, at distance $x_0 = x_a$ from the elastic axis (specifically, x_a = distance of the MC from the elastic axis).

Figure 3.21 shows the frequency response functions of all response variables along the whole beam, as computed by exact proposed and exact classical methods, for a point force $P = 1$ at $y_0 = 0.25 \cdot L$ and with frequency $\omega = 300$ rad/s. It is seen that the two methods are in excellent agreement, in both real and imaginary parts of the response variables. A further relevant comment is that bending deflection $H(y)$ and deflection $\Psi(y)x_a$ of the MC due to the torsional rotation $\Psi(y)$, reported in the first row of Figure 3.21, have the same order of magnitude, thus meaning that bending-torsion coupling effects are significant. Figure 3.21 also shows that the proposed solutions inherently satisfy the discontinuity conditions prescribed by the equations of motion: a slope discontinuity of the torsional rotation $\Psi(y)$ and a corresponding jump discontinuity of the torque $T(y)$ at the application points of the torsional-rotational damper ($y_2 = 0.5 \cdot L$), translational elastic support ($y_1 = 0.25 \cdot L$) and translational damper ($y_3 = 0.75 \cdot L$), as in fact their reaction forces, being eccentric with respect to the SC, produce also concentrated twisting moments (see support at y_1 and damper at y_3 in Figure 3.20); a slope discontinuity of the bending moment $M(y)$ and a corresponding jump discontinuity of the shear force $S(y)$ at the application

points of the translational elastic support ($y_1 = 0.25 \cdot L$) and translational damper ($y_3 = 0.75 \cdot L$).

Figure 3.22 shows the frequency response amplitudes for the bending deflection $H(y)$, as well as the deflection $\Psi(y)x_a$ of the MC due to the torsional rotation $\Psi(y)$, both computed at $y = 3L/5$, for a point force $P = 1$ with frequency ω spanning $[0, 700]$ rad/s, applied at $y_0 = 0.25 \cdot L$. Consistently with Figure 3.21, it is argued that bending-torsion coupling effects are significant, as indeed peaks of $H(y)$ and $\Psi(y)x_a$ attain the same order of magnitude over most of the frequency range. As in Figure 3.21, exact proposed and classical solutions are in a perfect agreement. Then, in order to provide an exhaustive description, Figures 3.23-3.24 compare the exact frequency response in Figure 3.22 to the corresponding one built by complex mode superposition, using $M = 10$ modes in Eq.(3.168). A very good matching is observed between exact solution and mode superposition solution. For an insight into the modal contributions, the frequency responses of the first four modes are also included in Figures 3.23-3.24. Finally, for a further assessment of the complex modal analysis approach, it is of interest to build the time-domain response by the Duhamel convolution integral (3.169), using $M = 1, 3, 10$ modes in Eq.(3.156) for the impulse response function. In particular, Figure 3.25 shows the bending deflection $h(y, t)$ at $y = 3L/5$, under a point force $P \cdot w(t)$, with $P = 1$ and $w(t) = \sin(250t)$, applied at $y_0 = 0.25L$ as for results in Figures 3.23-3.24; for comparison, the response obtained by the Duhamel convolution integral (3.169) when using the impulse response function built as inverse Fourier transform of the exact frequency response, is also included. The two solutions match very well when $M = 10$ modes are used in Eq.(3.156), mirroring the agreement between the corresponding frequency responses in Figure 3.23.

Next, attention is focused on the frequency response of the beam acted upon by a point force $P = 1$ with frequency $\omega = 300$ rad/s and application point y_0 spanning $[0, L]$. Figure 3.26 and Figure 3.27 show respectively real and imaginary parts of the total deflection frequency response measured at

distance $x_0 = x_a$ from the elastic axis, obtained by adding to the bending deflection $H(y)$ the contribution $\Psi(y)x_a$ due to the torsional rotation $\Psi(y)$, as computed by the exact proposed method. It is seen that the total deflection is symmetric, i.e. $H(y, y_0) - \Psi(y, y_0)x_a = H(y_0, y) - \Psi(y_0, y)x_a$, as expected since it represents indeed the so-called dynamic Green's function of the beam. The symmetry is well evident in the contour plots on the right column of Figures 3.26-3.27 .

As for computational advantages, the exact proposed method involves closed-form expressions (3.222) to compute the frequency response. Instead, the exact classical method requires inverting numerically, for each excitation frequency ω of interest and position of the point force, a 30×30 coefficient matrix, and a 24×24 matrix for the case of distributed force over $\left[\frac{1}{2}L,\ \frac{3}{4}L\right]$. Advantages of the proposed method are significant, especially to construct results in Figures 3.26-3.27 for load spanning the whole beam and, more generally, to carry out parametric investigations on the frequency response.

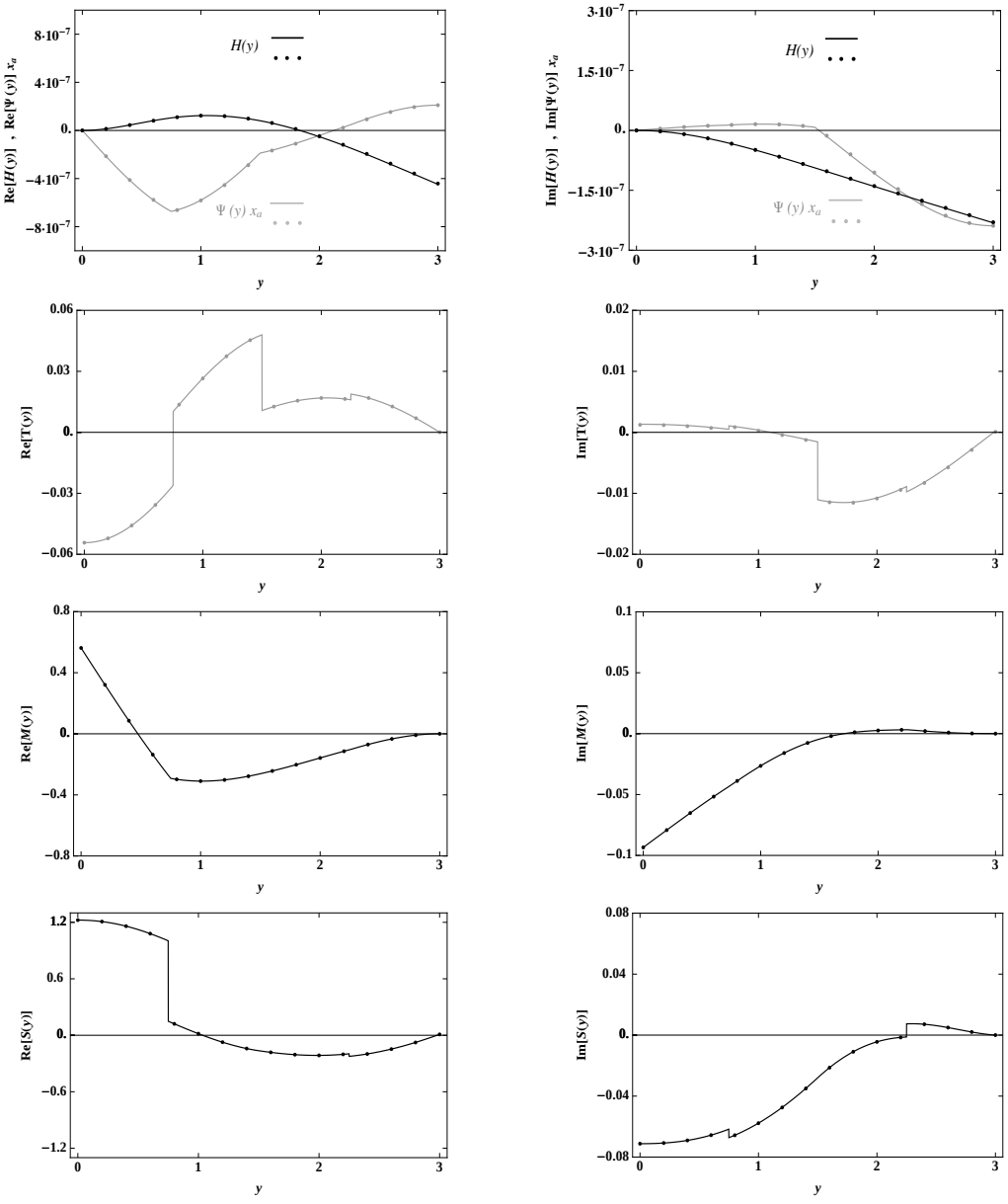

Figure 3.21: Beam in Figure 3.20, frequency response functions due to a transverse point force $P = 1$, applied at $y_0 = 0.25 \cdot L$ and at distance $x_0 = x_a$ from the elastic axis, with frequency $\omega = 300$ rad/s, as computed by exact proposed method (continuous lines) and exact classical method (dotted lines); real part (left column); imaginary part (right column).

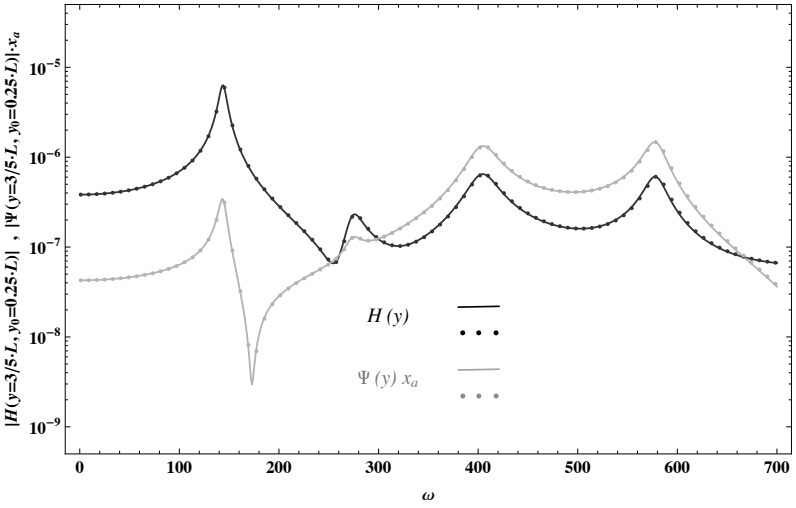

Figure 3.22: Beam in Figure 3.20, frequency response amplitudes for $H(y)$ and $\Psi(y)x_a$, both computed at $y = 3L/5$, for a transverse point force $P = 1$ applied at $y_0 = 0.25 \cdot L$ with frequency ω spanning $[0, 700]$ rad/s, as computed by exact proposed method (continuous lines) and exact classical method (dotted lines).

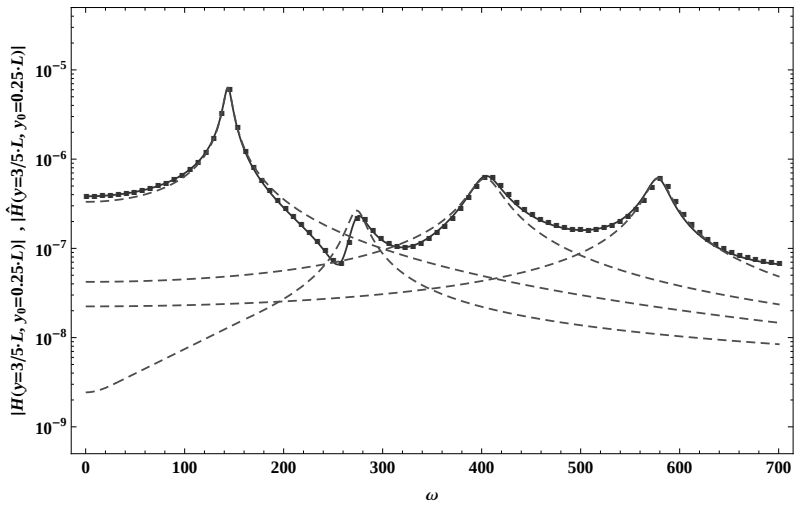

Figure 3.23: Beam in Figure 3.20, frequency response amplitudes for $H(y)$ computed at $y = 3L/5$, for a transverse point force $P = 1$ applied at $y_0 = 0.25 \cdot L$ with frequency ω spanning $[0, 700]$ rad/s, as computed by exact proposed method (continuous line) and mode superposition method: frequency response (3.168) with $M = 10$ (■); modal frequency responses for $k = 1, 2, 3, 4$ (dashed lines).

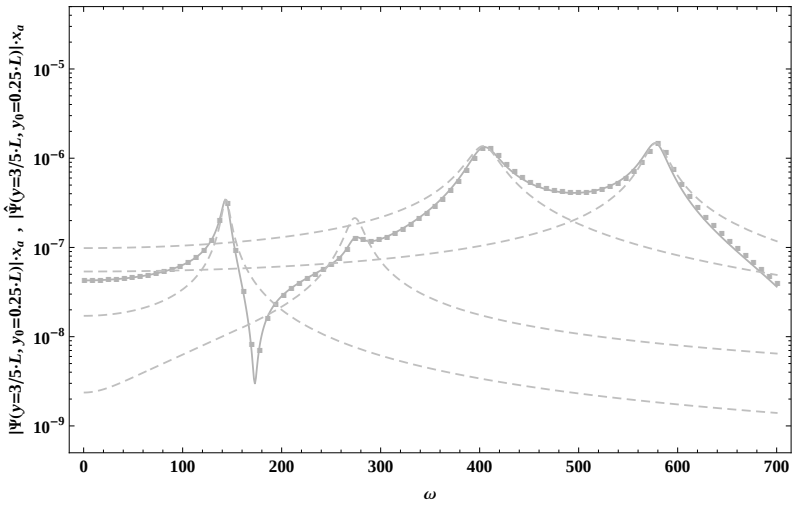

Figure 3.24: Beam in Figure 3.20, frequency response amplitudes for $\Psi(y)x_a$ computed at $y = 3L/5$, for a transverse point force $P = 1$ applied at $y_0 = 0.25 \cdot L$ with frequency ω spanning $[0, 700]$ rad/s, as computed by exact proposed method (continuous line) and mode superposition method: frequency response (3.168) with $M = 10$ (■); modal frequency responses for $k = 1, 2, 3, 4$ (dashed lines).

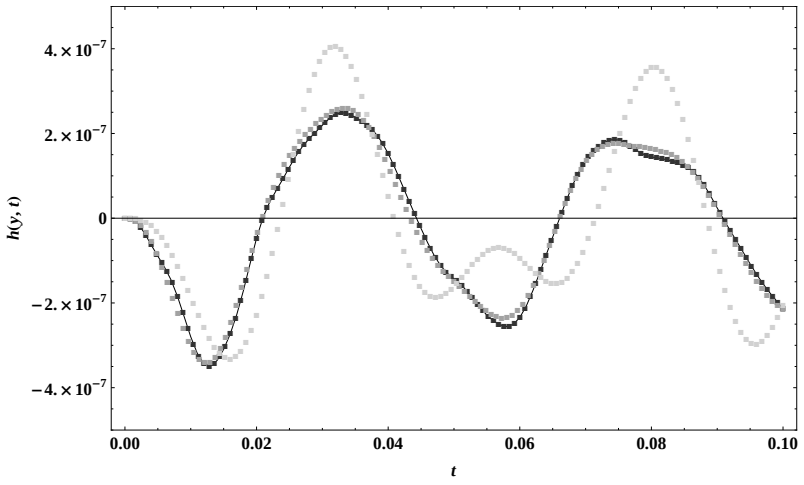

Figure 3.25: Beam in Figure 3.20, bending deflection $h(y, t)$ at $y = 3L/5$ under a transverse point force $P \cdot w(t)$, with $P = 1$ and $w(t) = \sin(250t)$, applied at $y_0 = 0.25L$, as computed by Eq.(3.169) using: (a) the impulse response function built as inverse Fourier transform of the exact frequency response (continuous line); (b) the impulse response function (3.156) with a number of modes $M = 10$ (■); $M = 3$ (■); $M = 1$ (■).

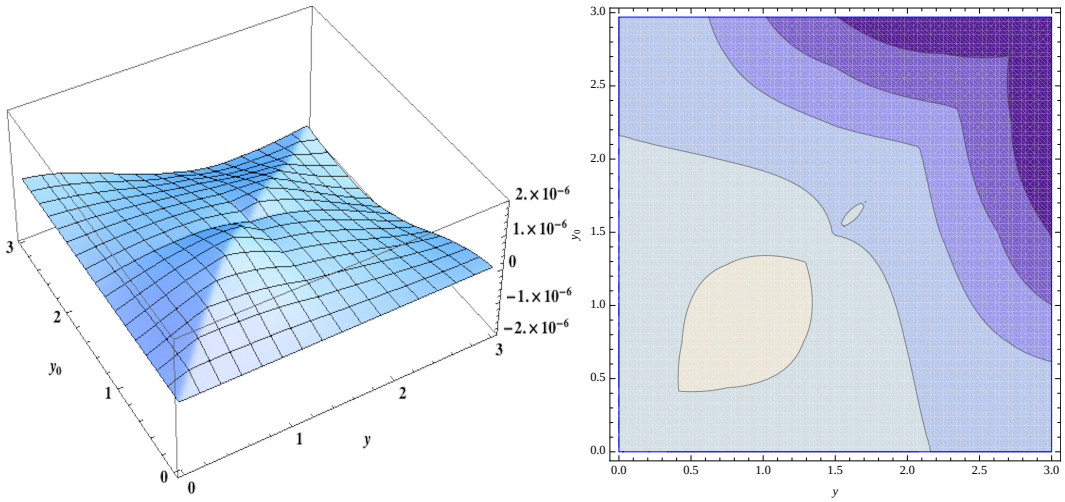

Figure 3.26: Beam in Figure 3.20, total deflection frequency response measured along the beam at distance $x_0 = x_a$ from the elastic axis, for a transverse point force $P = 1$ spanning the whole domain $[0, L]$, with frequency $\omega = 300$ rad/s; real part (left column) and corresponding contour plot (right column).

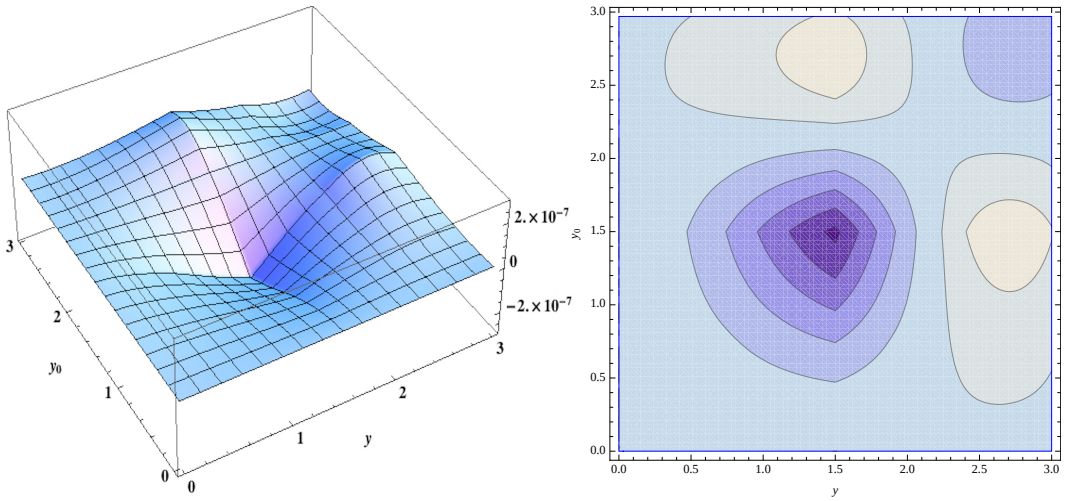

Figure 3.27: Beam in Figure 3.20, total deflection frequency response measured along the beam at distance $x_0 = x_a$ from the elastic axis, for a transverse point force $P = 1$ spanning the whole domain $[0, L]$, with frequency $\omega = 300$ rad/s; imaginary part (left column) and corresponding contour plot (right column).

Example B

Consider the clamped-clamped beam with a "Tee" cross section depicted in Figure 3.28, with the following parameters:
$I = 3.6624{\cdot}10^{-4}\,\mathrm{m}^4$, $J = 1.3791{\cdot}10^{-5}\,\mathrm{m}^4$, $I_\alpha = 13.0103\,\mathrm{kg{\cdot}m}$, $x_a = 0.1205\,\mathrm{m}$, $L = 6\,\mathrm{m}$, $m = 261.7562\,\mathrm{kg}\cdot\mathrm{m}^{-1}$, $E = 210\cdot10^9\mathrm{N}\cdot\mathrm{m}^{-2}$, $G = 80.7692\cdot10^9\mathrm{N}\cdot\mathrm{m}^{-2}$, $h = l = 0.5\mathrm{m}$, $t = 0.035\,\mathrm{m}$.

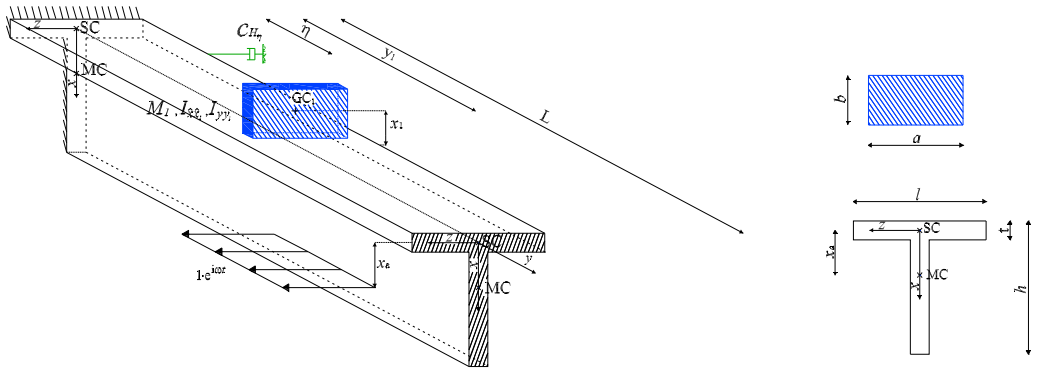

Figure 3.28: Clamped-clamped beam with "Tee" section carrying an attached mass and a pure viscous damper, subjected to a harmonically-varying transverse uniformly-distributed force.

First, it is assumed that the beam carries a mass M_1, modeled as a rectangular plate with $a = 0.5\,\mathrm{m}$ and $b = 1\,\mathrm{m}$, located at $y_1 = 0.5 \cdot L$; its gravity center along the x-axis is at distance $x_1 = -0.5175$ from the SC of the beam cross section. Bending and torsional vibrations are coupled in the $y-z$ plane because the MC of the beam cross section and the gravity center of the attached mass are eccentric, along the x-axis, with respect to the SC of the beam cross section (on the contrary, there is no coupling in the $x-y$ plane). Therefore, attention will focus on coupled bending-torsional dynamics in the $y-z$ plane, considering free and forced vibrations.

First, free vibration analysis is carried out. The characteristic equation is obtained as determinant of matrix $\mathbf{B}$ in Eq.(3.151), setting $\mathbf{r} = \mathbf{0}$. Table 3.6 reports the natural frequencies of the first three modes for different values of mass M_1, computed by exact proposed and classical methods. The natural

frequencies are real because no dampers are considered and, as expected, they decrease as M_1 increases. Figures 3.29, 3.30, 3.31 show the first three eigenfunctions of some response variables, associated with the first three natural frequencies in Table 3.6 (symbols Φ_H, Φ_Ψ, Φ_M, Φ_S, Φ_T are used in Figures 3.29, 3.30, 3.31 to indicate real eigenfunctions); particularly, it is assumed that $M_1 = 153.7\,\text{kg}$ and $I_{xx_1} = 3.20\,\text{kg}\cdot\text{m}^2$, $I_{yy_1} = 16.02\,\text{kg}\cdot\text{m}^2$. In order to show the coupling between bending and torsional responses, left and right columns of Figure 3.29 report respectively the bending deflection $\Phi_H(y)$, as well as the deflection of the MC of the beam cross section due to torsional response, computed as $\Phi_\Psi(y)x_a$. It can be noticed that bending and torsional contributions have similar order of magnitude in second and third mode, while the torsional contribution is dominant in the first mode.

Next, consider the beam in Figure 3.28 subjected to a harmonic transverse distributed force with frequency ω, acting on the interval $\frac{3}{4}L < y < L$ in z-direction, and applied at distance $x_c = x_a = 0.1205\,\text{m}$ from the elastic axis; again $M_1 = 153.7\,\text{kg}$ and $I_{xx_1} = 3.20\,\text{kg}\cdot\text{m}^2$, $I_{yy_1} = 16.02\,\text{kg}\cdot\text{m}^2$. Now it is of interest to study the forced frequency response when a translational viscous damper is applied to the beam for vibration mitigation. Specifically, in order to show how important are bending-torsion coupling effects in the beam response, the optimal position of the damper will be sought by adopting the present elementary coupled bending-torsion theory, as well as the pure bending Euler-Bernoulli theory only. For simplicity, it will be assumed that the translational viscous damper features a viscous coefficient $c_{H_\eta} = 5\cdot 10^3\,\text{Ns/m}$ and is applied at distance $x_\eta = 0$ from the elastic axis. Different positions will be explored along the y-axis.

For a first insight, assume that the viscous damper is applied at location $\eta = 0.5\cdot L$. Figure 3.32 shows the frequency response amplitude for the bending deflection $H(y)$ and the deflection of the MC of the beam cross section $\Psi(y)x_a$ due to torsional rotation, computed at $y = 0.14\cdot L$ for ω spanning $[0, 350]$. It is evident that coupling effects are significant, especially at second and third modes where the magnitude of the peaks is practically the

same for $H(y)$ and $\Psi(y)x_a$. It is also seen that the torsional response does not vanish as $\omega \to 0$ because, in the case under study, the distributed force has an eccentricity $x_c = 0.1205$ from the elastic axis. Next, in order to compare the coupled bending-torsion theory with the pure bending Euler-Bernoulli theory, the bending deflection frequency response $H(y)$ reported in Figure 3.32 is compared, in Figure 3.33, with the corresponding bending deflection frequency response that is obtained by the pure bending Euler-Bernoulli theory, referred to as $W(y)$ to avoid confusion (frequency dependence in $W(y)$ is omitted for brevity). It is noticed that $W(y)$, according to the Euler-Bernoulli theory, is the solution of the following uncoupled equation of motion:

$$EI\frac{\bar{d}^4 W}{dy^4} - m\omega^2 W - \sum_{j=1}^{N} P_j^{(W)}\delta(y-y_j) + \sum_{j=1}^{N} Mf_j^{(W)}\delta^{(1)}(y-y_j) - f(y) = 0 \tag{3.184}$$

where $P_j^{(W)}(\omega) = -\kappa_{P_j}(\omega)W(y_j)$, $Mf_j^{(W)}(\omega) = -\kappa_{M_j}(\omega)W'(y_j)$, being $W' = \dfrac{\bar{d}W}{dy}$. The solution of Eq.(3.184) can be obtained again via generalized functions or alternatively through the exact classical method. From Figure 3.33 it is well evident that the frequency responses are different, with the Euler-Bernoulli theory predicting its first mode at about $\omega = 301.5\,\text{rad/s}$, i.e. very close to the third mode of the coupled bending-torsion theory.

Further, in order to show how different may be the predictions of the coupled bending-torsion theory and the Euler-Bernoulli theory, it is assumed that the frequency of the distributed force in Figure 5.12 is $\omega = 301.5\,\text{rad/s}$, i.e. very close to the peaks of the coupled bending-torsion third mode and Euler-Bernoulli first mode in Figure 3.33. Let the application point of the viscous damper vary along the y-axis, in order to determine its optimal position according to the two theories. Figure 3.34 shows the bending deflection $W(y)$ along the whole beam according to the Euler-Bernoulli theory, while Figure 3.35 shows the bending deflection $H(y)$ along the beam according to the coupled bending-torsion theory. From Figure 3.34 it is seen that the viscous damper becomes ineffective near the clamped ends. On the contrary,

from Figure 3.35 it is apparent that the viscous damper becomes ineffective also when applied at the mid-span, consistently with Figure 3.29 where it is evident that a mid-span translational damper is not activated when the beam vibrates at its coupled bending-torsion third mode. Consistently with Figures 3.34-3.35, Figures 3.36-3.37 show the maximum value of the bending deflection along the beam, $H_{max} = max\left\{[|H(y)|, 0 < y < L]\right\}$ from the coupled bending-torsion theory and $W_{max} = max\left\{[|W(y)|, 0 < y < L]\right\}$ from the Euler-Bernoulli theory, for different values of the damper position. Figures 3.36-3.37 show that the optimal position of the damper considering Euler-Bernoulli theory is near $0.5 \cdot L$ while, for the same position, the damper is totally ineffective considering the coupled bending-torsion theory, as deduced also from Figure 3.29. It is then concluded that the Euler-Bernoulli theory would predict incorrectly the dynamics of the beam in Figure 3.28, and that bending-torsion coupling effects cannot be ignored when applying dampers for vibration mitigation.

	Mode 1		Mode 2		Mode 3	
$M_1\,(kg)$	C. M.	P. M.	C.M.	P.M.	C.M.	P.M.
100	106.351	106.352	281.789	281.789	301.495	301.493
153.7	93.4846	93.4844	266.263	266.261	301.492	301.491
200	85.3273	85.3276	258.696	258.695	301.490	301.490
250	78.4786	78.4782	253.227	253.223	301.489	301.488

Table 3.6: Beam in Figure 3.28, natural frequencies (rad/s) for different values of mass M_1, as computed by exact classical method (C.M.) and exact proposed method (P.M.).

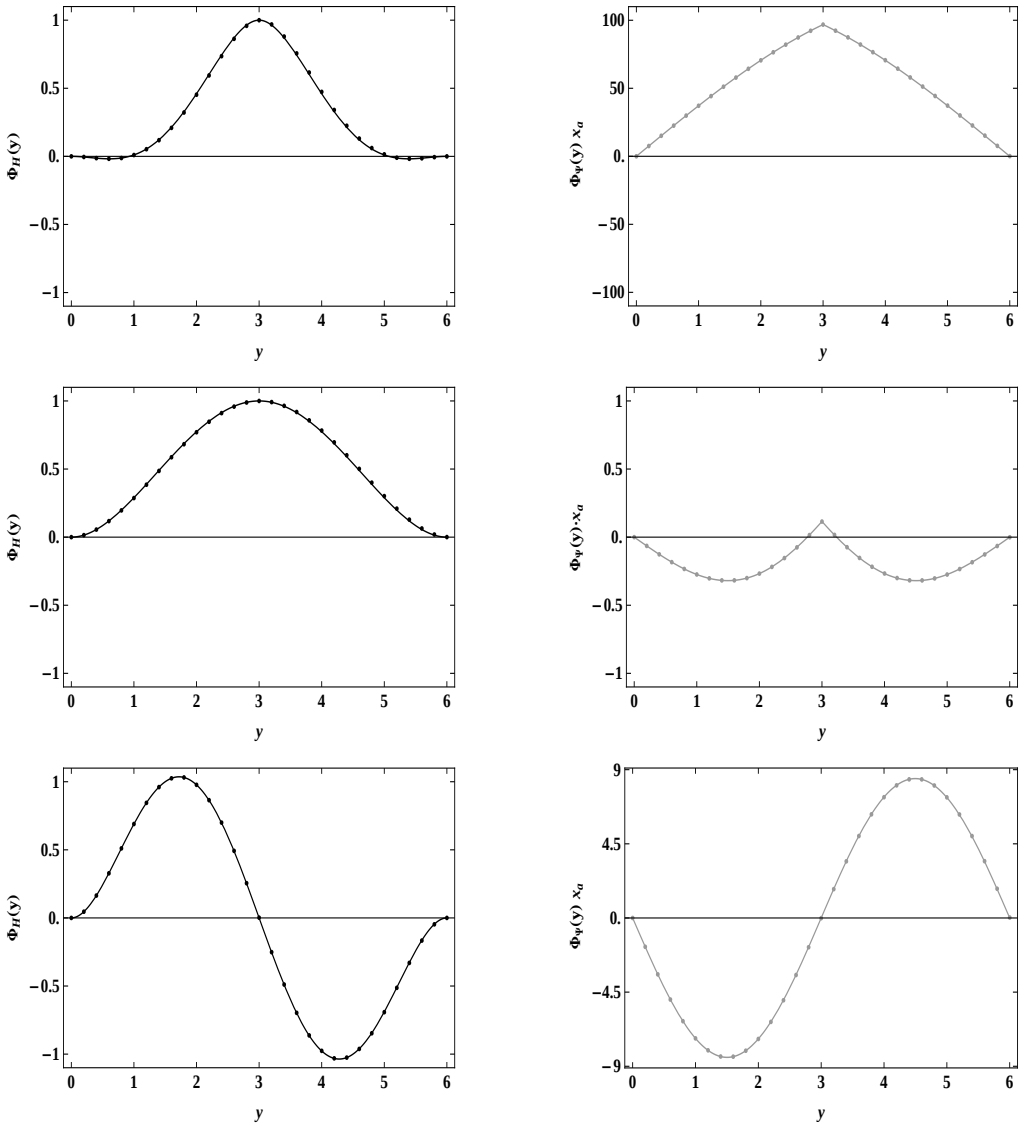

Figure 3.29: Beam in Figure 3.28, eigenfunctions of first 3 modes (from top to bottom): bending deflection (left column), compared with deflection of beam cross-section MC due to torsional response (right column), as computed by exact proposed method (continuous lines) and exact classical method (dotted lines).

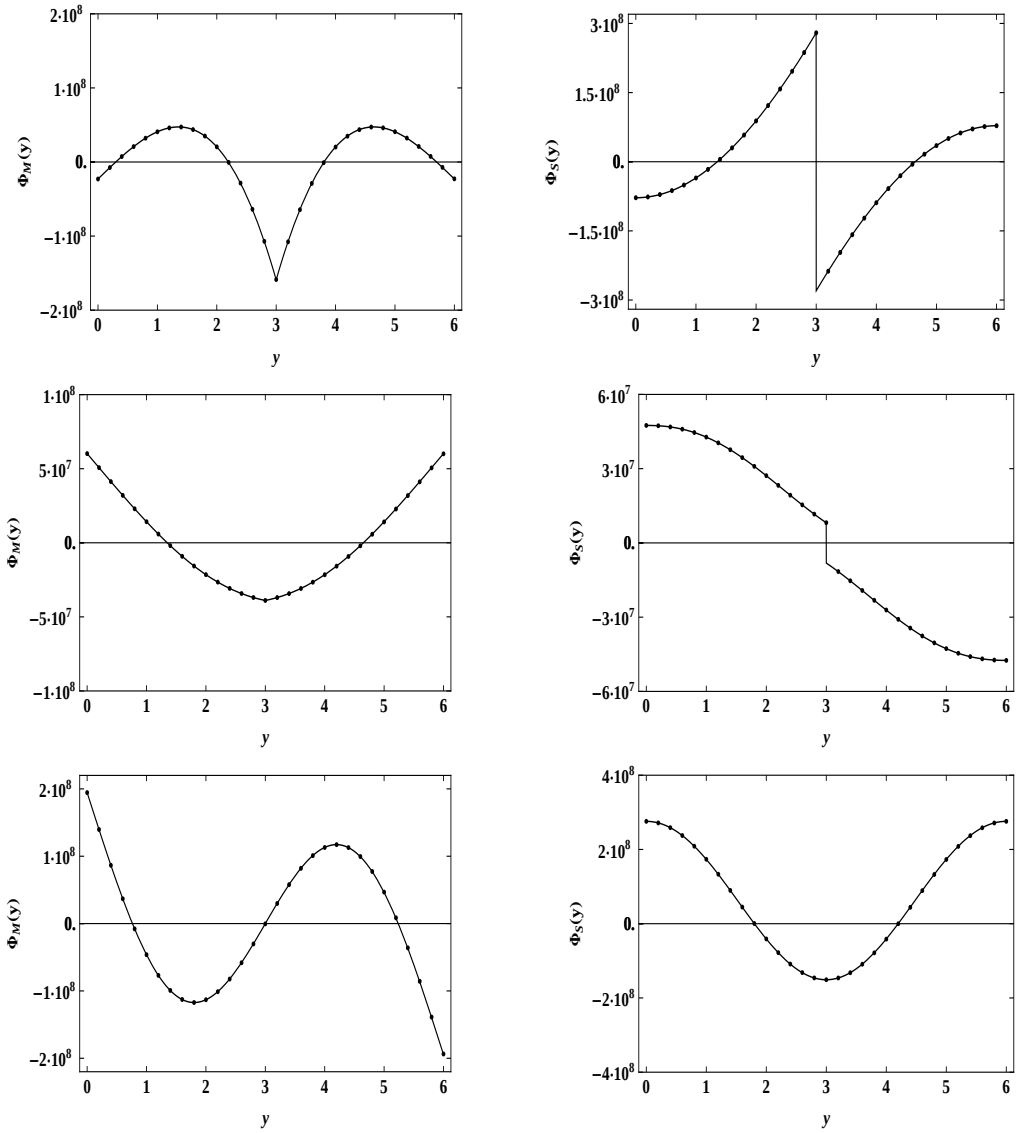

Figure 3.30: Beam in Figure 3.28, eigenfunctions of first 3 modes (from top to bottom): bending moment (left column), and shear force (right column), as computed by exact proposed method (continuous lines) and exact classical method (dotted lines).

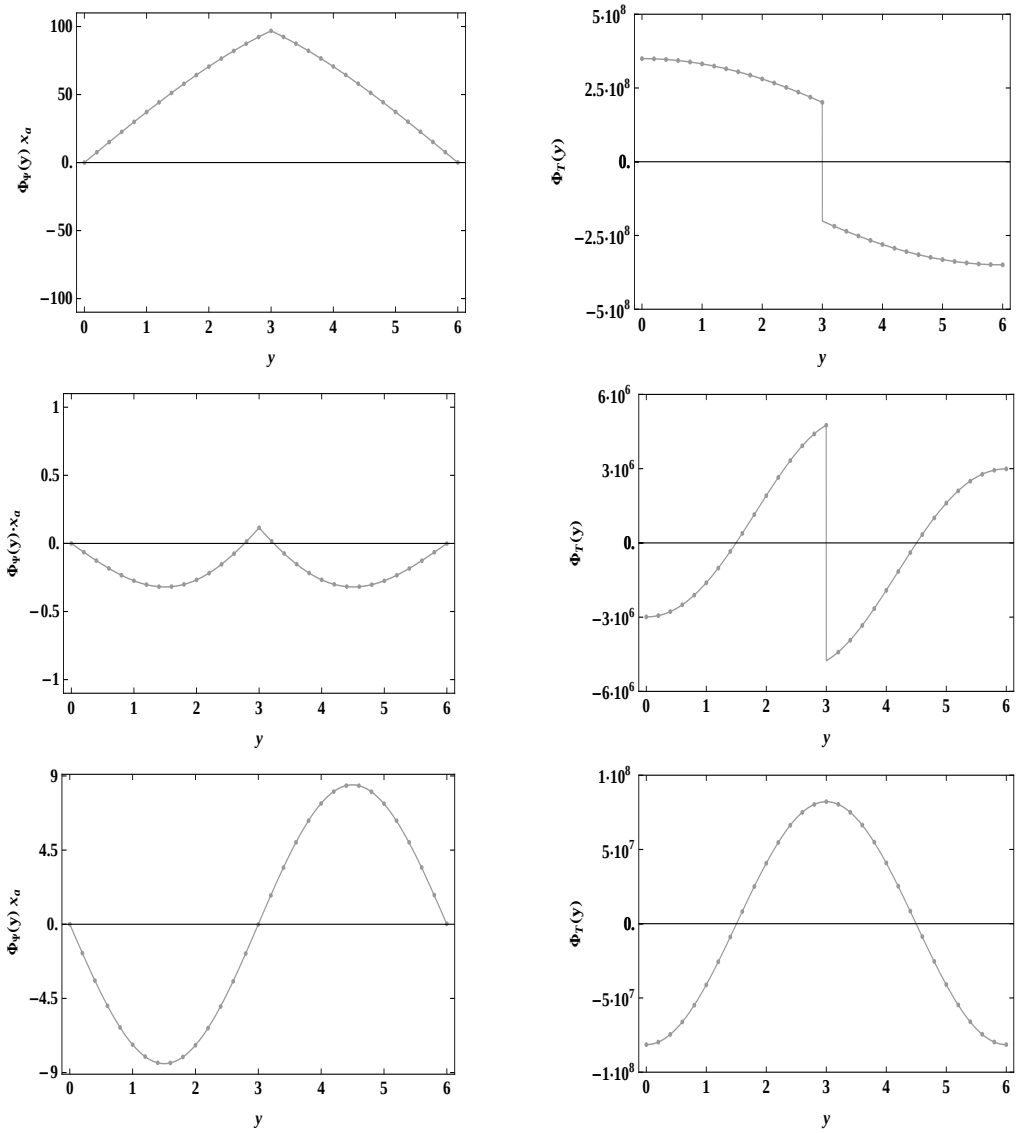

Figure 3.31: Beam in Figure 3.28, eigenfunctions of first 3 modes (from top to bottom): torsional rotation (left column), and torque (right column), as computed by exact proposed method (continuous lines) and exact classical method (dotted lines).

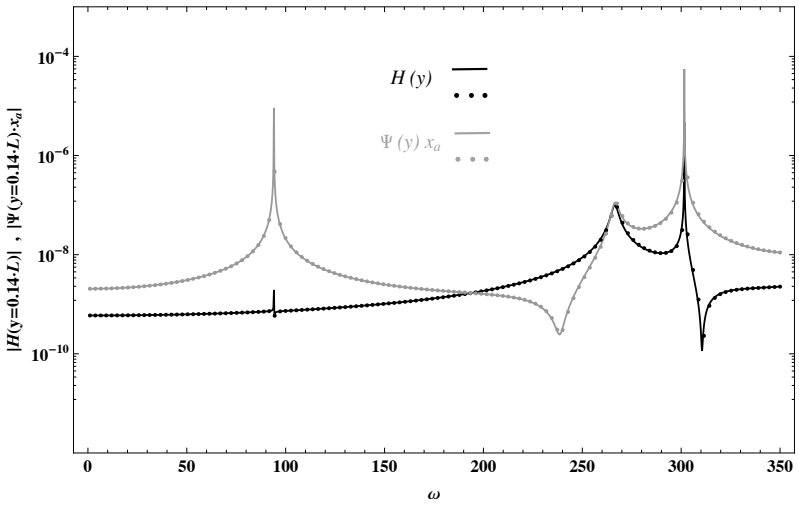

Figure 3.32: Beam in Figure 3.28, frequency response amplitude for $H(y)$ (black lines) and $\Psi(y)x_a$ (gray lines), both computed at $y = 0.14 \cdot L$ for a transverse uniformly-distributed force $f(y) = 1$ over $\left[\frac{3}{4}L, L\right]$; exact proposed method (continuous lines), exact classical method (dotted lines).

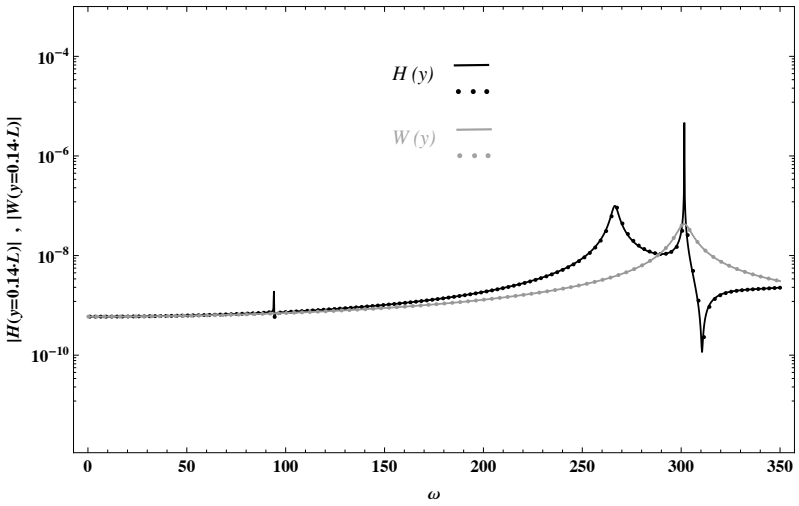

Figure 3.33: Beam in Figure 3.28, comparison between frequency response amplitudes for $H(y)$ (black lines) and $W(y)$ (gray lines), both computed at $y = 0.14 \cdot L$ for a transverse uniformly-distributed force $f(y) = 1$ over $\left[\frac{3}{4}L, L\right]$; exact proposed method (continuous lines), exact classical method (dotted lines).

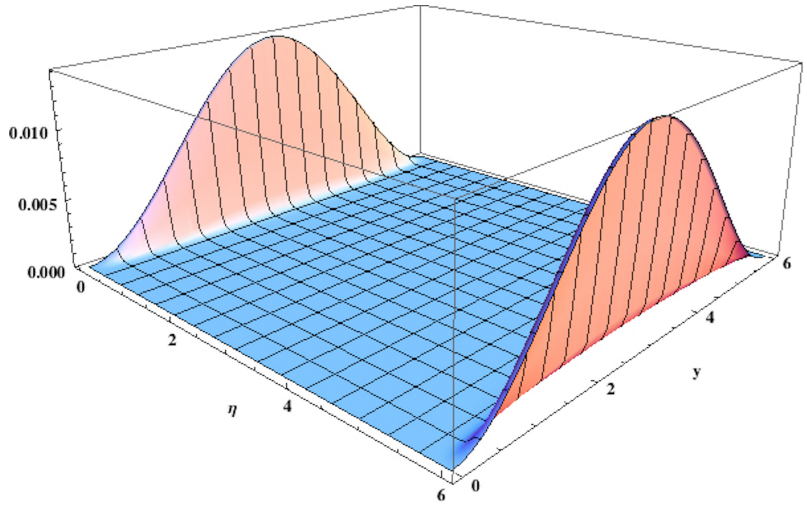

Figure 3.34: Beam in Figure 3.28, frequency response amplitude for $W(y)$ along the beam, due to a transverse uniformly-distributed force $f(y) = 1$ over $\left[\frac{3}{4}L, L\right]$, with frequency $\omega = 301.5$ rad/s, for damper position η varying over the whole domain $[0, L]$.

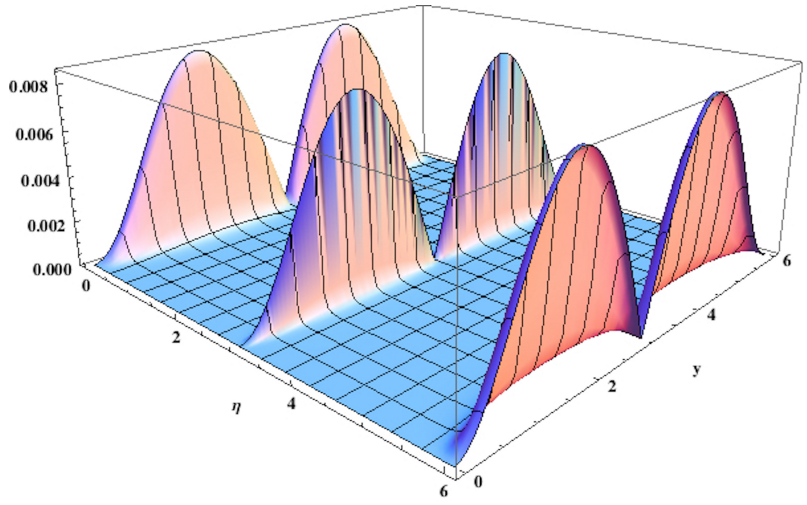

Figure 3.35: Beam in Figure 3.28, frequency response amplitude for $H(y)$ due to a transverse uniformly-distributed force $f(y) = 1$ over $\left[\frac{3}{4}L, L\right]$, with frequency $\omega = 301.5$ rad/s, for damper position η varying over the whole domain $[0, L]$.

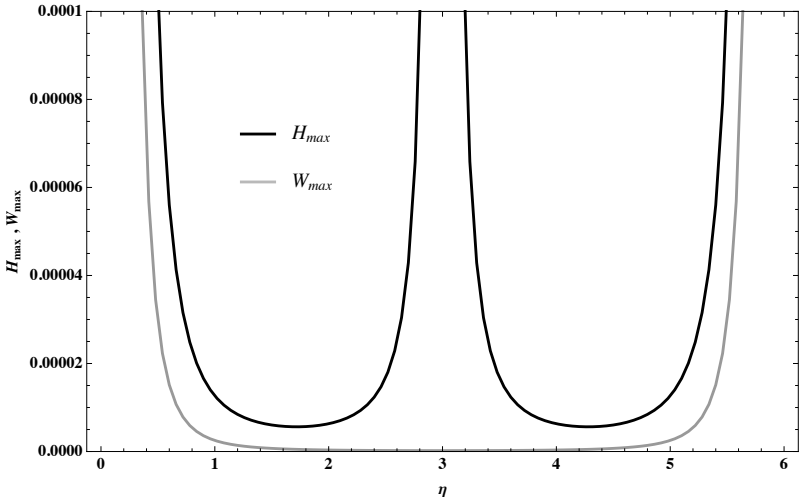

Figure 3.36: Beam in Figure 3.28, comparison between H_{max} and W_{max}, i.e. maxima amplitudes of frequency responses $H(y)$ and $W(y)$, for different damper positions η.

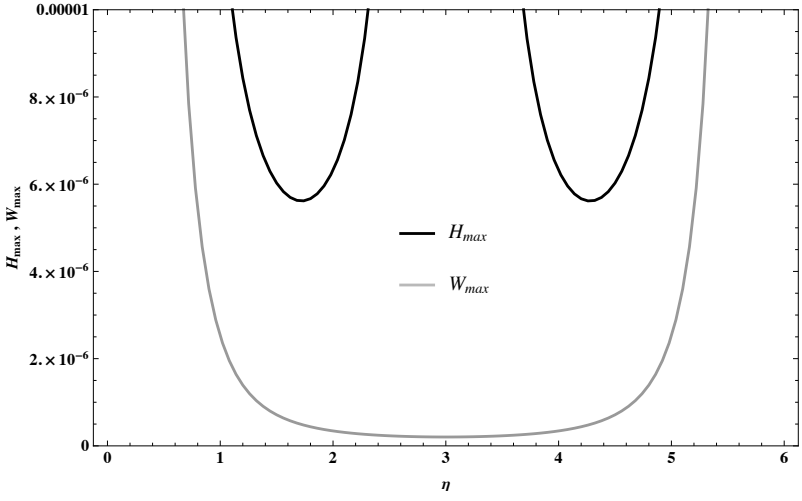

Figure 3.37: Beam in Figure 3.28, comparison between H_{max} and W_{max}, i.e. maxima amplitudes of frequency responses $H(y)$ and $W(y)$, for different damper positions η; zoomed view of Figure 3.36 for ordinate range $[0, 0.00001]$.

3.5 Coupled bending-torsional vibrations of discontinuous beams with mono symmetric cross sections (warping effects included)

As discussed in the previous Section, beams with mono-symmetric cross section are involved as basic components in different structures for engineering applications. Investigation on dynamics of such beams requires appropriate theories, since cross section asymmetry implies coupled-bending torsional vibrations; particularly, coupling effects arise because shear centre (SC) and mass center (MC) of the beam cross section do not coincide.

Different authors have investigated the dynamics of coupled bending-torsional beams, as seen in the previous Section. But, authors in refs.[45, 46, 47, 48, 52, 64], as well as refs.[50, 60, 62], assume that beams twist according to the Saint-Venant theory, i.e. warping effects of the beam cross section are not considered. This assumption is reasonable for beams with angular cross sections, with circular section or with compact sections, but for other types of beams will lead to wrong dynamic analysis. Timoshenko [53] was one of the first to present the set of coupled equations of motion including warping stiffness, obtaining the exact modal solutions for simply supported beams. Extending the Dokumaci's work [46] by including the warping effects, Bishop et al.[54] showed that omitting these effects leads to relevant errors in the coupled frequencies of a beam with thin-walled open cross section. Similar conclusions were drawn by Bercin and Tanaka [55] who, analyzing free vibrations of coupled bending-torsional Timoshenko beams with end cantilever conditions, showed that neglecting warping effects, rotatory inertia and shear effects may lead to relevant errors when thickness or modal index increase. In ref. [56], they extended the study to beams with arbitrary cross sections through the finite element method. A great impulse to the study of coupled bending-torsional problems was given by Banerjee [57], who gave exact analytical expressions for a coupled bending-torsional dynamic stiffness matrix,

for any B.C, including warping effects. Similarly to refs.[54, 55, 56], he underlined that warping effects may affect significantly the natural frequencies of some thin-walled open cross-section beams.

Forced vibration analysis of coupled bending-torsion beam including warping stiffness was led by Adam in ref.[63], where the solution of the governing equations of motion was found separating the response of the beam in a quasistatic and in a complementary part. More recently, Sapountzakis et al. in ref. [65, 66, 67] developed a boundary element method for the general flexural-torsional vibrations of beams of arbitrarily shaped constant cross section, taking into account warping effects and considering both free and forced vibrations.

As widely discussed in this thesis, many engineering problems involve beams carrying different types of attachments as dampers, supports and attached masses. Nevertheless, only few works have focused on coupled bending-torsional beams with attachments [68, 69] and [70, 71, 72, 73, 74] as shown in the previous Section.

This Section deals with the frequency response of coupled bending-torsional beams carrying an arbitrary number of attachments, particularly attached masses, translational dampers and torsional-rotational dampers, all featuring Kelvin-Voigt viscoelastic behavior. Unlike the previous Section, equations of motion are derived making use of coupled bending-torsion theory including warping effects and taking advantage of generalized functions (see Chapter 2) to model the discontinuities of response variables at the application points of dampers/masses. Novel exact expressions of the frequency response are obtained in closed analytical form, which hold for harmonically-varying polynomial loads arbitrarily placed along the beam, and any number of dampers/masses. The exact analytical expression of the dynamic Green's functions of the beam, i.e. the frequency response to an arbitrarily-placed point load, is also obtained. On the basis of the same analytical framework free vibration analysis is led. Specifically, exact natural frequencies and closed-form eigenfunctions will be calculated from a characteristic equation

built as determinant of a 8×8 matrix, for any number of dampers/masses. The final step would involve a complex modal analysis approach to obtain the modal frequency response functions and modal impulse response functions of the beam, upon introducing pertinent orthogonality conditions for the modes. Since this step is very similar to that developed in the previous Section, it is not reported for brevity.

Warping effects on natural frequencies and dynamics of the beam are discussed, comparing results with those obtained based on the elementary coupled bending-torsion theory [45, 46, 47, 48, 50, 52, 60, 62], i.e. neglecting warping effects.

The Section is organized as follows. Firstly, the equations governing the beams under study are formulated. Next, frequency response is derived. Finally, two numerical applications are proposed.

3.5.1 Problem statement

The beam under study is depicted in Figure 3.38: a straight uniform beam, referred to a right handed coordinate system (Oxyz), carrying an arbitrary number of translational and torsional-rotational Kelvin-Voigt dampers, as well as attached masses.

The beam has length L and its cross section is mono-symmetric, with x axis of symmetry. The elastic axis, i.e. the locus of the SCs of the beam cross sections, coincides with the y-axis; the mass axis, which is the locus of the MCs of the beam cross sections, is assumed to be at distance x_a from the elastic axis. Let $h(y,t)$, $\theta(y,t)$, $\psi(y,t)$, $\psi'(y,t)$ be the bending deflection in the z-direction, the bending rotation about the x-axis and the torsional rotation about the y-axis of the SCs and the torsion respectively, and $\mu(y,t)$, $s(y,t)$, $\tau(y,t)$ and $b(y,t)$ the bending moment, shear force, torque and bimoment, being t the time.

The application point of a damper/attached mass along the y-axis is indicated with y_j, with $0 < y_1 < \cdots < y_j < \cdots < y_N < L$, while stiffness and damping parameters of the j-th damper and properties of the j-th mass are

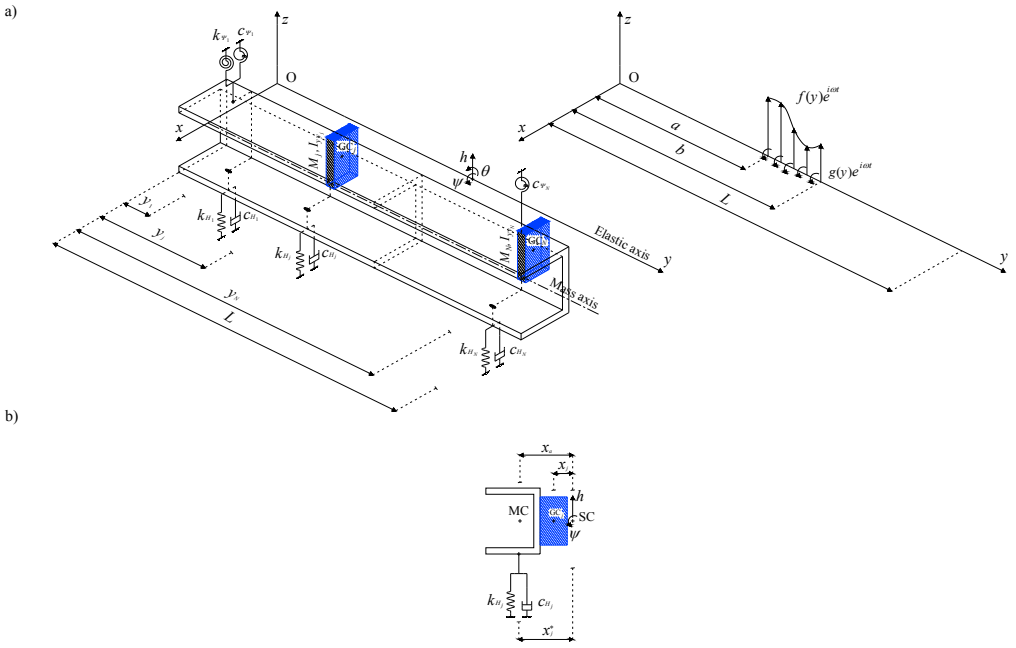

Figure 3.38: a) Beam with mono-symmetric cross section carrying an arbitrary number of Kelvin-Voigt dampers and attached masses (represented as shaded boxes), subjected to harmonically-varying distributed loads; b) Beam cross section at $y = y_j$.

denoted as follows:

- k_{H_j}, c_{H_j} for translational dampers, k_{Ψ_j}, c_{Ψ_j} for torsional-rotational dampers.
- M_j is the mass and I_{yy_j} the mass inertia moment about the y-axis in Figure 3.38.

In the context above, rigid translational or torsional-rotational supports can also be modeled, in approximate way, assuming suitably large numerical values for k_{H_j} or k_{Ψ_j}, and setting $c_{H_j} = c_{\Psi_j} = 0$.

As in the previous Section, two assumptions are made to ensure that twisting is coupled with bending in z-direction only:

1. The gravity center of the j-th attached mass is at distance $z_j = 0$ from the elastic axis.

2. The principal axes of the j-th attached mass are parallel to those of the beam cross section.

It is pointed out that, in this Section, bending and torsional vibrations are studied including the effects of warping stiffness in the equations of motion [53, 54, 55, 56, 57, 63, 65, 66, 67, 69]; rotatory inertia and shear deformation of the beam are not considered.

By using the coupled bending-torsion beam theory including warping effects and taking advantage of generalized functions (see Chapter 2), the following set of equations governing the flexural and torsional problems can be written (frequency dependence of the response variables is omitted for brevity):

$$\theta(y,t) = \frac{\bar{\partial} h(y,t)}{\partial y} \tag{3.185}$$

$$\mu(y,t) = EI\frac{\bar{\partial}\theta(y,t)}{\partial y} \tag{3.186}$$

$$s(y,t) = -\frac{\bar{\partial}\mu(y,t)}{\partial y} \tag{3.187}$$

$$\frac{\bar{\partial} s(y,t)}{\partial y} = m\frac{\partial^2 h(y,t)}{\partial t^2} - mx_a\frac{\partial^2\psi(y,t)}{\partial t^2} - \sum_{j=1}^{N} p_j(t)\delta(y-y_j) - f(y,t) \tag{3.188}$$

$$\tau(y,t) = GJ\frac{\bar{\partial}\psi(y,t)}{\partial y} - E\Gamma\frac{\bar{\partial}^3\psi(y,t)}{\partial y^3} \tag{3.189}$$

$$\begin{aligned}\frac{\bar{\partial}\tau(y,t)}{\partial y} &= I_\alpha\frac{\partial^2\psi(y,t)}{\partial t^2} - mx_a\frac{\partial^2 h(y,t)}{\partial t^2} + \sum_{J=1}^{N} p_j(t)x_j\delta(y-y_j) \\ &- \sum_{j=1}^{N} Mt_j\,\delta(y-y_j) - g(y,t)\end{aligned} \tag{3.190}$$

from which the coupled governing equations, for the flexural problem (3.191) and the torsional problem (3.192) can be derived

$$EI\frac{\bar{\partial}^4 h(y,t)}{\partial y^4} + m\frac{\partial^2 h(y,t)}{\partial t^2} - mx_a\frac{\partial^2 \psi(y,t)}{\partial t^2} - \sum_{j=1}^{N} p_j(t)\delta(y-y_j) - f(y,t) = 0 \tag{3.191}$$

$$\begin{aligned} E\Gamma\frac{\bar{\partial}^4 \psi(y,t)}{dy^4} - GJ\frac{\bar{\partial}^2 \psi(y,t)}{dy^2} + I_\alpha\frac{\partial^2 \psi(y,t)}{\partial t^2} - mx_a\frac{\partial^2 h(y,t)}{\partial t^2} \\ + \sum_{j=1}^{N} p_j(t)x_j\delta(y-y_j) - \sum_{j=1}^{N} mt_j(t)\delta(y-y_j) - g(y,t) = 0 \end{aligned} \tag{3.192}$$

where bar means generalized derivative (see Chapter 2), EI, $E\Gamma$ and GJ are respectively bending, warping and torsional rigidities, m is the mass per unit length, while I_α is the polar moment of inertia per unit length about the elastic axis. In Eqs (3.191)-(3.192) $p_j(t)$ and $mt_j(t)$ are concentrated force and twisting moment associated with dampers and attached masses at y_j.

3.5.2 Direct frequency analysis

Assume that the vibration response of the system in Figure 3.38 can be represented in the form

$$\mathbf{v} = \mathbf{Y}e^{i\omega t} \tag{3.193}$$

where $\mathbf{v} = \{h\ \theta\ \mu\ s\ \phi\ \ \phi'\ \tau\ b\}$ and $\mathbf{Y} = \{H\ \Theta\ M\ S\ \Phi\ \Phi'\ T\ B\}$ collect the response variable of the beam. Eq.(3.193) is a general form to represent:

1. The frequency response function, that is the steady state response under an harmonic force $f(y,t) = f(y)e^{i\omega t}$ and twisting moment $g(y,t) = g(y)e^{i\omega t}$ with any frequency ω, i.e. $\mathbf{Y} = \mathbf{Y}(x,\omega)$

2. Free vibration response setting $f(y,t) = g(y,t) = 0$, and being $\omega = \omega_n$ an eigenvalue and $\mathbf{Y} = \mathbf{Y}_n(x)$ the corresponding vectors of eigenfunc-

tions; in general, the damping in the system is not proportional, then eigenvalues and eigenfunctions will be complex.

Introducing Eq.(3.193) in equations of motion yelds

$$EI\frac{\bar{d}^4H}{dy^4} - m\omega^2 H + mx_a\omega^2\Psi - \sum_{j=1}^{N} P_j\delta(y-y_j) - f(y) = 0 \tag{3.194}$$

$$\begin{aligned} E\Gamma\frac{\bar{d}^4\Psi}{dy^4} - GJ\frac{\bar{d}^2\Psi}{dy^2} - I_\alpha\omega^2\Psi + m\omega^2 x_a H + \sum_{j=1}^{N} P_j x_j\delta(y-y_j) \\ - \sum_{j=1}^{N} Mt_j\delta(y-y_j) - g(y) = 0 \end{aligned} \tag{3.195}$$

In Eqs (3.194)-(3.195) P_j and Mt_j are concentrated force and twisting moment associated with dampers and attached masses at y_j, given as:

$$P_j = -\kappa_{P_j}(\omega)[H(y_j) - x_j\Psi(y_j)] \tag{3.196}$$

$$Mt_j = -\kappa_{T_j}(\omega)\Psi(y_j) \tag{3.197}$$

In Eq.(3.196)-(3.197) $H(y_j)$ and $\Psi(y_j)$ are the deflection and torsional rotation at $y = y_j$, and $\kappa_{P_j}(\omega)$, $\kappa_{T_j}(\omega)$ are frequency-dependent terms given as:

$$\kappa_{P_j}(\omega) = k_{H_j} + i\omega c_{H_j} - M_j\omega^2 \tag{3.198}$$

$$\kappa_{T_j}(\omega) = k_{\Psi_j} + i\omega c_{\Psi_j} - (I_{yy_j} - M_j x_j^2)\omega^2 \tag{3.199}$$

Eqs.(3.194)-(3.195) can be combined, by eliminating either H or Ψ, to obtain 8-th order differential equations for deflection and torsional rotation:

$$\alpha\frac{\bar{d}^8H}{dy^8}+\beta\frac{\bar{d}^6H}{dy^6}+\gamma\frac{\bar{d}^4H}{dy^4}+\eta\frac{\bar{d}^2H}{dy^2}+\lambda H+\frac{I_a\omega^2}{mx_a\omega^2}f(y)+\frac{GJ}{mx_a\omega^2}f^{[2]}(y) - \frac{E\Gamma}{mx_a\omega^2}f^{[4]}(y)-g(y)+R_{H_{ext}}(y)=0 \tag{3.200}$$

$$\alpha\frac{\bar{d}^8\Psi}{dy^8}+\beta\frac{\bar{d}^6\Psi}{dy^6}+\gamma\frac{\bar{d}^4\Psi}{dy^4}+\eta\frac{\bar{d}^2H}{dy^2}+\lambda H+f(y)-\frac{EI}{mx_a\omega^2}g^{[4]}(y)+\frac{m\omega^2}{mx_a\omega^2}g(y) + R_{\Psi_{ext}}(y)=0 \tag{3.201}$$

where $R_{H_{ext}}(y), R_{\Psi_{ext}}(y)$ are the following generalized functions:

$$R_{H_{ext}}(y)=\sum_{j=1}^{N}P_j\left[(\frac{I_a\omega^2}{mx_a\omega^2}-x_j)\delta(y-y_j)+\frac{GJ}{mx_a\omega^2}\delta^{(2)}(y-y_j) - \frac{E\Gamma}{mx_a\omega^2}\delta^{(4)}(y-y_j)\right]-\sum_{j=1}^{N}Mt_j\delta(y-y_j) \tag{3.202}$$

$$R_{\Psi_{ext}}(y)=\sum_{j=1}^{N}P_j\left[\frac{EIx_j}{mx_a\omega^2}\delta^{(4)}(y-y_j)-\frac{x_j-x_a}{x_a}\delta(y-y_j)\right] - \sum_{j=1}^{N}Mt_j\left[\frac{EI}{mx_a\omega^2}\delta^{(4)}(y-y_j)-\frac{m\omega^2}{mx_a\omega^2}\delta(y-y_j)\right] \tag{3.203}$$

while α, β, γ, η and λ are given as:

$$\alpha=\frac{E\Gamma EI}{mx_a\omega^2};\ \ \beta=-\frac{GJEI}{mx_a\omega^2};\ \ \gamma=-(\frac{EII_\alpha\omega^2}{mx_a\omega^2}+\frac{E\Gamma}{x_a}); \quad \eta=\frac{GJm\omega^2}{mx_a\omega^2};\ \ \lambda=-(mx_a\omega^2-\frac{m\omega^2I_\alpha\omega^2}{mx_a\omega^2}) \tag{3.204}$$

In Eqs.(3.202)-(3.203), $f^{[k]}(y)$ and $g^{[k]}(y)$ denote the k-th derivative of $f(y)$ and $g(y)$ with respect to y.

It is noticed that Eqs.(3.194)-(3.195) (as well as Eqs.(3.191)-(3.192)), governing the motion of the beam in Figure 3.38, have been written for a general case of dampers and masses occurring simultaneously at every location y_j. In addition, for simplicity, it has been assumed that the j-th damper and gravity center GC_j of the j-th mass are applied at the same distance x_j from the elastic axis, i.e. $x_j = x_j^*$ in Figure 3.38. It is possible to remove these assumptions with very simple changes in the derived solutions, as will be shown later.

Exact frequency response functions

In order to obtain the frequency response, assume that a harmonic distributed force $f(y)e^{i\omega t}$ and a harmonic distributed twisting moment $g(y)e^{i\omega t}$ act on the beam in Figure 3.38, on the interval (a, b) with $0 \leq a, b \leq L$; $f(y)$ is in z-direction and $g(y)$ is about the y-axis. For generality, it is assumed that $f(y)$ and $g(y)$ are arbitrary polynomial functions.

Applying the linear superposition principle, the vector $\mathbf{Y}(y) = [H\ \Theta\ M\ S\ \Psi\ \Psi'\ T\ B]$ containing all the response variables can be written as (again, frequency dependence is omitted for conciseness):

$$\mathbf{Y}(y) = \mathbf{\Omega}(y)\mathbf{c} + \sum_{j=1}^{N} \mathbf{J}(y, y_j)\mathbf{\Lambda}_j + \mathbf{Y}^{(f)}(y) + \mathbf{Y}^{(g)}(y) \tag{3.205}$$

where vector $\mathbf{\Lambda}_j = [P_j\ Mt_j]$ collects the unknown reaction force P_j and twisting moment Mt_j at location y_j, see Eqs.(3.196)-(3.197). Further, $\mathbf{c}^{\mathrm{T}} = [c_1\ c_2\ c_3\ c_4\ c_5\ c_6\ c_7\ c_8]$ is a vector of integration constants, while $\mathbf{\Omega}(y)$,

$\mathbf{J}(y, y_j)$, $\mathbf{Y}^{(f)}(y)$ and $\mathbf{Y}^{(g)}(y)$ are given as:

$$\mathbf{\Omega}(y) = \begin{bmatrix} \Omega_{H1} & \Omega_{H2} & \Omega_{H3} & \Omega_{H4} & \Omega_{H5} & \Omega_{H6} & \Omega_{H7} & \Omega_{H8} \\ \Omega_{\Theta 1} & \Omega_{\Theta 2} & \Omega_{\Theta 3} & \Omega_{\Theta 4} & \Omega_{\Theta 5} & \Omega_{\Theta 6} & \Omega_{\Theta 7} & \Omega_{\Theta 8} \\ \Omega_{M1} & \Omega_{M2} & \Omega_{M3} & \Omega_{M4} & \Omega_{M5} & \Omega_{M6} & \Omega_{M7} & \Omega_{M8} \\ \Omega_{S1} & \Omega_{S2} & \Omega_{S3} & \Omega_{S4} & \Omega_{S5} & \Omega_{S6} & \Omega_{S7} & \Omega_{S8} \\ \Omega_{\Psi 1} & \Omega_{\Psi 2} & \Omega_{\Psi 3} & \Omega_{\Psi 4} & \Omega_{\Psi 5} & \Omega_{\Psi 6} & \Omega_{\Psi 7} & \Omega_{\Psi 8} \\ \Omega_{\Psi' 1} & \Omega_{\Psi' 2} & \Omega_{\Psi' 3} & \Omega_{\Psi' 4} & \Omega_{\Psi' 5} & \Omega_{\Psi' 6} & \Omega_{\Psi' 7} & \Omega_{\Psi' 8} \\ \Omega_{T1} & \Omega_{T2} & \Omega_{T3} & \Omega_{T4} & \Omega_{T5} & \Omega_{T6} & \Omega_{T7} & \Omega_{T8} \\ \Omega_{B1} & \Omega_{B2} & \Omega_{B3} & \Omega_{B4} & \Omega_{B5} & \Omega_{B6} & \Omega_{B7} & \Omega_{B8} \end{bmatrix} \tag{3.206}$$

$$\mathbf{J}(y, y_j) = [\mathbf{J}^{(P)} \;\; \mathbf{J}^{(Mt)}] = \begin{bmatrix} J_H^{(P)} & J_H^{(Mt)} \\ J_\Theta^{(P)} & J_\Theta^{(Mt)} \\ J_M^{(P)} & J_M^{(Mt)} \\ J_S^{(P)} & J_S^{(Mt)} \\ J_\Psi^{(P)} & J_\Psi^{(Mt)} \\ J_{\Psi'}^{(P)} & J_{\Psi'}^{(Mt)} \\ J_T^{(P)} & J_T^{(Mt)} \\ J_B^{(P)} & J_B^{(Mt)} \end{bmatrix} \quad \text{for } \; j = 1, 2, \ldots N \tag{3.207}$$

$$\mathbf{Y}^{(f)}(y) = \int_a^b \mathbf{J}^{(P)}(y, \xi) f(\xi) d\xi \tag{3.208}$$

$$\mathbf{Y}^{(g)}(y) = \int_a^b \mathbf{J}^{(Mt)}(y, \xi) g(\xi) d\xi \tag{3.209}$$

Here, closed analytical expressions are derived for $\mathbf{\Omega}(y)$, $\mathbf{J}(y, y_j)$, $\mathbf{Y}^{(f)}(y)$ and $\mathbf{Y}^{(g)}(y)$ based on the theory of generalized functions in conjunction with the equations of coupled bending-torsion theory including warping effects. Details are given in Appendix A, where analytical expressions for $\mathbf{\Omega}(y)$ are derived from the solutions to the homogeneous equations associated with Eq.(3.200) and Eq.(3.201); for $\mathbf{J}(y, y_j)$ from particular integrals of Eq.(3.200)

and Eq.(3.201) associated with a unit point force $P = 1$ and unit twisting moment $Mt = 1$ applied at y_j, see Eqs.(3.202)-(3.203); for $\mathbf{Y}^{(f)}(y)$ and $\mathbf{Y}^{(g)}(y)$ from particular integrals of Eq.(3.200) and Eq.(3.201) associated with the external load. Specifically, in Appendix A the particular integrals of Eqs.(3.200)-(3.201) are obtained in a closed form by the proposed approach. Here, it is only reported the fundamental solution, from which all the closed form solutions are derived. The fundamental solution is the solution of the following equation:

$$\alpha\frac{\bar{d}^8X}{dy^8}+\beta\frac{\bar{d}^6X}{dy^6}+\gamma\frac{\bar{d}^4X}{dy^4}+\eta\frac{\bar{d}^2X}{dy^2}+\lambda X-\delta(y-y_0)=0 \tag{3.210}$$

where y_0 is an arbitrary location along the y-axis. It may be seen that the solution X takes the form (see Chapter 2)

$$X(y,y_0)=\sum_{j=1}^{8}\Omega_j(y)c_j+J^{(*)}(y,y_0) \tag{3.211}$$

where Ω_j denotes terms of the solution to the homogeneous equation associated with Eq.(3.210)

$$\begin{gathered}\Omega_1=\cos(\sqrt{r_1}y)\ ;\ \Omega_2=\sin(\sqrt{r_1}y)\ ;\ \Omega_3=\cos(\sqrt{r_2}y)\ ;\ \Omega_4=\sin(\sqrt{r_2}y)\ ;\\ \Omega_5=\cosh(\sqrt{r_3}y)\ ;\ \Omega_6=\sinh(\sqrt{r_3}y)\ ;\ \Omega_7=\cosh(\sqrt{r_4}y)\ ;\ \Omega_8=\sinh(\sqrt{r_4}y)\end{gathered} \tag{3.212}$$

while the particular integral $J^{(*)}$ is obtained by Laplace transform (see Chapter 2), and after some manipulations, in the following form:

$$\begin{aligned}J^{(*)}(y,y_0)=\frac{2}{d}\Big[&\sin(\sqrt{r_1}(y-y_0))\sqrt{r_2}\sqrt{r_3}\sqrt{r_4}(r_3+r_2)(r_4+r_2)(r_4-r_3)+\\&+\sin(\sqrt{r_2}(y-y_0))\sqrt{r_1}\sqrt{r_3}\sqrt{r_4}(r_3+r_1)(r_4+r_1)(r_3-r_4)+\\&+\sinh(\sqrt{r_3}(y-y_0))\sqrt{r_1}\sqrt{r_2}\sqrt{r_4}(r_4+r_1)(r_4+r_2)(r_1-r_2)+\\&+\sinh(\sqrt{r_4}(y-y_0))\sqrt{r_1}\sqrt{r_2}\sqrt{r_3}(r_1+r_3)(r_2+r_3)(r_2-r_1)]U(y-y_0)\end{aligned} \tag{3.213}$$

In Eq.(3.213), $U(\cdot)$ is the Unit-Step function (notice that the notation has been changed since the symbol "H" denotes now the bending deflection), $d = -2\alpha\sqrt{r_1}\sqrt{r_2}\sqrt{r_3}\sqrt{r_4}(r_2 - r_1)(r_3 - r_4)(r_1 + r_3)(r_2 + r_3)(r_1 + r_4)(r_2 + r_4)$ while $-r_1$, $-r_2$, r_3, r_4 ($r_1 > 0$, $r_2 > 0$, $r_3 > 0$, $r_4 > 0$) are the four solutions of the following 4-th order polynomial equation:

$$\alpha \cdot r^4 + \beta \cdot r^3 + \gamma r^2 + \eta r + \lambda = 0 \tag{3.214}$$

Eq.(3.210) with its solution is the basis to obtain closed-form expressions for the frequency response in Eq.(3.222), as explained in Appendix A.

Starting from Eq.(3.205), it is possible to obtain the frequency response $\mathbf{Y}(y)$ as closed-form function of the vector of integration constants $\mathbf{c}$ only, regardless of the number of attachments along the beam. For this purpose, consider Eqs.(3.196)-(3.197) for P_j and Mt_j. Upon using Eq.(3.205) for $H(y_j)$ and $\Psi(y_j)$, it can be seen that $H(y_j)$ and $\Psi(y_j)$ on the right hand sides of Eqs.(3.196)-(3.197) involve only unknowns $\mathbf{\Lambda}_k$ for $k < j$, as indeed the particular integrals in $\mathbf{J}(y_j, y_k)$ are not zero only for $y_j > y_k$ and vanish for $y_j \leq y_k$ (see Appendix A). This makes it possible to cast vector $\mathbf{\Lambda}_1$ at the location y_1 and vectors $\mathbf{\Lambda}_j$ at locations y_j, for $j = 2, \ldots, N$ in the following forms:

$$\mathbf{\Lambda}_1 = \mathbf{\Phi}_{\mathbf{\Omega}}(y_1)\mathbf{c} + \mathbf{\Phi}^{(f)}(y_1) + \mathbf{\Phi}^{(g)}(y_1) \tag{3.215}$$

$$\mathbf{\Lambda}_j = \mathbf{\Phi}_{\mathbf{\Omega}}(y_j)\mathbf{c} + \sum_{k=1}^{j-1} \mathbf{\Phi}_{\mathbf{J}}(y_j, y_k)\mathbf{\Lambda}_k + \mathbf{\Phi}^{(f)}(y_j) + \mathbf{\Phi}^{(g)}(y_j) \quad \text{for } j = 2, \ldots, N \tag{3.216}$$

In Eqs.(3.215)-(3.216) $\mathbf{\Phi}_{\mathbf{\Omega}}(y_j)$ is a 2×8 matrix given as:

$$\mathbf{\Phi}_{\mathbf{\Omega}}(y_j) = \begin{bmatrix} -\kappa_{P_j}(\omega)(\mathbf{\Omega}_1(y_j) - x_j\mathbf{\Omega}_5(y_j)) \\ -\kappa_{T_j}(\omega)\mathbf{\Omega}_5(y_j) \end{bmatrix} \tag{3.217}$$

being $\mathbf{\Omega}_i(y_j)$ the row vector coinciding with the i-th row of matrix $\mathbf{\Omega}(y_j)$.

Further, $\mathbf{\Phi_J}(y_j, y_k)$ is the 2×2 matrix:

$$\mathbf{\Phi_J}(y_j, y_k) = \begin{bmatrix} -\kappa_{P_j}(\omega)(\mathbf{J}_1(y_j, y_k) - x_j \mathbf{J}_5(y_j, y_k)) \\ -\kappa_{T_j}(\omega)\mathbf{J}_5(y_j, y_k) \end{bmatrix} \tag{3.218}$$

where $\mathbf{J}_i(y_j, y_k)$ is the row vector coinciding with the i-th row of matrix $\mathbf{J}(y_j, y_k)$, while $\mathbf{\Phi}^{(f)}(y_j)$ and $\mathbf{\Phi}^{(f)}(y_j)$ are the 2×1 vectors:

$$\mathbf{\Phi}^{(f)}(y_j) = \begin{bmatrix} -k_{P_j}(\omega)(Y_1^{(f)}(y_j) - x_j Y_5^{(f)}(y_j)) \\ -k_{T_j}(\omega) Y_5^{(f)}(y_j) \end{bmatrix} \tag{3.219}$$

$$\mathbf{\Phi}^{(g)}(y_j) = \begin{bmatrix} -k_{P_j}(\omega)(Y_1^{(g)}(y_j) - x_j Y_5^{(g)}(y_j)) \\ -k_{T_j}(\omega) Y_5^{(g)}(y_j) \end{bmatrix} \tag{3.220}$$

being $Y_i^{(f)}(y_j)$ and $Y_i^{(g)}(y_j)$ the i-th components of vectors $Y^{(f)}(y_j)$ and $Y^{(g)}(y_j)$. Next, starting from Eq.(3.215) for $\mathbf{\Lambda}_1$ and using Eq.(3.216), the following expression can be derived for $\mathbf{\Lambda}_j$ in terms of $\mathbf{c}$:

$$\begin{aligned} \mathbf{\Lambda}_j = {} & \mathbf{\Phi_\Omega}(y_j)\mathbf{c} + \sum_{(j,m)\in N_2^{(j)}} \mathbf{\Phi_J}(y_j, y_m)(\mathbf{\Phi_\Omega}(y_m)\mathbf{c} + \mathbf{\Phi}^{(f)}(y_m) + \mathbf{\Phi}^{(g)}(y_m)) + \\ & + \sum_{2<q\le j} \sum_{(j,m,n,\ldots,r,s)\in N_q^{(j)}} \mathbf{\Phi_J}(y_j, y_m)\mathbf{\Phi_J}(y_m, y_n)\ldots\mathbf{\Phi_J}(y_r, y_s)(\mathbf{\Phi_\Omega}(y_s)\mathbf{c} \\ & + \mathbf{\Phi}^{(f)}(y_s) + \mathbf{\Phi}^{(g)}(y_s)) \end{aligned} \tag{3.221}$$

where $N_q^{(j)}$ assumes the same meaning of the previous Sections. Hence, on replacing Eq.(3.221) for $\mathbf{\Lambda}_j$ in Eq.(3.205), the following relation is finally derived for the frequency response $\mathbf{Y}(y)$ in terms of $\mathbf{c}$ only:

$$\mathbf{Y}(y) = \tilde{\mathbf{Y}}(y)\mathbf{c} + \tilde{\mathbf{Y}}^{(fg)}(y) = \tilde{\mathbf{Y}}(y)\mathbf{c} + \tilde{\mathbf{Y}}^{(f)}(y) + \tilde{\mathbf{Y}}^{(g)}(y) \tag{3.222}$$

where

$$\tilde{\mathbf{Y}}(y) = \mathbf{\Omega}(y) + \sum_{j=1}^{N} \mathbf{J}(y, y_j)\mathbf{\Phi}_{\mathbf{\Omega}}(y_j) + \sum_{j=1}^{N} \mathbf{J}(y, y_j)\Bigg\{ \sum_{(j,m)\in N_2^{(j)}} \mathbf{\Phi}_{\mathbf{J}}(y_j, y_m)\mathbf{\Phi}_{\mathbf{\Omega}}(y_m) + \\ + \sum_{2<q\leq j} \sum_{(j,m,n,\ldots,r,s)\in N_q^{(j)}} \mathbf{\Phi}_{\mathbf{J}}(y_j, y_m)\mathbf{\Phi}_{\mathbf{J}}(y_m, y_n)\ldots\mathbf{\Phi}_{\mathbf{J}}(y_r, y_s)\mathbf{\Phi}_{\mathbf{\Omega}}(y_s)\Bigg\} \tag{3.223}$$

$$\tilde{\mathbf{Y}}^{(f)}(y) = \mathbf{Y}^{(f)}(y) + \sum_{j=1}^{N} \mathbf{J}(y, y_j)\mathbf{\Phi}^{(f)}(y_j) \\ + \sum_{j=1}^{N} \mathbf{J}(y, y_j)\Bigg\{ \sum_{(j,m)\in N_2^{(j)}} \mathbf{\Phi}_{\mathbf{J}}(y_j, y_m)\mathbf{\Phi}^{(f)}(y_m) + \\ + \sum_{2<q\leq j} \sum_{(j,m,n,\ldots,r,s)\in N_q^{(j)}} \mathbf{\Phi}_{\mathbf{J}}(y_j, y_m)\mathbf{\Phi}_{\mathbf{J}}(y_m, y_n)\ldots\mathbf{\Phi}_{\mathbf{J}}(y_r, y_s)\mathbf{\Phi}^{(f)}(y_s)\Bigg\} \tag{3.224}$$

$$\tilde{\mathbf{Y}}^{(g)}(y) = \mathbf{Y}^{(g)}(y) + \sum_{j=1}^{N} \mathbf{J}(y, y_j)\mathbf{\Phi}^{(g)}(y_j) \\ + \sum_{j=1}^{N} \mathbf{J}(y, y_j)\Bigg\{ \sum_{(j,m)\in N_2^{(j)}} \mathbf{\Phi}_{\mathbf{J}}(y_j, y_m)\mathbf{\Phi}^{(g)}(y_m) + \\ + \sum_{2<q\leq j} \sum_{(j,m,n,\ldots,r,s)\in N_q^{(j)}} \mathbf{\Phi}_{\mathbf{J}}(y_j, y_m)\mathbf{\Phi}_{\mathbf{J}}(y_m, y_n)\ldots\mathbf{\Phi}_{\mathbf{J}}(y_r, y_s)\mathbf{\Phi}^{(g)}(y_s)\Bigg\} \tag{3.225}$$

In Eq.(3.223), $\tilde{\mathbf{Y}}(y)$ depends on the beam parameters only, through matrices $\mathbf{\Omega}(y)$ and $\mathbf{J}(y, y_j)$, while $\tilde{\mathbf{Y}}^{(f)}(y)$ and $\tilde{\mathbf{Y}}^{(g)}(y)$ depend also on the applied load, as they include the particular integrals $\mathbf{Y}^{(f)}(y)$, $\mathbf{Y}^{(g)}(y)$ and the load dependent vectors $\mathbf{\Phi}^{(f)}(y)$, $\mathbf{\Phi}^{(g)}(y)$. Notice that all terms in Eq.(3.223) through Eq.(3.225) are readily available in closed analytical form, using expressions

in Appendix A.

Once obtained the vector $\mathbf{Y}(y)$ as function of the integration constants $\mathbf{c}$ only, the final step to derive the exact frequency response is to enforce the B.C. of the beam. This leads to 8 equations with general form:

$$\mathbf{Bc} = \mathbf{r} \rightarrow \mathbf{c} = (\mathbf{B})^{-1}\mathbf{r} \tag{3.226}$$

where vector $\mathbf{r}$ involves the load-dependent terms $\tilde{\mathbf{Y}}^{(f)}(y)$, $\tilde{\mathbf{Y}}^{(g)}(y)$ in Eqs.(3.224)-(3.225), computed at the beam ends, while $\mathbf{B}$ is a coefficient matrix with size 8×8 regardless of the number of dampers/masses. The vector of integration constants $\mathbf{c}$ can be obtained in a closed analytical form, as shown in Appendix C.

Substituting for $\mathbf{c}$ in Eq.(3.222), exact closed-form expressions are obtained for the frequency response $\mathbf{Y}(y)$ of the coupled bending-torsional beam with an arbitrary number of dampers/masses, under distributed polynomial loads $f(y)e^{i\omega t}$ and $g(y)e^{i\omega t}$. The closed-form expressions are available for all response variables in $\mathbf{Y}(y)$. Obviously, they hold also for point loads applied at any y_0 along the y-axis, simply setting $\mathbf{Y}^{(f)}(y) = \mathbf{J}^{(P)}(y, y_0)$ in Eq.(3.208) and $\mathbf{Y}^{(g)}(y) = \mathbf{J}^{(Mt)}(y, y_0)$ in Eq.(3.209). Remarkably, in this case Eq.(3.222) provides the exact closed-form expressions of the dynamic Green's functions of the beam with dampers/masses.

Eq.(3.222) can be used also if B.C. are not homogeneous, e.g. for end dampers or tip masses. Indeed, the end dampers or tip masses can be modeled as located at $y_1 = 0^+$ and $y_N = L^-$, and the B.C. can still be considered as homogeneous.

3.5.3 Advantages and remarks

Now, advantages of the proposed approach are discussed comparing the exact analytical frequency response functions (3.222) with the alternative exact expressions obtainable by a classical procedure. This consists in dividing the beam in uniform segments, each between two consecutive appli-

cation points of dampers/masses/point loads or under a distributed load, where the frequency response can be expressed using the solution to the homogeneous equations of motion, and including a particular integral for the segments where a distributed load is applied. For n segments, $8 \times n$ integration constants should be computed by enforcing the B.C. at beam ends and matching conditions among the solutions over adjacent segments. By using this approach, even with a low number of dampers/masses/loads, the coefficient matrix associated with the equations to be solved shall be re-inverted numerically for any forcing frequency of interest, and updated whenever dampers/masses/load change positions. Over this classical procedure, the proposed exact expression (3.222) has the following advantages:

- It is inherently able to satisfy all the required conditions at the dampers and point load locations, capturing jump and slope discontinuities of the response variables.

- The analytical form is easy to implement in any symbolic package, and can readily be computed for any frequency of interest, parameters of dampers (location, stiffness, damping), position of the loads, regardless of the number of dampers and positions of the dampers relative to the loads.

These two characteristics make Eq.(3.222) particularly suitable for optimization problems, where several solutions shall be built and compared for changing position and parameters of dampers/masses/loads.

At this stage, few remarks concern the changes to be made if the assumptions made previously are removed. First, the case of dampers and masses which do not occur simultaneously at a given location y_j is discussed. For instance, if only a translational damper occurs at y_j, $M_j = 0$ in Eq.(3.198) and $\kappa_{T_j}(\omega) = 0$ in Eqs.(3.199). This will automatically set equal to zero the 2^{nd} row in matrices $\mathbf{\Phi_\Omega}(y_j)$, $\mathbf{\Phi_J}(y_j, y_k)$, as well as vectors $\mathbf{\Phi}^{(f)}(y_j)$ and $\mathbf{\Phi}^{(g)}(y_j)$. In addition, being $Mt_j(\omega) = 0$ at $y = y_j$, the 2^{nd} column of matrix $\mathbf{\Phi_J}(y_m, y_j)$ shall be set equal to zero for any $y_m > y_j$. Similar changes will

be made if a rotational damper or a mass only occurs at y_j, as well as two dampers or a damper and a mass.

The final remark concerns the changes to be made when a translational damper and a mass occur simultaneously at a given location y_j, but at different distances x_j^* and x_j from the elastic axis (as shown in Figure 3.38). In this case, the equations of motion (3.194)-(3.195) are modified as follows:

$$EI\frac{\bar{d}^4H}{dy^4} - m\omega^2 H + mx_a\omega^2\Psi - \sum_{j=1}^{N}(P_j^* + P_j)\delta(y - y_j) - f(y) = 0 \quad (3.227)$$

$$\begin{aligned} E\Gamma\frac{\bar{d}^4\Psi}{dy^4} - GJ\frac{\bar{d}^2\Psi}{dy^2} - I_\alpha\omega^2\Psi + m\omega^2 x_a H + \sum_{j=1}^{N}(P_j^* x_j^* + P_j x_j)\delta(y - y_j) \\ - \sum_{j=1}^{N} Mt_j\delta(y - y_j) - g(y) = 0 \end{aligned} \quad (3.228)$$

where P_j^* is the reaction force associated with the damper applied at x_j^*, while P_j and Mt_j are the reaction force and twisting moment associated with the mass whose gravity center GC_j is applied at x_j, given as:

$$P_j^* = -\kappa_{P_j^*}[H(y_j) - x_j^*\Psi(y_j)] = -(k_{H_j} + i\omega c_{H_j})[H(y_j) - x_j^*\Psi(y_j)] \quad (3.229)$$

$$P_j = -\kappa_{P_j}[H(y_j) - x_j\Psi(y_j)] = M_j\omega^2[H(y_j) - x_j\Psi(y_j)] \quad (3.230)$$

$$Mt_j = -\kappa_{T_j}\Psi(y_j) = (I_{yy_j} - M_j x_j^2)\omega^2\Psi(y_j) \quad (3.231)$$

In this case, the vector $\mathbf{\Lambda}_j$ takes the form:

$$\mathbf{\Lambda}_j = [P_j^* \; P_j \; Mt_j] \quad (3.232)$$

while $\mathbf{J}(y, y_j)$, $\mathbf{\Phi}_{\mathbf{J}}(y_j, y_k)$, $\mathbf{\Phi}^{(f)}(y_j)$ and $\mathbf{\Phi}^{(g)}(y_j)$ become

$$\mathbf{J}(y, y_j) = [\mathbf{J}^{(P^*)}\ \mathbf{J}^{(P)}\ \mathbf{J}^{(Mt)}] \tag{3.233}$$

$$\begin{aligned}
\mathbf{\Phi}_{\mathbf{\Omega}}(y_j) &= \begin{bmatrix} -\kappa_{P_j^*}(\omega)(\mathbf{\Omega}_1(y_j) - x_j^*\mathbf{\Omega}_5(y_j)) \\ -\kappa_{P_j}(\omega)(\mathbf{\Omega}_1(y_j) - x_j\mathbf{\Omega}_5(y_j)) \\ -\kappa_{T_j}(\omega)\mathbf{\Omega}_5(y_j) \end{bmatrix} \\
\mathbf{\Phi}_{\mathbf{J}}(y_j, y_k) &= \begin{bmatrix} -\kappa_{P_j^*}(\omega)(\mathbf{J}_1(y_j, y_k) - x_j^*\mathbf{J}_5(y_j, y_k)) \\ -\kappa_{P_j}(\omega)(\mathbf{J}_1(y_j, y_k) - x_j\mathbf{J}_5(y_j, y_k)) \\ -\kappa_{T_j}(\omega)\mathbf{J}_5(y_j, y_k) \end{bmatrix}
\end{aligned} \tag{3.234}$$

$$\begin{aligned}
\mathbf{\Phi}^{(f)}(y_j) &= \begin{bmatrix} -k_{P_j^*}(\omega)(Y_1^{(f)}(y_j) - x_j^*Y_5^{(f)}(y_j)) \\ -k_{P_j}(\omega)(Y_1^{(f)}(y_j) - x_jY_5^{(f)}(y_j)) \\ -k_{T_j}(\omega)Y_5^{(f)}(y_j) \end{bmatrix} \\
\mathbf{\Phi}^{(g)}(y_j) &= \begin{bmatrix} -k_{P_j^*}(\omega)(Y_1^{(g)}(y_j) - x_j^*Y_5^{(g)}(y_j)) \\ -k_{P_j}(\omega)(Y_1^{(g)}(y_j) - x_jY_5^{(g)}(y_j)) \\ -k_{T_j}(\omega)Y_5^{(g)}(y_j) \end{bmatrix}
\end{aligned} \tag{3.235}$$

Notice that $\mathbf{J}^{(P^*)}$ in Eq.(3.233) has the same expression as $\mathbf{J}^{(P)}$ in Appendix B, with x_j^* replacing x_j. At this stage, the same procedure previously shown can be used to obtain the frequency response $\mathbf{Y}(y)$ by Eq.(3.222).

3.5.4 Numerical examples

Here, two numerical examples are presented to validate the exact method proposed in this Section and emphasize the importance of warping effects on the dynamics of coupled bending-torsional beams. Numerical results will be compared with those obtained by the classical exact method. An excellent agreement between the two methods will be found. However, computational advantages of the proposed method over the classical one will be always considerable, thanks to the closed-form expressions derived in this Section. Moreover, results in terms of natural frequencies and frequency response will

be compared with those obtained using the Euler-St.Venant coupled bending-torsion theory, i.e. neglecting warping effects. In this case, the following steady-state coupled equations will be used in every beam segment between two consecutive dampers/masses or under distributed loads $f(y)$, $g(y)$:

$$EI\frac{\bar{d}^4 H_{NW}}{dy^4} - m\omega^2 H_{NW} + mx_a\omega^2\Psi_{NW} - \sum_{j=1}^{N} P_j\delta(y-y_j) - f(y) = 0 \quad (3.236)$$

$$\begin{aligned} GJ\frac{\bar{d}^2\Psi_{NW}}{dy^2} + I_\alpha\omega^2\Psi_{NW} - m\omega^2 x_a H_{NW} - \sum_{j=1}^{N} P_j x_j\delta(y-y_j) \\ + \sum_{j=1}^{N} Mt_j\delta(y-y_j) - g(y) = 0 \end{aligned} \quad (3.237)$$

where $H_{NW}(y)$ and $\Psi_{NW}(y)$ denote deflection and torsional rotation, when warping effects are not considered. The solution to Eqs.(3.236)-(3.237) involves a load-dependent particular integral and six integration constants in every beam segment, which can be computed enforcing the beam B.C. along with matching conditions among the solutions over adjacent segments.

Example A involves the free vibration analysis of a beam with a channel cross section carrying elastic supports. Results in terms of natural frequencies will be found in excellent agreement with those available in literature [57].

In Example B, frequency response functions are obtained for a beam with a channel cross section carrying a damper and an attached mass, for different loadings. Further, the optimal position of the damper will be found by a parametric analysis, taking advantage of the closed-form expressions for the frequency response.

Example A

Consider the clamped-free beam with a channel cross section in Figure 3.39, whose properties are those reported in ref.[57]: $L = 7\,\mathrm{m}$, $d = 0.0889\,\mathrm{m}$, $b = 0.1524\,\mathrm{m}$, $t = 0.0071\,\mathrm{m}$, $EI = 0.1704 \cdot 10^7\,\mathrm{Nm}^2$, $GJ = 0.314 \cdot 10^4\,\mathrm{Nm}^2$, $E\Gamma = 0.1337 \cdot 10^4\,\mathrm{Nm}^4$, $m = 17.61\,\mathrm{kg\ m}^{-1}$, $I_\alpha = 0.1342\,\mathrm{kg\ m}$. The abscissa

of the MC is $x_a = 0.05626\,\mathrm{m}$.

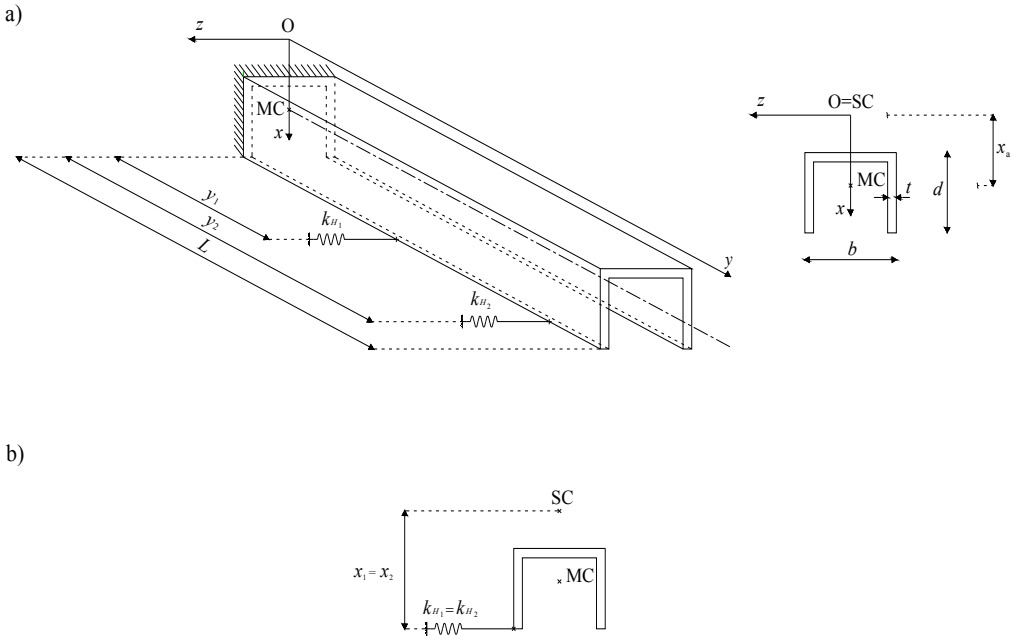

Figure 3.39: a) Cantilever beam with channel cross section carrying two translational elastic supports; b) Beam cross sections at $y = y_1$ and $y = y_2$.

The beam carries two translational elastic supports at $y_1 = 3\,\mathrm{m}$ and $y_2 = 6\,\mathrm{m}$, both applied at distance $x_1 = x_2 = 0.118\,\mathrm{m}$ from the SC of the beam cross section as shown in Figure 3.39; let k_{H_1} and k_{H_2} be the stiffness parameters of the elastic supports. Warping is fully constrained at $y = 0$ but is allowed through the whole beam.

Coupled bending-torsional vibrations will be investigated in the $y - z$ plane. Coupling effects arise in the $y - z$ plane only, as indeed the SC is eccentric with respect to the MC along the x-axis but not along the z-axis.

The characteristic equation is obtained as determinant of matrix $\mathbf{B}$ in Eq.(3.226), setting $\mathbf{r} = \mathbf{0}$. Table 3.7 reports the first three natural frequencies for different values of stiffness parameters k_{H_1} and k_{H_2}, calculated by proposed and classical methods; as expected, as the stiffness of the supports increases the natural frequencies increase. Results obtained by the two meth-

ods are in a very good agreement, but the proposed method is computationally more efficient, since the characteristic equation is built as determinant of the 8×8 matrix $\mathbf{B}$ in Eq.(3.226) while, instead, the characteristic equation of the classical method is constructed as determinant of a 24×24 matrix. Table 3.7 also reports the natural frequencies computed by proposed method and those computed by adopting the Euler-St.Venant coupled bending-torsion theory, i.e. neglecting warping effects. It is apparent from Table 3.7 that neglecting warping effects leads to relevant errors in the natural frequencies, as the modal index increases.

Figures 3.40-3.41 show the first three eigenfunctions of various response variables computed by proposed and classical methods, assuming that $k_{H_1} = k_{H_2} = 10^5\,\mathrm{N/m}$. The eigenfunctions are normalized so that pure bending deflection $\Phi_H(y)$ (being $\Phi_{(\cdot)}$ the normalized eigenfunction of a generic variable) is unitary at the tip, i.e. $\Phi_H(L) = 1$. For all three modes there is a great amount of coupling between bending and torsional responses as indeed, in the left column of Figure 3.40, it is evident that the pure bending deflection $\Phi_H(y)$ has the same order of magnitude of the deflection of the MC due to torsional response, computed as $\Phi_\Psi(y)x_a$ (notice that x_a is the distance between MC and SC of the beam cross section, see Figure 3.39). Torque eigenfunctions Φ_T, shown in the right column of Figure 3.40, exhibit jump discontinuities at the application points of the elastic supports; being applied at a distance $x_1 = x_2 = 0.118\,\mathrm{m} \neq 0$ from the elastic axis, in fact, the elastic supports produce external twisting moments as the beam deflects. Eigenfunctions of bending moment Φ_M and shear force Φ_S, shown in the left and right column of Figure 3.41, exhibit slope and jump discontinuities, respectively, at the application points y_1 and y_2 of the elastic supports. Bending rotation and bimoment are continuous along the whole domain and are not reported for brevity.

All the eigenfunctions built by the exact proposed and classical methods are in excellent agreement over the whole domain as shown in Figure 3.40-3.41. The eigenfunctions built by the proposed method inherently fullfill all

the required conditions at the application points y_1, y_2 of the elastic supports thanks to the use of generalized functions.

Finally, it is observed that ref.[57] provides the natural frequencies of the beam in Figure 3.39 when the supports at $y = 3\,\mathrm{m}$ and $y = 6\,\mathrm{m}$ are fixed and applied at the SC of the cross section, see Figure 3.42. This corresponds to assume $x_1 = x_2 = 0$ and a very large stiffness k_{H_1}, k_{H_2} in Eq.(3.226) (modeling fixed supports by using a very large stiffness is obviously an approximate approach). Assuming $k_{H_1} = k_{H_2} = 10^9\,\mathrm{N/m}$, Table 3.8 shows that the natural frequencies computed from Eq.(3.226) are in a very good agreement with those reported in ref.[57].

	Mode 1		Mode 2		Mode 3	
$k_{H_1} = k_{H_2}\,[N/m]$	C. M.	P. M.	C.M.	P.M.	C. M.	P. M.
10^3	21.3845	21.3848	52.8036	52.8033	105.658	105.652
10^5	43.3435	43.3431	73.7567	73.7563	121.328	121.326
10^7	49.8646	49.8644	180.663	180.668	228.652	228.657

	Mode 1		Mode 2		Mode 3	
$k_{H_1} = k_{H_2}\,[N/m]$	warping ignored	warping (P.M.)	warping ignored	warping (P.M.)	warping ignored	warping (P.M.)
10^3	21.0604	21.3848	47.6884	52.8033	95.7272	105.652
10^5	41.8841	43.3431	68.8591	73.7563	112.937	121.326
10^7	47.4662	49.8644	148.531	180.668	157.207	228.657

Table 3.7: Beam in Figure 3.39, natural frequencies calculated through classical method (C.M.) and proposed method (P.M.), with different stiffness values for the translational elastic supports. Natural frequencies obtained by Euler-St.Venant coupled bending-torsion theory (warping ignored) are included.

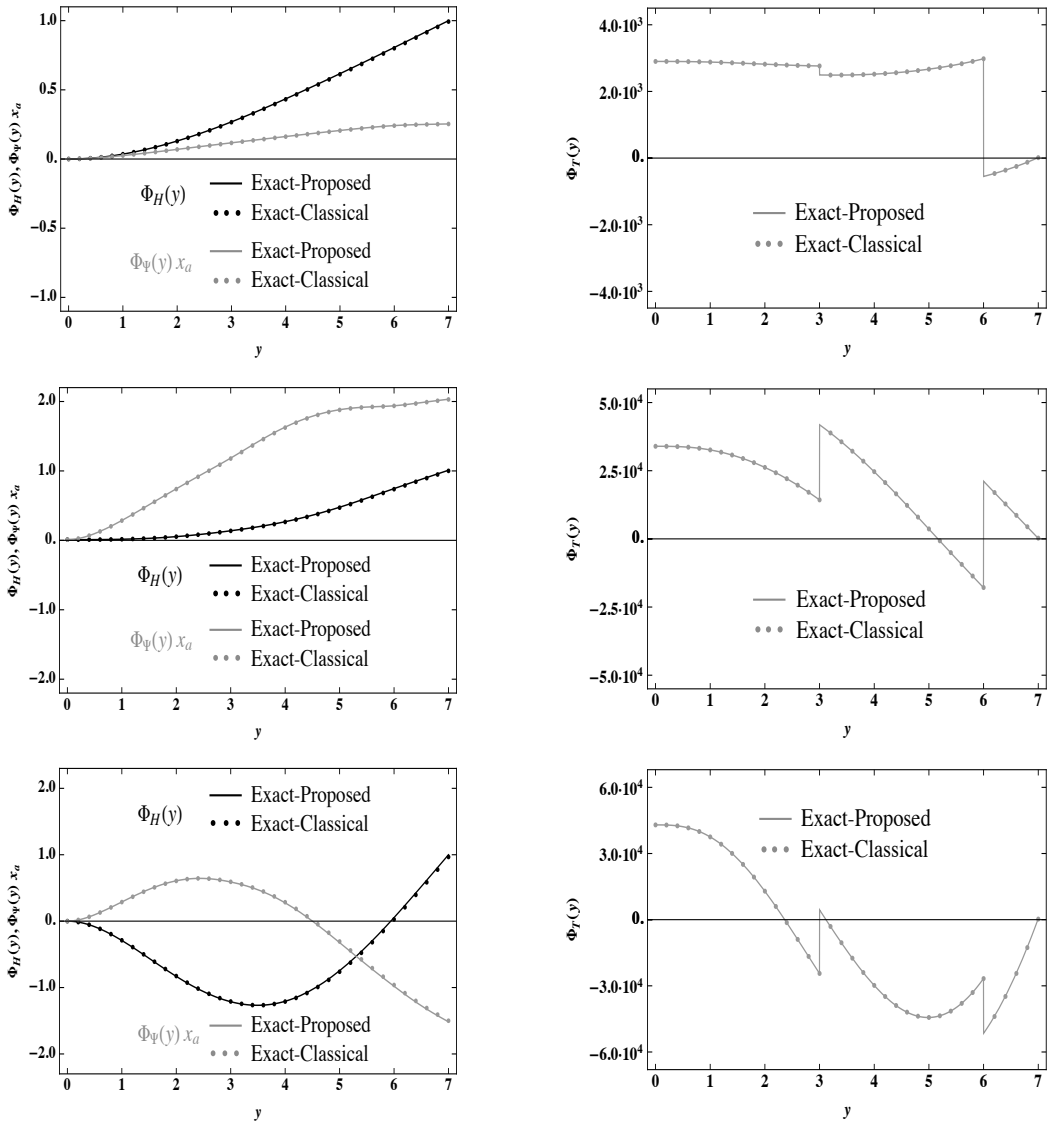

Figure 3.40: Beam in Figure 3.39, eigenfunctions of first 3 modes (from top to bottom): pure bending deflection compared with deflection of beam cross-section MC due to torsional response (left column); torque (right column).

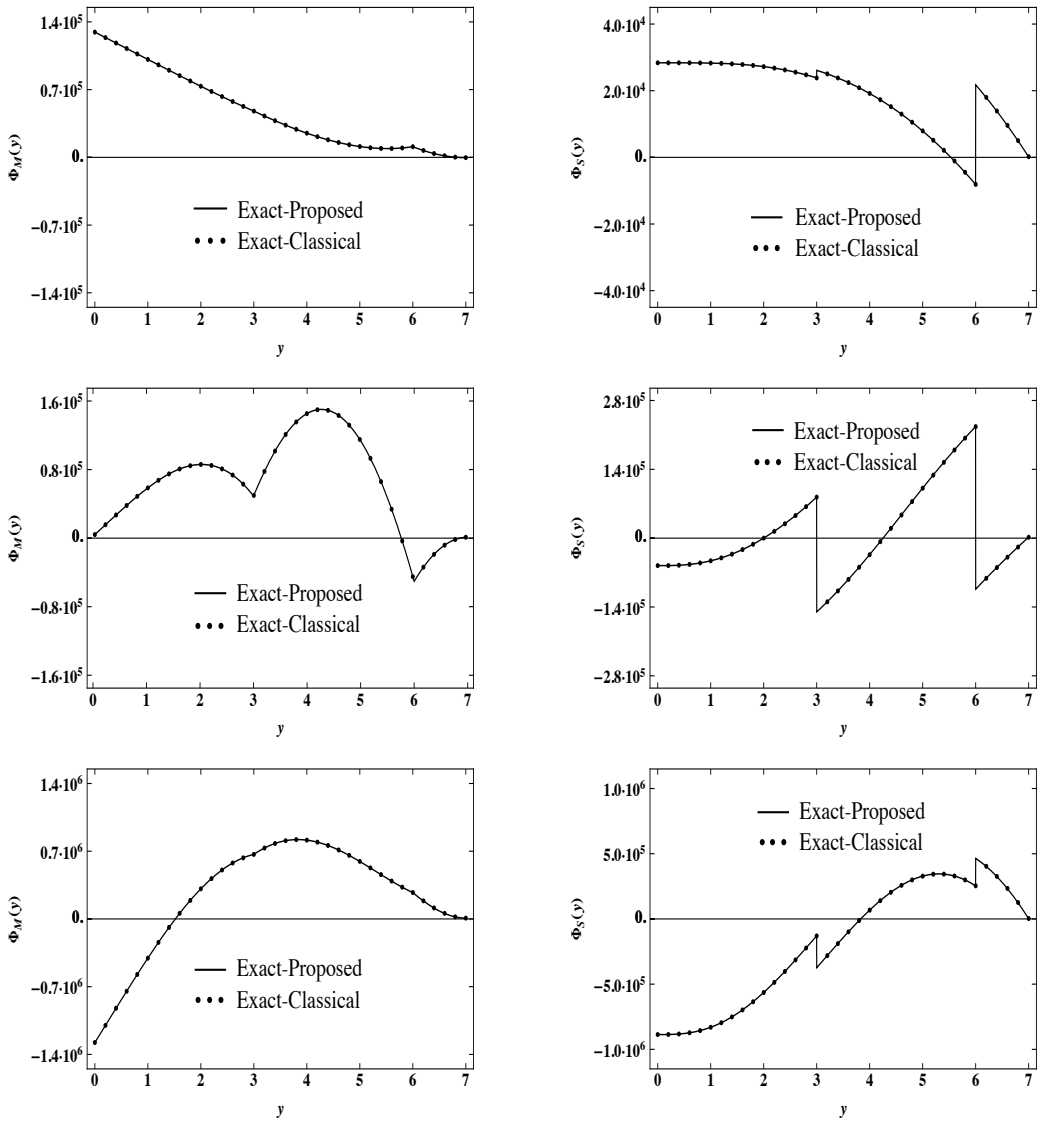

Figure 3.41: Beam in Figure 3.39, eigenfunctions of first 3 modes (from top to bottom): bending moment (left column); shear force (right column).

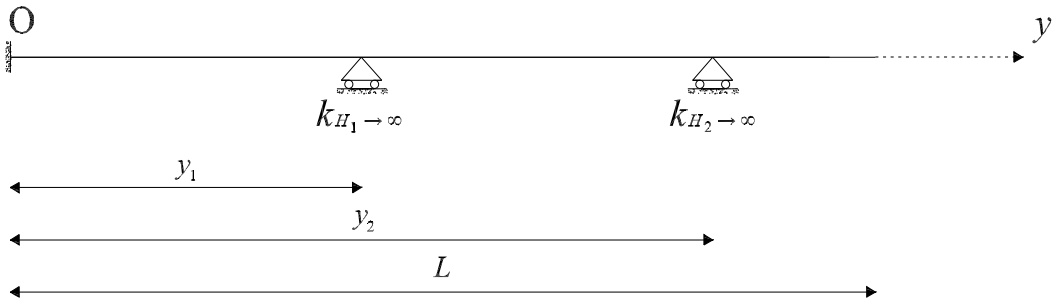

Figure 3.42: Cantilever beam with channel cross section considered in ref.[57].

	Mode 1		Mode 2		Mode 3	
$k_{H_1} = k_{H_2}\,[N/m]$	ref.[57]	P. M.	ref.[57].	P.M.	ref.[57]	P. M.
∞	38.4971	38.4966	121.516	121.518	205.523	205.525

Table 3.8: Beam in Figure 3.42, natural frequencies calculated through proposed method (P.M.) and compared to those obtained in ref.[57].

Example B

Consider the beam in Figure 3.43, whose properties are taken, again, as in ref.[57]: $L = 1.28\,\text{m}$, $d = 0.058\,\text{m}$, $t = 0.00125\,\text{m}$, $b = 0.1\,\text{m}$, $EI = 0.974 \cdot 10^5\,\text{Nm}^2$, $GJ = 11.21\,\text{Nm}^2$, $E\Gamma = 35.4\,\text{Nm}^4$, $m = 2.095\,\text{kg m}^{-1}$, $I_\alpha = 0.725\,10^{-2}\text{kg m}$. The abscissa of the MC is $x_a = 0.03771\,\text{m}$.

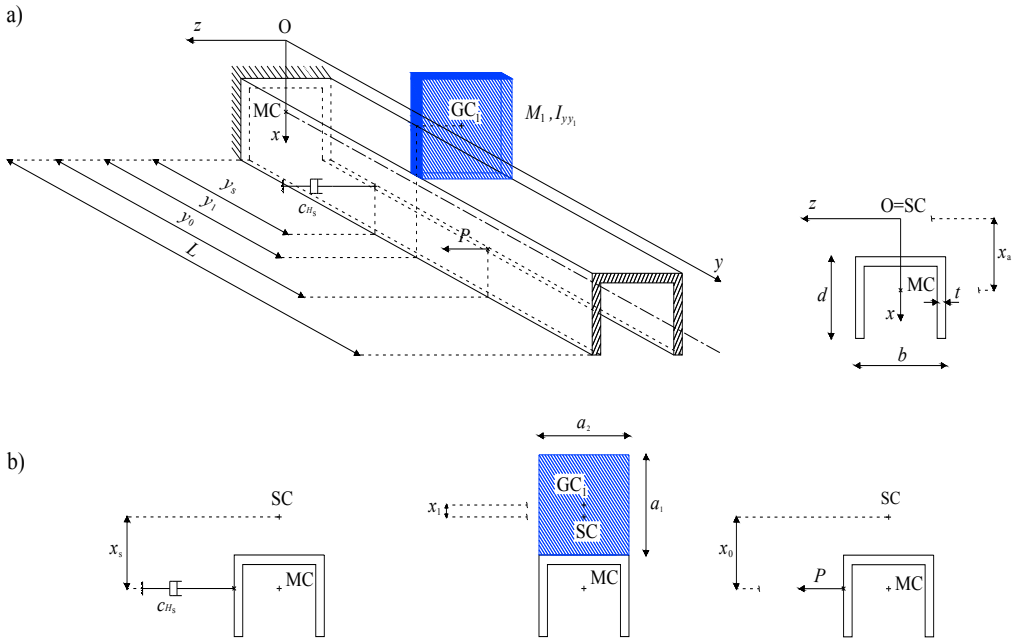

Figure 3.43: a) Clamped-clamped beam with channel cross section carrying a translational viscous damper and an attached mass, subjected to a harmonically-varying transverse point force; b) Beam cross sections at $y = y_s$, $y = y_1$ and $y = y_0$ (from left to right).

At $y_1 = 0.5L = 0.64\,\text{m}$ a mass M_1, modeled as a rigid rectangular plate with $a_1 = 0.1\,\text{m}$, $a_2 = 0.1\,\text{m}$, is attached to the beam, with its gravity center GC_1 located at distance $x_1 = -0.02869\,\text{m}$ with respect to the y-axis (i.e., the elastic axis); further, be I_{yy_1} its mass moment of inertia with respect to the y-axis. The beam is clamped at both ends so that warping is fully constrained in $y = 0$ and $y = L$, while it is allowed through the whole beam. Since both MC and GC_1 are eccentric with respect to SC along the x-axis

(see Figure 3.43), bending and torsional vibrations will be coupled only in the $y-z$ plane.

Firstly, a free vibration analysis is carried out, with characteristic equation built as determinant of matrix $\mathbf{B}$ in Eq.(3.226), setting $\mathbf{r}=\mathbf{0}$. Table 3.9 shows the first three natural frequencies for different values of the mass M_1, as calculated by proposed and classical method. Moreover, Table 3.9 shows the natural frequencies obtained from the Euler-St.Venant coupled bending-torsion theory, i.e. neglecting warping effects. A very good agreement is found among natural frequencies obtained by proposed and classical methods. It is also seen that natural frequencies with or without warping effects are significantly different. Finally, it is noticed that the natural frequencies generally decrease as the mass M_1 increases, as expected, while those of mode 3 with warping and mode 2 without warping effects do not vary. The reason is that, for these two modes, bending deflection and torsional rotation exhibit zero values at the application point $y_1 = 0.64\,\mathrm{m}$ of the mass M_1 (in the following, see Figure 3.44 for mode 3 with warping). Next, assuming $M_1 = 0.8\,\mathrm{kg}$ and $I_{yy_1} = 0.0013\,\mathrm{kg\ m^2}$, the eigenfunctions associated with the first three natural frequencies are reported in Figures 3.44-3.45, as computed by proposed and classical method. In Figure 3.44, where the eigenfunctions of pure bending deflection $\Phi_H(y)$ and deflection of the MC due to torsional rotation $\Phi_\Psi(y)x_a$ are reported, it can be observed that bending and torsional responses are significantly coupled, with torsional effects dominating in the first and third modes. Shear force $\Phi_S(y)$ and torque $\Phi_T(y)$ of first and second modes in Figure 3.45 exhibit jump discontinuities at the midspan, where the mass M_1 is located. These discontinuities are attributable respectively to the inertial transverse force of the mass M_1, and the non-zero arm ($x_1 = -0.02869\,\mathrm{m}$) that this force has with respect to the elastic axis. In addition, torque discontinuity is also attributable to the non-zero torsional inertia of the mass ($I_{yy_1} = 0.0013\,\mathrm{kg\ m^2}$). Shear forces $\Phi_S(y)$ and torque $\Phi_T(y)$ of mode 3 in Figure 3.45 are not discontinuous, consistently with the fact that the corresponding bending deflection $\Phi_H(y)$ and torsional rotation

$\Phi_\Psi(y)$ in Figure 3.44 exhibit zero values at the application point $y_1 = 0.64\,\mathrm{m}$ of the mass M_1.

In the following, attention is focused on forced vibrations. Let the beam be subjected to a harmonic transverse force $P = 1$ in z-direction with frequency ω. It is assumed that the force is applied at $y_0 = 0.9\,\mathrm{m}$ along the beam, at distance $x_0 = x_a = 0.03771\,\mathrm{m}$ from the elastic axis, i.e. at the MC of the cross section at $y_0 = 0.9\,\mathrm{m}$. Again, $M_1 = 0.8\,\mathrm{kg}$ and $I_{yy_1} = 0.0013\,\mathrm{kg\ m^2}$ are set. In addition, a translational viscous damper with damping parameter $c_{H_s} = 10\,\mathrm{Ns/m}$ is applied at distance $x_s = x_a = 0.03771\,\mathrm{m}$ from the elastic axis, i.e. at the abscissa of the MC. For vibration mitigation, the optimal position y_s of the damper along the beam axis will be sought, investigating whether, and to which extent, it is affected by considering or neglecting warping effects.

For a first insight into this issue, assume that the viscous damper is applied at $y_s = 0.5L = 0.64\,\mathrm{m}$. Figure 3.46 shows the frequency response amplitudes for pure bending deflection, $H(y)$, and deflection of the MC due to torsional rotation, $\Psi(y)x_a$, computed at $y = 0.4\,\mathrm{m}$ for ω spanning $(0, 3500)\,\mathrm{rad/s}$. Coupling between bending and torsional responses is evident through the whole frequency domain.

Next, using $H(y)$ and $\Psi(y)x_a$ in Figure 3.46, the frequency response amplitude for the total deflection of the MC is built, i.e. $|H(y) - \Psi(y)x_a|$, for comparison with the corresponding one built without warping effects, i.e. $|H_{NW}(y) - \Psi_{NW}(y)x_a|$, obtained from Eqs.(3.236)-(3.237) according to the Euler-St.Venant coupled bending-torsion theory. The comparison in Figure 3.47 shows that the frequency responses predicted by the two theories are very different, particularly the 1-st peak of $|H(y) - x_a\Psi(y)|$ and the 8-th peak of $|H_{NW}(y) - x_a\Psi_{NW}(y)|$ occur practically at the same frequency, i.e. $\omega = 772.069\,\mathrm{rad/s}$.

To further investigate the consequences of neglecting warping effects, assume that the harmonic transverse force $P = 1$ at $y_0 = 0.9\,\mathrm{m}$ has frequency $\omega = 772.07\,\mathrm{rad/s}$, which is very close to the frequency $\omega = 772.069\,\mathrm{rad/s}$

where the peaks of both $|H(y) - \Psi(y)x_a|$ and $|H_{NW}(y) - \Psi_{NW}(y)x_a|$ occur in Figure 3.47. Then, assume to vary the application point of the viscous damper along the beam, in order to determine its optimal position. Figures 3.48 and 3.49 show the frequency response amplitude for the total deflection of the MC with and without warping effects, computed respectively as $|H(y) - \Phi(y)x_a|$ (Figure 3.48) and $|H_{NW}(y) - \Psi_{NW}(y)x_a|$ (Figure 3.49) along the whole beam. Very different results are obtained, indeed when warping effects are considered the damper becomes progressively ineffective as its application point approaches the clamped ends, while when warping effects are neglected the damper is ineffective at various other points along the beam. To explain this result, it is useful to consider the undamped beam, i.e. the beam without damper. For this beam, Figures 3.50-3.51 show the mode shapes for the MC total deflection, i.e. $\Phi_H(y) - \Phi_\Psi(y)x_a$ and $\Phi_{H_{NW}}(y) - \Phi_{\Psi_{NW}}(y)x_a$ (x_a is the distance between MC and SC of the beam cross section, see Figure 3.43), which correspond to the peaks of the frequency response amplitudes $|(H(y) - \Psi(y)x_a)|$ and $|(H_{NW}(y) - \Phi_{NW}(y)x_a)|$ at $\omega = 772.069\,\text{rad/s}$ in Figure 3.47. Results in Figure 3.49 mirror the mode shape in Figure 3.51, as indeed the damper, which is applied at $x_s = x_a$, cannot be activated when located at the zero crossing points of the mode shape $\Phi_{H_{NW}}(y) - \Phi_{\Psi_{NW}}(y)x_a$ in Figure 3.51. The same conclusion can be drawn from Figure 3.48 and Figure 3.50. For a further insight into the results in Figures 3.48-3.49, Figure 3.52 shows the maximum value of the the frequency response amplitude for the MC total deflection along the beam, $[H - \Psi x_a]_{max} = \max[|H(y) - \Psi(y)x_a|, 0 < y < L]$ including warping effects and $[H_{NW} - \Psi_{NW}x_a]_{max} = \max[|H_{NW}(y) - \Psi_{NW}(y)x_a|, 0 < y < L]$ neglecting warping effects, for different values of the damper position. Figure 3.52 shows that the optimal position of the damper considering warping effects is at $y_s = 0.5\text{L} = 0.64\,\text{m}$ while, for the same position, the damper would be ineffective when warping effects are neglected. It is then concluded that the Euler-St.Venant coupled bending-torsion theory would predict incorrectly the dynamics of the beam in Figure 3.43, leading to erroneous results on the

optimal position of the damper.

	Mode 1		Mode 2		Mode 3	
$M_1\,[kg]$	C.M.	P.M.	C.M.	P.M.	C.M.	P.M.
0.8	772.072	772.070	2226.01	2226.02	2579.62	2579.67
1	739.003	739.004	2085.75	2085.77	2579.62	2579.67
1.5	673.426	673.429	1861.441	1861.44	2579.62	2579.67
2	621.746	621.749	1715.12	1715.14	2579.62	2579.67

	Mode 1		Mode 2		Mode 3	
$M_1\,[kg]$	warping ignored	warping (P.M.)	warping ignored	warping (P.M.)	warping ignored	warping (P.M.)
0.8	79.9692	772.070	192.999	2226.02	246.133	2579.67
1	76.6619	739.004	192.999	2085.77	239.687	2579.67
1.5	70.0723	673.429	192.999	1861.44	228.899	2579.67
2	64.8483	621.749	192.999	1715.14	221.977	2579.67

Table 3.9: Beam in Figure 3.43, natural frequencies of the beam calculated through classical method (C.M.) and proposed method (P.M.), for different values of the mass M_1; natural frequencies obtained by Euler-St.Venant coupled bending-torsion theory (warping ignored) are included.

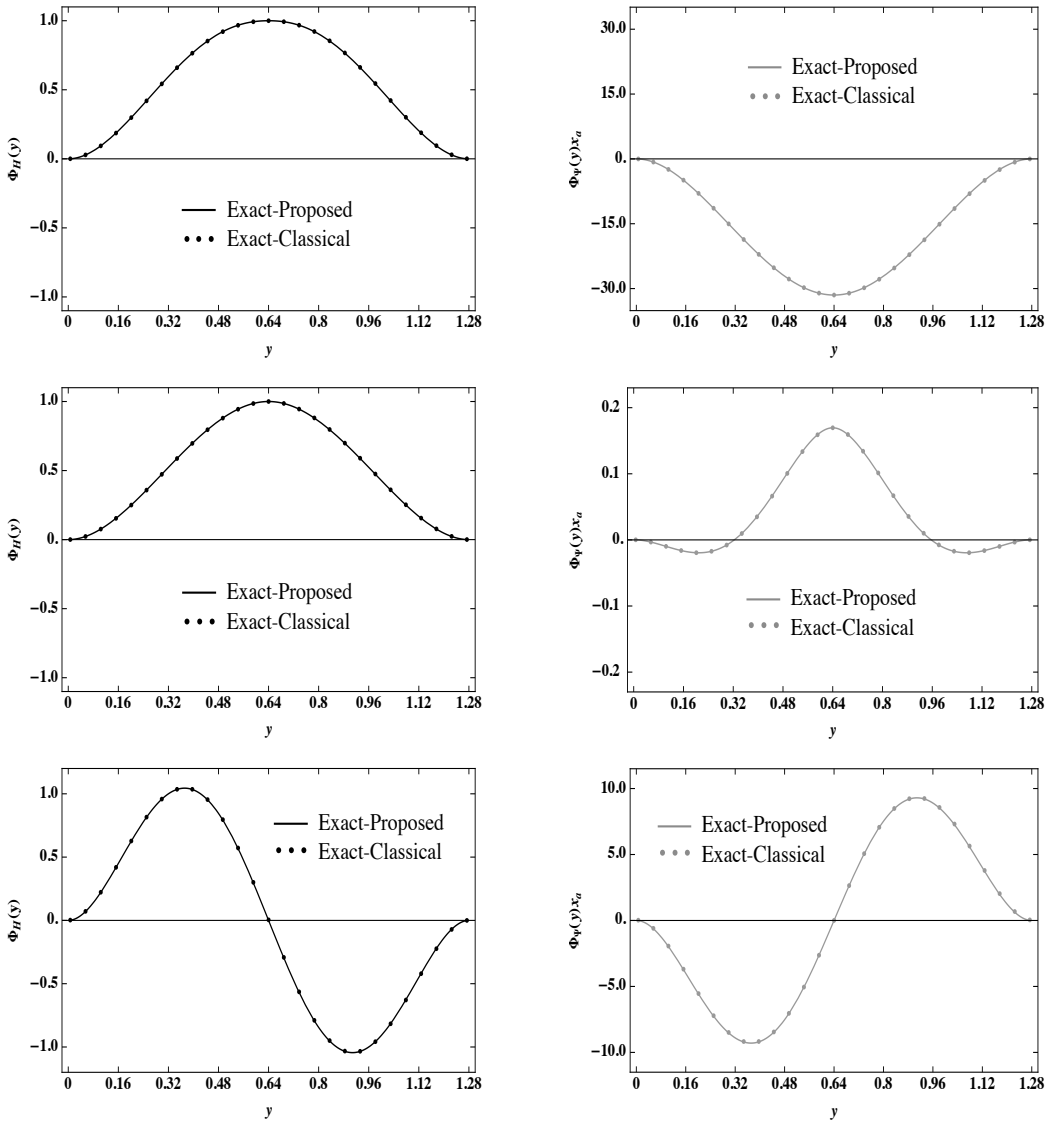

Figure 3.44: Beam in Figure 3.43, eigenfunctions of first 3 modes (from top to bottom): pure bending deflection (left column) compared with deflection of beam cross-section MC due to torsional response (right column).

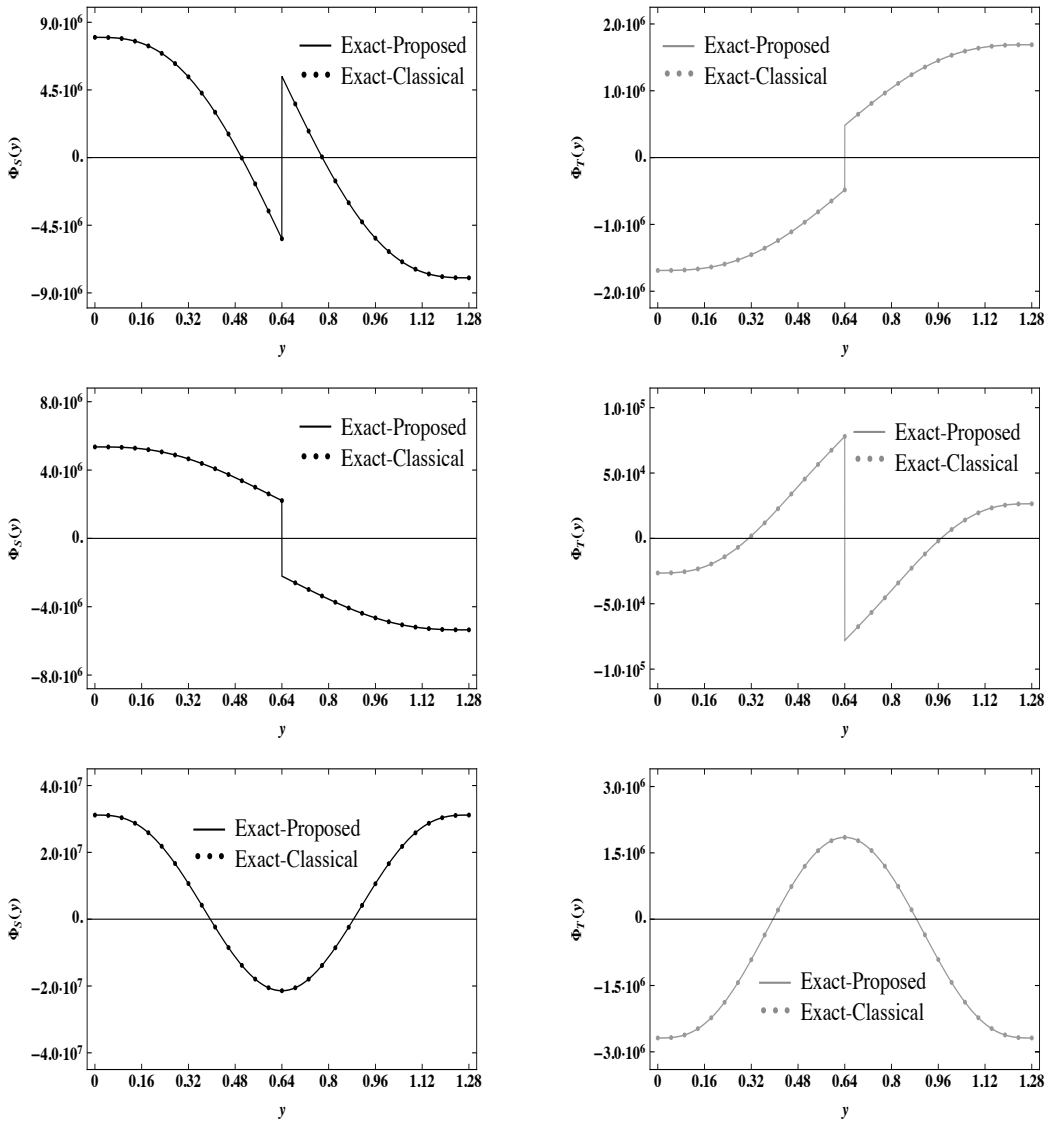

Figure 3.45: Beam in Figure 3.43, eigenfunctions of first 3 modes (from top to bottom): shear force (left column) and torque (right column).

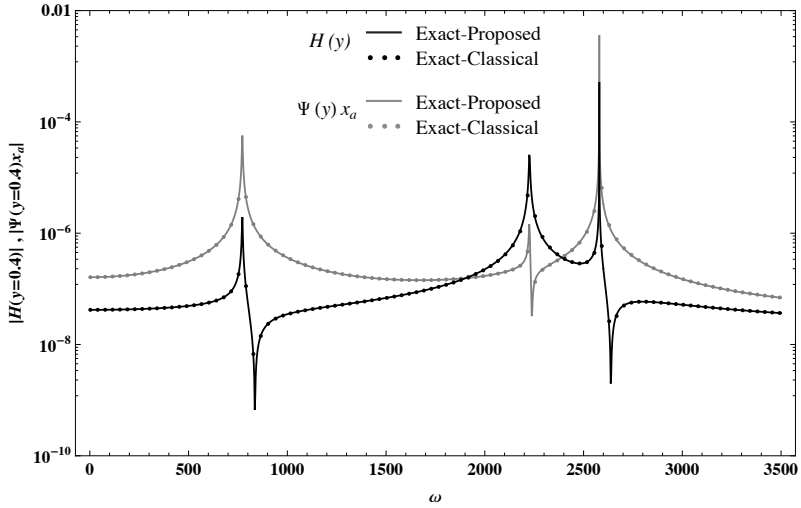

Figure 3.46: Beam in Figure 3.43, frequency response amplitudes for $H(y)$ and $\Psi(y)x_a$, computed at $y = 0.4\,\mathrm{m}$, for a point force P applied at $y_0 = 0.9\,\mathrm{m}$ with frequency ω spanning $[0, 3500]$ rad/s, as computed by exact proposed and classical methods.

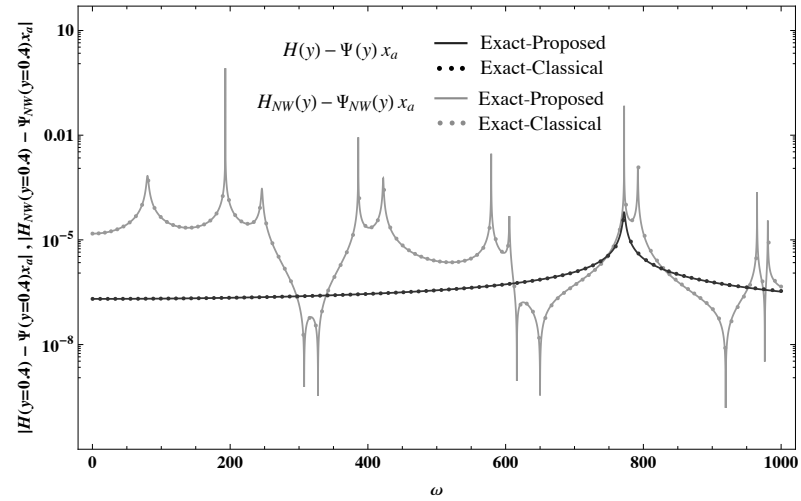

Figure 3.47: Beam in Figure 3.43, comparison between frequency response amplitudes for $H(y) - \Psi(y)x_a$ and $H_{NW}(y) - \Psi_{NW}(y)x_a$, computed at $y = 0.4\,\mathrm{m}$, for a point force P applied at $y_0 = 0.9\,\mathrm{m}$ with frequency ω spanning $[0, 1000]$ rad/s, as computed by exact proposed and classical methods.

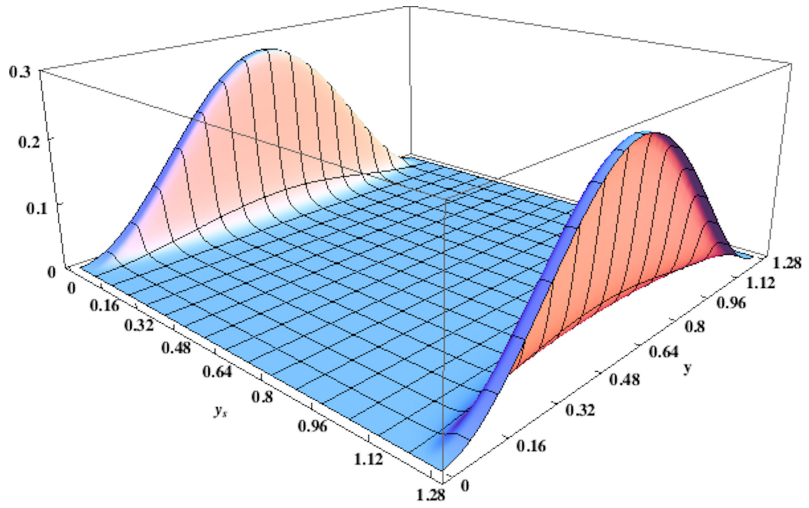

Figure 3.48: Beam in Figure 3.43, frequency response amplitude $|H(y) - \Psi(y)x_a|$ for MC total deflection along the whole beam, $0 \leq y \leq L$, due to a point force P applied at $y_0 = 0.9\,\text{m}$, with frequency $\omega = 772.07\,\text{rad/s}$, for varying damper position $0 < y_s < L$.

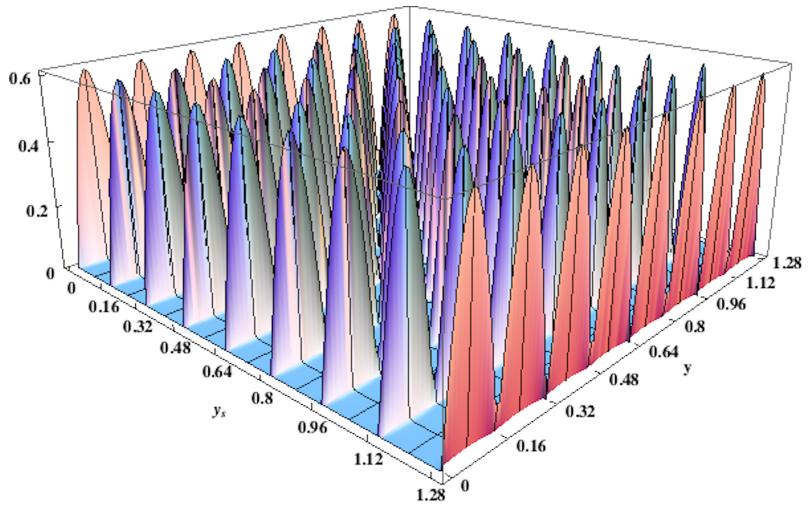

Figure 3.49: Beam in Figure 3.43, frequency response amplitude $|H_{NW}(y) - \Psi_{NW}(y)x_a|$ for MC total deflection along the whole beam, $0 \leq y \leq L$, due to a point force P applied at $y_0 = 0.9\,\text{m}$, with frequency $\omega = 772.07\,\text{rad/s}$, for varying damper position $0 < y_s < L$.

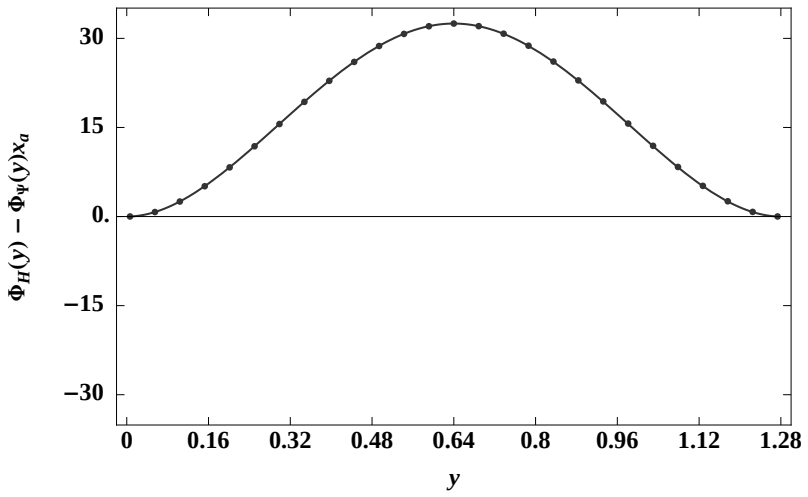

Figure 3.50: Beam in Figure 3.43, eigenfunction of the undamped mode corresponding to the peak at $\omega = 772.069\,\text{rad/s}$ in the frequency response amplitude $|H(y) - \Psi(y)x_a|$ for the MC total deflection, obtained in Figure 3.47 including warping effects.

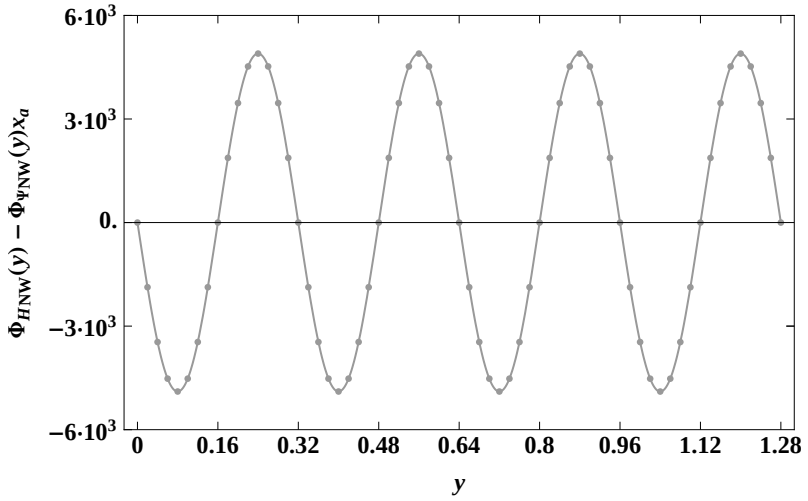

Figure 3.51: Beam in Figure 3.43, eigenfunction of the undamped mode corresponding to the peak at $\omega = 772.069\,\text{rad/s}$ in the frequency response amplitude $|H_{NW}(y) - \Psi_{NW}(y)x_a|$ for the MC total deflection, obtained in Figure 3.47 neglecting warping effects.

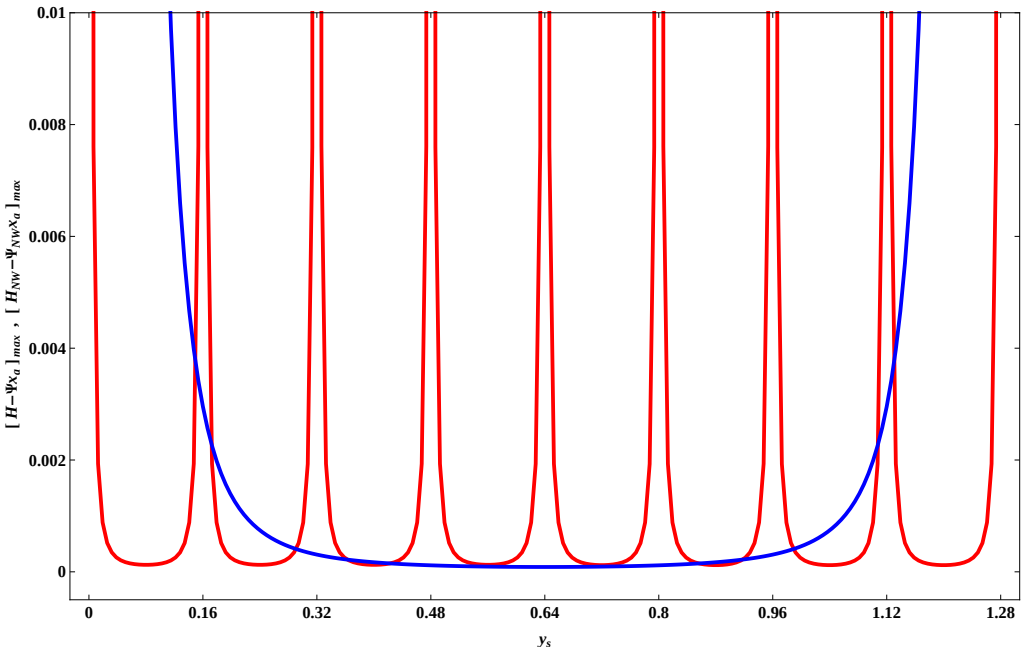

Figure 3.52: Beam in Figure 3.43, comparison between $[H - \Psi x_a]_{max}$ (—) and $[H_{NW} - \Psi_{NW} x_a]_{max}$ (—), i.e. maxima amplitudes of frequency responses $H(y) - \Psi(y)x_a$ and $H_{NW}(y) - \Psi_{NW}(y)x_a$, for MC total deflection computed over the whole beam, $0 \leq y \leq L$, for various damper positions $0 < y_s < L$.

3.6 Coupled bending-torsional vibrations of discontinuous beams with asymmetric cross sections

Future developments will provide generalization of the method to CCDS made up of beams with asymmetric cross section, neglecting or including warping effects. In the first case, appropriate combinations of the coupled equations of motion will lead, in the frequency domain, to a ten order differential equation governing the problem, while in the second case to a twelve order differential equation. Finding the fundamental solution of these problems (see Chapter 2) is the key step to obtain the dynamic Green's functions, frequency response functions of beams with dampers and to perform a complex modal analysis upon deriving pertinent orthogonality conditions.

In the next Section, an other mono-dimensional element will be considered: a two layer elastically bonded beam.

3.7 Flexural vibrations of discontinuous layered elastically bonded beams

In engineering applications, beams composed of two or more layers are widely used to increase the strength-to-weight and stiffness-to-weight ratio of structural components. If bonded by strong adhesives, the layers can be assumed to be rigidly interconnected, and a full composite action between the layers is developed. During the last decades a large amount of studies has been devoted to static and dynamic analysis of rigidly bonded composite structures for various engineering problems [75, 76, 77, 78, 79, 80, 81, 82, 83], providing engineers with various well established methods. However, in certain structural components such as composite steel concrete beams and layered wood beams with flexible shear connectors, a rigid bond between the

layers cannot be achieved. The deformation of the connectors results in an interlayer slip, which affects both strength and deformation of the structure. Existing literature has focused on static and dynamic analysis of layered elastically bonded beams. For instance, linear static analysis is performed in [84, 85, 86], and vibration problems are addressed in [87, 88, 89, 90, 91, 92]. In general all these studies have considered layered beams in a simple configuration, with uniform cross section and constraints at the beam ends only.

In this Section, the theory of generalized functions is used to reformulate and solve the vibration problem of two-layer elastically bonded beams with elastic translational supports and rotational joints. First, the governing equations of motion are presented. Then, a classical modal superposition approach is applied to build the dynamic response, with exact modes derived from an eigenvalue problem involving a 6×6 matrix, for any number of supports/joints. This result is obtained thanks to novel solutions of the equation of motion, built via the theory of generalized functions. Finally two illustrative examples are reported.

3.7.1 Problem Statement

In this Section the dynamic response of a beam composed of two elastically bonded layers, which carries an arbitrary number N of elastic translational supports and elastic rotational joints at abscissas x_j along the longitudinal x-axis, as shown in Figure 3.53, is analyzed. The layers are disposed about the transverse z-axis, with otherwise arbitrary shape and constant cross section. The beam is subjected to time-varying distributed loads $q(x;t)$ and concentrated forces $f_j(t)$ applied at abscissas x_j, inducing the dynamic lateral beam deflection $w(x;t)$, which, under the assumption of small deformations, is assumed to the same for each fiber at given x (no uplift between the layers). Variable t denotes time. The equation of flexural motion in terms of defection $w(x;t)$ is derived neglecting the effect of rotatory and longitudinal inertia and in absence of external axial forces. With these assumptions, conservation of

momentum in transverse direction, conservation of the angular momentum about the y-axis, and conservation of momentum in axial direction for the beam element yield the following equilibrium equations

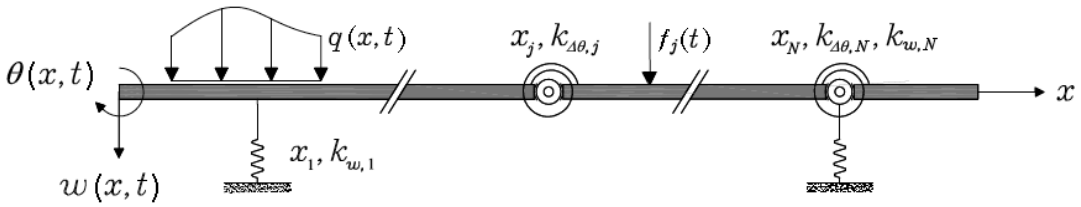

Figure 3.53: Two-layer elastically bonded beam

$$\frac{\bar{\partial} Q(x,t)}{\partial x} = -q(x,t) - f_j(t)\delta(x-x_j) - p_j(t)\delta(x-x_j) + \mu\frac{\partial^2 w(x,t)}{\partial t^2} \quad (3.238)$$

$$\frac{\bar{\partial} M(x,t)}{\partial x} = Q(x,t) \quad (3.239)$$

$$\frac{\bar{\partial} N(x,t)}{\partial x} = -T_1(x,t) + T_2(x,t) \quad (3.240)$$

in which the space-derivatives are generalized derivatives, as denoted by the over-bar, to capture the discontinuities of response variables at the elastic supports and joints, with $Q(x,t)$, $M(x,t)$, $N(x,t)$, $T1(x,t) = T2(x,t) = T(x,t)$ being the total shear force, the total bending moment, the total axial force, and the elastic interlaminar shear force transmitted between the upper and lower layer, respectively. The mass per unit length μ is calculated as $\mu = \sum_{i=1}^{2} \rho_i A_i$ with mass densities ρ_i and cross sectional areas A_i $(i = 1, 2)$ of the upper (subscript 1) and the lower layer. In Eq.(3.238), $p_j(t)$ is the reaction force exerted by the j-th elastic translational support of stiffness $k_{w,j}$

$$p_j(t) = -k_{w,j} w(x_j, t) \quad (3.241)$$

The total shear force $Q(x;t)$, the total bending moment $M(x;t)$ and the total axial force $N(x;t)$ are expressed in terms of the layer stress resultants as shown in Figure 3.54 and discussed in ref.[92]

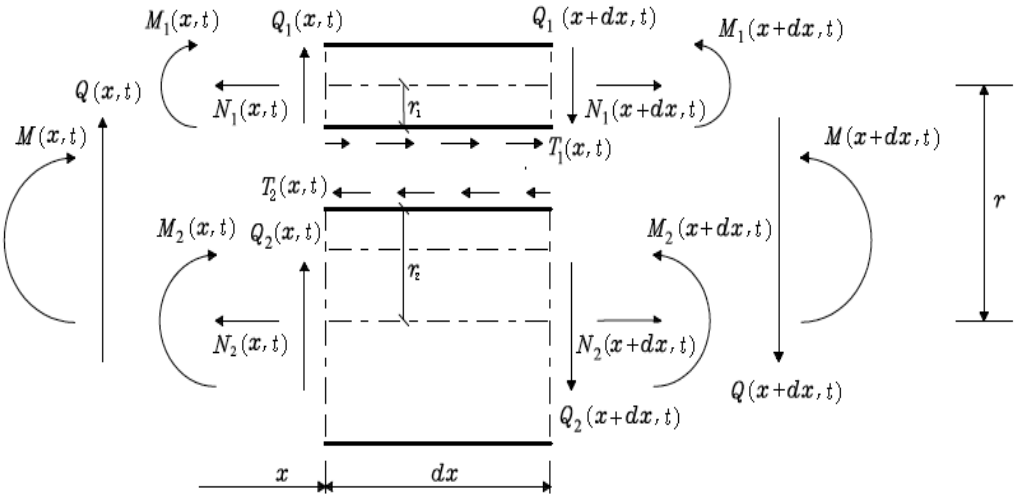

Figure 3.54: Infinitesimal two-layer beam element (according to ref.[92]).

$$Q(x,t) = Q_1(x,t) + Q_2(x,t) \tag{3.242}$$

$$M(x,t) = M_1(x,t) + M_2(x,t) - N_1(x,t)r \tag{3.243}$$

$$N(x,t) = N_1(x,t) + N_2(x,t) = 0 \tag{3.244}$$

where r represents the distance between the layer centroids, see Figure 3.54. Considering that Euler-Bernoulli hypothesis is not applicable to the total cross-section of the beam due to interlayer slip, but remains valid for each individual layer, and referring once more to Figure 3.54, the individual layer stress resultants are

$$Q_i(x,t) = \frac{\bar{\partial} M_i(x,t)}{\partial x} + T_i(x,t)r_i \tag{3.245}$$

$$M_i(x,t) = E_i I_i[-\frac{\bar{\partial} w(x,t)}{\partial x^2} + \Delta\Theta_j(t)\delta(x - x_j)] \quad \text{for } i = 1,2 \tag{3.246}$$

$$N_i(x,t) = E_i A_i \frac{\partial u_i(x,t)}{\partial x} \tag{3.247}$$

where E_1 and E_2 denote Young's moduli, and I_1 and I_2 are the principal moments of inertia of the cross-sectional areas of the upper and lower layer, respectively. The distances between the centroids of the single layers and

the interlayer are referred to as r_1 and r_2 (see Figure 3.54). Furthermore, $u_1(x,t)$ and $u2(x,t)$ are the longitudinal displacements at the centroid of the upper and lower layer, respectively. The relative rotation $\Delta\Theta_j(t)$ at the j-th elastic rotational joint is related to the corresponding bending moment $M(x_j,t)$ according to

$$\Delta\theta_j(t) = \theta(x_j^+,t) - \theta(x_j^-,t) = -\frac{M(x_j,t)}{k_{\Delta\theta,j}} \tag{3.248}$$

where $\theta(x,t) = \bar{\partial}w(x,t)/\partial x$ is the reaction of the cross section, assumed to be equal for both layers, while $k_{\Delta\theta_j}$ denotes the stiffness of the j-th rotational joint.

The elastic interlaminar shear force $T(x,t) = T1(x,t) = T2(x,t)$ between the upper and lower layer is a force per unit length and is related to the interlaminar slip (see Figure 3.55)

$$\Delta u(x,t) = u_2(x,t) - u_1(x,t) + r\frac{\bar{\partial}w(x,t)}{\partial x} \tag{3.249}$$

via Hooke's law, i.e.

$$T(x,t) = k_s\Delta_u(x,t) \tag{3.250}$$

with k_s being the elastic slip modulus. Differentiation of Eq.(3.250) with respect to x yields together with Eqs.(3.248), (3.242), (3.245) and taking into account that $\partial N_1(x,t)/\partial x = -T$, after some algebra,

$$r\frac{\bar{\partial}^2 w(x,t)}{\partial x^2} + \frac{1}{k_s}\frac{\bar{\partial}^2 N_1(x,t)}{\partial x^2} - N_1(x,t)(\frac{1}{E_1A_1} + \frac{1}{E_2A_2}) = 0 \tag{3.251}$$

Combining Eqs. (3.242), (3.245) allows the axial force in the upper layer $N_1(x;t)$ to be expressed as a function of the total bending moment $M(x,t)$ and the kinematic variables $w(x,t)$ and $\Delta\theta_j(t)$

$$N_1(x,t) = -\frac{1}{r}[M(x,t) + EI_0(\frac{\bar{\partial}w(x,t)}{\partial x^2} - \Delta\theta_j(t)\delta(x-x_j))] \tag{3.252}$$

with EI_0 denoting the bending stiffness corresponding to non-composite action (subscript 0),

$$EI_0 = \sum_{i=1}^{2} E_i I_i \tag{3.253}$$

Subsequently, Eq.(3.252) and its second derivative with respect to x are substituted into Eq.(3.251), yielding

$$\frac{\bar{\partial} w(x,t)}{\partial x^4} - \alpha^2 \frac{\bar{\partial}^2 w(x,t)}{\partial x^2} + k_s \frac{EA_0}{EA_p} \Delta\theta_j(t)\delta(x - x_j) - \Delta\theta_j \delta^{(2)}(x - x_j) = \\ + \frac{\alpha^2}{EI_\infty} M(x,t) - \frac{1}{EI_0} \frac{\bar{\partial}^2 M(x,t)}{\partial x^2} \tag{3.254}$$

In this equation, $EA_p = E_1 A_1 E_2 A_2$, EI_∞ is the bending stiffness corre-

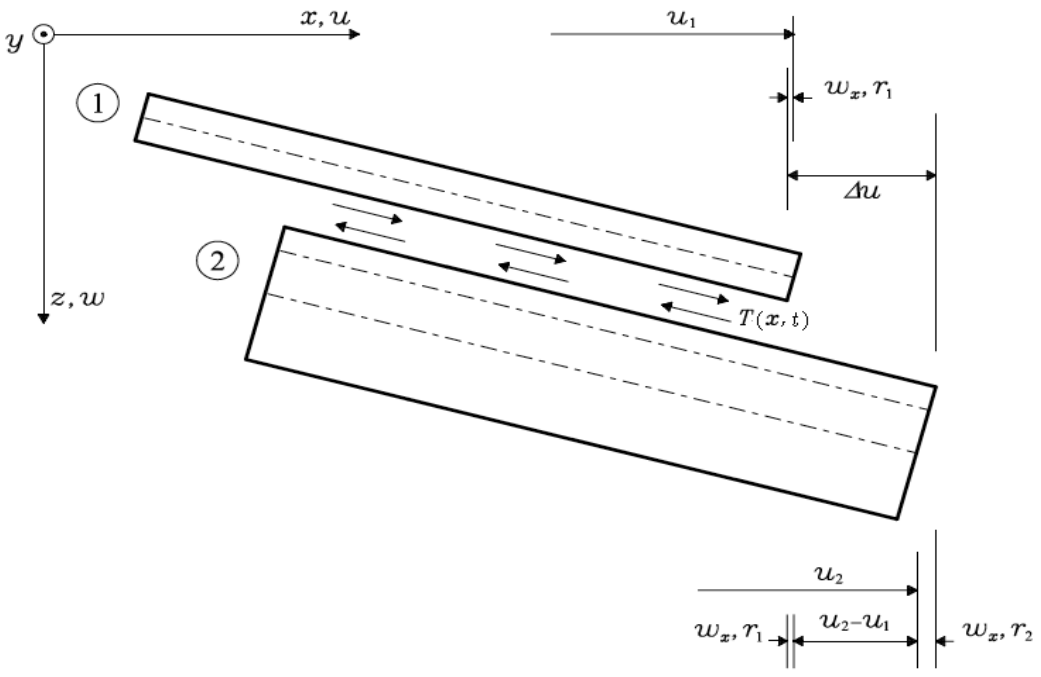

Figure 3.55: Deformed two-layer beam (according to ref.[92]).

sponding to a rigid interlayer connection (∞) and EA_0 is the longitudinal

stiffness for non-composite action, defined respectively as

$$EI_\infty = EI_0 + \frac{r^2 EA_p}{EA_0}, \quad EA_0 = \sum_{i=1}^{2} E_i A_i \tag{3.255}$$

while coefficient α^2 reads

$$\alpha^2 = k_s\left(\frac{EA_0}{EA_p} + \frac{r_2}{EI_0}\right) \tag{3.256}$$

Twice differentiation of Eq.(3.254) with respect to x and using Eqs.(3.238), finally the equation of motion in terms of $w(x,t)$

$$\begin{aligned}\frac{\bar{\partial} w(x,t)}{\partial x^6} - \alpha^2\frac{\bar{\partial}^4 w(x,t)}{\partial x^4} + \frac{\mu}{EI_0}\frac{\bar{\partial}^4 w(x,t)}{\partial x^2 \partial t^2} - \frac{\mu\alpha^2}{EI_\infty}\frac{\partial^2 w(x,t)}{\partial t^2} + \frac{\alpha^2}{EI_\infty p_j(t)}\delta(x-x_j) \\ - \frac{p_j(t)}{EI_0}\delta^{(2)}(x-x_j) + k_s\frac{EA_0}{EA_p}\Delta\theta_j(t)\delta^{(2)}(x-x_j) - \Delta\theta_j(t)\delta^{(4)}(x-x_j) \\ = -\frac{\alpha^2}{EI_\infty q(x,t)} - \frac{\alpha^2}{EI_\infty} f_j(t)\delta(x-x_j) + \frac{f_j(t)}{EI_0}\delta^{(2)}(x-x_j)\end{aligned} \tag{3.257}$$

Note that in Eq.(3.257), the reaction force $p_j(t)$ exerted by the j-th translational support and relative rotation $\Delta\theta_j(t)$ at the j.th rotational joints are unknown quantities.

In the present formulation, both limits $\alpha \to \infty$ (rigidly bonded beam) and $\alpha \to 0$ (no bonded beam) can be taken into account without numerical difficulties. If no supports and joints are present then $p_j = 0$ and $\Delta\theta_j = 0$ for any j. In such case, Eq.(3.257) reverts to the equation of motion of two-layer elastically bonded beam without discontinuities, as shown in ref.[91].

The solution of Eq.(3.257) is found together with the initial conditions $w(x, t = 0)$, $\partial w(x, t = 0)/\partial t = 0$, and the beam boundary conditions. In the following three classical boundary conditions are reported ([91]) with $x_b = 0, L$ denoting the beam ends.

- Simply supported end

$$w(x_b,t) = 0 \quad M_1(x_b,t) = M_2(x_b,t) = 0 \quad N_1(x_b,t) = 0 \tag{3.258}$$

- Clamped end

$$w(x_b,t)=0 \quad \frac{\bar{\partial} w(x_b,t)}{\partial x}=0 \quad \Delta u(x_b,t)=0 \tag{3.259}$$

- Free end

$$M_1(x_b,t)=M_2(x_b,t)=0 \quad N_1(x_b,t)=0 \quad Q(x_b,t)=0 \tag{3.260}$$

Upon solving Eq.(3.257) for $w(x;t)$, the stress resultants $M(x;t)$, $Q(x;t)$, $N_1(x;t)$ and the interlaminar shear force per unit length $T(x;t)$ can be built from the previous equations.

3.7.2 Direct Frequency analysis

Based on the standard separate variables approach, assuming $w(x,t)=\Phi(x)e^{i\omega t}$, with ω natural frequency for the free vibration deflection of the two-layer elastically bonded beam with elastic supports/joints, the following sixth ordinary differential equation for the deflection eigenfunction $\phi(x)$ is obtained

$$\begin{aligned}\frac{\bar{d}\Phi(x)}{dx^6}-\alpha^2\frac{\bar{d}^4\Phi(x)}{dx^4}-\frac{\mu\omega^2}{EI_0}\frac{\bar{d}^2\Phi(x)}{dx^2}+\frac{\mu\alpha^2\omega^2}{EI_\infty}\Phi(x)+\frac{\alpha^2}{EI_\infty P_j}\delta(x-x_j)\\ -\frac{P_j}{EI_0}\delta^{(2)}(x-x_j)+k_s\frac{EA_0}{EA_p}\Delta\Theta_j\delta^{(2)}(x-x_j)-\Delta\Theta_j(t)\delta^{(4)}(x-x_j)=0\end{aligned} \tag{3.261}$$

The eigenfunction for the bending moment $\Upsilon(x)$, the shear force $\Gamma(x)$, the axial force in the upper layer $\Sigma(x)$, and the elastic interlaminar shear force $\Psi(x)$, are similarly obtained [36]

$$\begin{aligned}\Upsilon(x)=-EI_\infty\frac{\bar{d}^2\Phi(x)}{dx^2}+\frac{EI_\infty}{\alpha^2}(\frac{\bar{d}^4\Phi(x)}{dx^4}-\frac{\mu\omega^2}{EI_0}\Phi(x))\\ +\frac{k_sEA_0EI_\infty}{EA_p\alpha^2}\Delta\Theta_j\delta(x-x_j)-\frac{EI_\infty}{\alpha^2}\Delta\Theta_j\delta^{(2)}(x-x_j)-\frac{EI_\infty}{EI_0\alpha^2}P_j\delta(x-x_j)\end{aligned} \tag{3.262}$$

$$\begin{aligned}\Gamma(x) = &-EI_\infty \frac{\bar{d}^3\Phi(x)}{dx^3} + \frac{EI_\infty}{\alpha^2}(\frac{\bar{d}^5\Phi(x)}{dx^5} - \frac{\mu\omega^2}{EI_0}\frac{\Phi(x)}{dx}) \\ &+ \frac{k_s EA_0 EI_\infty}{EA_p\alpha^2}\Delta\Theta_j\delta^{(1)}(x-x_j) \\ &- \frac{EI_\infty}{\alpha^2}\Delta\Theta_j\delta^{(3)}(x-x_j) - \frac{EI_\infty}{EI_0\alpha^2}P_j\delta^{(1)}(x-x_j)\end{aligned} \tag{3.263}$$

$$\begin{aligned}\Sigma(x) = &-\frac{1}{r}[(EI_0 - EI_\infty)\frac{\bar{d}^2\Phi(x)}{dx^2} + \frac{EI_\infty}{\alpha^2}(\frac{\bar{d}^4\Phi(x)}{dx^4} - \frac{\mu\omega^2}{EI_0}\Phi(x))] \\ &+ \frac{1}{r}\Delta\Theta_j\delta(x-x_j) - \frac{k_s EA_0 EI_\infty}{\tau EA_p\alpha^2}\Delta\Theta_j\delta(x-x_j) \\ &+ \frac{EI_\infty}{\tau\alpha^2}\Delta\Theta_j\delta^{(2)}(x-x_j) + \frac{EI_\infty}{\tau EI_0\alpha^2}P_j\delta(x-x_j)\end{aligned} \tag{3.264}$$

$$\begin{aligned}\Sigma(x) = &-\frac{1}{r}[(EI_0 - EI_\infty)\frac{\bar{d}^3\Phi(x)}{dx^3} + \frac{EI_\infty}{\alpha^2}(\frac{\bar{d}^5\Phi(x)}{dx^5} - \frac{\mu\omega^2}{EI_0}\frac{\bar{d}\Phi(x)}{dx})] \\ &+ \frac{1}{r}\Delta\Theta_j\delta^{(1)}(x-x_j) - \frac{k_s EA_0 EI_\infty}{\tau EA_p\alpha^2}\Delta\Theta_j\delta^{(1)}(x-x_j) \\ &+ \frac{EI_\infty}{\tau\alpha^2}\Delta\Theta_j\delta^{(3)}(x-x_j) + \frac{EI_\infty}{\tau EI_0\alpha^2}P_j\delta^{(1)}(x-x_j)\end{aligned} \tag{3.265}$$

The eigenfunction of rotation $\Theta(x)$ is found considering that

$$\Theta(x) = \frac{\bar{d}\Phi(x)}{dx} \tag{3.266}$$

while unknown quantities P_j and $\Delta\Theta_j$ at the application point of supports/joints are given by Eq.(3.241) and Eq.(3.248), respectively

$$P_j = -k_{w,j}\Phi(x_j) \tag{3.267}$$

$$\Delta\Theta_j = -\frac{\Upsilon(x_j)}{k_{\Delta\theta,j}} \tag{3.268}$$

Next, basing on the procedure shown in the previous Sections for other

mono dimensional elements, the eigenfunctions of the two-layer elastically bonded beam problem can be computed. For this purpose, the unknown eigenfunctions of the response variables are collected in vector $\mathbf{Y}(x) = [\Phi(x)\ \Theta(x)\ \Upsilon(x)\ \Gamma(x)\ \Sigma(x)\ \Psi(x)]^T$ and the unknown quantities P_j and $\Delta\Theta_j$ at the application points of elastic supports and joints are collected in vectors $\mathbf{\Lambda}_j = [P_j\ \Delta\Theta_j]$. Based on the linear superposition principle, vector $\mathbf{Y}(x)$ is built as the sum of the solution $\mathbf{\Omega}(x)\mathbf{c}$ to the homogeneous equation associated with Eq.(3.261), representing the eigenfunctions of the bare beam (i.e. the beam without supports/joints), and the particular solution $\mathbf{J}(x, x_j)\mathbf{\Lambda}_j$ associated with the unknowns P_j and $\Delta\Theta_j$, which account for the discontinuities of the response variables at support and joint locations, respectively

$$\mathbf{Y}(x) = \mathbf{\Omega}(x)\mathbf{c} + \sum_{j=1}^{N} \mathbf{J}(x, x_j)\mathbf{\Lambda}_j \tag{3.269}$$

where $\mathbf{c} = [c_1\ c_2\ c_3\ c_4\ c_5\ c_6]^T$ is a 6×1 vector of integration constants, while

$$\mathbf{\Omega}(x) = \begin{bmatrix} \Omega_{\Phi 1} & \Omega_{\Phi 2} & \Omega_{\Phi 3} & \Omega_{\Phi 4} & \Omega_{\Phi 5} & \Omega_{\Phi 6} \\ \Omega_{\Theta 1} & \Omega_{\Theta 2} & \Omega_{\Theta 3} & \Omega_{\Theta 4} & \Omega_{\Theta 5} & \Omega_{\Theta 6} \\ \Omega_{\Upsilon 1} & \Omega_{\Upsilon 2} & \Omega_{\Upsilon 3} & \Omega_{\Upsilon 4} & \Omega_{\Upsilon 5} & \Omega_{\Upsilon 6} \\ \Omega_{\Gamma 1} & \Omega_{\Gamma 2} & \Omega_{\Gamma 3} & \Omega_{\Gamma 4} & \Omega_{\Gamma 5} & \Omega_{\Gamma 6} \\ \Omega_{\Sigma 1} & \Omega_{\Sigma 2} & \Omega_{\Sigma 3} & \Omega_{\Sigma 4} & \Omega_{\Sigma 5} & \Omega_{\Sigma 6} \\ \Omega_{\Psi 1} & \Omega_{\Psi 2} & \Omega_{\Psi 3} & \Omega_{\Psi 4} & \Omega_{\Psi 5} & \Omega_{\Psi 6} \end{bmatrix} \tag{3.270}$$

$$\mathbf{J}(y, y_j) = [\mathbf{J}^{(P)}\ \ \mathbf{J}^{(\Delta\Theta)}] = \begin{bmatrix} J_{\Phi}^{(P)} & J_{\Phi}^{(\Delta\Theta)} \\ J_{\Theta}^{(P)} & J_{\Theta}^{(\Delta\Theta)} \\ J_{\Upsilon}^{(P)} & J_{\Upsilon}^{(\Delta\Theta)} \\ J_{\Gamma}^{(P)} & J_{\Gamma}^{(\Delta\Theta)} \\ J_{\Sigma}^{(P)} & J_{\Sigma}^{(\Delta\Theta)} \\ J_{\Phi}^{(P)} & J_{\Phi}^{(\Delta\Theta)} \end{bmatrix} \quad \text{for } j = 1, 2, \ldots N \tag{3.271}$$

In Eq.(3.271) superscripts P and $\Delta\Theta$ denote the particular integrals as-

sociated with a unit transverse force $P_j = 1$ and a unit relative rotation $\Delta\Theta_j = 1$, applied at $x = x_j$, respectively. All terms in Eq.(3.269) are available in a simple closed analytical form.

Following the procedure in the previous Section and adapting it to this problem its is possible to formulate ehe eigenvalue problem in this matrix form:

$$\mathbf{Bc} = \mathbf{0} \tag{3.272}$$

where $\mathbf{c}$ is a 6×6 matrix regardless of the number of supports/joints. The characteristic equation is the determinant of matrix $\mathbf{B}$, i.e. set$\mathbf{B} = 0$, whose roots ω_n are the natural frequencies of the beam. Once vector $\mathbf{c}$ is derived as non-trivial solution of Eq.(3.272) for the n-th natural frequency, the exact closed analytical expression for the corresponding vector of eigenfunctions $\mathbf{Y}_n(x)$ is finally built by Eq.(3.269). The eigenfunctions satisfy intrinsically all the required conditions at the application points of support/joints, thanks to the generalized functions involved in the particular integrals.

3.7.3 Classical Modal analysis and time domain response

Based on modal analysis, the beam deflection response $w(x,t)$ under an external excitation may be expressed as

$$w(x,t) = \sum_{n=1}^{\infty} R_n(t)\Phi_n(x) \tag{3.273}$$

where $R_n(x)$ denotes the n-th deflection eigenfunction derived in Section 3.1, while $R_n(x)$ is the corresponding time-dependent modal coordinate.

Modal series Eq.(3.273) is substituted into the equation of motion Eq.(3.261), mutiplied by the m-th eigenfunction $\Phi_m(x)$, and integrated over beam length

L. Then, considering the orthogonality relations

$$-\frac{\mu}{EI_0}\int_0^L \frac{\bar{d}^2\Phi_m(x)}{dx^2}\Phi_n dx+\frac{\mu\alpha}{EI_\infty}\int_0^L \Phi_n\Phi_m dx+\sum_{h=1}^{2}\Phi_n(x_b)C_h[\Phi_m(x_b)] = m_m\delta_{mn} \tag{3.274}$$

where $x_b = 0,\ L$; δ_{mn} is the Kronocker delta, C_h denotes a linear homogenous differential operator containing derivatives of the boundaries, for example

- simply supported or clamped end

$$C_1 = C_2 = 0 \tag{3.275}$$

and m_m is the modal mass

$$m_m = -\frac{\mu}{EI_0}\int_0^L \frac{\bar{d}^2\Phi_m(x)}{dx^2}\Phi_m(x)+\frac{\mu\alpha^2}{EI_\infty}\int_0^L \Phi_m^2(x)dx+\sum_{h=1}^{2}\Phi_m(x_b)C_h[\Phi_m(x_b,t)] \tag{3.276}$$

the ordinary equation for modal coordinate $R_m(t)$, is written as

$$\frac{d^2R_m(t)}{dt^2}+\omega_m^2R_m(t) = \frac{1}{m_m}V_m(t)\ , \quad \text{for } m = 1,\dots,\infty \tag{3.277}$$

with modal loading V_m

$$\begin{aligned} V_m(t) = {} & \frac{\alpha^2}{EI_\infty}\int_0^L \Phi_m(x)q(x,t)dx - \frac{1}{EI_0}\int_0^L \Phi_m(x)\frac{\partial q(x,t)}{\partial x^2}dx \\ & + \frac{\alpha}{EI_\infty}\int_0^L \Phi_m(x)f_j(t)\delta(x-x_j)dx - \frac{1}{EI_0}\int_0^L \Phi_m(x)f_j(t)\delta^{(2)}(x-x_j)dx \\ & + \sum_{h=1}^{2}\Phi_m(x_b)C_h[q(x_b,t)] \end{aligned} \tag{3.278}$$

Within a linear theory, assuming proportional viscous damping, Eq.(3.277) can be modified as

$$\frac{d^2R_m(t)}{dt^2}+2\xi_m\omega_m\frac{dR_m(t)}{dt}+\omega_m^2R_m(t) = \bar{}m_mV_m(t) \tag{3.279}$$

For quiet initial conditions, the time domain solution of Eq.(3.279) is given

by the well-known Duhamel's convolution integral,

$$R_m(t) = \frac{1}{m_m \omega_{dm}} \int_0^t V_m(\tau) exp[-\xi_m \omega_m (t-\tau)] d\tau \tag{3.280}$$

with the m-th damped natural frequency $\omega_{dm} = \omega_m \sqrt{1-\xi_m^2}$.

Chapter 4

Extension of the proposed approach to coupled plane frames-discrete systems: Deterministic Analysis

The method proposed in Chapter 3 is now extended to perform the deterministic dynamic analysis of coupled plane frame-discrete systems.

Thanks to the closed form expressions derived in Chapter 3 for frequency response functions, the exact DSM and LV will be built for every mono-dimensional element with sizes that do not depend on the number of subsystems. This is the basis to build the exact global DSM and LV of coupled frame-discrete systems. Plane frames made up of 2-D assembly of beams with symmetric cross section will be considered only.

Finally, for plane frames coupled with mass-spring subsystems, a novel modal analysis approach is developed to compute the time domain response.

4.1 Exact dynamic stiffness matrix and load vectors of coupled beams-discrete systems

In this Section, the DSM and LV are built for different types of coupled beams-discrete systems. For this purpose, these systems are treated as two node elements with each node featuring a fixed number of degrees of freedom which depends on the kind of beam and vibration problem considered. Firstly, beams with symmetric cross section are dealt with. For these beams uncoupled axial and flexural vibrations are considered and each node features 3 degrees of freedom (axial displacement, defection and rotation). Next, beams with mono symmetric cross section are considered. These beams show coupled bending-torsion vibrations and then each node feature 3 (deflection, bending rotation, torsional rotation) or 4 (deflection, bending rotation, torsional rotation, torsion) degrees of freedom depending on the inclusion or not of the warping effects.

4.1.1 Exact dynamic stiffness matrix and load vectors of discontinuous beams with symmetric cross section

Refer to the beam ends in Figure 3.1 as nodes with 3 degrees of freedom each (axial displacement, deflection, and rotation), and assume, for generality, arbitrary transverse polynomial loads. Nodal equations can be built using Eq.(3.54) for the bending response $\mathbf{Y}(x,\omega)$, and Eq.(3.110) for axial displacement $U(x,\omega)$ and axial force $N(x,\omega)$ collected in $\mathbf{Z}(x,\omega)$.

Using Eq.(3.54) for $\mathbf{Y}(x,\omega) = [V\ \Theta\ M\ S]^T$ and Eq.(3.110) for $U(x,\omega)$ and $N(x,\omega)$ to build the vector of nodal displacements/rotations $\mathbf{u} = [u_1\ v_1\ \theta_1\ u_2\ v_2\ \theta_2]^T$ with $u_1 = U(0,\omega)$, $v_1 = V(0,\omega)$, $\theta_1 = \Theta(0,\omega)$, $u_2 = U(L,\omega)$, $v_2 = V(L,\omega)$, $\theta_2 = \Theta(L,\omega)$, and the vector of nodal forces/moments $\mathbf{f} = [H_1\ T_1\ C_1\ H_2\ T_2\ C_2]$, with $H_1 = -N(0,\omega)$, $T_1 = -S(0,\omega)$, $C_1 = M(0,\omega)$,

$H_2 = -N(L,\omega)$, $T_2 = -S(L,\omega)$, $C_2 = M(L,\omega)$, (positive sign conventions for the nodal forces/moments agree with those for the nodal displacements/rotations), the following nodal equations can be written:

$$\mathbf{u} = \mathbf{\Gamma b} + \mathbf{u}^{(f)} \tag{4.1}$$

$$\mathbf{f} = \mathbf{\Xi b} + \mathbf{f}^{(f)} \tag{4.2}$$

with $\mathbf{u}^{(f)} = [\tilde{W}_1^{(f)}(0)\ \tilde{Y}_1^{(f)}(0)\ \tilde{Y}_2^{(f)}(0)\ \tilde{W}_1^{(f)}(L)\ \tilde{Y}_1^{(f)}(L)\ \tilde{Y}_2^{(f)}(L)]$, $\mathbf{u}^{(f)}$ $= [-\tilde{W}_1^{(f)}(0) - \tilde{Y}_4^{(f)}(0)\ \tilde{Y}_3^{(f)}(0)\ \tilde{W}_2^{(f)}(L)\ \tilde{Y}_4^{(f)}(L)\ -\tilde{Y}_3^{(f)}(L)]^T$, $\mathbf{b} = [a_1\ a_2\ c_1$ $c_2\ c_3\ c_4]^T$, whereas $\mathbf{\Gamma}$ and $\mathbf{\Xi}$ are

$$\mathbf{\Gamma} = \begin{bmatrix} U_{11}(0) & U_{12}(0) & 0 & 0 & 0 & 0 \\ 0 & 0 & \tilde{Y}_{11}(0) & \tilde{Y}_{12}(0) & \tilde{Y}_{13}(0) & \tilde{Y}_{14}(0) \\ 0 & 0 & \tilde{Y}_{21}(0) & \tilde{Y}_{22}(0) & \tilde{Y}_{23}(0) & \tilde{Y}_{24}(0) \\ U_{11}(0) & U_{12}(L) & 0 & 0 & 0 & 0 \\ 0 & 0 & \tilde{Y}_{11}(L) & \tilde{Y}_{12}(L) & \tilde{Y}_{13}(L) & \tilde{Y}_{14}(L) \\ 0 & 0 & \tilde{Y}_{11}(L) & \tilde{Y}_{12}(L) & \tilde{Y}_{13}(L) & \tilde{Y}_{14}(L) \end{bmatrix} \tag{4.3}$$

$$\mathbf{\Xi} = \begin{bmatrix} -N_{11}(0) & -N_{12}(0) & 0 & 0 & 0 & 0 \\ 0 & 0 & -\tilde{Y}_{41}(0) & -\tilde{Y}_{42}(0) & -\tilde{Y}_{43}(0) & -\tilde{Y}_{44}(0) \\ 0 & 0 & \tilde{Y}_{31}(0) & \tilde{Y}_{32}(0) & \tilde{Y}_{33}(0) & \tilde{Y}_{34}(0) \\ U_{11}(0) & U_{12}(L) & 0 & 0 & 0 & 0 \\ 0 & 0 & \tilde{Y}_{41}(L) & \tilde{Y}_{42}(L) & \tilde{Y}_{43}(L) & \tilde{Y}_{44}(L) \\ 0 & 0 & -\tilde{Y}_{31}(L) & -\tilde{Y}_{32}(L) & -\tilde{Y}_{33}(L) & -\tilde{Y}_{34}(L) \end{bmatrix} \tag{4.4}$$

In Eqs. (4.3) and (4.4), $U_{11}(x)$, $U_{12}(x)$, $N_{11}(x)$, $N_{12}(x)$ are taken from Eqs. (3.110), whereas $\tilde{Y}_{ij}$ and $\tilde{Y}_i^{(f)}$ denotes the (i, j) element of matrix in Eq.(3.54) and i-th element of vector $\tilde{\mathbf{Y}}^{(f)}$, in Eq.(3.54). Based on Eqs.(4.1)

and (4.2), the following nodal matrix relation can be derived

$$\mathbf{f} = \mathbf{\Sigma\Gamma}^{-1}(\mathbf{u} - \mathbf{u}^{(f)}) + \mathbf{f}^{(f)} = \mathbf{D}(\omega)\mathbf{u} + \mathbf{q} \tag{4.5}$$

where

$$\mathbf{D}(\omega) = \mathbf{\Sigma\Gamma}^{-1} \tag{4.6}$$

$$\mathbf{q}(\omega) = -\mathbf{\Sigma\Gamma}^{-1}\mathbf{u}^{(f)} + \mathbf{f}^{(f)} \tag{4.7}$$

In Eqs.(4.6) and (4.7), $\mathbf{D}(\omega)$ and $\mathbf{q}(\omega)$ are the exact 6×6 DSM and the exact 6×1 LV of the two node beam element with an arbitrary number of dampers. Respective, sizes of $\mathbf{D}(\omega)$ and $\mathbf{q}(\omega)$ are 6×6 and 6×1 regardless of the number of dampers.

Matrix $\mathbf{D}(\omega)$ in Eq.(4.6) is available in a closed form, because the inverse matrix $\mathbf{\Gamma}^{-1}$ can be inverted, in a symbolic form, from Eq.(4.3) for $\mathbf{\Gamma}$. Pertinent formulae for inversion are given in Appendix B. Also, vector $\mathbf{q}$ in Eq. (4.7) can be computed in a closed form, for any polynomial load, based on the symbolic inverse matrix $\mathbf{\Gamma}^{-1}$ and closed-form expressions for $\mathbf{u}^{(f)}$ and $\mathbf{f}^{(f)}$ in Eqs.(4.1) and (4.2). Finally, notice that there is a formal correspondence between Eq.(4.5) and the standard equilibrium equation of a two-node beam element in the FE method. However, unlike in the FE method, $\mathbf{D}(\omega)$ and $\mathbf{q}(\omega)$ are the exact DSM and the exact LV.

These are considerable advantages over the exact classical method that, in general, provides numerical solutions. Indeed, terms in the dynamic stiffness matrix would be computed column by column, enforcing unit displacements/rotations at the ends, and the coefficient matrix associated with the equations to be solved should be inverted numerically, for each frequency of interest.

Remarkably, the size of $\mathbf{D}(\omega)$ and $\mathbf{q}(\omega)$ is 6×6 and 6×1, respectively, for any number of dampers/masses and loads along the two-node beam element. Therefore, within a standard finite element assembling procedure, $\mathbf{D}(\omega)$ and $\mathbf{q}(\omega)$ will be used in the next Section to build the exact global

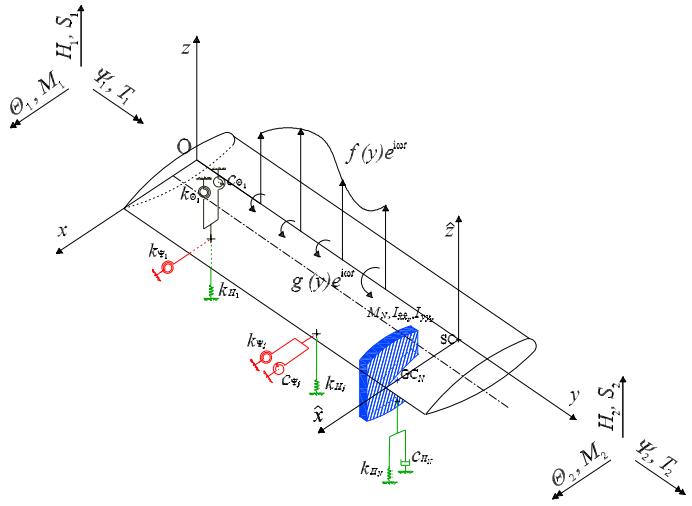

Figure 4.1: Two-node beam element for the beam in Figure 3.19.

dynamic stiffness matrix and load vector of frames, whose size will depend only on the number of beam-to-column nodes regardless of the number of in-span dampers/masses and loads along every structural member. On using the derived closed-form expressions, this is feasible in any finite element commercial code for frequency response of frames.

Next, the exact DSM and LV will be built for coupled systems made up of beams with mono symmetric cross section.

4.1.2 Exact dynamic stiffness matrix and load vector of discontinuous beams with mono symmetric cross section (warping effects neglected)

Consider the beam in Figure 3.19 as a two-node finite element with nodes at the two ends, each featuring 3 degrees of freedom, as shown in Figure 4.1. For generality, consider the case of harmonically-varying, arbitrarily-placed polynomial load.

Using Eq.(3.143) to build the vector of nodal displacements/rotations $\mathbf{u} = [H(0)\ \Theta(0)\ \Psi(0)\ H(L)\ \Theta(L)\ \Psi(L)]^{\mathrm{T}} = [H_1\ \Theta_1\ \Psi_1\ H_2\ \Theta_2\ \Psi_2]^{\mathrm{T}}$ and the vec-

tor of nodal forces/moments $\mathbf{f} = [-S(0)\ -M(0)\ -T(0)\ S(L)\ M(L)\ T(L)]^{\mathrm{T}} = = [S_1\ M_1\ T_1\ S_2\ M_2\ T_2]^{\mathrm{T}}$ (positive sign conventions for nodal forces/moments agree with those for nodal displacements/rotations), the following expressions can be written:

$$\mathbf{u} = \mathbf{A}\mathbf{c} + \tilde{\mathbf{u}}_f + \tilde{\mathbf{u}}_g \ ; \ \mathbf{f} = \mathbf{Z}\mathbf{c} + \tilde{\mathbf{f}}_f + \tilde{\mathbf{f}}_g \tag{4.8}$$

where $\mathbf{A}$ and $\mathbf{Z}$ are

$$\mathbf{A} = \begin{bmatrix} \tilde{\mathbf{Y}}_1(0) \\ \tilde{\mathbf{Y}}_2(0) \\ \tilde{\mathbf{Y}}_5(0) \\ \tilde{\mathbf{Y}}_1(L) \\ \tilde{\mathbf{Y}}_2(L) \\ \tilde{\mathbf{Y}}_5(L) \end{bmatrix}; \quad \mathbf{Z} = \begin{bmatrix} -\tilde{\mathbf{Y}}_4(0) \\ -\tilde{\mathbf{Y}}_3(0) \\ -\tilde{\mathbf{Y}}_6(0) \\ \tilde{\mathbf{Y}}_4(L) \\ \tilde{\mathbf{Y}}_3(L) \\ \tilde{\mathbf{Y}}_6(L) \end{bmatrix} \tag{4.9}$$

denoting with $\tilde{\mathbf{Y}}_j(y)$ the j-th row of matrix $\tilde{\mathbf{Y}}(y)$, while $\tilde{\mathbf{u}}_f$, $\tilde{\mathbf{u}}_g$, $\tilde{\mathbf{f}}_f$, $\tilde{\mathbf{f}}_g$ are

$$\tilde{\mathbf{u}}_f = \begin{bmatrix} \tilde{Y}_1^{(f)}(0) \\ \tilde{Y}_2^{(f)}(0) \\ \tilde{Y}_5^{(f)}(0) \\ \tilde{Y}_1^{(f)}(L) \\ \tilde{Y}_2^{(f)}(L) \\ \tilde{Y}_5^{(f)}(L) \end{bmatrix}; \quad \tilde{\mathbf{u}}_g = \begin{bmatrix} \tilde{Y}_1^{(g)}(0) \\ \tilde{Y}_2^{(g)}(0) \\ \tilde{Y}_5^{(g)}(0) \\ \tilde{Y}_1^{(g)}(L) \\ \tilde{Y}_2^{(g)}(L) \\ \tilde{Y}_5^{(g)}(L) \end{bmatrix}; \quad \tilde{\mathbf{f}}_f = \begin{bmatrix} -\tilde{Y}_4^{(f)}(0) \\ -\tilde{Y}_3^{(f)}(0) \\ -\tilde{Y}_6^{(f)}(0) \\ \tilde{Y}_4^{(f)}(L) \\ \tilde{Y}_3^{(f)}(L) \\ \tilde{Y}_6^{(f)}(L) \end{bmatrix}; \quad \tilde{\mathbf{f}}_g = \begin{bmatrix} -\tilde{Y}_4^{(g)}(0) \\ -\tilde{Y}_3^{(g)}(0) \\ -\tilde{Y}_6^{(g)}(0) \\ \tilde{Y}_4^{(g)}(L) \\ \tilde{Y}_3^{(g)}(L) \\ \tilde{Y}_6^{(g)}(L) \end{bmatrix} \tag{4.10}$$

denoting with $\tilde{Y}_j^{(f)}(y)$, $\tilde{Y}_j^{(g)}(y)$ respectively the j-th element of the vectors $\tilde{\mathbf{Y}}^{(f)}(y_j)$, $\tilde{\mathbf{Y}}^{(g)}(y_j)$.

Based on Eq.(4.8) the following nodal matrix relation can be derived:

$$\mathbf{f} = \mathbf{Z}\mathbf{A}^{-1}(\mathbf{u} - \tilde{\mathbf{u}}_f - \tilde{\mathbf{u}}_g) + \tilde{\mathbf{f}}_f + \tilde{\mathbf{f}}_g = \mathbf{D}\mathbf{u} + \tilde{\mathbf{q}} \tag{4.11}$$

where

$$\mathbf{D} = \mathbf{Z}\mathbf{A}^{-1} \tag{4.12}$$

$$\tilde{\mathbf{q}} = -\mathbf{Z}\mathbf{A}^{-1}(\tilde{\mathbf{u}}_f + \tilde{\mathbf{u}}_g) + \tilde{\mathbf{f}}_f + \tilde{\mathbf{f}}_g \tag{4.13}$$

In Eqs.(4.12)-(4.13), $\mathbf{D} = \mathbf{D}(\omega)$ and $\tilde{\mathbf{q}} = \tilde{\mathbf{q}}(\omega)$ are the exact 6×6 dynamic stiffness matrix and the exact load vector 6×1 of the two-node beam element, respectively. Matrix $\mathbf{D}$ is available in a closed form, using closed-form expressions (3.144) for $\tilde{\mathbf{Y}}$ in $\mathbf{A}$ and $\mathbf{Z}$ given as Eq.(4.9), and building the 6×6 inverse matrix $\mathbf{A}^{-1}$ in a symbolic form, as shown in Appendix C. Likewise, also load vector $\tilde{\mathbf{q}}$ can be computed in a closed form for any point/polynomial load, using closed-form expressions (3.145)-(3.146) for $\tilde{\mathbf{u}}_f$, $\tilde{\mathbf{u}}_g$, $\tilde{\mathbf{f}}_f$ and $\tilde{\mathbf{f}}_g$ in Eq.(4.10). As discussed previously for the case of beams with symmetri cross sections, these are considerable advantages over the exact classical method that, in general, provides numerical solutions.

Remarkably, the size of $\mathbf{D}$ and $\tilde{\mathbf{q}}$ is 6×6 and 6×1, respectively, for any number of dampers/masses and loads along the two-node beam element. Therefore, within a standard finite element assembling procedure, $\mathbf{D}$ and $\tilde{\mathbf{q}}$ can be used to build the exact global dynamic stiffness matrix and load vector of frames, whose size will depend only on the number of beam-to-column nodes regardless of the number of in-span dampers/masses and loads along every structural member. On using the derived closed-form expressions, this is feasible in any finite element commercial code for frequency response of frames.

4.1.3 Exact dynamic stiffness matrix and load vector of discontinuous beams with mono symmetric cross section (warping effects included)

In this subsection, the exact DSM and the LV will be built for beams with mono symmetric cross section for which coupled bending-torsion theory,

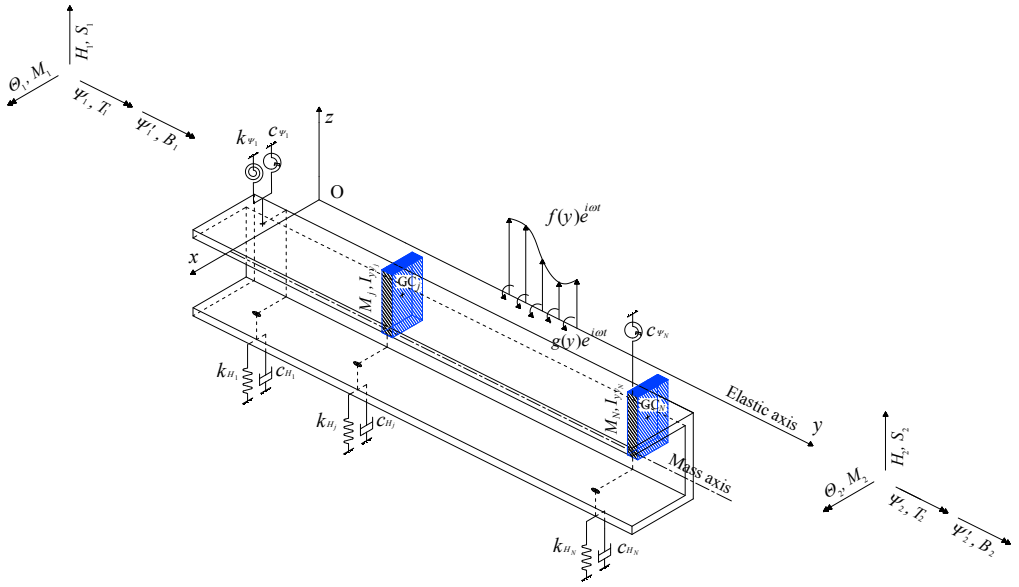

Figure 4.2: Two-node beam element for the beam in Figure 3.38.

including warping effect, is adopted. Here, a different approach to build the DSM and LV will be adopted with respect to that used in the previous subsections.

Consider the beam in Figure 3.38 as a two-node finite element with nodes at the two ends, each featuring 4 degrees of freedom, as shown in Figure 4.2. For generality, consider the case of arbitrary polynomial load.

Eq.(3.222) can be used to build the vector of nodal displacements $\mathbf{u} = [H(0)\ \Theta(0)\ \Psi(0)\ \Psi'(0)\ H(L)\ \Theta(L)\ \Psi(L)\ \Psi'(L)] = [H_1\ \Theta_1\ \Psi_1\ \Psi'_1\ H_2\ \Theta_2\ \Psi_2\ \Psi'_2]$ and the vector of nodal forces $\mathbf{f} = [-S(0) - M(0) - T(0) - B(0)\ S(L)\ M(L)\ T(L)\ B(L)] = [S_1\ M_1\ T_1\ B_1\ S_2\ M_2\ T_2\ B_2]$ (positive sign conventions are shown in Figure 4.2). Then, the following nodal relations holds:

$$\mathbf{f} = \mathbf{D}\mathbf{u} + \mathbf{q}_0 \tag{4.14}$$

where $\mathbf{D} = \mathbf{D}(\omega)$ is the dynamic stiffness matrix, while $\mathbf{q}_0 = \mathbf{q}_0(\omega)$ is the nodal load vector attributable to the external loads acting on the beam.

It will be shown that elements of both matrix $\mathbf{D}$ and vector $\mathbf{q}_0$ can be

derived in closed analytical form based on the frequency response (3.222), on assuming that both ends are clamped.

Be $\mathbf{G}^{(d)}(y, y_0) = [H^{(d)}\ \Theta^{(d)}\ M^{(d)}\ S^{(d)}\ \Psi^{(d)}\ \Psi'^{(d)}\ T^{(d)}\ B^{(d)}]$, for $d = H$, Θ, Ψ, Ψ', the frequency response vector of the beam in Figure 3.38, subjected to a harmonic unit deflection $He^{i\omega t}$, with $H = 1$, harmonic unit bending rotation $\Theta e^{i\omega t}$, with $\Theta = 1$, harmonic unit torsional rotation $\Psi e^{i\omega t}$, with $\Psi = 1$ and harmonic unit torsion $\Psi' e^{i\omega t}$, with $\Psi' = 1$, applied at the beam ends $y_0 = 0$ and $y_L = L$. It is noticed that $\mathbf{G}^{(d)}(y, y_0)$ takes the form (3.222) with no load-dependent terms $\tilde{\mathbf{Y}}^{(f)}(y)$, $\tilde{\mathbf{Y}}^{(g)}(y)$, i.e.:

$$\mathbf{G}^{(d)}(y, y_0) = \tilde{\mathbf{Y}}(y)\mathbf{c}^{(d,y_0)} \qquad \text{for} \qquad \mathbf{c}^{(d,y_0)} = \mathbf{A}^{-1}\mathbf{e}^{(d,y_0)} \qquad d = H, \Theta, \Psi, \Psi' \tag{4.15}$$

In Eq.(4.15), matrix $\mathbf{A}$ takes the form

$$\mathbf{A} = \begin{bmatrix} \tilde{\mathbf{Y}}_1(0) \\ \tilde{\mathbf{Y}}_2(0) \\ \tilde{\mathbf{Y}}_5(0) \\ \tilde{\mathbf{Y}}_6(0) \\ \tilde{\mathbf{Y}}_1(L) \\ \tilde{\mathbf{Y}}_2(L) \\ \tilde{\mathbf{Y}}_5(L) \\ \tilde{\mathbf{Y}}_6(L) \end{bmatrix} \tag{4.16}$$

denoting with $\tilde{\mathbf{Y}}_j(y)$ the j-th row of matrix $\tilde{\mathbf{Y}}(y)$, while vectors $\mathbf{e}^{(d,y_0)}$ are given as:

$$\mathbf{e}^{(H,y_0)} = \begin{bmatrix} 1 & 0 & 0 & 0 & 0 & 0 & 0 & 0 \end{bmatrix};\ \mathbf{e}^{(\Theta,y_0)} = \begin{bmatrix} 0 & 1 & 0 & 0 & 0 & 0 & 0 & 0 \end{bmatrix} \tag{4.17}$$

$$\mathbf{e}^{(\Psi,y_0)} = \begin{bmatrix} 0 & 0 & 1 & 0 & 0 & 0 & 0 & 0 \end{bmatrix};\ \mathbf{e}^{(\Psi',y_0)} = \begin{bmatrix} 0 & 0 & 0 & 1 & 0 & 0 & 0 & 0 \end{bmatrix} \tag{4.18}$$

if $y_0 = 0$ and

$$\mathbf{e}^{(H,y_0)} = \begin{bmatrix} 0 & 0 & 0 & 0 & 1 & 0 & 0 & 0 \end{bmatrix};\ \mathbf{e}^{(\Theta,y_0)} = \begin{bmatrix} 0 & 0 & 0 & 0 & 0 & 1 & 0 & 0 \end{bmatrix} \tag{4.19}$$

$$\mathbf{e}^{(\Psi,y_0)} = \begin{bmatrix} 0 & 0 & 0 & 0 & 0 & 0 & 1 & 0 \end{bmatrix};\ \mathbf{e}^{(\Psi',y_0)} = \begin{bmatrix} 0 & 0 & 0 & 0 & 0 & 0 & 0 & 1 \end{bmatrix} \tag{4.20}$$

if $y_0 = L$

At this stage, the elements of matrix $\mathbf{D}$ can be built based on Eq.(4.15). In particular, bearing in mind that the elements of the dynamic stiffness matrix $\mathbf{D}$ are the nodal forces due to unit displacements at the nodes, and taking into account the relations between nodal forces and stress resultants, it yields

$$\mathbf{D} = \begin{bmatrix} -S^{(H)}(0,0) & -S^{(\Theta)}(0,0) & -S^{(\Psi)}(0,0) & -S^{(\Psi')}(0,0) & -S^{(H)}(0,L) & -S^{(\Theta)}(0,L) & -S^{(\Psi)}(0,L) & -S^{(\Psi')}(0,L) \\ -M^{(H)}(0,0) & -M^{(\Theta)}(0,0) & -M^{(\Psi)}(0,0) & -M^{(\Psi')}(0,0) & -M^{(H)}(0,L) & -M^{(\Theta)}(0,L) & -M^{(\Psi)}(0,L) & -M^{(\Psi')}(0,L) \\ -T^{(H)}(0,0) & -T^{(\Theta)}(0,0) & -T^{(\Psi)}(0,0) & -T^{(\Psi')}(0,0) & -T^{(H)}(0,L) & -T^{(\Theta)}(0,L) & -T^{(\Psi)}(0,L) & -T^{(\Psi')}(0,L) \\ -B^{(H)}(0,0) & -B^{(\Theta)}(0,0) & -B^{(\Psi)}(0,0) & -B^{(\Psi')}(0,0) & -B^{(H)}(0,L) & -B^{(\Theta)}(0,L) & -B^{(\Psi)}(0,L) & -B^{(\Psi')}(0,L) \\ S^{(H)}(L,0) & S^{(\Theta)}(L,0) & S^{(\Psi)}(L,0) & S^{(\Psi')}(L,0) & S^{(H)}(0,L) & S^{(\Theta)}(L,L) & S^{(\Psi)}(L,L) & S^{(\Psi')}(L,L) \\ M^{(H)}(L,0) & M^{(\Theta)}(L,0) & M^{(\Psi)}(L,0) & M^{(\Psi')}(L,0) & M^{(H)}(L,L) & M^{(\Theta)}(L,L) & M^{(\Psi)}(L,L) & M^{(\Psi')}(L,L) \\ T^{(H)}(L,0) & T^{(\Theta)}(L,0) & T^{(\Psi)}(L,0) & T^{(\Psi')}(L,0) & T^{(H)}(L,L) & T^{(\Theta)}(L,L) & T^{(\Psi)}(L,L) & T^{(\Psi')}(L,L) \\ B^{(H)}(L,0) & B^{(\Theta)}(L,0) & B^{(\Psi)}(L,0) & B^{(\Psi')}(L,0) & B^{(H)}(L,L) & B^{(\Theta)}(L,L) & B^{(\Psi)}(L,L) & B^{(\Psi')}(L,L) \end{bmatrix} \tag{4.21}$$

where $S^{(d)}(y,y_0)$, $M^{(d)}(y,y_0)$, $T^{(d)}(y,y_0)$, $B^{(d)}(y,y_0)$ for $d = H,\ \Theta,\ \Psi,\ \Psi'$, are given by Eq.(4.15) with $y = 0, L$ and $y_0 = 0, L$. It is worth remarking that all elements in Eq.(4.21) for $\mathbf{D}$ are readily available in a closed form. Indeed, in Eq.(4.15) $\tilde{\mathbf{Y}}(y)$ is available in exact analytical form as explained in Chapter 3, and $\mathbf{c}^{(d,y_0)}$ can be built in a closed analytical form, as shown in Appendix C.

Next, denote by $\mathbf{Y}_0 = \begin{bmatrix} H_0 & \Theta_0 & M_0 & S_0 & \Psi_0 & \Psi_0' & T_0 & B_0 \end{bmatrix}$ the frequency response vector (3.222) of the beam in Figure 4.2 under loads $f(y)$, $g(y)$, when both ends of the beam are clamped. Be $\mathbf{c}^{(fg)}$ the pertinent vector of integration constants in Eq.(3.222) where, in this case, superscript (fg) distinguishes vector $\mathbf{c}^{(fg)}$ from vectors $\mathbf{c}^{(H,y_0)}$, $\mathbf{c}^{(\Theta,y_0)}$, $\mathbf{c}^{(\Psi,y_0)}$ and $\mathbf{c}^{(\Psi',y_0)}$ associated with unit deflection, bending rotation, torsional rotation and torsion at the beam ends, see Eq.(4.15). Vector $\mathbf{c}^{(fg)}$ is computed by the following equation:

$$\mathbf{B}\mathbf{c}^{(fg)} = \mathbf{e}^{(fg)} \ \rightarrow \ \mathbf{c}^{(fg)} = \mathbf{B}^{-1}\mathbf{e}^{(fg)} \tag{4.22}$$

$$\begin{aligned} \mathbf{e}^{(fg)} = -[&\tilde{H}^{(fg)}(0)\ \tilde{\Theta}^{(fg)}(0)\ \tilde{\Psi}^{(fg)}(0)\ \tilde{\Psi}'^{(fg)}(0) \\ &\tilde{H}^{(fg)}(L)\ \tilde{\Theta}^{(fg)}(L)\ \tilde{\Psi}^{(fg)}(L)\ \tilde{\Psi}'^{(fg)}(L)]^T \end{aligned} \tag{4.23}$$

Using the closed form expression (3.222), taking advantage of the closed form expression for $\mathbf{c}^{(fg)}$ (derived in Appendix C) and in view of relations between nodal forces and stress resultants, the exact load vector $\mathbf{q}_0$ in Eq.(4.14) is then given in the closed form

$$\mathbf{q}_0 = \begin{bmatrix} -S_0(0) & -M_0(0) & -T_0(0) & -B_0(0) & S_0(L) & M_0(L) & T_0(L) & B_0(L) \end{bmatrix}^T \tag{4.24}$$

where S_0, M_0, T_0 and B_0 are the components of vector $\mathbf{Y}_0$.

Summarizing, in Eqs.(4.21)-(4.24), $\mathbf{D} = \mathbf{D}(\omega)$ and $\mathbf{q}_0 = \mathbf{q}_0(\omega)$ are the exact 8×8 dynamic stiffness matrix and the exact load vector 8×1 of the two-node beam element, respectively. Matrix $\mathbf{D}$ and load vector $\mathbf{q}_0$ can be computed in a closed form or any point/polynomial load, and these are considerable advantages over the exact classical method (see comments for

beams with symmetric cross sections).

Remarkably, the size of $\mathbf{D}$ and $\mathbf{q}_0$ is 8×8 and 8×1, respectively, for any number of dampers and masses along the two-node beam element. Therefore, a finite-element assembly of these two-node beam elements will feature an exact global dynamic stiffness matrix and an exact load vector whose size depends only on the number of connecting nodes between the beam elements, regardless of the number of in-span dampers/masses and loads along them.

Now, some numerical examples are presented to show the exactness and efficiency of the proposed method in computing the DSM and LV of coupled beams-discrete systems.

4.1.4 Numerical examples

Discontinuous beams with mono symmetric cross section (warping effects neglected)

Consider the beam studied in Example A in Figure 3.20. It is of interest to build the exact dynamic stiffness matrix (4.12) and exact load vector (4.13), considering the beam in Figure 3.20 as a two-node finite element with nodes at the two ends, each featuring 3 degrees of freedom, as shown in Figure 4.3. For two values of the frequency ω, Table 4.1 and Table 4.2 report the terms of the exact dynamic stiffness matrix (4.12) and exact load vector (4.13), the latter for a uniformly-distributed force $f(y) = 1$ over $\left[\frac{1}{2}L,\ \frac{3}{4}L\right]$. Corresponding terms obtained from the exact classical method, included for comparison, are identical. As expected, the dynamic stiffness matrix is symmetric.

As for computational advantages, the exact proposed method involves closed-form expressions (3.222) to compute the frequency response as well as (4.12) and (4.13) to compute dynamic stiffness matrix and load vector. Instead, the exact classical method requires inverting numerically, for each excitation frequency ω of interest and position of the point force, a 30×30 coefficient matrix, and a 24×24 matrix for the case of distributed force over $\left[\frac{1}{2}L,\ \frac{3}{4}L\right]$.

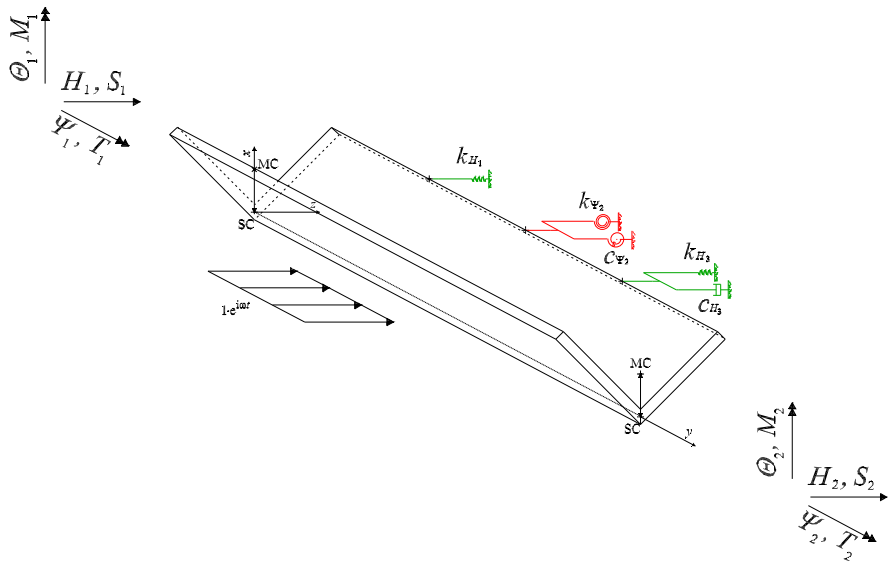

Figure 4.3: Two-node beam element for the beam in Figure 3.20 under a harmonically-varying transverse uniformly-distributed force $f(y)e^{i\omega t}$, $f(y) = 1$ over $[\frac{1}{2}L, \frac{3}{4}L]$.

Now, consider the beam studied in Example B in Figure 3.28. It is of interest to build the exact load vector (4.13), considering the beam in Figure 3.28 as a two-node finite element with nodes at the two ends, each featuring 3 degrees of freedom, as shown in Figure 4.4. For two values of the frequency ω, Table 4.3 and Table 4.4 report the terms of the exact load vector (4.13) for two different loadings: a uniformly-distributed force $f(y) = 1$ over $\left[\frac{3}{4}L,\ L\right]$, and a linearly-distributed force $f(y)$ over $\left[\frac{3}{4}L,\ L\right]$, with $f(\frac{3}{4}L) = 1$ and $f(L) = 0$. Again, corresponding terms obtained from the exact classical method, included for comparison, are coincident.

	$\omega = 200$ rad/s		$\omega = 500$ rad/s	
D.S.M. terms	C. M.	P. M.	C.M.	P.M.
D_{11}	21815.2+1933.91i	21815.2+1933.91i	654792+414900i	654792+414900i
$D_{12} = D_{21}$	353597+1453.81i	353597+1453.81i	656852+167775i	656852+167775i
$D_{13} = D_{31}$	8454.40-280.509i	8454.40-280.509i	-164253-35575.1i	-164253-35575.1i
$D_{14} = D_{41}$	-425901+5101.04i	-425901+5101.04i	-1625830-47274.1i	-1625830-47274.1i
$D_{15} = D_{51}$	553684-2718.62i	553684-2718.62i	981031-14165.6i	981031-14165.6i
$D_{16} = D_{61}$	1877.44-532.366i	1877.44-532.366i	100557+15525.9i	100557+15525.9i
D_{22}	881691+1107.09i	881691+1107.09i	942620+75632.3i	942620+75632.3i
$D_{23} = D_{32}$	2411.68-193.611i	2411.68-193.611i	-80027.1-12466.7i	-80027.1-12466.7i
$D_{24} = D_{42}$	-553606+4097.27i	-553606+4097.27i	-1000410+48002.9i	-1000410+48002.9i
$D_{25} = D_{52}$	530045-2162.78i	530045-2162.78i	729833-35824.8i	729833-35824.8i
$D_{26} = D_{62}$	1322.13-403.824i	1322.13-403.824i	19952.5+776.019i	19952.5+776.019i
D_{33}	454.697+61.6750i	454.697+61.6750i	14857.8+3523.07i	14857.8+3523.07i
$D_{34} = D_{43}$	1865.24-420.617i	1865.24-420.617i	96226.5+ 20589.1i	96226.5+ 20589.1i
$D_{35} = D_{53}$	-1323.51+249.563i	-1323.51+249.563i	-16370.8 - 6200.12i	-16370.8 - 6200.12i
$D_{36} = D_{63}$	-342.949+72.8168i	-342.949+72.8168i	-13663.2 - 2686.8i	-13663.2 - 2686.8i
D_{44}	22640.3 +18311.7i	22640.3 +18311.7i	504424+ 583779i	504424+ 583779i
$D_{45} = D_{54}$	-354005-9373.04i	-354005-9373.04i	-587499-257741i	-587499-257741i
$D_{46} = D_{64}$	8376.59-1471.16i	8376.59-1471.16i	-151958-49184.1i	-151958-49184.1i
D_{55}	881885+4820.26i	881885+4820.26i	913130+116780i	913130+116780i
$D_{56} = D_{65}$	-2374.36+778.738i	-2374.36+778.738i	73798.4+ 20731.1i	73798.4+ 20731.1i
D_{66}	461.855+147.472i	461.855+147.472i	13977.2+ 4467.95i	13977.2+ 4467.95i

Table 4.1: Beam in Figure 4.3, numerical values of dynamic stiffness matrix (D.S.M.) terms for two different values of frequency ω, as computed by exact classical method (C.M.) and exact proposed method (P.M.).

	$\omega = 200$ rad/s		$\omega = 500$ rad/s	
L.V. terms	C. M.	P. M.	C.M.	P.M.
$\tilde{q}_1$	-0.29186+0.00625i	-0.29186+0.00625i	-0.59510-0.08716i	-0.59510-0.08716i
$\tilde{q}_2$	-0.23172+0.00456i	-0.23172+0.00456i	-0.26494 -0.00483i	-0.26494 -0.00483i
$\tilde{q}_3$	0.00569-0.00107i	0.00569-0.00107i	0.04294+0.01496i	0.04294+0.01496i
$\tilde{q}_4$	-0.57072+0.01399i	-0.57072+0.01399i	0.44549+0.27199i	0.44549+0.27199i
$\tilde{q}_5$	0.35744-0.00766i	0.35744-0.00766i	-0.55589-0.11453i	-0.55589-0.11453i
$\tilde{q}_6$	0.01668-0.001686i	0.01668-0.001686i	-0.08743-0.02474i	-0.08743-0.02474i

Table 4.2: Beam in Figure 4.3, numerical values of load vector (L.V.) terms for a uniformly-distributed force $f(y) = 1$ over $[\frac{1}{2}L, \frac{3}{4}L]$ for two values of forcing frequency ω, as computed by exact classical method (C.M.) and exact proposed method (P.M.).

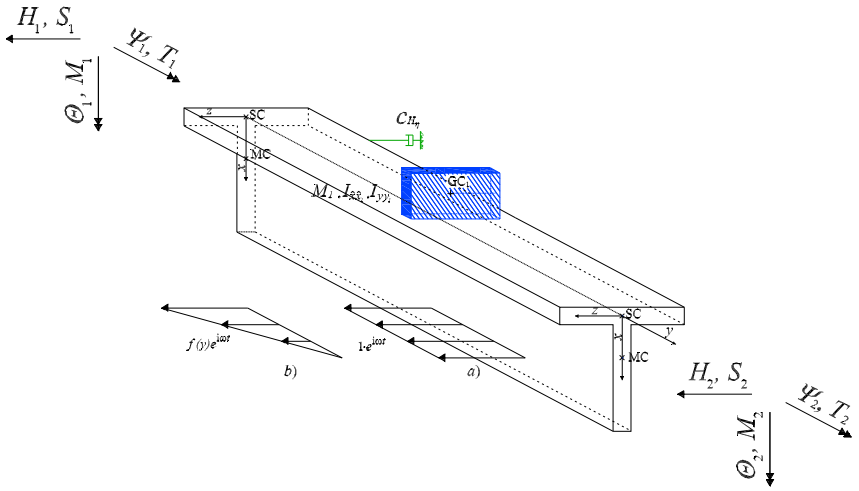

Figure 4.4: Two-node beam element for beam in Figure 3.28 under two different harmonically-varying transverse distributed forces $f(y)e^{i\omega t}$: a) uniformly-distributed force $f(y) = 1$ over $[\frac{3}{4}L, L]$; b) linearly-distributed force $f(y)$ over $[\frac{3}{4}L, L]$ with $f(\frac{3}{4}L) = 1$ and $f(L) = 0$.

Discontinuous beams with mono symmetric cross section (warping effects included)

Consider the beam of Example B in Figure 3.43. Assume that the beam is loaded by a harmonic uniformly-distributed force over $[0.5L, 0.8L]$, with $f(y) = 1$, and consider the beam as a two-node finite element with nodes at the two ends, each featuring 4 degrees of freedom, as shown in Figure 4.5. It is of interest to compare the proposed exact expressions of dynamic stiffness matrix (4.21) and load vector (4.24), with the corresponding ones obtained from the exact classical method. For two values of the frequency ω, Table 4.5 and Table 4.6 show that proposed and classical methods provide identical terms for the dynamic stiffness matrix and load vector, thus confirming the exactness of expressions (4.21) and (4.24). As expected, notice that the dynamic stiffness matrix is symmetric.

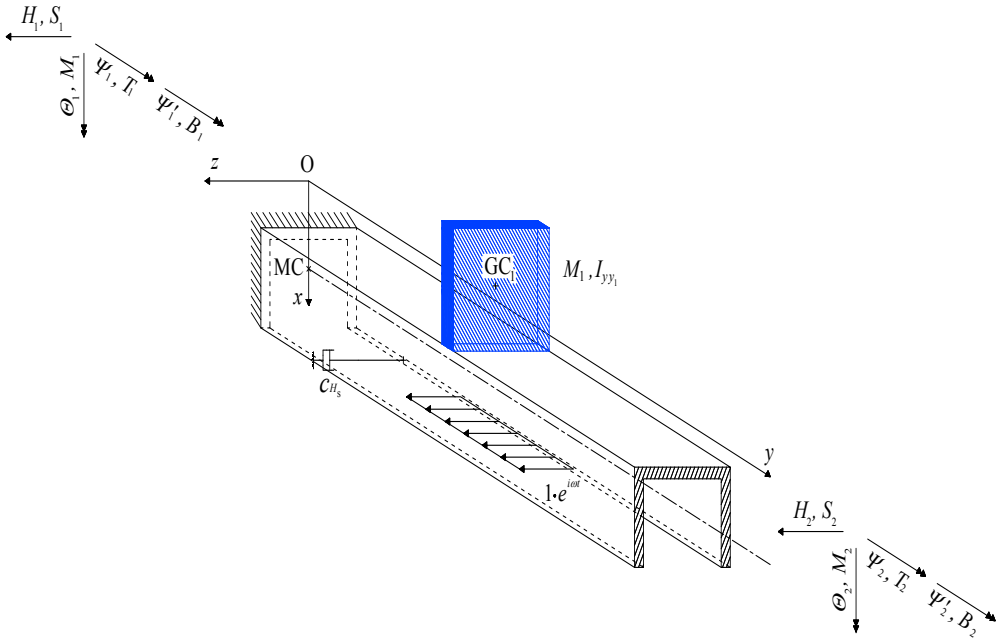

Figure 4.5: Two-node beam element for the beam in Figure 3.43.

	$\omega = 150$ rad/s		$\omega = 350$ rad/s	
L.V. terms	C. M.	P. M.	C.M.	P.M.
$\tilde{q}_1$	-0.14776+0.003584i	-0.14776+0.003584i	0.17416+0.00737i	0.17416+0.00737i
$\tilde{q}_2$	-0.26507+0.00517i	-0.26507+0.00517i	0.54803+0.00104i	0.54803+0.00104i
$\tilde{q}_3$	-0.02821-0.00004i	-0.02821-0.00004i	0.14347-0.00407i	0.14347-0.00407i
$\tilde{q}_4$	-1.58165+0.00358i	–1.58165+0.00358i	-0.24449+0.00737i	-0.24449+0.00737i
$\tilde{q}_5$	0.96365-0.00517i	0.96365-0.00517i	-0.58737-0.00105i	-0.58737-0.00105i
$\tilde{q}_6$	0.13508-0.00004i	0.13508-0.00004i	0.00239-0.00408i	0.00239-0.00408i

Table 4.3: Beam in Figure 4.4, numerical values of load vector (L.V.) terms for a uniformly-distributed force $f(y) = 1$ over $[\frac{3}{4}L, L]$ for two values of frequency ω, as computed by exact classical method (C.M.) and exact proposed method (P.M.).

	$\omega = 150$ rad/s		$\omega = 350$ rad/s	
L.V. terms	C. M.	P. M.	C.M.	P.M.
$\tilde{q}_1$	-0.10862+0.00258i	-0.10862+0.00258i	0.12221+0.00458i	0.12221+0.00458i
$\tilde{q}_2$	-0.19263+0.00373i	-0.19263+0.00373i	0.35061+0.00065i	0.35061+0.00065i
$\tilde{q}_3$	-0.01847-0.00003i	-0.01847-0.00003i	0.08615-0.00253i	0.08615-0.00253i
$\tilde{q}_4$	-0.79853+0.00258i	-0.79853+0.00258i	0.09138+0.00457i	0.09138+0.00457i
$\tilde{q}_5$	0.61942-0.00372i	0.61942-0.00372i	-0.39707-0.00065i	-0.39707-0.00065i
$\tilde{q}_6$	0.05893-0.00003i	0.05893-0.00003i	-0.03587-0.00254i	-0.03587-0.00254i

Table 4.4: Beam in Figure 4.4, numerical values of load vector (L.V.) terms for a linearly-distributed force $f(y)$ over $[\frac{3}{4}L, L]$, with $f(\frac{3}{4}L) = 1$ and $f(L) = 0$, for two values of frequency ω, as computed by exact classical method (C.M.) and exact proposed method (P.M.).

	$\omega = 500$ rad/s		$\omega = 1000$ rad/s	
D.S.M. terms	C. M.	P. M.	C.M.	P.M.
D_{11}	241500+1829.73i	241500+1829.73i	-695268. + 1162.99i	-695268. + 1162.99i
$D_{12} = D_{21}$	291359+566.084i	291359+566.084i	93577.3+ 433.186i	93577.3+ 433.186i
$D_{13} = D_{31}$	9843.13-108.484i	9843.13-108.484i	9985.44+133.947i	9985.44+133.947i
$D_{14} = D_{41}$	1750.99-32.7418i	1750.99-32.7418i	-1645.52 + 36.4161i	-1645.52 + 36.4161i
$D_{15} = D_{51}$	-708613+1829.73i	-708613+1829.73i	-1127630+1162.99i	-1127630+1162.99i
$D_{16} = D_{61}$	403354-566.084i	403354-566.084i	541261-433.186i	541261-433.186i
$D_{17} = D_{71}$	3567.86-108.484i	3567.86-108.484i	-17081.9+133.947i	-17081.9 + 133.947i
$D_{18} = D_{81}$	-1037.87+32.7418i	-1037.87+32.7418i	4813.01-36.4161i	4813.01-36.4161i
D_{22}	287634+175.136i	287634+175.136i	235501+161.351i	235501+161.351i
$D_{23} = D_{32}$	1696.59-33.5629i	1696.59-33.5629i	-524.491+49.8917i	-524.491 + 49.8917i
$D_{24} = D_{42}$	374.021-10.1297	374.021-10.1297	-646.395 + 13.564i	-646.395 + 13.564i
$D_{25} = D_{52}$	-403354+566.084i	-403354+566.084i	-541261. + 433.186i	-541261. + 433.186i
$D_{26} = D_{62}$	166269-175.136	166269-175.136	209794-161.351i	209794-161.351i
$D_{27} = D_{72}$	981.411-33.5629i	981.411-33.5629i	-3701.36 + 49.8917i	-3701.36 + 49.8917i
$D_{28} = D_{82}$	-272.214+10.1297i	-272.214+10.1297	1104.58-13.564i	1104.58-13.564i
D_{33}	-1148.99+6.43197i	1148.99+6.43197i	1227.52+15.4272i	1227.52+ 15.4272i
$D_{34} = D_{43}$	-169.498+1.94125i	-169.498+1.94125i	789.718+4.19417i	789.718+4.19417i
$D_{35} = D_{53}$	3567.86-108.484i	3567.86-108.484i	-17081.9+133.947i	-17081.9+133.947i
$D_{36} = D_{63}$	-981.411+33.5629i	-981.411+33.5629i	3701.36-49.8917i	3701.36-49.8917i
$D_{37} = D_{73}$	-1000.36+6.43197i	-1000.36+6.43197i	3270.42+15.4272i	3270.42+15.4272i
$D_{38} = D_{83}$	365.745-1.94125i	365.745-1.94125i	-816.495-4.19417i	-816.495-4.19417i
D_{44}	34.1894+0.585893i	34.1894+0.585893i	332.663+1.14027i	332.663+1.14027i
$D_{45} = D_{54}$	1037.87-32.7418i	1037.87-32.7418i	-4813.01+36.416i	-4813.01 + 36.416i
$D_{46} = D_{64}$	-272.214+10.1297i	-272.214+10.1297i	1104.58-13.564i	1104.58-13.564i
$D_{47} = D_{74}$	-365.745+1.94125i	-365.745+1.94124i	816.495+4.19417i	-206.821-1.14027i
$D_{48} = D_{84}$	123.894-0.58589i	123.894-0.58589i	-206.821-1.14027i	-206.821-1.14027i
D_{55}	241500+1829.73i	241500+1829.73i	-695268+1162.99i	-695268+1162.99i
$D_{56} = D_{65}$	-291359-566.084i	-291359-566.084i	-93577.3-433.186i	-93577.3-433.186i
$D_{57} = D_{75}$	9843.13-108.484i	9843.13-108.484i	9985.44+133.947i	9985.44+133.947i
$D_{58} = D_{85}$	-1750.99+32.7418i	-1750.99+32.7418i	1645.52-36.416i	1645.52-36.416i
D_{66}	287634+175.136i	287634+175.136i	235501+161.351i	235501+161.351i
$D_{67} = D_{76}$	-1696.59 + 33.5629i	-1696.59 + 33.5629i	524.491-49.8917i	524.491-49.8917i
$D_{68} = D_{86}$	287634+ 175.136i	287634+ 175.136i	-646.395+13.564i	-646.395+13.564i
D_{77}	-1148.99 + 6.43197i	-1148.99 + 6.43197i	1227.52+15.4272i	1227.52+15.4272i
$D_{87} = D_{78}$	169.498-1.94125i	169.498-1.94125i	-789.718-4.19417i	-789.718-4.19417i
D_{88}	34.1894+0.58589i	34.1894+0.58589i	332.663+1.14027i	332.663+1.14027i

Table 4.5: Beam in Figure 4.5, numerical values of dynamic stiffness matrix terms for two values of frequency ω, as computed by exact classical method (C.M.) and exact proposed method (P.M.).

	$\omega = 500$ rad/s		$\omega = 1000$ rad/s	
L.V. terms	C. M.	P. M.	C.M.	P.M.
$(q_0)_1$	-0.14054+0.00077i	-0.14054+0.00077i	-0.05877-0.00057i	-0.05877-0.00057i
$(q_0)_2$	-0.04681+0.00024i	-0.04681+0.00024i	-0.02863-0.00021i	-0.02863-0.00021i
$(q_0)_3$	0.00907-0.00004i	0.00907-0.00004i	-0.01353-0.00006i	-0.01353-0.00006i
$(q_0)_4$	0.00286-0.00001i	0.00286-0.00001i	-0.00355-0.00002i	-0.00355-0.00002i
$(q_0)_5$	-0.30701+0.00077i	-0.30701+0.00077i	-0.23942-0.00057i	-0.23942-0.00057i
$(q_0)_6$	0.07770-0.00025i	0.07770-0.00024i	0.06185+0.00022i	0.06185+0.00022i
$(q_0)_7$	0.01551-0.00004i	0.01551-0.00004i	-0.23942-0.00057i	-0.23942-0.00057i
$(q_0)_8$	-0.00405+0.00001i	-0.00405+0.00001i	-0.00594-0.00006i	-0.00594-0.00006i

Table 4.6: Beam in Figure 4.5, numerical values of load vector terms for a uniformly-distributed force $f(y) = 1$ over $[0.5L, 0.8L]$ for two values of frequency ω, as computed by exact classical method (C.M.) and exact proposed method (P.M.).

4.2 Exact frequency response and free vibrations of coupled plane frame-discrete systems

4.2.1 Frequency response

Consider a plane frame made by assembling beams with symmetric cross section, carrying an arbitrary number of KV dampers snd subjected to harmonically varying, arbitrarily-placed point/polynomial loads, as shown in Figure 4.6. The global DSM and LV of the frame can be built by a standard FE-like assembling procedure of DSM and LV of the individual frame members, given by Eqs.(4.6) and (4.7). For this purpose, Eq.(4.7) is written for the generic frame member (e) between two beam to- column nodes in the form $\mathbf{f}_{loc}^{(e)} = \mathbf{D}^{(e)}(\omega)\mathbf{u}_{loc}^{(e)} + \mathbf{q}_{loc}^{(e)}$, where subscript "loc" indicates that all quantities are referred to the local coordinate system. Enforcing equilibrium

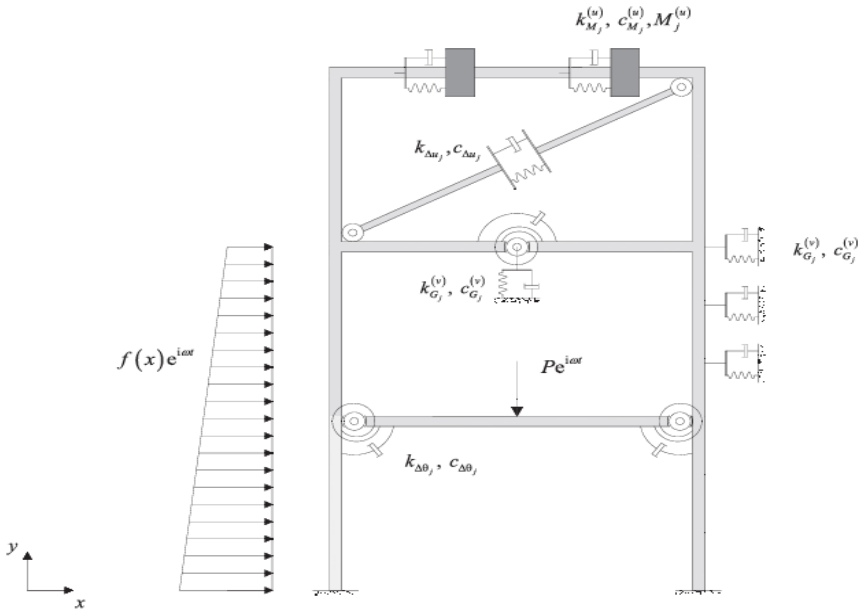

Figure 4.6: Plane frame with KV dampers.

at the beam-to-column nodes and the external kinematic BC of the frame, leads to the following global equilibrium equations:

$$\mathbf{D}_{GL}(\omega)\mathbf{U} = \mathbf{F} \tag{4.25}$$

$$\mathbf{D}_{GL}(\omega) = \sum_{e=1}^{N_e} (\mathbf{T}^{(e)}\mathbf{L}^{(e)})^T \mathbf{D}^{(e)}(\omega)\mathbf{T}^{(e)}\mathbf{L}^{(e)} \tag{4.26}$$

$$\mathbf{F} = -\sum_{e=1}^{N_e} (\mathbf{T}^{(e)}\mathbf{L}^{(e)})^T \mathbf{q}_{loc}^{(e)} + \mathbf{F}^{(0)} \tag{4.27}$$

For each frame member (e), $\mathbf{T}^{(e)}$ relates the local reference system to the global reference system, $\mathbf{u}_{loc} = \mathbf{T}^{(e)}\mathbf{u}^{(e)}$, whereas $\mathbf{L}^{(e)}$ relates $\mathbf{u}^{(e)}$ to the global vector of displacements $\mathbf{U} = [U_1\ U_2\ U_3 \dots]$, i.e., $\mathbf{u}^{(e)} = \mathbf{L}^{(e)}\mathbf{U}$. In Eq. (4.26), $\mathbf{D}_{GL}(\omega)$ is the exact global DSM; in Eq. (4.27) $\mathbf{F}$ is the exact global LV which includes the contribution of loads acting along the frame members and the vector $\mathbf{F}^{(0)}$ of external nodal forces, if they exist. Notice that $\mathbf{F}^{(0)}$ may include also the reaction forces of ETDs or ERDs applied at nodes. In this case, the i-th component of vector $\mathbf{F}$ will include an additional term $F_i = \kappa_{eq_i}(\omega)U_i$, with $\kappa_{eq_i}(\omega)$ frequency-dependent stiffness of the nodal damper, depending on whether the damper is a translational or a rotational one.

At this stage, the exact FRM of the frame, $\mathbf{H}(\omega)$, can be derived by matrix inversion:

$$\mathbf{U} = \mathbf{H}(\omega)\mathbf{F}, \quad \text{for } \mathbf{H}(\omega) = [\mathbf{D}_{GL}(\omega)]^{-1} \tag{4.28}$$

Upon computing $\mathbf{U}$ from Eq.(4.28), the exact FRFs of all response variables can be built in any frame member using Eq.(3.54) for $\mathbf{Y}(x)$ and Eqs.(3.110) for $U(x)$ and $N(x)$, where vector $\mathbf{b}$ pertaining to the frame member is computed as $\mathbf{b} = (\mathbf{\Gamma}^{(e)})^{-1}[\mathbf{u}_{loc}^{(e)} - (\mathbf{u}_{loc})^{(e)}]$; where, for $\mathbf{u}_{loc}^{(e)} = \mathbf{T}^{(e)}\mathbf{L}^{(e)}\mathbf{U}$.

4.2.2 Free vibrations

All natural frequencies of the plane structure in Figure 4.6 can be computed as roots of the global dynamic stiffness matrix given by Eq.(4.26), using the well-known Wittrick-Williams algorithm [19]. The implementation requires the number J_i of "clamped-clamped" natural frequencies, which fall below any arbitrary trial frequency, of the two node i-th member with dampers. Adopting the approach proposed in a recent paper on frames composed of multi-cracked members [18], J_i can be computed applying the W-W algorithm to every i-th member with clamped ends and using, for this specific purpose, the dynamic stiffness matrix built by assembling the dynamics stiffness matrices of member segments connected at the internal points where dampers occur.

For every computed natural frequency ω, the nodal displacement vector $\mathbf{U}$ will be built as non-trivial solution of $\mathbf{D}_{GL}\mathbf{U} = \mathbf{0}$ (Eq.(4.25)). Corresponding eigenfunctions for all response variables in the i-th member will be built from Eq.(3.54) for $\tilde{\mathbf{Y}}(x)$ and Eqs.(3.110) for $\tilde{\mathbf{Z}}(x)$ imposing the loading terms equal to zero, where the set of six (4 for $\tilde{\mathbf{Y}}(x)$ and 2 for $\tilde{\mathbf{Z}}(x)$) integration constants for the i-th member $\mathbf{c}^{(i)}$ are obtained as $\mathbf{c}^{(i)} = (\tilde{\mathbf{\Gamma}})^{-1}\tilde{\mathbf{U}}^{(i,nod)}$, with $\tilde{\mathbf{U}}^{i,nod} = \mathbf{T}^{(i)}\mathbf{L}^{(i)}\mathbf{U}$. The displacement of the masses in the subsystems can readily be computed from deflection/axial-displacement of the application point, using free-vibration equilibrium equations of the masses.

Notice that some changes in notations have been applied for simplicity and response variables in the local coordinate system of every member have been denoted as $\tilde{(\ )}$, in addition $\tilde{\mathbf{U}}^{(i,nod)} = \mathbf{u}_{loc}^{(i)}$.

Now, it is shown that relevant orthogonality conditions hold for vibration modes of plane frames coupled with mass-spring subsystems.

Orthogonality conditions

For the n-th mode, be $\tilde{V}_n^{(i)}(x)$, $\tilde{U}_n^{(i)}(x)$ the deflection and axial-displacement eigenfunction of the i-th member in the local coordinate system, for which

the following equations hold

$$EI^{(i)}\frac{\bar{d}^4\tilde{V}_n^{(i)}(x)}{dx^4} - \tilde{B}_n^{(i)}(x) - m^{(i)}\omega_n^2\tilde{V}_n^{(i)}(x) = 0 \tag{4.29}$$

$$EA^{(i)}\frac{\bar{d}^2\tilde{U}_n^{(i)}(x)}{dx^4} - \tilde{A}_n^{(i)}(x) + m^{(i)}\omega_n^2\tilde{U}_n^{(i)}(x) = 0 \tag{4.30}$$

where $\tilde{A}^{(i)}(x)$ and $\tilde{B}^{(i)}(x)$ contain the reaction force of the spring-sub-system in axial and vertical direction respectively. On multiplying Eq.(4.29) by deflection $V_m^{(i)}(x)$ and Eq.(4.30) by axial displacement $\tilde{U}_m^{(i)}(x)$, integrating over the length $L^{(i)}$, summing up, yields

$$\begin{aligned}(\tilde{\mathbf{p}}_n^{(i,nod)})^T\tilde{\mathbf{U}}_m^{(i,nod)} = &\int_0^{L^{(i)}}(\frac{\bar{d}^2\mathbf{U}_n^{(i)}}{dx^2})^T\mathbf{K}^{(i)}\frac{\bar{d}^2\tilde{\mathbf{U}}_m^{(i)}}{dx^2}dx - \int_0^{L^{(i)}}(\tilde{\mathbf{F}}_n^{(i)})^T\tilde{\mathbf{U}}_m^{(i)}dx \\ &- m^{(i)}\omega_n^2\int_0^{L^{(i)}}(\tilde{\mathbf{U}}_n^{(i)})^T\tilde{\mathbf{U}}_m^{(i)}dx\end{aligned} \tag{4.31}$$

where for the i-th member

$$\begin{aligned}&\tilde{\mathbf{U}}_m^{(i)}(x) = [\tilde{U}_m^{(i)}(x)\ \tilde{V}_m^{(i)}(x)];\ \tilde{\mathbf{U}}_n^{(i)}(x) = [\tilde{U}_n^{(i)}(x)\ \tilde{V}_n^{(i)}(x)];\\ &\tilde{\mathbf{F}}_n^{(i)}(x) = [\tilde{A}_n^{(i)}(x)\ \tilde{B}_n^{(i)}(x)];\end{aligned} \tag{4.32}$$

$$\mathbf{K} = \begin{bmatrix} EA^{(i)} & 0 \\ 0 & EI^{(i)} \end{bmatrix} \tag{4.33}$$

where $\tilde{\mathbf{p}}^{(i,nod)} = \mathbf{f}$ in Eq.(4.2) for each member, imposing $\mathbf{f}^{(f)} = \mathbf{0}$. Next, being $\mathbf{P}_n^{(i,nod)}$ and $\mathbf{U}_m^{(i,nod)}$ the nodal forces and modal displacements expressed in the global coordinate system (that can be related to the same quantities in the local coordinate system), it can be shown that the following relation holds

$$\sum_{i=1}^{Ne}(\mathbf{P}_n^{(i,nod)})^T\mathbf{U}_m^{(i,nod)} \tag{4.34}$$

From Eq.(4.34), and the same relation written inverting the subscripts,

the following two orthogonality conditions can be derived

$$(\omega_m^2 - \omega_n^2) \sum_{i=1}^{Ne} m^{(i)} \int_0^{L^{(i)}} (\tilde{\mathbf{U}}_m^{(i)})^T \mathbf{U}_n^{(i)} dx + Q(\omega_m, \omega_n) \tag{4.35}$$

$$\begin{aligned} &(\omega_m - \omega_n) \sum_{i=1}^{Ne} \int_0^{L^{(i)}} (\frac{\bar{d}^2 \tilde{\mathbf{U}}_m^{(i)}}{dx^2})^T \mathbf{K}^{(i)} \frac{\bar{d}^2 \tilde{U}_n^{(i)}}{dx^2} dx \\ &\quad + \omega_m \omega_n (\omega_m - \omega_n) \sum_{i=1}^{Ne} m^{(i)} \int_0^{L^{(i)}} (\tilde{\mathbf{U}}_m^{(i)})^T \tilde{\mathbf{U}}^{(i)} dx + Z(\omega_m, \omega_n) \end{aligned} \tag{4.36}$$

where $Q(\omega_m, \omega_n)$ and $Z(\omega_m, \omega_n)$ are given as

$$Q = \sum_{i=1}^{Ne} \sum_{j=1}^{N^{(i)}} (\tilde{\mathbf{U}}_m^{(i)}(x_j^{(i)}))^T (\mathbf{K}_{ABj}^{(i)}(\omega_n) - \mathbf{K}_{ABj}^{(i)}(\omega_m)) \tilde{\mathbf{U}}_n^{(i)}(x_j^{(i)}) \tag{4.37}$$

$$\begin{aligned} Z = &\sum_{i=1}^{Ne} \sum_{j=1}^{N^{(i)}} (\tilde{\mathbf{U}}^{(i)}(x_j^{(i)}))(\omega_m \mathbf{K}_{AB_j}^{(i)}(\omega_n) - \omega_n \mathbf{K}_{AB_j}^{(i)}(\omega_m)) \tilde{\mathbf{U}}_n^{(i)}(x_j^{(i)}) \\ &+ (\omega_n - \omega_m) \sum_{i=1}^{Ne} \sum_{j=1}^{N^{(i)}} \frac{\tilde{M}_n^{(i)}(x_j)}{k_{\Delta\Theta_j}^{(i)}} \Big(\tilde{M}_m^{(i)}(x_j) \\ &+ \frac{EI}{k_{\Delta\Theta_j}^{(i)}} \int_0^{L^{(i)}} \tilde{M}_m^{(i)}(x_j) \delta(x - x_j^{(i)}) \delta(x - x_j^{(i)}) dx \Big) \end{aligned} \tag{4.38}$$

for

$$\mathbf{K}_{ABj}^{(i)}(\omega) = \begin{bmatrix} k_{A_j}^{(i)}(\omega) & 0 \\ 0 & k_{B_j}^{(i)}(\omega) \end{bmatrix} \tag{4.39}$$

with $\kappa_{A_j}^{(i)}(\omega)$ and $\kappa_{B_j}^{(i)}(\omega)$ frequency-dependent stiffness of the mass-spring subsystems acting in axial and vertical direction.

4.3 Novel exact modal analysis of plane frame with mass-spring sub-systems

Now, short hints are given concerning a novel exact modal analysis approach [23] for vibration analysis of plane frames, which are coupled with discrete mass-spring subsystems and include elastic rotational joints modelling local flexibility. Specifically, exploiting the orthogonality conditions derived in the previous Section, the plane frame response under arbitrary loads is obtained by modal impulse and modal frequency response functions, under the assumption of proportional damping. The solutions are exact and can be used as benchmark for classical finite-element solutions. The approach is formulated for various mass-spring subsystems, acting in transverse and axial directions relative to every member.

Starting from bending and axial motion equations of the ith member under impulsive loading written in the local coordinate system of the member:

$$EI^{(i)}\frac{\bar{\partial}^4\tilde{v}_n^{(i)}(x,t)}{dx^4} - \tilde{b}_n^{(i)}(x,t) + m^{(i)}\ddot{\tilde{v}}_n^{(i)}(x,t) - \tilde{q}_y^{(i)}(x)\delta(t) = 0 \tag{4.40}$$

$$EA^{(i)}\frac{\bar{\partial}^2\tilde{u}_n^{(i)}(x,t)}{dx^4} - \tilde{a}_n^{(i)}(x,t) - m^{(i)}\ddot{\tilde{u}}_n^{(i)}(x) + \tilde{q}_x(x)^{(i)}\delta(t) = 0 \tag{4.41}$$

where $\tilde{q}_y^{(i)}(x)\delta(t)$ and $\tilde{q}_x^{(i)}(x)\delta(t)$ are space-dependent impulsive loads at $t = 0$, it can be demonstrated after several algebraic manipulations and exploiting the property in Eq.(4.34) and the orthogonality conditions (Eqs.(4.35)-(4.36)), that the impulse response function of the generic mth mode can be finally derived in a closed form, from which the equation governing the impulse response function of every mode can be also deduced. This closed form expression allows to compute the response of the plane structure in Figure 4.6 to arbitrary loads, with any space-distribution along the members.

Chapter 5

Proposed approach to the dynamic analysis of coupled continuous-discrete systems: Stochastic analysis

The method developed in Chapters 3 and 4 to perform the deterministic response of CCDS is now extended to stochastic excitations.

Firstly, on the basis of exact expressions for the frequency response functions derived in Chapter 3 and 4, exact closed-form expressions are built for stationary response of single beams and plane frames under stationary point/polynomial loads for any number of discrete elements (dampers, masses, etc...).

Next, non-stationary response is built for beams and plane frames. Specifically, on the basis of the exact closed expressions for modal impulse response function derived in Chapters 3 and 4, an efficient implementation of the Monte Carlo simulation under non-stationary input is obtained.

Finally, some sources of non-linearity are introduced in the behavior of both the primary continuous structure/systems and discrete elements. At this regard, for stationary excitations a novel statistical linearization tech-

nique is developed for determining second-order response statistics of beams with symmetric cross section with in-span elastic concentrated supports. The nonlinearities considered relate both to the support restoring forces, and to the assumption of relatively large beam displacements. A significant novel aspect of the technique is the utilization of constrained modes, involving generalized functions in their definition, computed in exact closed form in Chapter 3; in this way, shear-force discontinuity at the support locations can be readily accounted for. It is underlined that this approach is presented only for beams with symmetric cross section, but can be potentially extended to the other mono-dimensional elements taken in consideration in this thesis.

5.1 Stationary response

In this Section, exact closed form expressions are built for the stationary response of discontinuous beams with symmetric cross section and their 2-D assembly (plane frames). Next, stationary response is built for discontinuous beams with mono symmetric cross section.

5.1.1 Discontinuous beams with symmetric cross section and plane frames

Consider a beam with symmetric cross section as in Figure 4.6, subjected to a distributed random load $f(x,t) = f(x)f(t)$, with $f(t)$ a stationary process with Power Spectral Density (PSD) $S_{ff}(\omega)$. The PSD of the response variables in vector $\mathbf{Y}(y)$ (see Chapter 3, Section 2) will be obtained in the general form as

$$S_{Y_iY_i}(x,\omega) = |Y_i(x,\omega)|^2 S_{ff}(\omega) \tag{5.1}$$

where $Y_i(x)$ is given as Eq.(3.54), with integration constants $\mathbf{c}$ derived upon introducing the BC.

Eq.(5.1) provides the response variables along the beam. The same equa-

tions can be used to calculate the response in every tuned mass dampers or spring mass system, using the pertinent frequency response functions. Similar response are obtained for the axial response variable and are not here reported.

For a stationary input with $S_{ff}(\omega)$ acting on a frame as shown in Figure 4.6, Eq.(5.1) can be used to compute the PSD of the response in every frame member (e). For this case, the set of integration constants $\mathbf{c}$ to be used in Eq.(3.54) for $Y_i(x)$ is computed as the vector $\mathbf{b} = (\Gamma^{(e)})^{-1}[\mathbf{u}_{loc}^{(e)} - (\mathbf{u}_{loc}^{(f)})^{(e)}]$ pertinent to the frame member (where $\mathbf{u}_{loc}^{(e)} = \mathbf{T}^{(e)}\mathbf{L}^{(e)}\mathbf{U}$).

It is underlined that the exact PSD of any response variable in Eq.(5.1) can readily be derived also for multivariate stationary inputs acting on beam or a frame, based on the linear superposition principle.

Finally, some remarks are given regarding the advantages of Eq.(5.1) for the exact PSD with respect to alternative existing methods. For a single beam, the exact PSD (Eq.(5.1)) inherently fulfills all required conditions at the application points of dampers and in general of discrete elements (discontinuities and continuities of all response variables). The analytical form is easy to implement in any symbolic package as Mathematica [2] and can be readily compute for any parameters, position of the loads, regardless of the number of dampers and position of dampers relative to the loads. The advantages are considerable over the alternative exact approach where the exact FRF is built by expressing the steady-state response over every uniform beam segment between two consecutive damper locations in a trigonometric form with four unknown integration constants, to be computed by enforcing the BC, and a set of matching conditions at the damper locations between the responses over contiguous beam segments. By this approach, in fact, the coefficient matrix associated with the equations to be solved has to be reinverted numerically for any forcing frequency of interest, and updated whenever dampers/load positions change; also, the size inevitably increases with the number of dampers.

For a plane frame, the exact PSD (Eq.(5.1)) inherently fulfills all the re-

quired conditions at the dampers locations, since these conditions are fulfilled by the DSM and LV for each frame member (e). The size of the FRM and LV (Eqs.(4.26)-(4.27)) depends only on the total number of beam-to-columns nodes, regardless of number and position of dampers and loads in each frame member. The FRF and LV can readily be updated for any changing parameter of the dampers and loads, and position of the loads relative to the dampers, by simply updating the local DSM and LV of the frame members in Eq.(4.6) and Eq.(4.7).

Furthermore, for a single beam and frame, the exact PSD of all response variables can serve ad benchmark solution for the corresponding PSD built by a standard FE method with two-node beam elements. Further advantages are that, in a standard FE method, a mesh node shall be inserted at the application point of any damper or point load, and remeshing may be required whenever damper/loads change position.

5.1.2 Discontinuous beams with mono symmetric cross section (warping effects neglected)

In this Section, the stationary response of coupled bending-torsion beams with supports and attached masses will be obtained making use of the exact frequency response functions derived in Chapter 3.

Response to concentrated loads

Consider the beam in Figure 3.19 subjected to a finite number K of stationary concentrated transverse forces $P_r(t)$, assumed to be statistically dependent. Every force acts in z-direction at y_r, and at distance x_c from the y-axis (elastic axis). The power spectral density functions of the deflection, $S_{HH}(y,\omega)$, and all the other response variables in vector $\mathbf{Y}(y,\omega) = [H\ \Theta\ M\ S\ \Psi\ T]$, can be obtained by the following expressions involving the

cross spectral density functions of the forces $S_{P_rP_s}(\omega)$:

$$S_{Y_iY_i}(y,\omega)=\sum_{r=1}^{K}\sum_{s=1}^{K}\Big\{\Big[Y^*_{(f),i}(y,y_r,\omega)Y_{(f),i}(y,y_s,\omega)+Y^*_{(g),i}(y,y_r,\omega)Y_{(g),i}(y,y_s,\omega)+ Y^*_{(f),i}(y,y_r,\omega)Y_{(g),i}(y,y_s,\omega)+Y^*_{(g),i}(y,y_r,\omega)Y_{(f),i}(y,y_s,\omega)\Big]S_{P_rP_s}(\omega)\Big\} \tag{5.2}$$

where the asterisk denotes complex conjugate. In Eq.(5.2) $Y_{(f),i}(y,\xi,\omega)$, $Y_{(g),i}(y,\xi,\omega)$ are given as Eq.(3.143) imposing $\mathbf{Y}^{(f)}=0$ and $\mathbf{Y}^{(g)}=0$ respectively, built by direct integration, where $\mathbf{F}(y,\omega)=\mathbf{J}^{(P)}(y,\xi,\omega)$ in Eq.(3.136) and $\mathbf{G}(y,\omega)=\mathbf{J}^{(Mt)}(y,\xi,\omega)$ in Eq.(3.137). Alternatively, $Y_{(f),i}(y,\xi,\omega)$ and $Y_{(g),i}(y,\xi,\omega)$ may be computed by Eqs.(3.180)-(3.181) built via the normal mode method, on truncating to a sufficient number of modes. In this case, $f(y)=\delta(y-y_r)$ and $g(y)=\delta(y-y_r)$ shall be set in Eqs.(3.182)-(3.183) for every concentrated force $P_r(t)$.

Response to distributed loads

Assume now that the beam in Figure 3.19 is acted upon by a stationary distributed transverse load $f(y,t)$, acting in z-direction and applied at distance x_c from the y-axis (elastic axis). The load is randomly varying with respect to time only. If $S_{ff}(\omega)$ denotes the power spectral density function of $f(y,t)$, the power spectral density functions of all response variables can be obtained as follows:

$$S_{Y_iY_i}(y,\omega)=\Big[|Y_{(f),i}(y,\omega)|^2+|Y_{(g),i}(y,\omega)|^2+Y^*_{(f),i}(y,\omega)Y_{(g),i}(y,\omega)+Y^*_{(g),i}(y,\omega)Y_{(f),i}(y,\omega)\Big]S_{ff}(\omega) \tag{5.3}$$

where $Y_i^{(f)}(y,\omega)$, $Y_i^{(g)}(y,\omega)$ are given respectively as Eq.(3.143) imposing $\mathbf{Y}^{(f)}=0$ and $\mathbf{Y}^{(g)}=0$ respectively or, again, Eqs.(3.180)-(3.181) on truncating to an appropriate number of modes.

It is worth remarking that Eqs.(5.2)-(5.3) can readily be implemented

in analytical form, thanks to the closed analytical expressions built for the frequency response functions (3.143) and (3.180)-(3.181). Advantages are significant over the exact classical method for computing the power spectral density of the response. By the classical method, in fact, the frequency response functions are built dividing the beam in uniform segments, each between two consecutive application points of supports/masses/point loads or under a distributed load, where the response is expressed in terms of 6 unknown integrations constants. For n segments, a set of $(6 \times n)$ equations, built by enforcing the B.C. and suitable matching conditions between the solutions over adjacent segments, shall be solved numerically for every forcing frequency. In addition, the set of $(6 \times n)$ equations shall be updated whenever supports/masses/load change positions.

5.1.3 Numerical Examples

Two numerical examples are proposed in order to demonstrate the validity of the exact proposed method and emphasize the importance of the bending-torsion coupling effects in the stochastic dynamics of mono-symmetric beams with attachments. In both examples power spectral density function of some response variables will be computed, making use of the derived exact expressions (two-sided power spectral densities will always be reported). Two beams will be considered, with angular and "Tee" cross sections, for which warping can generally be neglected according to engineering practice.

Consider the clamped-clamped beam with angular cross section shown in Figure 5.1. Properties are chosen as follows:
$I = 1.0174 \cdot 10^{-5}\mathrm{m}^4$, $J = 9.6666 \cdot 10^{-8}$, $I_\alpha = 0.0549\mathrm{kg} \cdot \mathrm{m}$, $x_a = 0.0512\mathrm{m}$, $L = 3\mathrm{m}$, $m = 7.83\,\mathrm{kg} \cdot \mathrm{m}^{-1}$, $E = 70 \cdot 10^9 \mathrm{N} \cdot \mathrm{m}^{-2}$, $G = 26.3158 \cdot 10^9\,\mathrm{N} \cdot \mathrm{m}^{-2}$, $c_h = 3 \cdot 10^2\,\mathrm{Nm}^{-2}\mathrm{s}$, $c_\psi = 2.105 \cdot \mathrm{Ns}$, $b = 0.15\mathrm{m}$, $t = 0.01\,\mathrm{m}$.

Two translational elastic supports are located at $y_1 = 0.25L$ and $y_3 = 0.75L$, both applied at distance $x_1 = x_3 = 0.1025\,\mathrm{m}$ from the SC of the beam cross section. Further a torsional-rotational elastic support is located at $y_2 = 0.5L$ as shown in Figure 5.1.

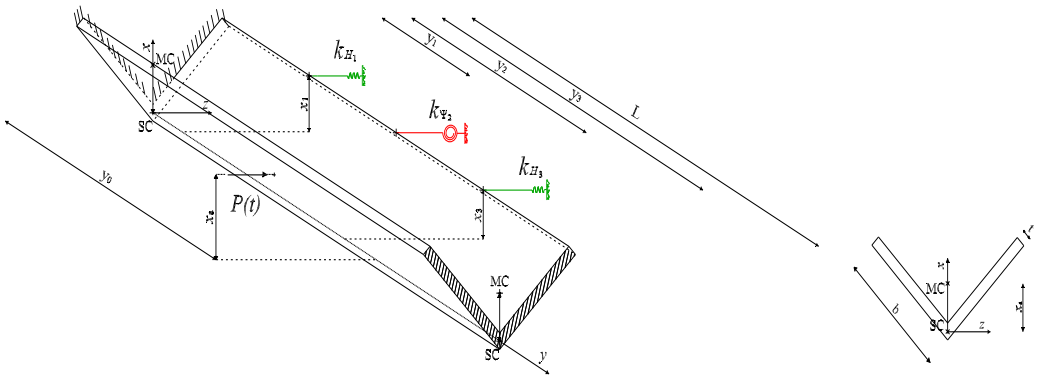

Figure 5.1: Clamped-clamped beam with angular cross-section carrying elastic supports and subjected to a stationary concentrated force $P(t)$ applied at $y_0 = 0.35L$.

Since we are interested in dealing with coupled bending-torsional vibrations, the beam response will be investigated in the $y - z$ plane, where coupling arises due to the eccentricity of the SC with respect to the MC along the x-axis, see Figure 5.1.

First, free vibration analysis is carried out. Table 5.1 reports the natural frequencies of the first three modes, with various stiffness values k_{H_1}, k_{H_3} for the translational elastic supports, as computed by: (1) the exact proposed method, with characteristic equation obtained as determinant of the 6×6 matrix $\mathbf{B}$ in Eq.(3.171); (2) the exact classical method, with characteristic equation given as determinant of a 24×24 matrix obtained by dividing the beam in 4 segments and enforcing internal matching conditions along with the beam B.C. The two methods are in excellent agreement. It is also observed that, as expected, the modal frequencies increase as k_{H_1} and k_{H_3} increase. Figure 5.2 shows the eigenfunctions of some response variables, associated with the modal frequencies in Table 5.1, computed by exact proposed and classical methods; particularly it is assumed that $k_{H_1} = k_{H_3} = 10^5\,\mathrm{N/m}$ and $k_{\Psi_2} = 10^4\,\mathrm{Nm}$. The left column of Figure 5.2 reports the bending deflection $H_n(y)$ compared to the deflection of the cross-section MC due to torsional response, computed as $\Psi_n(y)x_a$ (where x_a is the distance between the SC and MC along x-axis); these response variables are compared in order to show

the amount of coupling between the bending and torsional contributions. Particularly, notice that $H_n(y)$ and $\Psi_n(y)x_a$ have similar order of magnitude in first and third mode, while the torsional contribution is dominant in the second mode. Moreover, it is evident from Figure 5.2 that $\Psi_n(y)$ exhibits slope discontinuities at the abscissas y_1, y_2, y_3 where the elastic supports are located, while slope discontinuities in the torsional rotation mirrors the jump discontinuities in the torque $T_n(y)$, that is depicted in the right column of Figure 5.2.

Now, attention is focused on the response to random loads. Assume that the beam is acted upon by a stationary white-noise concentrated force $P(t)$ acting in z-direction with two-sided $S_{PP}(\omega) = S_0 = 1\,\mathrm{N}^2\mathrm{s}$, applied at $y_0 = 0.35L$ along the y-axis (elastic axis), at distance $x_0 = x_a$ from the y-axis. Figure 5.3 shows the power spectral density functions of the bending deflection, $H(y)$, as well as the deflection of the MC due to torsional rotation, $\Psi(y)x_a$, calculated at $y = 3L/7$. The power spectral densities are obtained using Eq.(5.2), with the exact frequency response functions built via direct integration, and the frequency response functions (3.180)-(3.181) built via normal mode method, truncated to the first 10 modes. It is observed that the two results are in excellent agreement. Furthermore, Figure 5.3 shows that twisting contributes significantly to the deflection of the MC, thus confirming the importance of accurate methods to capture bending-torsion coupling effects in the beam response. For completeness, Figure 5.4 shows the power spectral density functions of the torque moment $T(y)$ at $y = 3L/7$. Again, power spectral densities obtained with the proposed exact and truncated frequency response functions are in perfect agreement.

	Mode 1		Mode 2		Mode 3	
$k_{H_1} = k_{H_3}$	C. M.	P. M.	C.M.	P.M.	C.M.	P.M.
10^2	337.696	337.695	446.964	446.961	714.346	714.347
10^3	337.942	337.941	447.224	447.221	714.387	714.385
10^4	340.386	340.383	449.802	449.806	714.763	714.767
10^5	362.823	362.821	474.136	474.134	718.593	718.591
10^6	481.192	481.196	626.428	626.425	754.477	754.472

Table 5.1: Beam in Figure 5.1, natural frequencies (rad/s) with various stiffness values for the translational elastic supports k_{H_1} and k_{H_3}, as computed by exact classical method (C.M.) and exact proposed method (P.M.).

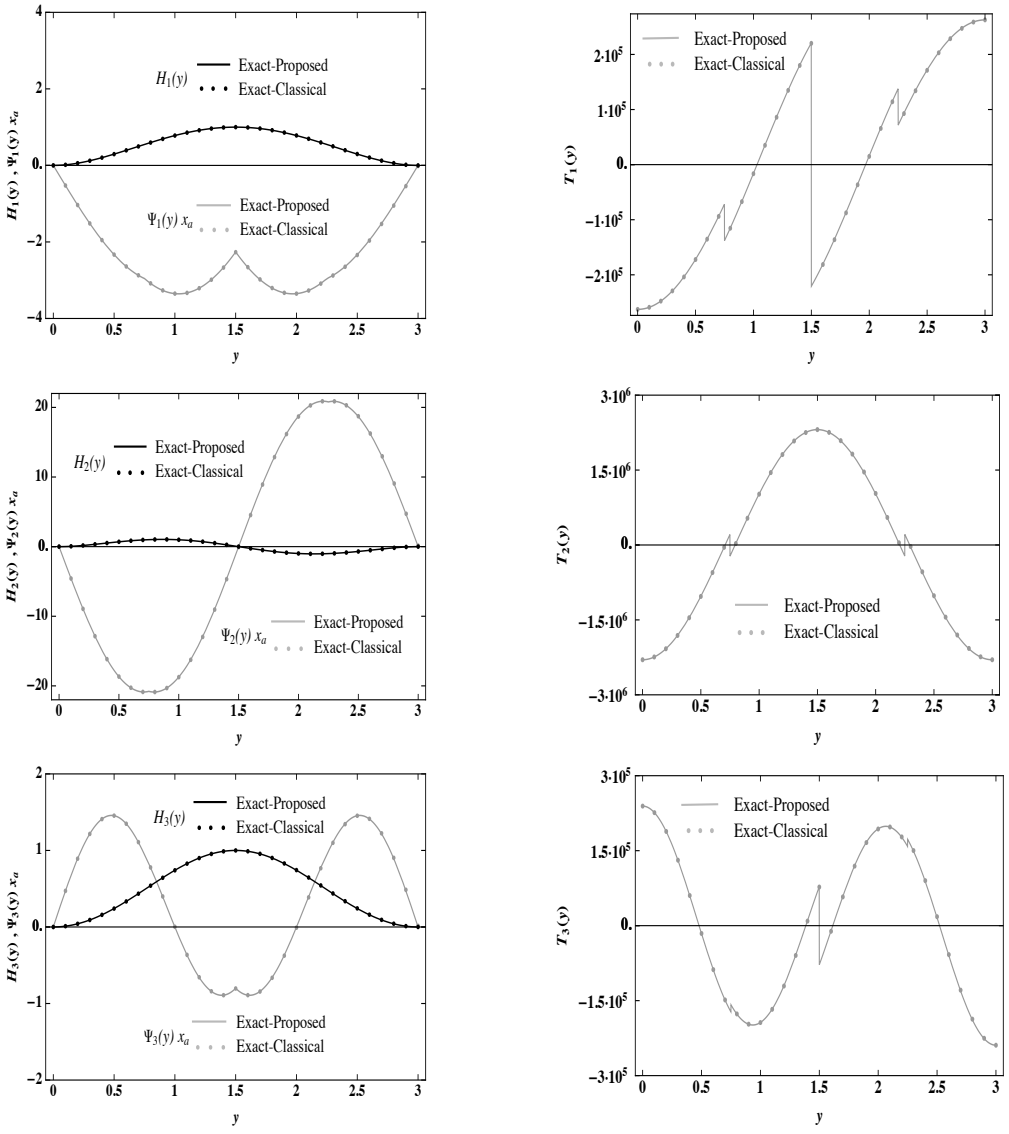

Figure 5.2: Beam in Figure 5.1, eigenfunctions of first 3 modes (from top to bottom): pure bending deflection compared with deflection of cross-section MC due to torsional response (left column); torque (right column).

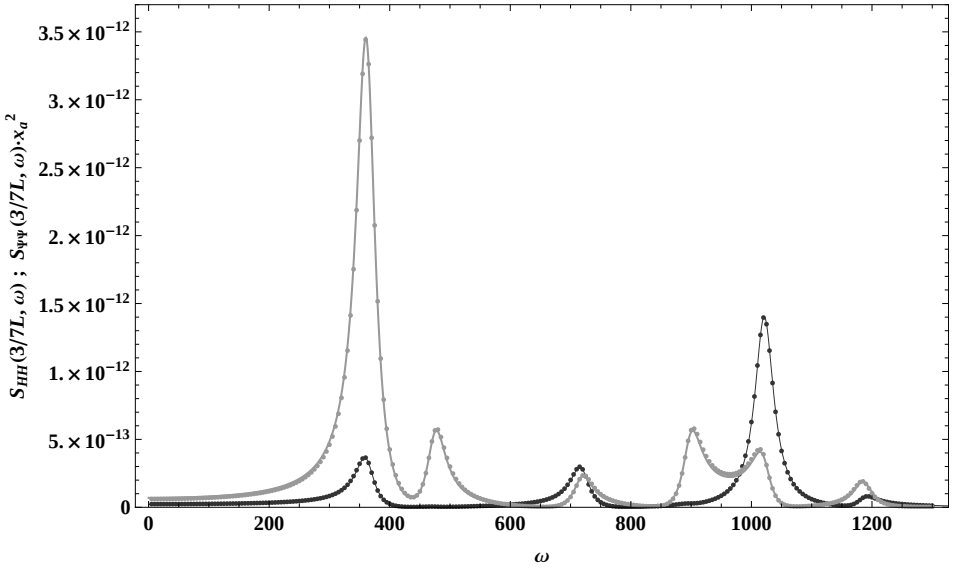

Figure 5.3: Beam in Figure 5.1, power spectral densities of pure bending deflection $S_{HH}(y,\omega)$ (black) and deflection of the cross-section MC due to torsional rotation $S_{\Psi\Psi}(y,\omega)x_a^2$ (gray), computed at $y = 3/7L$, with frequency response functions built via direct integration (continuous line) and normal mode method (dotted line).

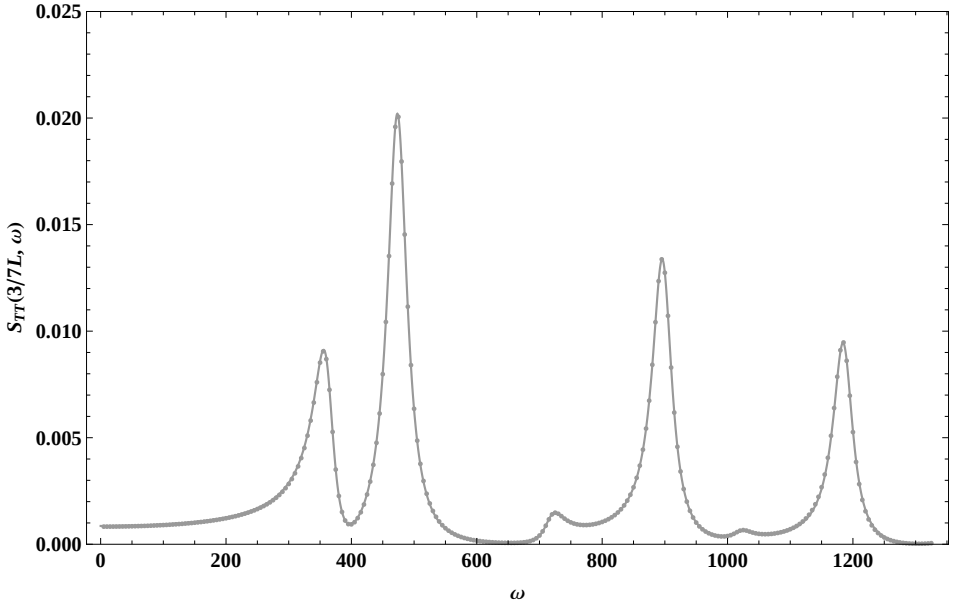

Figure 5.4: Beam in Figure 5.1, power spectral densities of torque $S_{TT}(y,\omega)$, computed at $y = 3/7L$, with frequency response functions built via direct integration (continuous line) and normal mode method (dotted line).

Example B

This example deals with the cantilever beam with a "Tee" cross section depicted in Figure 5.5, whose properties are chosen as follows: $I = 3.66244 \cdot 10^{-4}\text{m}^4$, $J = 1.37915 \cdot 10^{-5}$, $I_\alpha = 13.01\text{kg} \cdot \text{m}$, $x_a = 0.1205\text{m}$, $L = 6\text{m}$, $m = 261.76\,\text{kg} \cdot \text{m}^{-1}$, $E = 210 \cdot 10^9\text{N} \cdot \text{m}^{-2}$, $G = 80.7692 \cdot 10^9\,\text{N} \cdot \text{m}^{-2}$, $c_h = 3 \cdot 10^3\text{Nm}^{-2}\text{s}$, $c_\psi = 149.1 \cdot \text{Ns}$, $h = l = 0.5\,\text{m}$, $t = 0.035$ m.

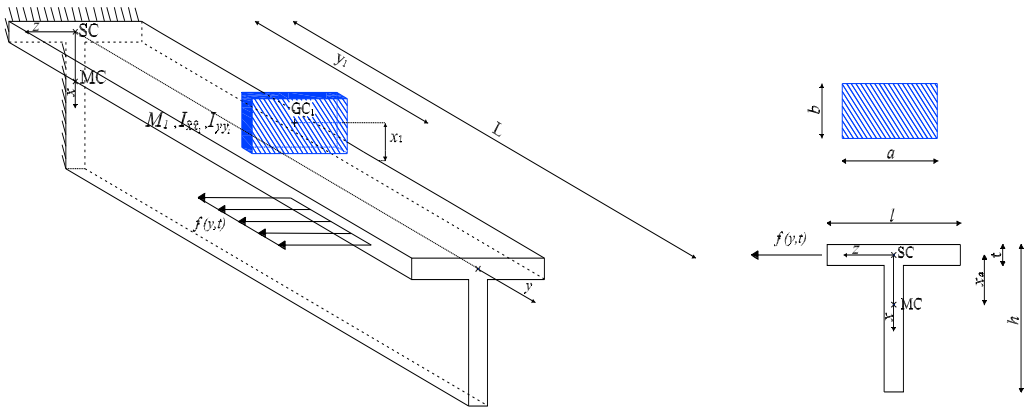

Figure 5.5: Beam with "Tee" cross section carrying an attached mass, subjected to a stationary white noise $f(y,t)$ uniformly distributed over $[0.7L, 0.9L]$.

As shown in Figure 5.5 a mass $M_1 = 50\,\text{kg}$, modeled as a rigid rectangular plate with $a = 0.5\,\text{m}$ and $b = 0.6\,\text{m}$, is attached at $y_1 = 0.5 \cdot L$; let be $I_{\hat{x}\hat{x}_1} = 1.042\,\text{kg m}^2$ and $I_{yy_1} = 2.542\,\text{kg m}^2$ the mass inertia moment with respect to the $\hat{x}$ and y-axis respectively and $x_1 = -0.3175\,\text{m}$ the distance, along the x-axis, between the SC and the gravity center GC_1.

Assume that the beam is acted upon by a stationary white-noise distributed force $f(y,t)$ with two-sided $S_{ff}(\omega) = S_0 = 10^7\text{N}^2 s$, acting in z-direction over the interval $[0.7L, 0.9L]$. Specifically, it is assumed that the force is applied along the elastic axis, i.e. at zero distance from the cross-section SCs (see Figure 5.5). Figures 5.6-5.7 show the power spectral density functions of the bending deflection, $H(y)$, and torsional rotation, $\Psi(y)$, calculated at the tip $y = L$ making use of Eq.(5.3). Again, the power spectral

densities are obtained in two different ways, i.e. making use of the derived exact frequency response and that built through the modal normal mode method (see Eqs.(3.180)-(3.182)), considering the first ten modes. It is seen that the results are in perfect agreement. As shown in Figure 5.7, the torsional response tends to zero. This is consistent with the fact that a static distributed force applied at the SC induces no torsional response.

Next, in order to underline the importance of bending-torsion coupling effects in the dynamic response, the stochastic response of the beam, obtained by the coupled Euler-St.Venant bending-torsion theory, is compared to that obtained with the pure bending Euler-Bernoulli theory, which ignores coupling effects and, as such, does not capture any torsional response. Again assume that the beam is acted upon by a stationary white-noise distributed force $f(y,t)$ with $S(\omega) = S_0 = 10^7\,\mathrm{N^2s}$, acting in z-direction over the interval $[0.7L, 0.9L]$. Figure 5.8 shows the comparison between the power spectral density functions of the bending deflection $S_{HH}(y,\omega)$ (previously depicted in Figure 5.6) with those obtained by the Euler-Bernoulli theory, referred to as $S_{HH_{EB}}(y)$ to avoid confusion. Specifically, $S_{HH_{EB}}(y,\omega)$ is obtained from exact frequency response functions built via direct integration or normal mode method, starting from the following steady-state equation of motion:

$$EI\frac{\bar{d}^4 H_{EB}}{dy^4} - (m\omega^2 - c_h i\omega)H_{EB} - \sum_{j=1}^{N} P_j\delta(y-y_j) + \sum_{j=1}^{N} M f_j \delta^{(1)}(y-y_j) - f(y) = 0 \tag{5.4}$$

As shown in Figure 5.8 the PSD responses are very different, with the Euler-Bernoulli theory which fails to capture several peaks of the response. For a further insight, Figure 5.8 shows, in linear scale, a zoom of the plot in Figure 5.7 in the frequency range $[0, 300]$rad/s. It can be observed that, for small values of the frequency ω the PSD responses are almost equivalent, but as the frequency ω increases the effect of coupling become relevant and the two responses become very different. This is in accordance with Figure 5.7.

The different predictions between the two theories are even more evident

computing the time evolution of variance of the bending deflection responses at the tip $h(y = L, t)$ and $h_{EB}(y = L, t)$, shown in Figure 5.9. For this purpose, Monte Carlo simulations are performed by numerical integration of Eq.(3.176) with a time step $\Delta t = 0.001\,\mathrm{s}$. White noise samples have been simulated by the harmonic superposition method by Shinozuka and Deodatis [93], according to which the generic sample of the excitation process is given as:

$$W(t) = \sum_{i=1}^{M} \sqrt{4S_0 \Delta\omega} \cos(\omega_i t + \phi_i) \tag{5.5}$$

where $M = 1 \cdot 10^5$, $\Delta\omega = 0.02$, and ϕ_i are M realizations of a random variable uniformly distributed in $[0, 2\pi]$. For both theories, Figure 5.9 shows that after the transient, the variance of the displacement computed by numerical simulations agree very well with the stationary value obtained integrating the corresponding power spectra density functions. However, the variance computed by Euler-Bernoulli theory is completely different and in this case, well higher than that computed by the coupled Euler-St.Venant bending-torsion theory. It can then be concluded that the Euler-Bernoulli theory would predict incorrectly the dynamics of the beam in Figure 5.5, and that bending-torsion coupling effects cannot be neglected when applying random loads.

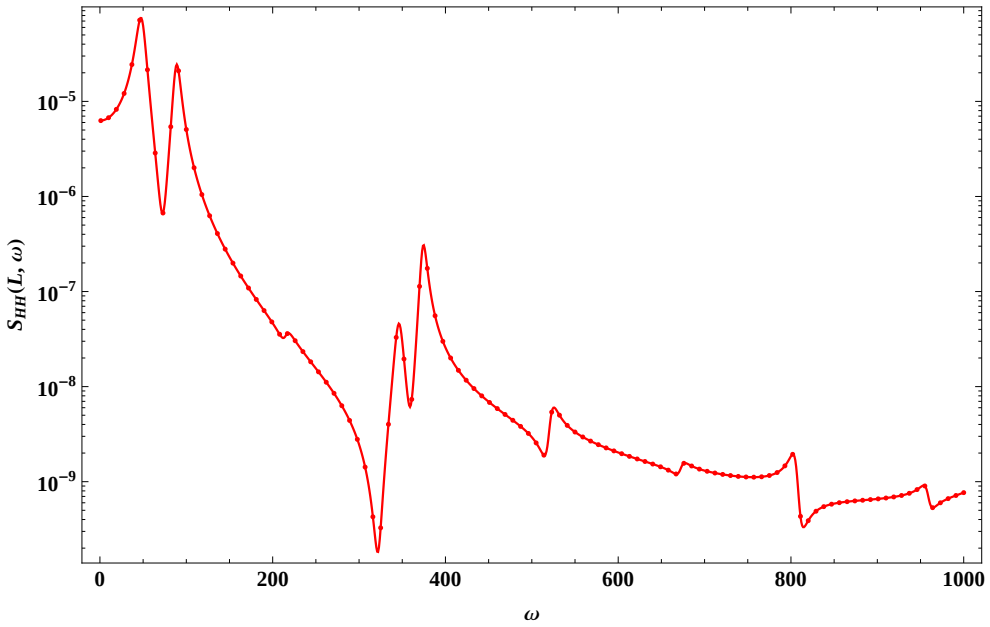

Figure 5.6: Beam in Figure 5.5, power spectral density of bending deflection $S_{HH}(y, \omega)$, computed at $y = L$, with frequency response functions built via direct integration (continuous line) and normal mode method (dotted line).

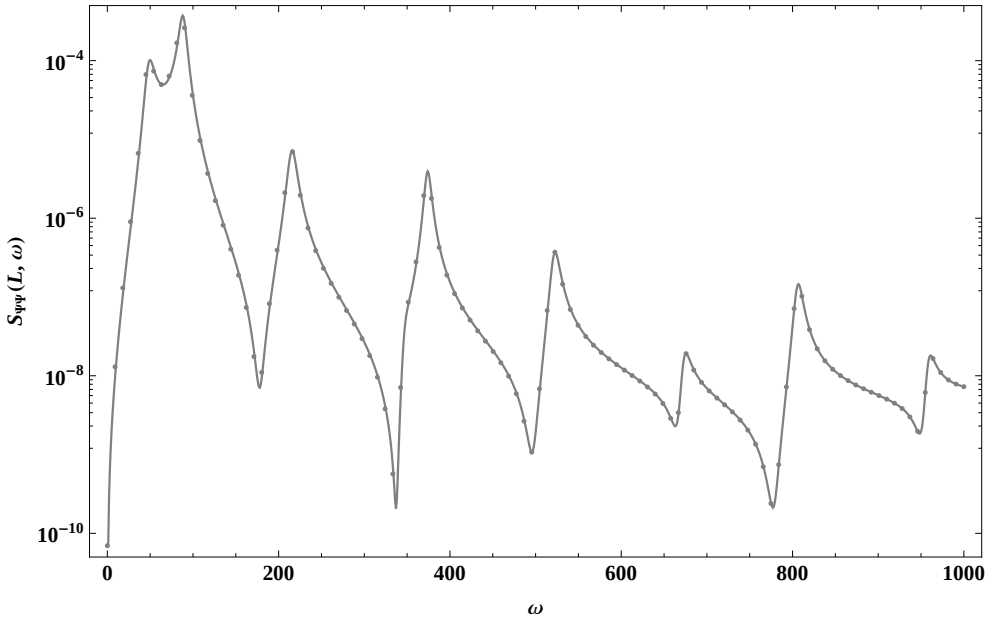

Figure 5.7: Beam in Figure 5.5, power spectral density of torsional rotation $S_{\Psi\Psi}(y, \omega)$, computed at $y = L$, with frequency response functions built via direct integration (continuous line) and normal mode method (dotted line).

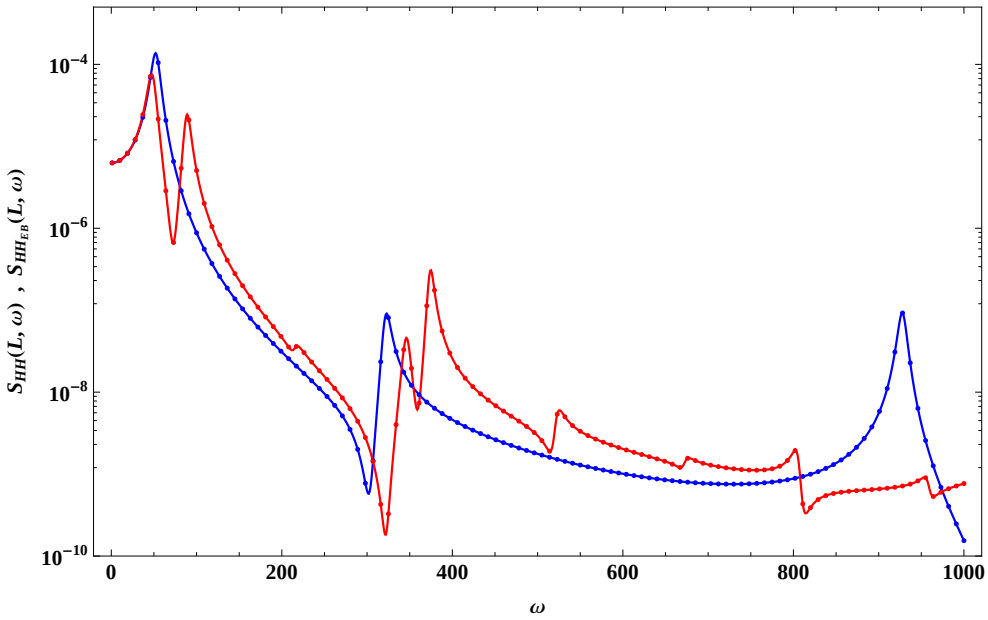

Figure 5.8: Beam in Figure 5.5, power spectral densities of pure bending deflection $S_{HH}(y,\omega)$ (red) obtained by Euler-St.Venant coupled bending-torsion theory and deflection $S_{HH_{EB}}(y,\omega)$ (blue) obtained by Euler-Bernoulli theory, computed at $y = L$, with frequency response functions built via direct integration (continuous line) and normal mode method (dotted line).

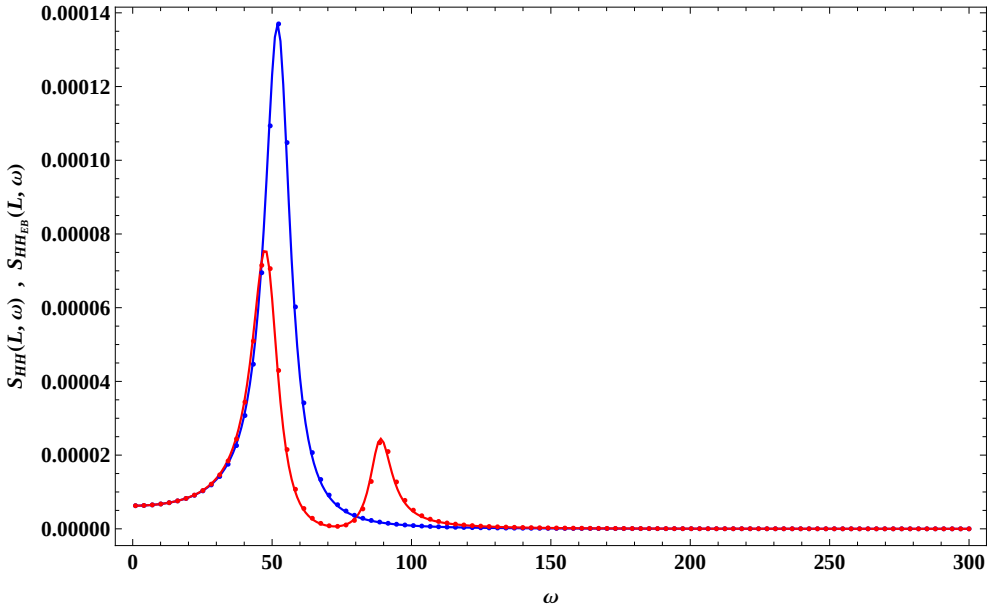

Figure 5.9: Beam in Figure 5.5, zoomed view (in linear scale) of Figure 5.15.

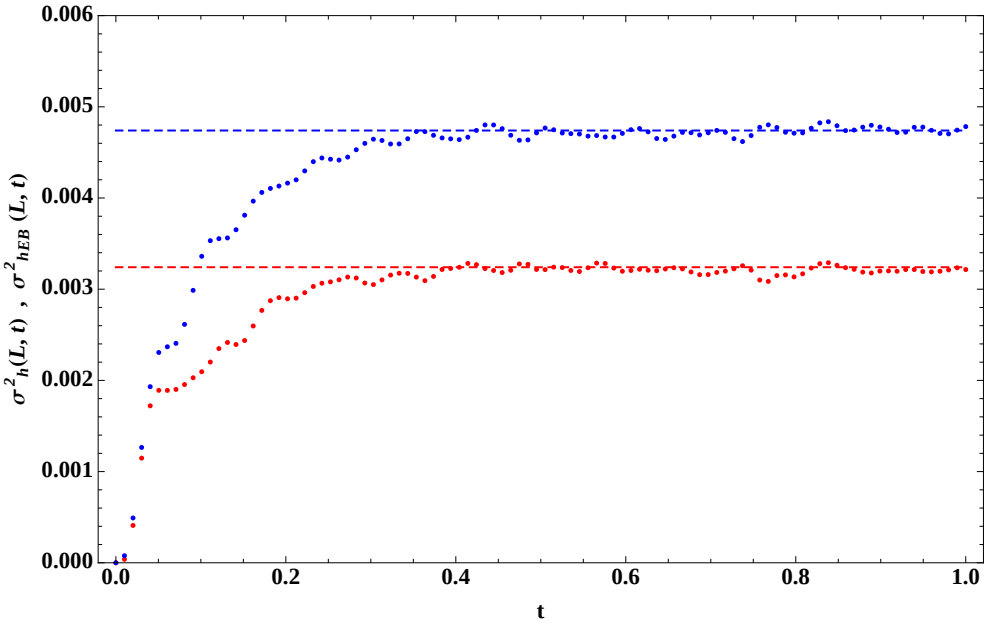

Figure 5.10: Beam in Figure 5.5, time-dependent variance of pure bending deflection $\sigma_h^2(L,t)$ (dotted red line) obtained by Euler-St.Venant coupled bending-torsion theory and $\sigma_{h_{EB}}^2(L,t)$ (dotted blue line) obtained by Euler-Bernoulli theory, computed at $y = L$, along with corresponding stationary value obtained by integrating the power spectral density function.

5.2 Non-stationary response

The response to non-stationary loads can be obtained by an efficient Monte Carlo simulation. This relies on the closed analytical expressions for the impulse response functions obtained in Chapter 3 for discontinuous beams with symmetric cross sections (Eqs.(3.63)) and with mono symmetric cross section (Eq.(3.156)). Indeed, every sample of the response process can be built making use of the Duhamel convolution integral. For example, for beams with symmetric cross section the vector samples of all response variable is given as follows (see Chapter 3 for notation)

$$\mathbf{y}(x,t) = \int_0^t \mathbf{I}_{RF}(x, t-\tau) f(\tau) d\tau \tag{5.6}$$

A similar expression can be found for response variable of beams with mono symmetric cross section. From Eq.(5.6) numerical or analytical solution can be obtained; for example, analytical solutions can be obtained for exponentially-modulated harmonic loads. Further, Eq.(5.6) provide the response variable along the beam. The same equations can be used to calculate the response in every TMD or in every subsystems, using the pertinent frequency response functions as well as the eigenfunctions in the TMD or the subsystems. Indeed, the latter can be easily derived from the deflection of the attachment point.

Notice that also analytical/numerical solutions built by Eq.(5.6), involve remarkable advantages compared to a standard FE approach. Indeed, the latter provides only numerical solutions with accuracy depending on mesh refinement and requires updating/refining the mesh whenever dampers and loads change position along the beam/frame.

5.3 Non-linear analysis: A novel statistical linearization solution approach

In this Section, a statistical linearization approach is developed for determining the response of stochastically excited beams with non-linear supports along their span.

Statistical linearization, due to its versatility and low computational cost, has been a widely used technique to find solutions of non-linear stochastic problems in dynamics. Specifically, it has been one of the most successful approximate solution techniques in the field of nonlinear stochastic dynamics for determining second-order response statistics [94]. In its standard formulation and implementation, and primarily due to its Gaussian response assumption, statistical linearization has proven to be versatile in addressing a wide range of nonlinearity forms, while exhibiting a reasonably low computational cost. A detailed presentation of the technique can be found in the books by Roberts and Spanos [95], and by Socha [96], whereas indicative recent generalizations have been developed to account for joint time-frequency analysis, for fractional derivative operators, and for systems with singular matrices [97, 98, 99, 100, 101, 102].

In this Section, attention is focused on the application of the technique to beam vibrations. All the pertinent works in literature [103, 104, 105] dealt with beams having doubly-symmetric cross section and where non-linearity derives from the assumption of moderately large displacement. In this regard, the novelty of the technique consists in considering non-linearity also in the constitutive law of the supports located along the beam span. A significant novelty aspect of the developed approach is the utilization of constrained modes, computed in Chapter 3, which involve appropriate generalized functions and can inherently account for shear-force discontinuities at the support locations. Employing these modes in the linearized modal equations yields accurate and computationally efficient solutions for the second-order statistics of the response. Results obtained by the proposed statistical linearization

approach are compared with Monte Carlo simulation data. These are generated by dividing the beam in finite elements of equal length and discretizing the beam equation into a set of second-order differential equations via the boundary integral method (BIM). The set of differential equations is then solved via a numerical Newmark integration scheme. Some illustrative numerical examples are considered for assessing the accuracy of the proposed statistical linearization solution approach.

It is remarked that the novel statistical linearization approach shows several advantages with respect to other linearization approaches due to the employ of exact closed form for constrained modes. However, all the advantages and consideration will be discussed in the next Section.

5.3.1 In-span supported beams with symmetric cross section

Problem statement

Consider the beam of length L depicted in Figure 5.11, resting on an arbitrary number of non-linear elastic supports. Let the beam be excited by a transverse distributed random load $f(x,t)$, with x being the axial coordinate and t the time. Applying D'Alembert's principle and utilizing generalized functions, the partial differential equation

$$EI\frac{\partial^4 v(x,t)}{\partial x^4}+m\frac{\partial^2 v(x,t)}{\partial t^2}+c\frac{\partial v(x,t)}{\partial t}-N\frac{\partial^2 v(x,t)}{\partial x^2}+\sum_{r=1}^{N}\{F_r\delta(x-x_r)\}=f(x,t) \tag{5.7}$$

governing the beam response is derived, where $v(x,t)$ is the beam deflection and N is the axial force given by

$$N=\frac{EA}{2L}\int_0^L\left[\frac{\partial v(x,t)}{\partial x}\right]^2 dx \tag{5.8}$$

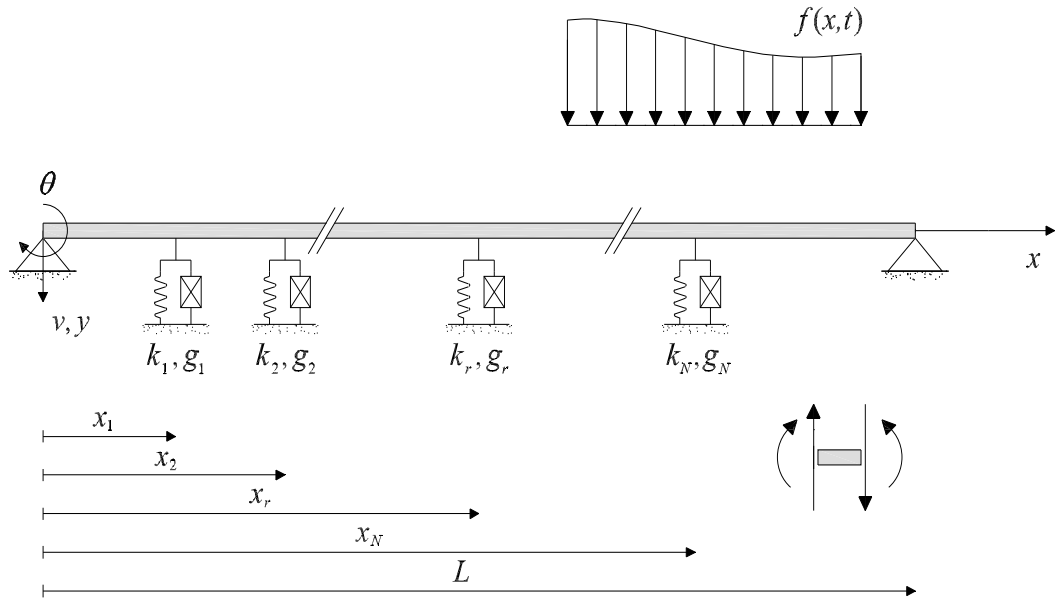

Figure 5.11: Non-linear beam resting on an arbitrary number of non-linear elastic supports; the crossed box indicates arbitrary non-linearity. Positive sign conventions are reported.

The nonlinearity in Eq.(5.8) relates to the assumption of relatively large beam displacements, while EA is the axial rigidity, EI is the flexural rigidity, and m represents the mass per unit length. The symbol F_r is the non-linear restoring force related to the support at location x_r, expressed as

$$F_r = k_r v(x_r, t) + g_r(v(x_r, t)) \tag{5.9}$$

where $k_r v(x_r, t)$ and $g_r(v(x_r, t))$ are the linear and non-linear parts of the restoring force, respectively, and k_r is a stiffness coefficient.

Next, it is assumed that the distributed load $f(x, t)$ can be expressed in the separable form:

$$f(x, t) = f(x)f(t) \tag{5.10}$$

where $f(x)$ is a deterministic function of the axial coordinate only, while $f(t)$ is a stationary zero-mean Gaussian process with a two-sided power spectral density function $S(\omega)$ and correlation function $R(t - \tau_1, t - \tau_2)$ expressed via

the Wiener-Kinshine relationship as

$$R(t-\tau_1, t-\tau_2) = E\Big[f(t-\tau_1)f(t-\tau_2)\Big] = \int_{-\infty}^{\infty} S(\omega)e^{i\omega(\tau_2-\tau_1)}d\omega \qquad (5.11)$$

Statistical linearization solution approach

Due to lack of exact solutions in the literature for the non-linear stochastic response of the beam in Figure 5.11, a statistical linearization solution approach is developed next. For this purpose, the beam deflection $v(x,t)$, of Eq.(5.7), is represented as

$$v(x,t) = \sum_{n=1}^{\infty} V_n(x)y_n(t) \qquad (5.12)$$

where y_n are the modal amplitudes and V_n are the modes of a corresponding linear ($N = 0$, i.e. small displacements are considered, and $F_r = k_r v(x_r, t)$) beam (Figure 5.12) associated with the non-linear problem of Eq.(5.7), governed by the differential equation

$$EI\,\frac{d^4V_n(x)}{dx^4} - m\omega_n^2 V_n(x) + \sum_{r=1}^{N}\{k_r V_n(x_r)\delta(x-x_r)\} = 0 \qquad (5.13)$$

In Eq.(5.13), ω_n is the n-th natural frequency related to the modes V_n, which can be obtained from Eq.(5.13) in a closed analytical form [13, 21] as shown in Chapter 3. Note that the derived modes inherently account for shear-force discontinuities at the support locations, as shown by Failla [21], and fully described in Chapter 3. It is remarked that this method developed by Failla [21] leads to a characteristic (frequency) equation expressed as a determinant of a 4×4 matrix, irrespective of the number of supports along the beam. This significant advantage enables the statistical linearization treatment of an arbitrary number of supports along the beam at a low computational cost.

The orthogonality condition (O.C.) among the modes V_n is expressed as

$$(\omega_n - \omega_m)\int_0^L V_m(x)V_n(x)dx = \Delta_{mn} \qquad (5.14)$$

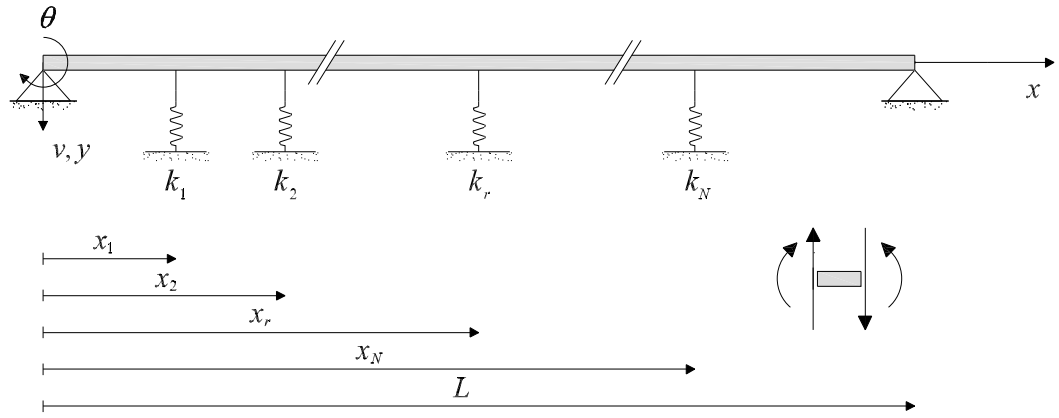

Figure 5.12: Corresponding linear beam associated with the non-linear beam in Figure 5.11.

where $\Delta_{mn} = 0$ if $m \neq n$ and $\Delta_{mn} = \mu_{nn}$ if $m = n$. It is noticed that the form of O.C. in Eq.(5.14) is equivalent to that related to a linear beam without any kind of supports.

The closed-form analytical expressions of modes $V_n(x)$ allow a rather straightforward and efficient formulation of the proposed statistical linearization solution procedure. Indeed, introducing Eq.(5.12) in Eq.(5.7) and exploiting the O.C. in Eq.(5.14), after some algebra, the following set of non-linear ordinary differential equations is obtained for the n-th modal amplitude y_n:

$$\begin{aligned} &\ddot{y}_n + \frac{c}{m}\dot{y}_n + \omega_n^2 y_n - \frac{EA}{2Lm\mu_{nn}} \sum_{m=1}^{\infty}\sum_{i=1}^{\infty}\sum_{j=1}^{\infty} K_{ij} R_{mn} y_m y_i y_j \\ &\quad + \sum_{r=1}^{N} \left\{ \frac{V_n(x_r)}{m\mu_{nn}} g_r \left(\sum_{j=1}^{\infty} V_j(x_r) y_j \right) \right\} = \frac{1}{m\mu_{nn}} \int_0^L V_n(x) f(x) dx f(t) \\ &\quad = \frac{P_n}{m\mu_{nn}} f(t) \end{aligned} \tag{5.15}$$

for $n = 1, 2, \ldots,$ where

$$K_{mn} = \int_0^L V'_m(x) V'_n(x) dx \quad ; \quad R_{mn} = \int_0^L V_m(x) V''_n(x) dx \tag{5.16}$$

Next, according to statistical linearization [103, 104, 105], an approximate solution of Eq.(5.15) is sought for by considering the equivalent system

$$\ddot{y}_n + \frac{c}{m}\dot{y}_n + \omega_{eq,n}^2 y_n = \frac{1}{m\mu_{nn}}\int_0^L V_n(x)f(x)dx f(t) = \frac{P_n}{m\mu_{nn}}f(t) \tag{5.17}$$

for $n = 1, 2, \ldots$, where $\omega_{eq,n}$ is the n-th equivalent natural frequency, determined by an error minimization procedure in a mean square sense. Specifically, denoting by ϵ_n the error between the nonlinear equation (5.15) and the linearized one (5.17), $\omega_{eq,n}$ is evaluated as the solution of the equation

$$\frac{\partial}{\partial \omega_{eq,n}^2} E\Big[\epsilon_n^2\Big] = 0 \qquad \text{for } n = 1, 2, \ldots \tag{5.18}$$

Eq.(5.18) yelds an expression for $\omega_{eq,n}$ in the form

$$\begin{aligned}\omega_{eq,n}^2 = \omega_n^2 - \frac{EA}{2Lm\mu_{nn}}\frac{1}{E\Big[y_n^2\Big]}\sum_{m=1}^{\infty}\sum_{i=1}^{\infty}\sum_{j=1}^{\infty}K_{ij}R_{mn}E\Big[y_n y_m y_i y_j\Big] \\ + \sum_{r=1}^{N}\left\{\frac{V_n(x_r)}{m\mu_{nn}E\Big[y_n^2\Big]}E\Big[y_n g_r\Big(\sum_{j=1}^{\infty}V_j(x_r)y_j\Big)\Big]\right\}\end{aligned} \tag{5.19}$$

The various expectations in Eq.(5.19) can be calculated as explained next. Consider the time domain linear input-output relationship

$$y_n = \frac{P_n}{m\mu_{nn}}\int_{-\infty}^{\infty} h_n(\tau)f(t-\tau)d\tau \quad \text{for } n = 1, 2\ldots \tag{5.20}$$

where $h_n(t)$ is the impulse response function associated with the linear system in Eq.(5.17) and related to the transfer function of the same system, $H_n(\omega)$, through its Fourier transform, i.e.,

$$h_n(t) = \frac{1}{2\pi}\int_{-\infty}^{\infty} H_n(\omega)e^{i\omega_n t}d\omega \quad \text{and} \quad H_n(\omega) = \int_{-\infty}^{\infty} h_n(t)e^{-i\omega_n t}d\omega \tag{5.21}$$

Next, substituting Eq.(5.20) in Eq.(5.19) and using Eqs.(5.21)-(5.11), the

second-order moment of y_n is evaluated as

$$E\Big[y_n^2\Big] = \left(\frac{P_n}{m\mu_{nn}}\right)^2 \int_{-\infty}^{\infty} H_n(-\omega)S(\omega)H_n(\omega)d\omega \tag{5.22}$$

while the cross statistics $E\Big[y_n y_m y_i y_j\Big]$ are evaluated as

$$E\Big[y_n y_m y_i y_j\Big] = \frac{P_n P_m P_i P_j}{m^4 \mu_{nn}\mu_{mm}\mu_{ii}\mu_{jj}}(S_{nm}S_{ij} + S_{ni}S_{mj} + S_{nj}S_{mi}) \tag{5.23}$$

where

$$S_{nm} = \int_{\infty}^{\infty} H_n(\omega)S(\omega)H_m(-\omega)d\omega \tag{5.24}$$

In deriving Eq.(5.23), Eq.(5.20) for y_n, and Eq.(5.21) for $h_n(t)$ have been utilized. Further, the relationship [105]

$$E\Big[z_1 z_2 z_3 \dots z_m\Big] = \sum_{all\ independent\ pairs} \left(\prod_{j\neq k} E\Big[z_j z_k\Big]\right) \tag{5.25}$$

which applies for Gaussian random processes with zero mean, is also considered, yielding for the input $f(t)$

$$\begin{aligned} E\Big[f(t-\tau_1)f(t-\tau_2)f(t-\tau_3)f(t-\tau_4)\Big] = \\ E\Big[f(t-\tau_1)f(t-\tau_2)]E[f(t-\tau_3)f(t-\tau_4)\Big] \\ +E\Big[f(t-\tau_1)f(t-\tau_3)]E[f(t-\tau_2)f(t-\tau_4)\Big] \\ +E\Big[f(t-\tau_1)f(t-\tau_4)]E[f(t-\tau_2)f(t-\tau_3)\Big] \end{aligned} \tag{5.26}$$

Next, depending on the specific form of the nonlinearity function $g(v(x_r,t))$, the expectation of the last term on the right hand side of Eq.(5.19) can be expressed as a function of the response second-order statistics. Overall, taking

into account Eqs.(5.22)-(5.23), Eq.(5.19) becomes

$$\omega_{eq,n}^2 = \omega_n^2 - \frac{EA}{2L}\frac{1}{m^3 P_n S_{nn}} \sum_{m=1}^{\infty}\sum_{i=1}^{\infty}\sum_{j=1}^{\infty} K_{ij} R_{nm} \frac{P_m P_i P_j}{\mu_{mm}\mu_{ii}\mu_{jj}} (S_{nm}S_{ij} + S_{ni}S_{mj} + S_{nj}S_{mi}) + \sum_{r=1}^{N}\left\{ \frac{V_n(x_r)}{m\mu_{nn}E\left[y_n^2\right]} E\Big[y_n g_r\Big(\sum_{j=1}^{\infty} V_j(x_r) y_j\Big)\Big]\right\} \tag{5.27}$$

Clearly, as $\omega_{eq,n}$ depends on S_{nm} via Eq.(5.27), and S_{nm} also depends on $\omega_{eq,n}$ via Eq.(5.24), an iterative solution approach can be established. In particular, setting at the first iteration $\omega_{eq,n} = \omega_n$ and employing a convergence criterion of the form $|\omega_{eq,n}^{(i+1)} - \omega_{eq,n}^{(i)}| < \epsilon$, the values of $\omega_{eq,n}$ and S_{nm} are obtained after few iterations.

Once the numerical values for each equivalent frequency are obtained, the variance of the beam deflection can be easily computed as

$$\sigma_v^2(x) = E\Big[v^2(x,t)\Big] = \sum_{i=1}^{M}\sum_{j=1}^{M} V_i(x)V_j(x)\frac{P_i P_j}{m\mu_{ii}\mu_{jj}} S_{ij} \tag{5.28}$$

Considerations and remarks

The method developed in the previous Section extends the conventional statistical linearization procedure related to non-linear beams under the assumption of moderately large displacements [103, 104, 105]. The main novelty herein consists in accounting for nonlinearities associated not only with the assumption of moderately large beam displacements, but also with the constitutive law of the supports along the span.

It is noteworthy that the modes V_n employed for this problem and obtained from Eq.(5.13) are constrained modes, i.e. inherently account for shear-force discontinuities at the support locations, as shown in Chapter 4. Specifically, Eq.(5.13) involves the linear part of the support forces (5.9). As a result, substituting Eq.(5.12) for the deflection $v(x,t)$ into Eq.(5.7) and using the O.C. (5.14) yields non-linear modal equations (5.15) where the terms associ-

ated with the supports involve only the non-linear part of the support forces (5.9). Note that different and more complex expressions for the non-linear modal equations (5.15) would be obtained if the employed modes were, for instance, the unconstrained ones corresponding to a beam without any kind of supports. Denoting the latter by $V_n^{(b)}$, they satisfy the equation

$$EI\,\frac{d^4V_n^{(b)}(x)}{dx^4} - m\omega_{(b),n}^2 V_n^{(b)}(x) = 0 \tag{5.29}$$

In this case, the beam deflection $v(x,t)$ would be represented as

$$v(x,t) = \sum_{n=1}^{\infty} V_n^{(b)} z_n(t) \tag{5.30}$$

and then terms associated with the supports in the non-linear modal equations (5.15) would depend on both the linear and nonlinear parts of the support forces (5.9). In particular, Eq.(5.15) would be expressed as

$$\begin{aligned}
&\ddot{z}_n + \frac{c}{m}\dot{z}_n + \omega_{n,(b)}^2 z_n - \frac{EA}{2Lm\mu_{nn}^{(b)}} \sum_{m=1}^{\infty}\sum_{i=1}^{\infty}\sum_{j=1}^{\infty} K_{ij}^{(b)} R_{mn}^{(b)} z_m z_i z_j \\
&\quad + \sum_{r=1}^{N}\left\{ k_r \frac{V_n^{(b)}(x_r)}{m\mu_{nn}^{(b)}} \sum_{j=1}^{\infty} V_j^{(b)}(x_r) z_j \right\} + \sum_{r=1}^{N}\left\{ \frac{V_n^{(b)}(x_r)}{m\mu_{nn}} g\left(\sum_{j=1}^{\infty} V_j^{(b)}(x_r) z_j \right) \right\} \\
&\quad = \frac{P_n^{(b)}}{m\mu_{nn}^{(b)}} f(t)
\end{aligned} \tag{5.31}$$

for $n = 1, 2, \ldots$.

Consequently, more terms would be involved in the error minimization procedure yielding increased computational effort and potentially less accu-

rate results. Indeed, Eq.(21) would take the form

$$\begin{aligned}\omega_{eq,n}^2 = \omega_{n,(b)}^2 &- \frac{EA}{2Lm\mu_{nn}^{(b)}} \frac{1}{E\left[z_n^2\right]} \sum_{m=1}^{\infty}\sum_{i=1}^{\infty}\sum_{j=1}^{\infty} K_{ij}^{(b)} R_{mn}^{(b)} E\left[z_n z_m z_i z_j\right] \\ &+ \sum_{r=1}^{N}\left\{ k_r \frac{V_n^{(b)}(x_r)}{m\mu_{nn}^{(b)} E\left[z_n^2\right]} E\left[z_n \sum_{j=1}^{\infty} V_j^{(b)}(x_r) z_j\right]\right\} \\ &+ \sum_{r=1}^{N}\left\{ \frac{V_n^{(b)}(x_r)}{m\mu_{nn} E\left[z_n^2\right]} E\left[z_n g\left(\sum_{j=1}^{\infty} V_j^{(b)}(x_r) z_j\right)\right]\right\}\end{aligned} \tag{5.32}$$

In addition, as can be seen from Eq.(5.29), unconstrained modes do not inherently account for shear force discontinuities at the support locations, thus rendering the constrained modes V_n the overall preferred choice.

A further important observation is that constrained modes V_n and corresponding frequencies ω_n are obtained by solving a characteristic equation expressed as the determinant of a 4×4 matrix, for any number of supports and any type of beam B.C. This is possible by employing the technique developed in the previous Chapter [21], which makes use of appropriate generalized functions to handle shear-force discontinuities at the support locations. The technique provides also closed-form analytical expressions for modes V_n.

Obviously, the same modes V_n and frequencies ω_n can be determined by applying a standard approach as described in Chapter 1, i.e. enforcing internal matching conditions between the free-vibration responses to the left and right of every support location. In this case, the characteristic equation would be obtained as the determinant of a $4(N+1) \times 4(N+1)$ matrix for N supports.

Both the technique by Failla [21] and the standard approach are exact. However, the technique by Failla [21] renders the statistical linearization approach computationally more efficient as the characteristic equation providing modes V_n and frequencies ω_n is always obtained as the determinant of a 4×4 matrix irrespective of the number of supports.

Monte Carlo simulations

Results obtained by statistical linearization are validated against Monte Carlo simulations data, generated by utilizing the boundary integral method (BIM) in conjunction with a Newmark integration scheme. First, samples of the zero-mean stationary Gaussian process $f(t)$ in Eq.(5.10) are produced by employing the spectral representation method by Shinozuka and Deodatis [93], that is:

$$f(t) = \sum_{i=1}^{M^*} \sqrt{4S(\omega)\Delta_\omega}\cos(\omega_i t + \phi_i) \tag{5.33}$$

where $\Delta\omega$ is a constant step on the frequency axis; $\omega_k = k\Delta\omega$ are M^* equally spaced frequencies and ϕ_k are M^* random phases uniformly distributed in $[0, 2\pi]$. Next, following the BIM [106], the differential equation of motion (5.7) is replaced by a surrogate one of the same maximum order with respect to the axial coordinate, i.e.,

$$\frac{\partial^4 v(x,t)}{\partial x^4} = b(x,t) \tag{5.34}$$

where $b(x,t)$ is an unknown time- and space-dependent fictitious load. Treating the time t as a parameter, the solution of Eq.(5.34) can be written as

$$v(x,t) = c_1 + c_2 x + c_3 x^2 + c_4 x^3 + \int_0^L G_P(x,\xi) b(\xi,t) d\xi \tag{5.35}$$

where $c_i = c_i(t)$ $(i = 1, 2, 3, 4)$ are time-dependent functions determined by the beam B.C. The integral in Eq.(5.35) represents the convolution between the fictitious load $b(x,t)$ and $G_P(x,\xi)$, which is the particular solution of the equation

$$\frac{d^4 G(x,\xi)}{dx^4} = \delta(x-\xi) \tag{5.36}$$

yelding

$$G_P(x,\xi) = \frac{1}{12}|x-\xi|(x-\xi)^2 \tag{5.37}$$

Next, dividing the beam in N^* elements of equal length Δx, and assuming that the fictitious load $b(x,t)$ is constant over each element, the expression

for the deflection (5.35) becomes

$$v(x,t) = c_1 + c_2 x + c_3 x^2 + c_4 x^3 + \sum_{j=1}^{N^*} b(\xi_j, t) \int_j G_P(x,\xi) d\xi \tag{5.38}$$

where $\int_j$ is the integral over the j-th element.

Collocating the equation of motion at the nodal points and making use of Eq.(5.38) to express the beam displacement and its subsequent derivatives at the nodal points, the following set of non-linear second-order differential equations is obtained; that is

$$\begin{aligned} m\mathbf{G}\ddot{\mathbf{b}}(t) + c\mathbf{G}\dot{\mathbf{b}}(t) + EI\mathbf{b}(t) - \frac{EA}{2L}\mathbf{F}[\mathbf{b}(t), \mathbf{G}] \\ + \frac{1}{\Delta x}\mathbf{K}\mathbf{G}\mathbf{b}(t) + \frac{1}{\Delta x}\sum_{r=1}^{N}\Big\{\mathbf{F}_r[\mathbf{b}(t), \mathbf{G}]\Big\} = \mathbf{q}(t) \end{aligned} \tag{5.39}$$

where $\mathbf{b}(t)$ is the vector containing the fictitious load evaluated at the nodal points, $\mathbf{G}$ is a matrix whose elements contain the integral of $G_P(x,\xi)$ over each element and take into account the beam B.C., $\mathbf{F}[\mathbf{b}(t), \mathbf{G}]$ is a non-linear vector function related to the large beam displacement contribution, while $\mathbf{K}$ is the diagonal matrix

$$\mathbf{K} = \begin{bmatrix} k_1 & 0 & \dots & 0 \\ 0 & k_2 & \dots & 0 \\ \vdots & \vdots & \ddots & 0 \\ 0 & \dots & 0 & k_N \end{bmatrix} \tag{5.40}$$

In Eq.(5.39) $\mathbf{F}_r$ is a non-linear vector function related to the non-linear part of the r-th restoring force; $\mathbf{q}(t)$ is the vector of the external time-varying force evaluated at the nodal points. It is remarked that in deriving Eq.(5.39), the Dirac's delta function $\delta(x)$ is handled as a finite impulse of unit area and of length Δx. In this way, any concentrated action (external point forces or reactions of the supports) is replaced by a uniform distributed action over the beam finite element of length Δx.

5.3.2 Numerical examples

To demonstrate the accuracy of the developed statistical linearization approach, two numerical examples are considered. In Example A, a simply supported beam with cubic nonlinearities in the supports is studied, while Example B deals with a clamped-clamped beam resting on supports with bilinear stiffness. In both examples, results obtained by statistical linearization are compared with Monte Carlo simulation data, for various values of the support parameters and the nonlinearity degree.

Example A: Cubic stiffness nonlinearities

Consider the simply supported beam depicted in Figure 5.13, where the nonlinear behavior of the supports at locations $x_1 = 3.75\,\text{m}$ and $x_2 = 8.25\,\text{m}$ is expressed by Eq.(5.9), which takes the specific form

$$F_r = k_{C_r} v(x_r, t) + \epsilon_r k_{C_r} v^3(x_r, t) \tag{5.41}$$

The beam is subjected to a white noise uniformly-distributed load with $f(x) = 1$ and power spectral density (PSD) S_0. Beam properties are summarized in Table 5.2; linear and non-linear coefficients of the supports are denoted as k_{C_1}, k_{C_2} and ϵ_1, ϵ_2, respectively.

Further, to proceed with the statistical linearization solution treatment, attention is directed first to the free vibration of the linear beam shown in Figure 5.14, obtained by setting $\epsilon_1 = \epsilon_2 = 0$ and $N = 0$. For this beam, a modal analysis is pursued according to the proposed method and the standard approach (see subsection "Considerations and remarks") for comparison. Table 5.3 shows the first three natural frequencies for various values of the coefficient $k = k_{C_1} = k_{C_2}$. Results obtained by the two methods coincide. Figure 5.15 shows the eigenfunctions associated with the first three natural frequencies for $k_{C_1} = k_{C_2} = 10^5\,\text{N/m}$. Specifically, the eigenfunctions of beam displacement and shear force are shown on the left and right columns, respectively. It can be readily seen that the eigenfunctions computed by the

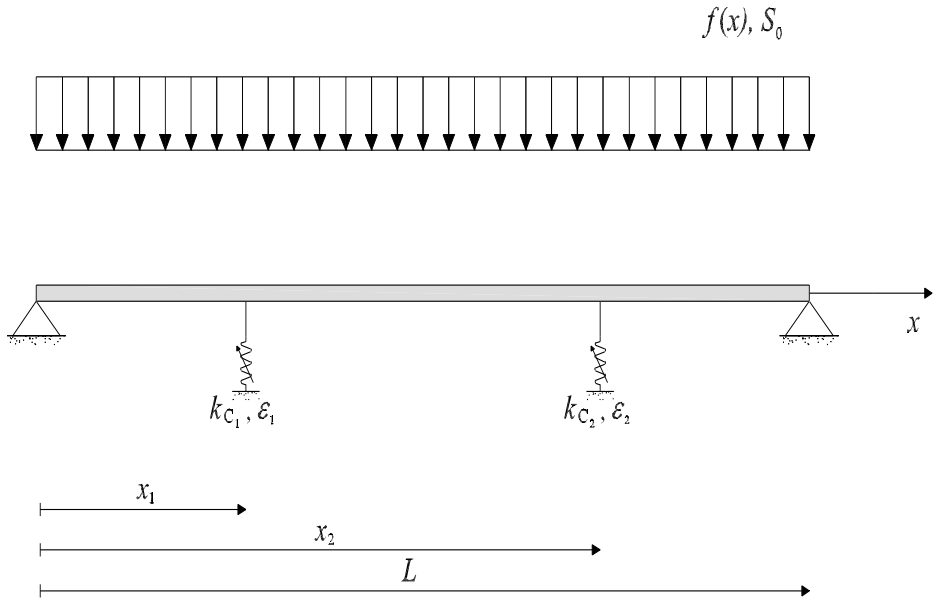

Figure 5.13: Simply supported non-linear beam resting on two non-linear supports with cubic stiffness nonlinearities.

approach in Appendix I inherently account for the presence of the supports at locations x_1 and x_2, as the shear force exhibits jump discontinuities at these locations. As before, a perfect agreement is observed with results obtained by the standard approach. The eigenfunctions computed according to Appendix I are used next to implement the statistical linearization approach proposed in subsection "Statistical linearization solution approach".

In this regard, consider the non-linear beam shown in Figure 5.13 with parameters values $S_0 = 2{\cdot}10^2\,\mathrm{N^2s}$; and $k_{C_1} = k_{C_2} = 10^5\,\mathrm{N/m}$. The response of the beam is represented via Eq.(5.12) by using the first three eigenfunctions, while applying the error minimization equation (5.18), Eq.(5.19) takes the form

$$\omega_{eq,n}^2 = \omega_n^2 - \frac{EA}{2Lm\mu_{nn}} \frac{1}{E\left[y_n^2\right]} \sum_{m=1}^{\infty}\sum_{i=1}^{\infty}\sum_{j=1}^{\infty} K_{ij} R_{mn} E\left[y_n y_m y_i y_j\right] + \sum_{r=1}^{2} \left\{ \frac{\epsilon_r k_{C_r}}{m\mu_{nn} E\left[y_n^2\right]} \sum_{m=1}^{\infty}\sum_{i=1}^{\infty}\sum_{j=1}^{\infty} V_n(x_r) V_m(x_r) V_i(x_r) V_j(x_r) E\left[y_n y_m y_i y_j\right] \right\} \tag{5.42}$$

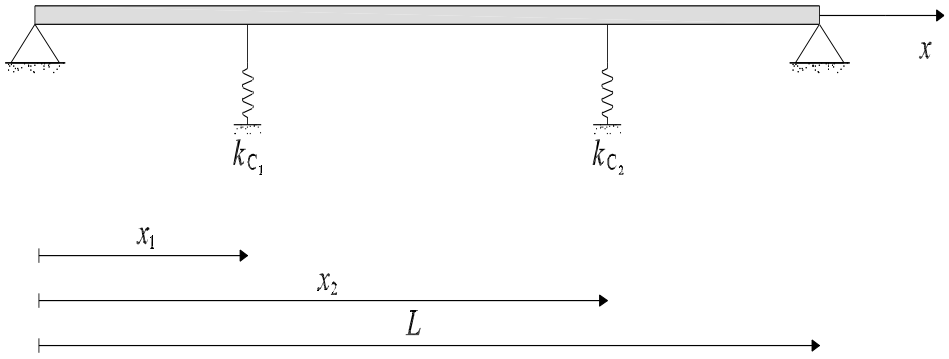

Figure 5.14: Corresponding linear beam associated with the non-linear beam in Figure 5.13.

The cross-statistics which depend on cubic stiffness nonlinearities can be easily expressed as functions of second-order statistics (see Eqs.(5.23)-(5.24)-(5.25)-(5.26)). By starting from an initial value of the n-th equivalent frequency equal to the n-th natural frequency of the linear beam shown in Figure 5.14, i.e. $\omega_{eq,n} = \omega_n$, a number of iterations from 6 to 10, as the nonlinearity selected in the application increases, are needed to obtain a convergent solution with a tolerance $\epsilon < 10^{-5}$. Figure 5.16 (a), (b), (c), (d) shows for increasing values of $\epsilon = \epsilon_1 = \epsilon_2$, (a) $\epsilon = 10^2\,\mathrm{N/m^3}$, (b) $\epsilon = 2 \cdot 10^2\,\mathrm{N/m^3}$, (c) $\epsilon = 5 \cdot 10^2\,\mathrm{N/m^3}$, (d) $\epsilon = 10^3\,\mathrm{N/m^3}$, the stationary variance σ_v^2 of the beam deflection $v(x,t)$ along the whole domain ($0 \leq x \leq L$). Black continuous lines represent the statistical linearization results and black dotted lines the Monte Carlo simulations data, obtained by employing 5000 samples and dividing the beam in 24 elements ($\Delta x = 0.5\,\mathrm{m}$); the dashed black line represents the response for $\epsilon = 0$. In addition, gray continuous lines represent the response of the beam without any source of non-linearity (i.e. $N = 0$, $\epsilon = 0$), in order to quantify the impact of non-linear effects on the system response. In Figure 5.16, it can be seen that results obtained by the statistical linearization approach exhibit satisfactory accuracy, which (as anticipated) decreases as the non-linearity degree increases. Nevertheless, even for strong nonlinearity cases, such as in Figure 5.16 (d) where the response variance is

almost one third that of the corresponding linear beam, the maximum percentage error as compared to Monte Carlo simulations data is approximately only 15%.

Next, for fixed values of $\epsilon = 2 \cdot 10^2\,\mathrm{N/m}^3$ and $S_0 = 2 \cdot 10^2\,\mathrm{N}^2\mathrm{s}$, the values of k_{C_1} and k_{C_2} are varied. Figure 5.17 (a), (b), (c), (d) shows the stationary variance σ_v^2 of the beam deflection $v(x,t)$ along the domain $0 \leq x \leq L$ for increasing values of $k = k_{C_1} = k_{C_2}$, namely (a) $k = 2 \cdot 10^5\,\mathrm{N/m}$, (b) $k = 5 \cdot 10^5\,\mathrm{N/m}$, (c) $k = 10^6\,\mathrm{N/m}$ and (d) $k = 10^{10}\,\mathrm{N/m}$. The continuous, dotted, gray and dashed lines have the same representation as in Figure 5.16; the gray continuous line still represents the variance of the linear beam, but with changing values of k. Clearly, for an increasing value of k, the beam becomes stiffer and exhibits a more linear behavior under the same excitation magnitude. Thus, the statistical linearization accuracy increases as well. The limiting case of a very large stiffness coefficient value corresponds to two rigid supports at the locations x_1 and x_2. As seen in Fig.5.17 (d), for this case the solution obtained by statistical linearization coincides with the available exact solution for the linear beam.

For completeness, Figure 5.18 (b), (c), (b*), (c*) compares the same results previously shown in Figure 5.17 (b), (c) with those obtained by performing statistical linearization with the unconstrained modes, i.e. the modes of the beam without any kind of supports. Specifically, Figures 5.18 (b), (c) refers to constrained modes, while Figures 5.18 (b*), (c*) refers to unconstrained ones; an equal number of modes are used for both sets, i.e. $M = 3$. Figure 5.18 clearly shows that using unconstrained modes does not lead to satisfactory results, especially as k increases. This result is somewhat anticipated (as explained in the Section "Considerations and Remarks") as the constrained-mode shear force exhibits jump discontinuities at the application points of supports, while the unconstrained-mode shear force is continuous over the whole beam axis, as a result of the infinitely differentiable unconstrained modes. Furthermore, constrained mode shapes progressively become very different as compared to the unconstrained ones as the stiffness of the

supports k increases; consequently, results obtained by using unconstrained modes become less and less accurate.

L	$12\,\mathrm{m}$
A	$0.004275\,\mathrm{m}^2$
EI	$3.05 \cdot 10^6\,\mathrm{Nm}^2$
m	$33.13\,\mathrm{kg/m}$
c	$92.85\,\mathrm{kg/ms}$

Table 5.2: Beam properties.

	$k = 10^5$		$k = 2 \cdot 10^5$		$k = 5 \cdot 10^5$		$k = 10^6$	
Mode	C. M.	P. M.	C.M.	P.M.	C.M.	P.M.	C.M.	P.M.
1	33.5233	33.5236	42.5235	42.5232	61.7784	61.7781	83.7422	83.7421
2	88.1225	88.1222	92.7854	92.7853	105.258	105.256	122.435	122.437
3	187.161	187.163	187.274	187.272	187.615	187.612	188.263	188.261

Table 5.3: Natural frequencies of beam in Figure 5.14 for different values of k.

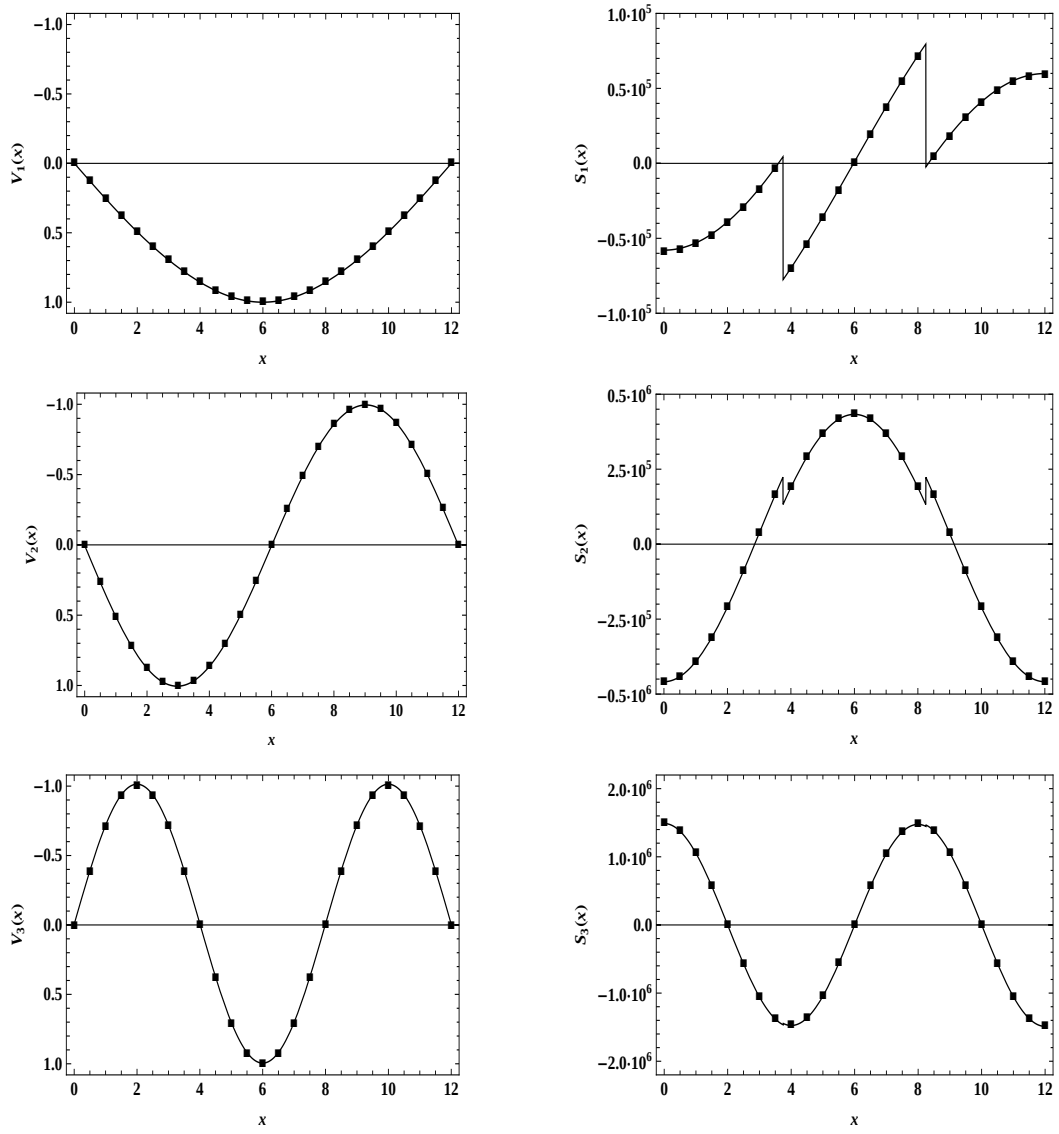

Figure 5.15: Beam in Figure 5.14, eigenfunctions of first 3 modes (from top to bottom): pure bending deflection (left column), and shear force (right column) computed by the generalized function approach (—) and the standard approach (∎).

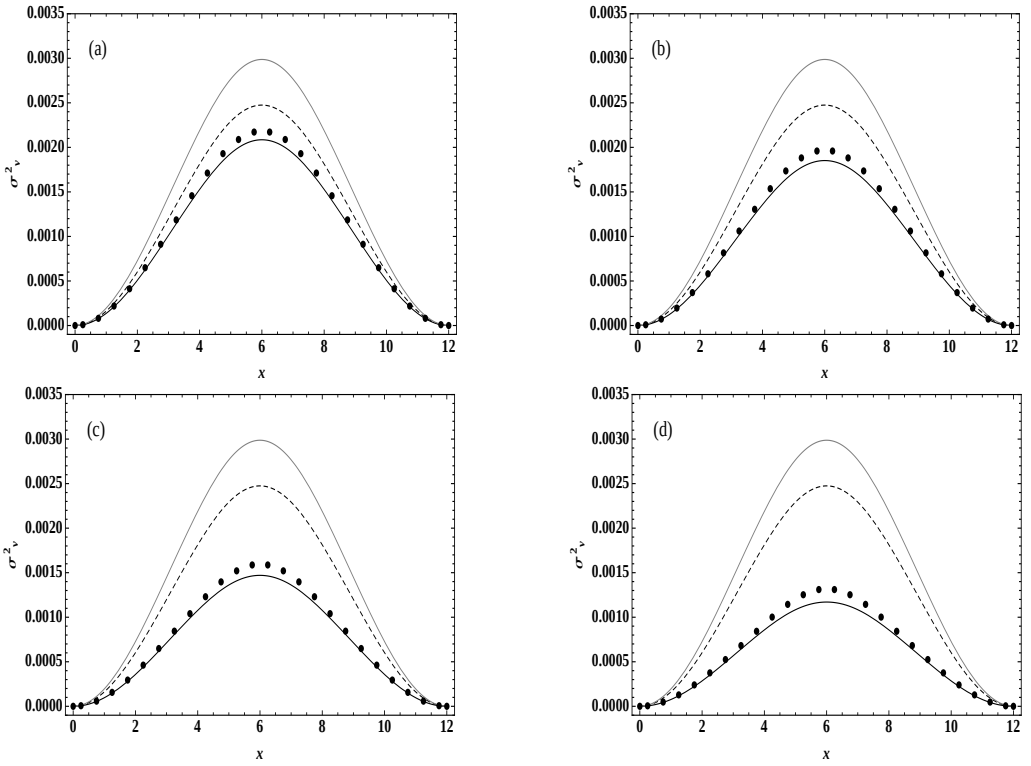

Figure 5.16: Beam in Figure 5.13: variance of beam displacement computed along $[0, L]$ for $\epsilon = 0$, $N = 0$ (—); for $\epsilon = 0$ (- - -); for various values of ϵ, (a) $\epsilon = 10^2\,\mathrm{N/m^3}$, (b) $\epsilon = 2 \cdot 10^2\,\mathrm{N/m^3}$, (c) $\epsilon = 5 \cdot 10^2\,\mathrm{N/m^3}$, (d) $\epsilon = 10^3\,\mathrm{N/m^3}$, statistical linearization (—), Monte Carlo (•).

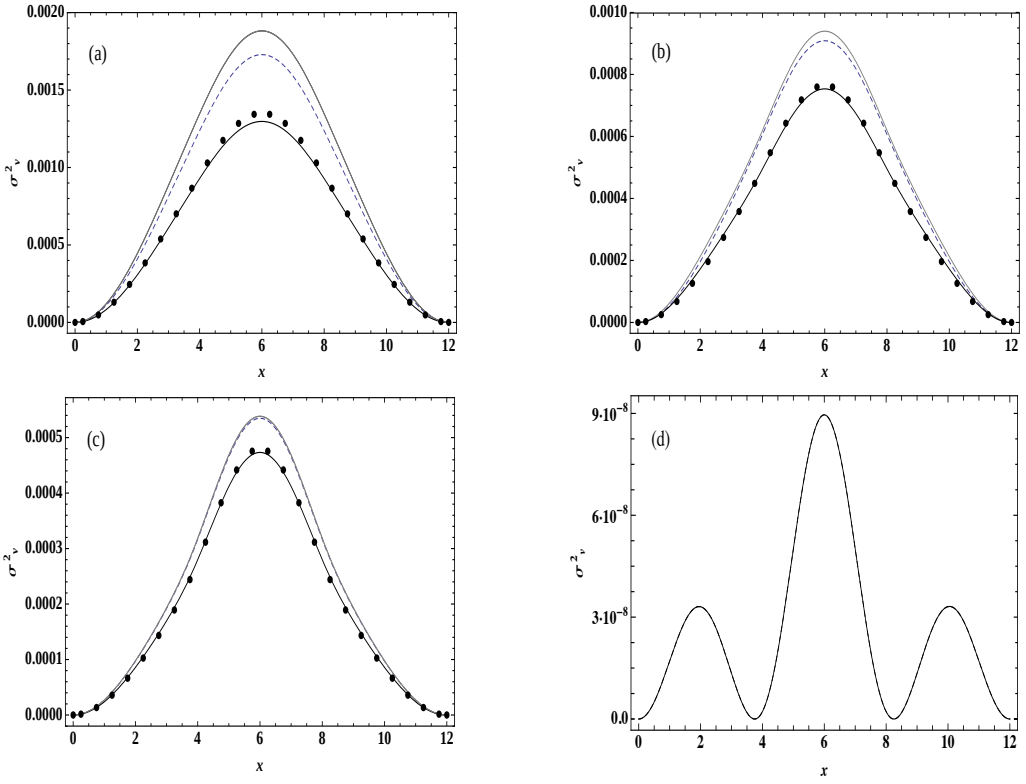

Figure 5.17: Beam in Figure 5.13: variance of beam displacement computed along $[0, L]$ for $\epsilon = 0$, $N = 0$ (—); for $\epsilon = 0$ (- - -); for various values of k, (a) $k = 2 \cdot 10^5\,\mathrm{N/m}$, (b) $k = 5 \cdot 10^5\,\mathrm{N/m}$, (c) $k = 10^6\,\mathrm{N/m}$, (d) $k = 10^{10}\,\mathrm{N/m}$, statistical linearization (—), Monte Carlo (•).

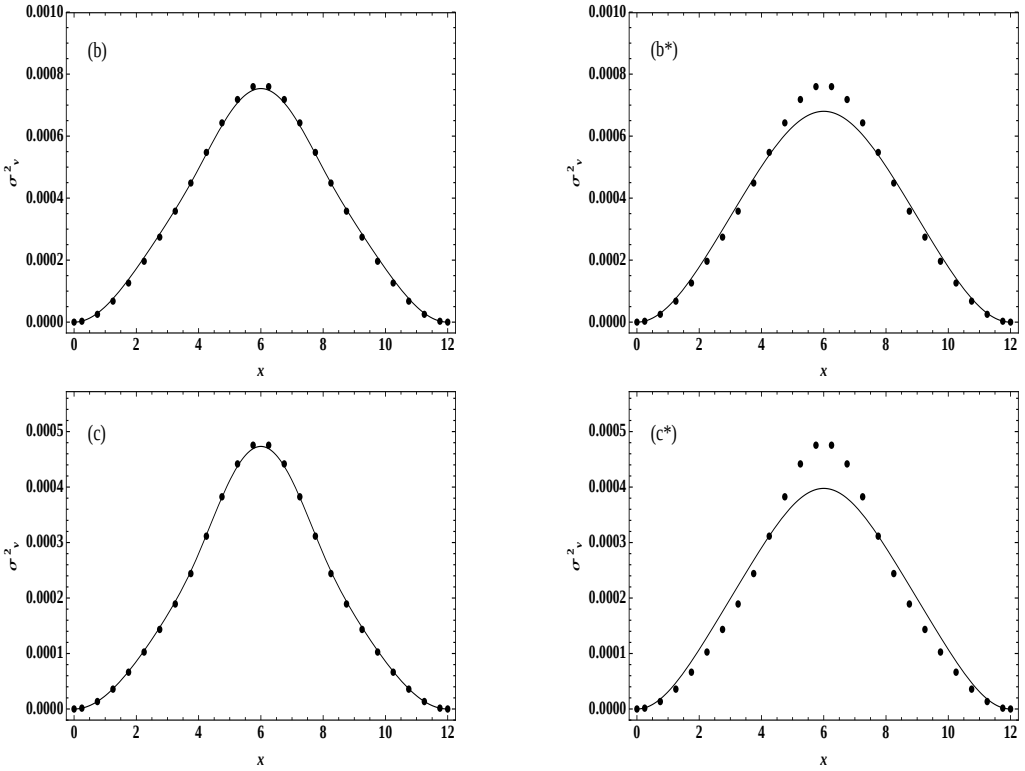

Figure 5.18: Beam in Figure 5.13: variance of beam displacement computed along $[0, L]$ using constrained modes (b), (c) and unconstrained modes (b*), (c*) for two values of k, (b)-(b*) $k = 5 \cdot 10^5\,\mathrm{N/m}$, (c)-(c*) $k = 10^6\,\mathrm{N/m}$, statistical linearization (—), Monte Carlo (•).

Example B: Bilinear stiffness nonlinearities

Consider the clamped-clamped beam depicted in Figure 5.19, resting on two supports with bilinear stiffness nonlinearities at locations $x_1 = 3.25\,\mathrm{m}$ and $x_2 = 8.75\,\mathrm{m}$. In this case, Eq.(5.9) takes the specific form

$$\begin{aligned} F_r = {} & k_{B_r}^{(1)} v(x_r,t) + (k_{B_r}^{(2)} - k_{B_r}^{(1)})\{(v(x_r,t) - \beta_r)U(v(x_r,t) - \beta_r) \\ & + (v(x_r,t) + \beta_r)U(-v(x_r,t) - \beta_r)\} \end{aligned} \tag{5.43}$$

The beam is excited by white noise uniformly distributed with $f(x) = 1$ and PSD S_0. The values for the beam properties are the same as in Example A, while the parameters of the two bilinear stiffness supports at locations x_1 and x_2 are denoted as $k_{B_1}^{(1)}$, $k_{B_1}^{(2)}$, β_1 and $k_{B_2}^{(1)}$, $k_{B_2}^{(2)}$, β_2, respectively.

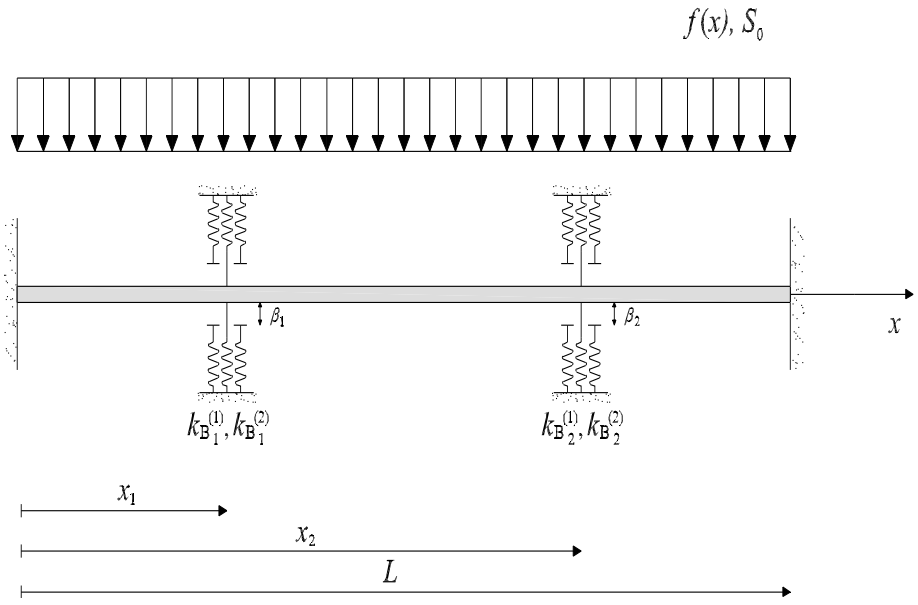

Figure 5.19: Clamped-clamped non-linear beam resting on two non-linear supports with bilinear stiffness nonlinearities.

In a similar manner as in example A, the corresponding linear beam shown in Figure 5.20 with $k_{B_1}^{(1)} = k_{B_1}^{(2)}$, $k_{B_2}^{(1)} = k_{B_2}^{(2)}$ and $N = 0$ is considered next for performing a modal analysis (see Chapter 3) and for deriving the first 3 natural frequencies. These are reported in Table 5.4 for various values of

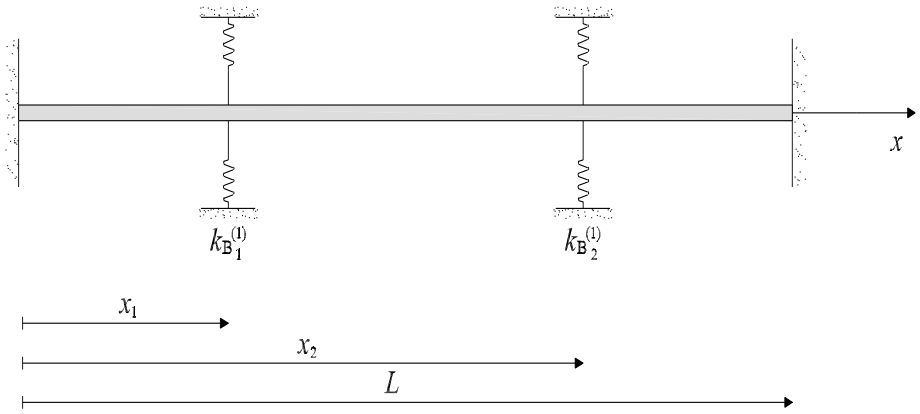

Figure 5.20: Corresponding linear beam associated with the non-linear beam in Figure 5.19.

the stiffness $k_B^{(1)} = k_{B_1}^{(1)} = k_{B_2}^{(1)}$, while the corresponding modes are shown in Figure 5.21 for $k_B^{(1)} = 10^5\,\mathrm{N/m}$. The procedure developed by Failla [21] and standard approach provide coincident results. The eigenfunctions determined according to the procedure by Failla [21] and described in Chapter 3 inherently account for shear-force discontinuities at support locations thanks to the use of generalized functions. They are used next for the statistical linearization solution approach.

Focusing on the non-linear beam shown in Figure 5.19 with the parameter values $S_0 = 2 \cdot 10^2\,\mathrm{N^2s}$, $k_B^{(1)} = k_{B_1}^{(1)} = k_{B_2}^{(1)} = 10^5\,\mathrm{N/m}$ and $\beta = \beta_1 = \beta_2 = 0.005\,\mathrm{m}$. The response of the beam is represented via Eq.(5.12) by using the first three eigenfunctions, while applying the error minimization equation (5.18), Eq.(5.19) takes the form

$$\omega_{eq,n}^2 = \omega_n^2 - \frac{EA}{2Lm\mu_{nn}} \frac{1}{E\Big[y_n^2\Big]} \sum_{m=1}^{\infty}\sum_{i=1}^{\infty}\sum_{j=1}^{\infty} K_{ij}R_{mn}E\Big[y_n y_m y_i y_j\Big] + \sum_{r=1}^{2}\Bigg\{\frac{(k_{B_r}^{(2)} - k_{B_r}^{(1)})V_n(x_r)}{m\mu_{nn}E\Big[y_n^2\Big]}\Bigg(E\Big[\Big(\sum_{j=1}^{\infty}V_j(x_r)y_j - \beta_r\Big)U\Big(\sum_{j=1}^{\infty}V_j(x_r)y_j - \beta_r\Big)y_n\Big] + E\Big[\Big(\sum_{j=1}^{\infty}V_j(x_r)y_j + \beta_r\Big)U\Big(-\sum_{j=1}^{\infty}V_j(x_r)y_j - \beta_r\Big)y_n\Big]\Bigg)\Bigg\} \tag{5.44}$$

The expectations which depend on the bilinear stiffness nonlinearities can be computed as follows. Denote $a_r = \sum_{k=1}^{\infty} V_k(x_r) y_k - \beta_r$; it follows that

$$\mu_{a_r} = E[a_r] = -\beta_r \tag{5.45}$$

$$\mu_{y_n} = E[y_n] = 0 \tag{5.46}$$

$$\sigma_{a_r}^2 = E[a_r^2] - E^2[a_r] = \sum_{k=1}^{\infty}\sum_{j=1}^{\infty} V_k(x_r) V_j(x_r) E[y_k y_j] \tag{5.47}$$

$$\sigma_{y_n}^2 = E[y_n^2] - E^2[y_n] = E[y_n^2] \tag{5.48}$$

$$\rho_{a_r y_n} = \frac{\sigma_{a_r y_n}}{\sigma_{a_r}\sigma_{y_n}} = \frac{E[a_r y_n] - E[a_r]E[y_n]}{\sigma_{a_r}\sigma_{y_n}} \tag{5.49}$$

Further, the expectation in the last term of Eq.(5.44) can be computed as

$$\begin{aligned} E\Big[a_r U[a_r] y_n\Big] &= \int_0^{\infty}\int_{-\infty}^{\infty} a_r y_n p_{a_r y_n}(a_r, y_n) da_r dy_n \\ &= \frac{1}{2}\rho_{a_r y_n}|\sigma_{y_n}|\left(|\sigma_{a_r}| + \sigma_{a_r}\mathrm{Erf}\left[\frac{\mu_{a_r}}{\sqrt{2}\sigma_{a_r}}\right]\right) \end{aligned} \tag{5.50}$$

with $p_{a_r y_n}(a_r, y_n)$ being the joint Gaussian probability density function of a_r and y_n [107]. In a similar manner, denoting $b_r = -\sum_{k=1}^{\infty} V_k(x_r) y_k - \beta_r$, also the joint probability density function $p_{b_r y_n}$ will be Gaussian with

$$\mu_{b_r} = \mu_{a_r}; \quad \sigma_{b_r} = \sigma_{a_r}; \quad \rho_{b_r y_n} = -\rho_{a_r y_n} \tag{5.51}$$

It follows that

$$E\Big[b_r U[b_r] y_n\Big] = -E\Big[a_r U[a_r] y_n\Big] = -\frac{1}{2}\rho_{a_r y_n}|\sigma_{y_n}|\left(|\sigma_{a_r}| + \sigma_{a_r}\mathrm{Erf}\left[\frac{\mu_{a_r}}{\sqrt{2}\sigma_{a_r}}\right]\right) \tag{5.52}$$

Note that all the expectations depending on bilinear stiffness nonlinearities

(5.50)-(5.52) are expressed as functions of second-order statistics and, consequently, the statistical linearization solution approach can be readily applied. By starting from an initial value of the n-th equivalent frequency equal to the n-th natural frequency of the linear beam shown in Figure 5.20, i.e. $\omega_{eq,n} = \omega_n$, a number of iterations from 6 to 10, as the nonlinearity selected in the application increases, are needed to obtain a convergent solution with a tolerance $\epsilon < 10^{-5}$.

The performance of statistical linearization is assessed for increasing value of $k_B^{(2)} = k_{B_1}^{(2)} = k_{B_2}^{(2)}$. In this regard, Figure 5.22 (a), (b), (c), (d) shows the stationary variance σ_v of the beam deflection $v(x,t)$ along the whole domain ($0 \leq x \leq L$), for (a) $k_B^{(2)} = 2 \cdot k_B^{(1)}$, (b) $k_B^{(2)} = 3 \cdot k_B^{(1)}$, (c) $k_B^{(2)} = 4 \cdot k_B^{(1)}$, (d) $k_B^{(2)} = 5 \cdot k_B^{(1)}$. As in Example A, black continuous lines represent the statistical linearization results, black dotted lines the Monte Carlo simulation data obtained by employing 5000 samples and dividing the beam in 24 elements ($\Delta_x = 0.5\,\mathrm{m}$); and the dashed black line represents the response for $k_B^{(1)} = k_B^{(2)}$. In addition, gray continuous lines represent the response of the beam without any source of non-linearity (i.e. $k_B^{(1)} = k_B^{(2)}$ and $N = 0$), in order to quantify the nonlinearity degree and its impact on the beam response. It can be readily seen in Figure 5.22 that statistical linearization exhibits, in general, satisfactory accuracy, even for a relatively high non-linearity degree.

Finally, assuming that the value of $k_B^{(2)}$ is fixed at $k_B^{(2)} = 10^6\,\mathrm{N/m}$, further comparisons are included between statistical linearization solutions considering constrained modes and unconstrained modes, for various values of $k_B^{(1)}$, (a)-(a*) $k_B^{(1)} = 1/4 \cdot k_B^{(2)}$, (b)-(b*) $k_B^{(1)} = 4/5 \cdot k_B^{(2)}$. Figure 5.23 (a), (b), (a*), (b*) shows the variance σ_v^2 obtained by using both sets of modes. Specifically, Figures 5.23 (a), (b) refer to constrained modes, while Figures 5.23 (a*), (b*) refer to unconstrained ones. The same number of modes, $M = 3$, are selected for both sets. Figure 5.23 clearly shows, as in Example A, that unconstrained modes are not able to capture the beam response variance as well as the constrained ones, especially as the stiffness $k_B^{(1)}$ increases.

	$k_B^{(1)} = 10^5$		$k_B^{(1)} = 2 \cdot 10^5$		$k_B^{(1)} = 5 \cdot 10^5$		$k_B^{(1)} = 10^6$	
Mode	C. M.	P. M.	C.M.	P.M.	C.M.	P.M.	C.M.	P.M.
1	53.6736	53.6734	59.435	59.436	73.7113	73.7116	91.7611	91.7612
2	134.091	134.093	138.162	138.162	149.593	149.595	166.585	166.581
3	255.097	255.096	255.588	255.588	257.104	257.101	259.743	259.741

Table 5.4: Natural frequencies of beam in Figure 5.20 for different values of $k_B^{(1)}$.

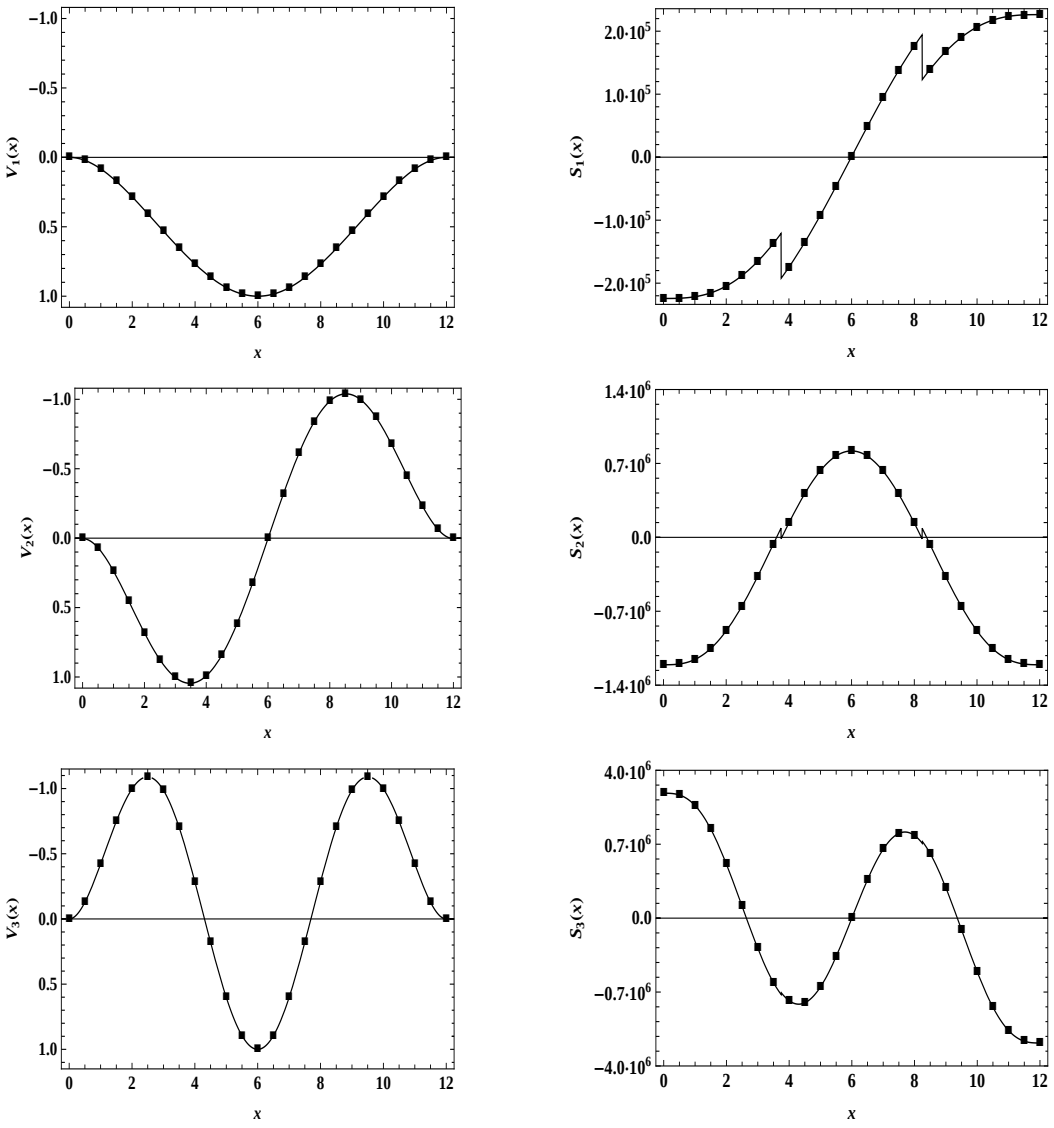

Figure 5.21: Beam in Figure 5.20, eigenfunctions of first 3 modes (from top to bottom): pure bending deflection (left column), and shear force (right column) computed by the generalized functions approach (—) and the standard approach (■).

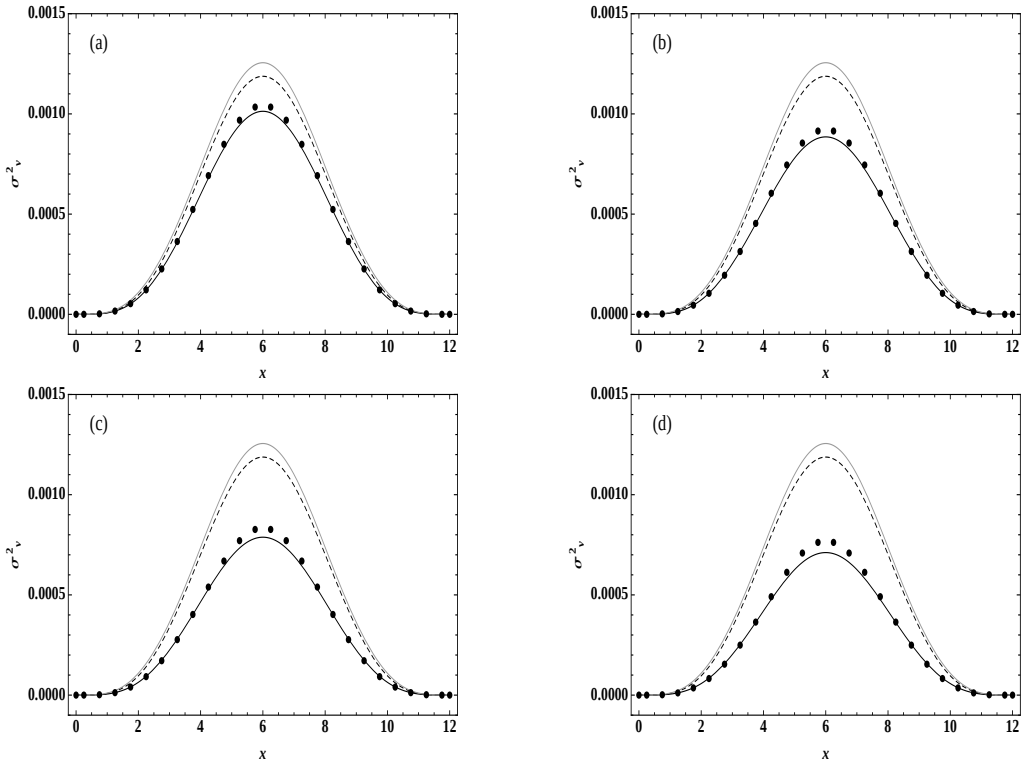

Figure 5.22: Beam in Figure 5.19: variance of beam displacement computed along $[0, L]$ for $k_B^{(1)} = k_B^{(2)}$, $N = 0$ (—); for $k_B^{(1)} = k_B^{(2)}$ (- - -); for various values of $k_B^{(2)}$, (a) $k_B^{(2)} = 2 \cdot k_B^{(1)}$, (b) $k_B^{(2)} = 3 \cdot k_B^{(1)}$, (c) $k_B^{(2)} = 4 \cdot k_B^{(1)}$, (d) $k_B^{(2)} = 5 \cdot k_B^{(1)}$, statistical linearization (—), Monte Carlo (•).

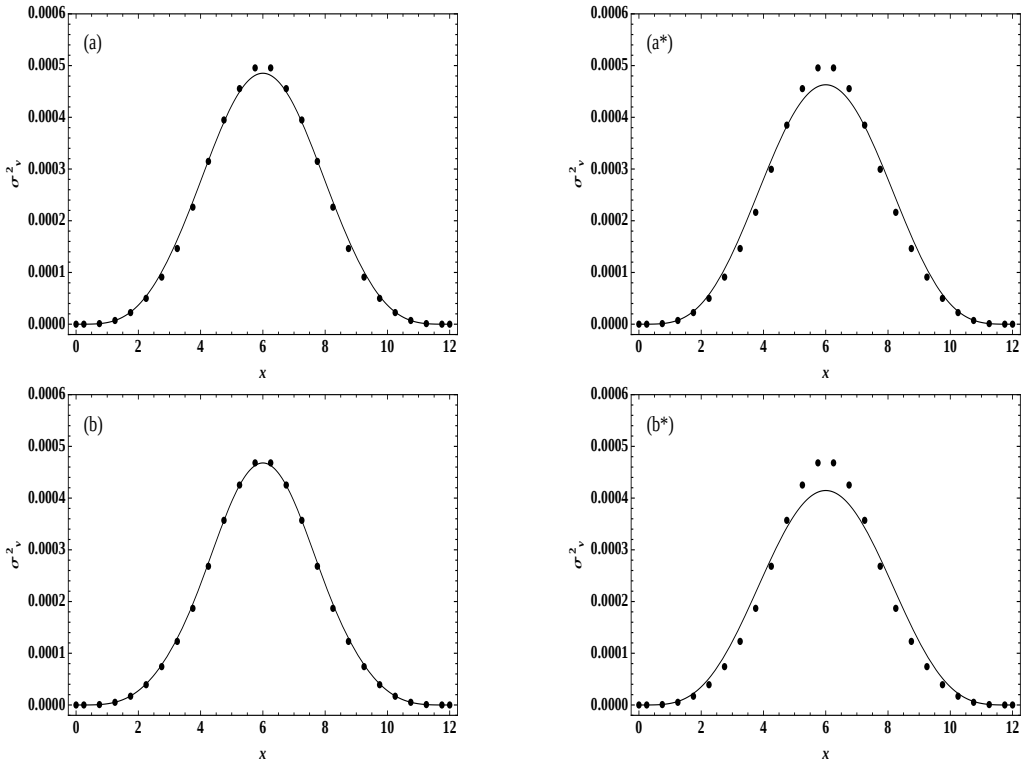

Figure 5.23: Beam in Figure 5.19: variance of beam displacement computed along $[0, L]$ using constrained modes (a), (b) and unconstrained modes (a*), (b*) for two values of $k_B^{(1)}$, (a)-(a*) $k_B^{(1)} = 1/2 \cdot k_B^{(2)}$, (b)-(b*) $k_B^{(1)} = 4/5 \cdot k_B^{(2)}$, statistical linearization (—), Monte Carlo (•).

Chapter 6

Concluding Remarks

In this thesis, an innovative and efficient approach, based on generalised functions, has been proposed for evaluating the deterministic and stochastic response of coupled continuous-discrete systems (CCDS). Specifically, attention has been focused on structural and mechanical systems. Indeed, the primary structures/systems considered are mono-dimensional elements as beams, columns and their 2-D assembly (plane frames). The discrete elements considered, to be coupled with the primary structure/system, are control devices as dampers, tuned mass dampers, spring-mass-systems; stiffeners as springs/supports, transversal ribs; additional attached masses; rotational/translational springs or dampers modeling a crack or a damage.

In Chapter 3, the proposed approach is developed for deterministic excitations acting on CCDS. Firstly, uncoupled flexural and axial vibrations of discontinuous beams with symmetric cross section are investigated; afterwards, the approach is extended to beams with mono symmetric and asymmetric cross section, which show coupled bending-torsional vibrations, and to flexural vibrations of composite beams. Specifically, it is shown that the dynamic Green's functions of the bare beam, i.e. the beam without discrete elements, can be used and combined to build exact closed form expressions of the frequency response of the CCDS to point/polynomial load. This involves 2 or 4 or 6 or 8 or 10 or 12 integration constants only (notice that the number

of integration constants depend on the beam and vibration problem considered), regardless of the number of dampers/discrete elements. This is the basis to obtain: a) for a single beam, the exact frequency response function (FRF) once enforcing the boundary conditions, and (in Chapter 4) the exact dynamic stiffness matrix (DSM) and load vector (LV); b) for a plane frame consisting of an assembly of beams with symmetric cross section, the exact global DSM and LV by a finite element assembling procedure and the corresponding exact FRF by inverting the global DSM (in Chapter 4); from the nodal displacement solution, exact FRFs are derived in every frame member in a closed form. The size of the FRM and LV depends only on the number of beam-to-columns nodes, regardless of the number of point/polynomial loads and dampers along the frame members. All the closed form expressions are inherently able to satisfy all the required condition at the discrete elements and point loads locations, capturing jump and slope discontinuities of response variables; further, the analytical form is easy to implement in any symbolic package, and can readily be computed for any frequency of interest, parameters of dampers (location, stiffness, damping), position of the loads, regardless of the number of dampers and positions of the dampers relative to the loads.

Next, since for generality the damping in beams is not proportional due to concentrated dampers, a novel complex modal analysis approach is led to obtain the modal impulse response function, to be used for time domain analysis. While, for plane frames coupled with mass-spring sub-systems (i.e. without concentrated dampers), a novel classical exact modal analysis is developed to perform time domain analysis.

In Chapter 5, the proposed approach is extended to stochastic excitations. Particularly, the exact stationary response is computed using the exact FRF for a single beam computed in Chapter 3, and the exact frequency response matrix (FRM) and LV for a plane frame computed in Chapter 4. Next, exploiting closed form expressions for modal impulse response functions, the response to non-stationary loads is computed for beams and frames via an

efficient Monte Carlo simulations.

Finally, a solution method is proposed to compute the stationary response of single beams with symmetric cross section coupled with nonlinear in-span supports; a distributed non-linearity is considered also due to the assumption of relatively large beam displacement. A significant novelty aspect of the developed approach is the utilization of the constrained modes, computed in Chapter 3, which involve appropriate generalized functions and can inherently account for shear-force discontinuities at the support locations.

Bibliography

[1] P. A. M. Dirac, *The Principle of Quantum Mechanics*, 3rd ed., Oxford: Oxford University Press, (1947).

[2] Mathematica. Version 8.0, Wolfram Research Inc., Champaign.

[3] W. H. Macaulay, *Note on the deflection of the beams*, Messenger of Mathematics, 48, pp. 129-130 (1919).

[4] R. J. Brungraber, *Singularity functions in the solution of beam-deflection problems*, Journal of Engineering Education (Mechanics Division Bulletin), 1.55 (9), pp. 278-280 (1965).

[5] R. P. Kanwal, *Generalized functions theory and applications*, Academic Press, New York (1983).

[6] A. Yavari, S. Sarkani, E. T. Moyer Jr, *On applications of generalized functions to beam bending problems*, International Journal of Solids and Structures, 37, pp. 5675-5705 (2000)

[7] G. Falsone, *The use of generalised functions in the discontinuous beam bending differential equation*, International Journal of Engineering Education, 18, 3, pp. 337-343 (2002).

[8] B. Biondi, S. Caddemi, *Closed form solutions of Euler-Bernoulli beams with singularities*, International Journal of Solids and Structures, 42, pp. 3027-3044 (2005).

[9] B. Biondi, S. Caddemi, *Euler-Bernoulli beams with mutiple singularities in the flexural stiffness*, European Journal of Solids and Structures, 42, pp. 3027-3044 (2005).

[10] A. Palmeri, A. Cicirello, *Physically-based Dirac's delta functions in the static analysis of multi-cracked Euler-Bernoulli and Timoshenko beams*, International Journal of Solids and Structures, 48, pp. 2184-2195 (2011).

[11] Failla G, Santini A, *On Euler-Bernoulli discontinuous beam solutions via uniform-beam Green's functions*, International journal of solids and structures, 44, pp. 7666-7687 (2007).

[12] E. I. Shifrin, R. Ruotolo, *Natural frequencies of a beam with an arbitrary number of cracks*, Journal of Sound and Vibration, 222, 3, pp. 409-423 (1999).

[13] J. Wang, P. Qiao, *Vibration of beams with arbitrary discontinuities and boundary conditions*, Journal of Sound and Vibration, 38, pp. 12-27 (2007).

[14] G. Failla, A. Santini, *A solution method for Euler-Bernoulli vibrating discontinuous beams*, Mechanics Research Communications, 35, pp. 517-529 (2008).

[15] L. Meirovitch, *Elements of Vibration Analysis*, McGraw-Hill, New York (1975).

[16] W.T. Thomson, *Theory of Vibration with Applications*, Prentice Hall, Englewood Cliffs, NJ (1988).

[17] S. Caddemi, I. Caliò, *Exact closed-form solution for the vibration modes of the Euler-Bernoulli beam with multiple open cracks*, Journal of Sound and Vibration, 327, pp. 473-489 (2009).

[18] S. Caddemi, I. Caliò, *The exact dynamic stiffness matrix of multi-cracked Euler-Bernoulli beam and applications to damaged frame structures*, Journal of Sound and Vibration 332, pp. 3049-3063 (2013).

[19] F. W. Williams, W.H. Wittrick, *An automatic computational procedure for calculating natural frequencies of skeletal structures*, International Journal of Mechanical Sciences, 12, pp. 781-791 (1970).

[20] G. Failla, *On the dynamics of viscoelastic discontinuous beams*, Mechanics Research Communications, 60, pp. 52-63 (2014).

[21] G. Failla, *An exact generalised function approach to frequency response analysis of beams and plane frames with the inclusion of viscoelastic damping*, Journal of Sound and Vibration, 360, pp. 171-202 (2016).

[22] G. Failla, *Stationary Response of Beams and Frames with Fractional Dampers through Exact Frequency Response Functions*, Journal of Engineering Mechanics, 143, 5 (2017).

[23] G. Failla, *An exact modal analysis approach to vibration analysis of structures with mass-spring subsystems and rotational joints*, Journal of Sound and Vibrations, 430, pp. 191-219 (2019).

[24] R. Ruotolo, C. Surace, *Natural frequencies of a bar with multiple cracks*, Journal of Sound and Vibration, 272, 301-316 (2004).

[25] N. T. Khiem, T. V. Lien, *A simplified method for natural frequency analysis of a multiple cracked beam*, Journal of Sound and Vibration 245 (4), pp. 737-751 (2001).

[26] Q. S. Li, *Free vibration analysis of non-uniform beams with an arbitrary number of cracks and concentrated masses*, Journal of Sound and Vibration 272, pp. 301-316 (2004).

[27] S. Sorrentino, S. Marchesiello, B. A. D. Piombo, *A new analytical technique for vibration analysis of non-proportionally damped beams*, Journal of Sound and Vibration, 265, pp. 765-782 (2003).

[28] S. Sorrentino, A. Fasana, S. Marchesiello, *Analysis of non-homogeneous Timoshenko beams with generalized damping distirbutions*, Journal of Sound and Vibration, 304, pp. 779-792 (2007).

[29] S. W. Hong, J. W. Kim, *Modal analysis of mulit-span Timoshenko beams connected or supported by resilient joints with damping*, Jounral of Sound and Vibration, 227, (4), pp. 787-806.

[30] H. B. Tang, C.J. Wu, X.Q. Huang, *Vibration analysis for a coupled beam-sdof system by using the recurrence equation method*, Journal of Sound and Vibration 311, pp. 912-923 (2008).

[31] J. S. Wu, D. W. Chen, *Dynamic analysis of a uniform cantilever beam carrying a number of elastically mounted point masses with dampers*, Journal of Sound and Vibration 229, (3) pp. 549-578 (2000).

[32] M. Gurgoze, H. Erol, *On the frequency response function of a damped cantilever simply supported in-span and carrying a tip mass*, Journal of Sound and Vibration, 225, (3), pp. 489-500 (2002).

[33] M. Gürgöze, H. Erol, *Dynamic response of a viscously damped cantilever with a viscous end condition*, Journal of Sound and Vibration 298 pp. 132-153 (2006).

[34] A. Burlon, G. Failla, F. Arena, *Exact frequency response analysis of axially loaded beams with viscoelastic dampers*, Inter-

national Journal of Mechanical Sciences, 115-116, pp. 370-384 (2016).

[35] A. Burlon, G. Failla, F. Arena, *Coupled bending and torsional free vibrations of beams with in-span supports and attached masses*, European Journal of Mechanics, A/Solids, n. 66, pp. 387-411 (2017).

[36] Di Lorenzo, S., Adam, C., Burlon, A., Failla, G., Pirrotta, A., *Flexural vibrations of discontinuous layered elastically bonded beams*, Composites Part B: Engineering, 137, pp. 102-111 (2018).

[37] A. Burlon, G. Failla, F. Arena, *Coupled bending-torsional frequency response of beams with attachments: exact solutions including warping effects*, Acta Mechanica 229, pp. 2445-2475 (2018).

[38] Burlon A, G. Failla G, Arena F, *Exact stochastic analysis of coupled bending-torsion beams with in-span supports and masses*, Probabilistic engineering mechanics, 54, pp. 53-64 (2018).

[39] Burlon A, G. Failla, Arena F, *Exact frequency response of two-node coupled bending-torsional beam element with attachments*, Applied mathematical modelling, pp. 508-537, (2018).

[40] Burlon A, I. Kougioumtzoglou, G. Failla, F. Arena, *Nonlinear random vibrations of beams with in-span supports via statistical linearization with constrained modes*, Journal of Engineering Mechanics, (Article in press).

[41] W. D. Pilkey, *Some properties and applications of singularity functions based on the theory of distributions*, Journal of the Franklin Institute 277, 5, pp. 464-497 (1964).

[42] G. Oliveto, A. Santini, E. Tripodi. *Complex modal analysis of a flexural vibrating beam with viscous end conditions*, Journal of Sound and Vibration 200, (3), pp. 327-345 (1997).

[43] E. Veletsos, C.E. Ventura, *Modal analysis of non-classically damped linear systems*, Earthquake Engineering and Structural Dynamics, 14, pp. 217-243 (1986).

[44] S. Caddemi, I. Caliò, F. Cannizzaro, *Influence of anelastic end support on the dynamic stability of Beck's column with multiple weak sections*, International Journal of Non-Linear Mechanics, 69, pp.14-28 (2015).

[45] P. O. Friberg, *Coupled vibrations of beams-an exact dynamic element stiffness matrix*, International Journal of Numerical Methods in Engineering, 19, pp. 479-493 (1983).

[46] E. Dokumaci, *An exact solution for coupled bending and torsion vibrations of uniform beam having single cross sectional symmetry.* Journal of Sound and Vibration 119, (3), pp. 443-449 (1987).

[47] W. L. Hallauer, R. Y. L. Liu, *Beam bending-torsion dynamic stiffness method for calculation of exact vibrations modes*, Journal of Sound and Vibration, 85, (1), pp. 105-113 (1982).

[48] J. R. Banerjee, *Coupled bending-torsional dynamic stiffness matrix for beam elements*, International Journal of Numerical Methods in Engineering, 28, pp. 1283-1298 (1989).

[49] J. R. Banerjee, *Explicit frequency equation and mode shapes of a cantilever beam coupled in bending and torsion*, Journal of Sound and Vibration, 224, (2), pp. 267-281 (1999).

[50] S. M. Hashemi, M. J. Richard, *A Dynamic Finite Element (DFE) method for free vibrations of bending-torsion coupled beams*, Aerospace Science and Technology, 4, pp. 41-55 (2000).

[51] S. H. R. Eslimy-Isfahany, J. R. Banerjee, *Use of generalized mass in the interpretation of dynamic response of bending-torsion coupled beams*, Journal of Sound and Vibration, 238, (2), pp. 295-308 (2000).

[52] S. H. R. Eslimy-Isfahany, J. R. Banerjee, A. J. Sobey, *Response of a bending-torsion coupled beam to deterministic and random loads*, Journal of Sound and Vibration, 195, (2), pp. 267-283 (1996).

[53] S. Timoshenko, D. H. Young, W. J. R. Weaver, *Vibrations Problems in Engineering*, Wiley, New York, (1974).

[54] R.E.D. Bishop, S. M. Cannon, S. Miao, *On coupled bending and torsional vibration of uniform beams*, Journal of Sound and Vibration, 131, pp. 457-464 (1989).

[55] A. N. Bercin, M. Tanaka, *Coupled flexural-torsional vibrations of Timoshenko beams*, Journal of Sound and Vibration, 207, (1) pp. 47-59 (1997).

[56] M. Tanaka, A. N. Bercin, *Finite element modeling of the coupled bending and torsional free vibration of uniform beams with an arbitrary cross-section*, Applied Mathematical Modeling, 21, (6), pp. 339-344 (1997).

[57] J. R. Banerjee, S. Guo, W. P. Howson, *Exact dynamic stiffness matrix of a bending-torsion coupled beam including warping*, Computers & Structures, 59, pp. 613-621 (1996).

[58] J. R. Banerjee, F. W. Williams, *Coupled bending torsional dynamic stiffness matrix of an axially loaded Timoshenko beam*

element, International Journal of Solids and Structures 6, pp. 749-762 (1994).

[59] M. S. Hashemi, M.J. Richard, *Free vibration analysis of axially loaded bending-torsion coupled beams: a dynamic finite element*, Computer & Structures, 77, pp. 711-724 (2000).

[60] L. Jun, L. Wanyou, S. Rongying, H. Hongxing, *Coupled bending and torsional vibration of nonsymmetrical axially loaded thin-walled Bernoulli-Euler beams*, Mechanics Research Communications, 31, pp. 697-711 (2004).

[61] L. Jun, L. Wanyou, S. Rongying, H. Hongxing, *Coupled bending and torsional vibration of axially loaded Bernoulli-Euler beams including warping effects*, Applied Acousics, 65 pp. 153-170 (2004).

[62] L. Jun, S. Rongying, H. Hongxing, J. Xianding, *Coupled bending and torsional vibration of axially loaded thin walled Timoshenko beams*, International Journal of Mechanical Sciences, 46, pp. 229-320.

[63] C. Adam, *Forced vibrations of elastic bending-torsion coupled beams*, Journal of Sound and Vibration, 221, (2), pp. 273-287 (1999).

[64] H. Han, D. Cao, L. Liu, *Green?s functions for forced vibration analysis of bending-torsion coupled Timoshenko beam*, Applied Mathematical Modeling, 45, pp. 621-635 (2017).

[65] E.J. Sapountzakis, G. C. Tsiatas, *Flexural-torsional vibrations of beams by BEM*, Computational Mechanics, 39, pp. 409-417 (2007).

[66] E. J. Sapountzakis, V. J. Mokos, *Dynamic analysis of 3-D beam elements including warping and shear deformation effects*, International Journal of Solids and Structures 43, pp. 6707-6726 (2006).

[67] E. J. Sapountzakis, J. A. Dourakopoulos, *Shear deformation effect in flexural-torsional vibrations of beams by BEM*, Acta Mechanica, 203, pp. 197-221 (2009).

[68] D. C. D. Oguamanam, *Free vibration of beams with finite mass rigid tip load and flexural-torsional coupling*, International Journal of Mechanical Sciences, 45, pp. 963-979 (2003).

[69] H. Gokdag, O. Kopmaz, *Coupled bending and torsional vibration of a beam with in span and tip attachments*, Journal of Sound and Vibration, 287 pp. 591-610 (2005).

[70] Y. R.Yang, L. C. Zhao, *Subharmonic bifurcation analysis of wing with store flutter*, Journal of Sound and Vibration, 157, (3), pp. 477-484 (1992).

[71] F. H. Gern, L. Librescu, *Effects of externally mounted stores and aerolasticity of advanced swept cantilevered aircraft wings*, Aerospace Science and Technology, 5, pp. 321-333 (1998).

[72] S. A. Fazelzadeh, A. Mazidi, H. Kalantari, *Bending-torsional flutter of wings with an attached mass subjected to a follower force*, Journal of Sound and Vibration, 323, pp. 148-162 (2009).

[73] P. Mardanpour, D. H. Hodges, R. Neuhart, N. Graybeal, *Engine placement effect on nonlinear trim and stability of flying wing aircraft*, Journal of Aircraft. 50, (6), pp. 1716-1725 (2013).

[74] P. Mardanpour, P. W. Richards, O. Nabipour, D. H. Hodges, *Effect of multiple engine placement on aerolastic trim and sta-*

bility of flying wing aircraft, Journal of Fluids and Structures, 44, pp. 67-86 (2014).

[75] J. M. Whitney, N. J. Pagano, *Shear deformation in heterogeneous anisotropic plates*, Journal of Applied Mechanics 37, pp. 1031-1036 (1970).

[76] A. Apuzzo, R. Barretta, R. Luciano, *Some analytical solutions of functionally graded Kirchhoff plates*, Composites Part B: Engineering 68, pp. 266-269 (2015).

[77] G. W. Swift, R. A. Heller, *Layered beam analysis*, Journal of the Engineering Mechanics Division, 100 pp. 267-282 (1974).

[78] R. Heuer, *Static and dynamic analysis of transversely isotropic*, moderately thick sandwich beams by analogy, Acta Mechanica 91 pp. 1-9 (1992).

[79] J. N. Reddy, *An evaluation of equivalent-single-layer and layer-wise theories of composite laminates*, Composite Structures 25 (1993) pp. 21-35.

[80] R. Barretta, R. Luciano, Analogies between Kirchhoff plates and functionally graded Saint-Venant beams under torsion, Continuum Mechanics and Thermodynamics, 27, (3) pp. 499-505 (2015).

[81] A. Pagani, Y. Yan, E. Carrera, *Exact solutions for static analysis of laminated, box and sandwich beams by refined layer-wise theory*, Composites Part B: Engineering 131 (Supplement C) pp. 62-75 (2017).

[82] V. Kahya, *Buckling analysis of laminated composite and sandwich beams by the finite element method*, Composites Part B: Engineering 91 (Supplement C) pp.126-134 (2016).

[83] M. Filippi, E. Carrera, *Bending and vibrations analyses of laminated beams by using a zig-zag-layer-wise theory*, Composites Part B: Engineering 98 (Supplement C) pp. 269-280 (2016).

[84] J. R. Goodman, E. P. Popov, *Layered beam systems with interlayer slip*, Journal of the Structural Division, 94, pp. 2535-2548 (1968).

[85] U. A. Girhammar, V. K. A. Gopu, *Composite beam-columns with interlayer slip-exact analysis*, Journal of Structural Engineering, 119, pp. 1265-1282 (1993).

[86] S. Simon, S. Miran, T. Goran, P. Igor, *Analytical solution of two-layer beam taking into account interlayer slip and shear deformation*, Journal of Structural Engineering, 116, pp. 886-894 (2007).

[87] S. Chonan, *Vibration and stability of sandwich beams with elastic bonding*, Journal of Sound and Vibration, 85, pp. 525-537 (1982).

[88] U. A. Girhammar, D. Pan, *Dynamic analysis of composite members with interlayer slip*, International Journal of Solids and Structures, 30, pp. 797-823 (1993).

[89] C. Adam, R. Heuer, A. Jeschko, *Flexural vibrations of elastic composite beams with interlayer slip*, Acta Mechanica, 125, pp. 17-30 (1997).

[90] S. W. Hansen, R. D. Spies, *Structural damping in laminated beams due to interfacial slip*, Journal of Sound and Vibration, 204, pp. 183-202, (1997).

[91] C. Adam, R. Heuer, A. Raue, F. Ziegler, *Thermally induced vibrations of composite beams with interlayer slip*, Journal of Thermal Stresses, 23, pp. 747-772 (2000).

[92] R. Heuer, C. Adam, *Piezoelectric vibrations of composite beams with interlayer slip*, Acta Mechanica ,140, pp. 247-263 (2000).

[93] M. Shinozuka, G. Deodatis, *Simulation of stochastic processes by spectral representation*, Applied Mechanics, 44, pp. 191-204 (1991).

[94] I. Elishakoff, S. H. Crandall, *Sixty years of stochastic linearization technique*, Meccanica, 52, (1-2), pp. 299-305 (2017)

[95] J. B. Roberts, P. D. Spanos, *Random vibration and statistical linearization*, Wiley, New York (1991).

[96] L. Socha, *Linearization methods for stochastic dynamic system*, Springer, Berlin (2008)

[97] P. D, Spanos, I. A. Kougioumtzoglou, *Harmonic wavelets based statistical linearization for response evolutionary power spectrum determination*, Probabilistic Engineering Mechanics 27, pp. 57-68 (2012).

[98] I. A. Kougioumtzoglou, *Stochastic joint time-frequency response analysis of nonlinear structural systems*, Journal of Sound and Vibrations, 332, pp. 7153-7173 (2013).

[99] I. A. Kougioumtzoglou, P. D. Spanos, *Harmonic wavelets based response evolutionary power spectrum determination of linear and nonlinear oscillators with fractional derivative elements*, International Journal of Non-Linear Mechanics 80, pp. 66-75 (2016)

[100] V. Fragkoulis, I. A. Kougioumtzoglou, A. Pantelous, *Statistical linearization of nonlinear structural systems with singular matrices*, Journal of Engineering Mechanics, 142 (9), pp. 1-11 (2016).

[101] I. A. Kougioumtzoglou, V. Fragkoulis, A. Pantelous, A. Pirrotta, *Random vibration of linear and nonlinear structural systems with singular matrices: A frequency domain approach*, Journal of Sound and Vibrations, 404, pp. 84-101 (2017).

[102] I. Petromichelakis, A. F. Psaros, I. A. Kougioumtzoglou, *Stochastic response determination and optimization of a class of nonlinear electromechanical energy harvesters: A Wiener path integral approach*, Probabilistic Engineering Mechanics, 53, 116-125 (2018)

[103] R. E. Herbert, *On the stresses in a nonlinear beam subject to random excitation*, International Journal of Solids and Structures, 1 (2), pp. 235-242. (1965).

[104] P. D. Spanos, G. Malara, (2014). *Nonlinear random vibrations of beams with fractional derivative elements*, Journal of Engineering Mechanics, 140, 9 (2014).

[105] P. Seide, *Nonlinear stresses and deflections of beams subjected to random time dependent uniform pressure*, Journal of Engineering for Industry, 98, pp. 1014-1020 (1975).

[106] J. T. Katsikadelis, G. C. Tsiatas, G. C. (2003). *Large deflection analysis of beams with variable stiffness*, Acta Mechanica, 164, pp. 1-13 (2003).

[107] J. Honerkamp, *Statistical Physics: An advanced approach with applications web-enhanced with problems and solutions*. Springer Science & Business Media (2013).

Appendix A

Analytical expressions of dynamic Green's functions of bare beams

A.1 Beams with symmetric cross section

The full set of Green's functions $\mathbf{G}^{(r)}(x, x_0)$ in Eq.(3.23), for $r = P, W, \Delta\Theta, \Delta V$, can be built starting from Eq.(3.37) for $G_V^{(P)}$, i.e. the deflection response to a point force $P = 1$ at $x = x_0$, using Eqs.(3.26)-(3.36).

Matrix $\mathbf{\Omega}$ in Eq.(3.23) contains the solutions of the homogeneous equations associated with Eqs.(3.19)-(3.22), and can easily be constructed as follows:

$$\begin{aligned} &\Omega_{V_1}(x) = e^{-\beta x};\ \Omega_{V_2}(x) = e^{\beta x};\\ &\Omega_{V_3}(x) = \cos(\beta x);\ \Omega_{V_1}(x) = \sin(\beta x); \end{aligned} \tag{A.1}$$

$$\begin{aligned} &\Omega_{V_1}(x) = -\beta e^{-\beta x};\ \Omega_{V_2}(x) = \beta e^{\beta x};\\ &\Omega_{V_3}(x) = -\beta\cos(\beta x);\ \Omega_{V_1}(x) = \beta\sin(\beta x); \end{aligned} \tag{A.2}$$

$$\begin{aligned} &\Omega_{V_1}(x) = -EI\beta^2 e^{-\beta x};\quad \Omega_{V_2}(x) = -EI\beta^2 e^{\beta x};\\ &\Omega_{V_3}(x) = EI\beta^2\cos(\beta x);\quad \Omega_{V_1}(x) = EI\beta^2\sin(\beta x); \end{aligned} \tag{A.3}$$

$$\begin{aligned}\Omega_{S_1}(x) &= EI\beta^3 e^{-\beta x}; \quad \Omega_{V_2}(x) = -EI\beta^3 e^{\beta x};\\ \Omega_{V_3}(x) &= -EI\beta^3 \cos(\beta x); \quad \Omega_{V_1}(x) = EI\beta^3 \sin(\beta x);\end{aligned} \tag{A.4}$$

The particular integrals $\mathbf{J}^{(r)}(x, x_0)$ in Eq.(3.23) for $r = P, W, \Delta\Theta, \Delta V$ can be can be constructed using Eqs.(3.26)-(3.36), as follows.

Particular integrals $\mathbf{J}^{(P)}$ for a point load $P = 1$ at $x = x_0$:

$$J_V^{(P)}(x, x_0) = \alpha[\sinh(\beta(x - x_0)) + \sinh(\beta(x - x_0))]H(x - x_0) \tag{A.5}$$

$$\begin{aligned}J_\Theta^{(P)}(x, x_0) &= \frac{\bar{d} J_V^{(P)}(x, x_0)}{dx}\\ &= \alpha\beta[\cosh(\beta(x - x_0)) + \cos(\beta(x - x_0))]H(x - x_0)\end{aligned} \tag{A.6}$$

$$\begin{aligned}J_M^{(P)}(x, x_0) &= -EI\frac{\bar{d}^2 J_V^{(P)}(x, x_0)}{dx^2}\\ &= -EI\alpha\beta^2[\sinh(\beta(x - x_0)) + \sin(\beta(x - x_0))]H(x - x_0)\end{aligned} \tag{A.7}$$

$$\begin{aligned}J_S^{(P)}(x, x_0) &= -EI\frac{\bar{d}^3 J_V^{(P)}(x, x_0)}{dx^3}\\ &= -EI\alpha\beta^3[\cosh(\beta(x - x_0)) + \cos(\beta(x - x_0))]H(x - x_0)\end{aligned} \tag{A.8}$$

Particular integrals $\mathbf{J}^{(W)}(x, x_0)$ for a point moment $W = 1$ at $x = x_0$:

$$\begin{aligned}J_V^{(W)}(x, x_0) &= \frac{\bar{d} J_V^{(P)}(x, x_0)}{dx_0}\\ &= -\alpha\beta[\cosh(\beta(x - x_0))\gamma_1 - \cos(\beta_2(x - x_0))]H(x - x_0)\end{aligned} \tag{A.9}$$

$$\begin{aligned}J_\Theta^{(W)}(x, x_0) &= \frac{\bar{d} J_V^{(W)}(x, x_0)}{dx}\\ &= -\alpha\beta^2[\sinh(\beta(x - x_0)) + \sin(\beta_2(x - x_0))]H(x - x_0)\end{aligned} \tag{A.10}$$

$$\begin{aligned} J_M^{(W)}(x,x_0) &= -EI\frac{\bar{d}^2 J_V^{(W)}(x,x_0)}{dx^2} \\ &= EI\alpha\beta^3[\cosh(\beta(x-x_0))+\cos(\beta(x-x_0))]H(x-x_0) \end{aligned} \tag{A.11}$$

$$\begin{aligned} J_S^{(W)}(x,x_0) &= -EI\frac{\bar{d}^3 J_V^{(W)}(x,x_0)}{dx^3} - 1\cdot\delta(x-x_0) \\ &= EI\alpha\beta^4[\sinh(\beta(x-x_0))+\cos(\beta(x-x_0))]H(x-x_0) \end{aligned} \tag{A.12}$$

Particular integrals $\mathbf{J}^{(\Delta V)}(x,x_0)$ for a relative rotation $\Delta\Theta = 1$ at $x = x_0$:

$$\begin{aligned} J_V^{(\Delta\Theta)}(x,x_0) &= EI\frac{\bar{d}^2 J_V^{(P)}(x,x_0)}{dx_0^2} \\ &= EI\alpha\beta^2[\sinh(\beta(x-x_0))+\sin(\beta_2(x-x_0))]H(x-x_0) \end{aligned} \tag{A.13}$$

$$\begin{aligned} J_\Theta^{(\Delta\Theta)}(x,x_0) &= \frac{\bar{d}J_V^{\Delta\Theta}(x,x_0)}{} \\ &= EI\alpha\beta^3[\cosh(\beta(x-x_0))+\cos(\beta(x-x_0))]H(x-x_0) \end{aligned} \tag{A.14}$$

$$\begin{aligned} J_M^{(\Delta\Theta)}(x,x_0) &= -EI\frac{\bar{d}^2 J_V^{(\Delta\Theta}(x,x_0)}{dx^2} + EI\delta(x-x_0) \\ &= -EI^2\alpha\beta^4[\sinh(\beta(x-x_0))-\sin(\beta(x-x_0))]H(x-x_0) \end{aligned} \tag{A.15}$$

$$\begin{aligned} J_S^{(\Delta\Theta)}(x,x_0) &= -EI\frac{\bar{d}^3 J_V^{(\Delta\Theta)}(x,x_0)}{dx^3} + EI\delta^{(1)}(x-x_0) \\ &= EI^2\alpha\beta^5[\cosh(\beta(x-x_0))-\cos(\beta(x-x_0))]H(x-x_0) \end{aligned} \tag{A.16}$$

Particular integrals $\mathbf{J}^{(\Delta V)}(x,x_0)$ for a relative rotation $\Delta V = 1$ at $x = x_0$:

$$J_V^{(\Delta V)}(x,x_0) = -EI\frac{\bar{d}^3 J_V^{(P)}(x,x_0)}{dx^3} = EI\alpha\beta^3[\cosh(\beta(x-x_0))\gamma_1 + \cos(\beta(x-x_0))]H(x-x_0) \tag{A.17}$$

$$J_\Theta^{(\Delta V)}(x,x_0) = \frac{\bar{d}^2 J_V^{(\Delta V)}(x,x_0)}{dx^2} + EI\delta^{(1)}(x-x_0) = EI\alpha\beta^4[\sinh(\beta(x-x_0)) - \sin(\beta(x-x_0))]H(x-x_0) \tag{A.18}$$

$$J_M^{(\Delta V)}(x,x_0) = -EI\frac{\bar{d}^2 J_V^{(\Delta V)}(x,x_0)}{dx^2} + EI\delta^{(1)}(x-x_0) = -EI^2\alpha\beta^5[\cosh(\beta(x-x_0)) - \cos(\beta(x-x_0))]H(x-x_0) \tag{A.19}$$

$$J_S^{(\Delta V)}(x,x_0) = -EI\frac{\bar{d}^3 J_V^{(\Delta V}(x,x_0)}{dx^3} + EI\delta^{(2)}(x-x_0) = EI^2\alpha\beta^6[\sinh(\beta(x-x_0)) + \sin(\beta(x-x_0))]H(x-x_0) \tag{A.20}$$

where $\alpha = \alpha(\omega) = 2^{-1}EI^{-1/4}m^{-3/4}\omega^{-3/2}$, $\beta = \beta(\omega) = EI^{-1/4}m^{1/4}\omega^{1/2}$, and $EI\alpha\beta^3 = 1/2$

A.2 Axially loaded beams with symmetric cross section

Starting from Eq.(3.85) for the deflection response to a unit point force $P = 1$ at a generic abscissa $x = x_0$, the full set of Green's functions $\mathbf{G}^{(r)}(x,x_0)$ for $r = P, \Delta\Theta$ can be built. Matrix $\mathbf{\Omega}$ in Eq.(3.85) includes solutions of the homogeneous equation associated with Eqs.(3.80)-(3.81) and can easily be

constructed using EB governing equations (obviously, terms in matrix $\mathbf{\Omega}$ do not depend on the loading function and, for this, do not carry superscript "r"):

$$\Omega_{V1}(x) = e^{\beta_1 x};\ \Omega_{V2}(x) = e^{-\beta_1 x};\ \Omega_{V3}(x) = e^{\beta_2 x};\ \Omega_{V4}(x) = e^{-\beta_2 x} \tag{A.21}$$

$$\Omega_{\Theta 1}(x) = \beta_1 e^{\beta_1 x};\ \Omega_{\Theta 2}(x) = -\beta_1 e^{-\beta_1 x};\ \Omega_{\Theta 3}(x) = \beta_2 e^{\beta_2 x};\ \Omega_{\Theta 4}(x) = -\beta_2 e^{-\beta_2 x} \tag{A.22}$$

$$\Omega_{\hat{M}1}(x) = -\beta_1^2 e^{\beta_1 x};\ \Omega_{M2}(x) = -\beta_1^2 e^{-\beta_1 x};\ \Omega_{M3}(x) = -\beta_2^2 e^{\beta_2 x};\ \Omega_{M4}(x) = -\beta_2^2 e^{-\beta_2 x} \tag{A.23}$$

$$\Omega_{S1}(x) = -\beta_1^3 e^{\beta_1 x};\ \Omega_{S2}(x) = \beta_1^3 e^{-\beta_1 x};\ \Omega_{S3}(x) = -\beta_2^3 e^{\beta_2 x};\ \Omega_{S4}(x) = \beta_2^3 e^{-\beta_2 x} \tag{A.24}$$

The vectors of particular integrals $\mathbf{J}^{(r)}(x, x_0)$ in Eq.(3.82), for $r = P, \Delta\Theta$, can be constructed, as follows.

Vector of particular integrals $\mathbf{J}^{(P)}(x, x_0)$ for a point load $P = 1$ at $x = x_0$:

$$J_V^{(P)}(x, x_0) = [\sinh(\beta_1(x - x_0))\gamma_1 + \sinh(\beta_2(x - x_0))\gamma_2] \cdot H(x - x_0) \tag{A.25}$$

$$\begin{aligned} J_\Theta^{(P)}(x, x_0) &= \frac{\bar{d} J_V^{(P)}(x, x_0)}{dx} \\ &= [\beta_1 \cosh(\beta_1(x - x_0))\gamma_1 + \beta_2 \cosh(\beta_2(x - x_0))\gamma_2] \cdot H(x - x_0) \end{aligned} \tag{A.26}$$

$$J_M^{(P)}(x,x_0) = -\frac{\bar{d}J_\Theta^{(P)}(x,x_0)}{dx} = -[\beta_1^2\sinh(\beta_1(x-x_0))\gamma_1 + \beta_2^2\sinh(\beta_2(x-x_0))\gamma_2]\cdot H(x-x_0) \tag{A.27}$$

$$J_S^{(P)}(x,x_0) = -\frac{\bar{d}J_M^{(P)}(x,x_0)}{dx} = -[\beta_1^3\cosh(\beta_1(x-x_0))\gamma_1 + \beta_2^3\cosh(\beta_2^3(x-x_0))\gamma_2]\cdot H(x-x_0) \tag{A.28}$$

Vector of particular integrals $\mathbf{J}^{\Delta\Theta}(x,x_0)$ for a relative rotation $\Delta\Theta = 1$ at $x = x_0$:

$$J_V^{(\Delta\Theta)}(x,x_0) = \frac{\bar{d}^2J_V^{(P)}(x,x_0)}{dx^2} = [\beta_1^2\sinh(\beta_1(x-x_0))\gamma_1 + \beta_2^2\sinh(\beta_2(x-x_0))\gamma_2]\cdot H(x-x_0) \tag{A.29}$$

$$J_\Theta^{(\Delta\Theta)}(x,x_0) = \frac{\bar{d}J_V^{(\Delta\Theta)}(x,x_0)}{dx} = [\beta_1^3\cosh(\beta_1(x-x_0))\gamma_1 + \beta_2^3\cosh(\beta_2(x-x_0))\gamma_2]\cdot H(x-x_0) \tag{A.30}$$

$$J_M^{(\Delta\Theta)}(x,x_0) = -\frac{\bar{d}^2J_\Theta^{(\Delta\Theta)}(x,x_0)}{dx} + \Delta\Theta\cdot\delta(x-x_0) = -[\beta_1^4\sinh(\beta_1(x-x_0))\gamma_1 + \beta_2^4\sinh(\beta_2(x-x_0))\gamma_2]\cdot H(x-x_0) \tag{A.31}$$

$$J_S^{(\Delta\Theta)}(x,x_0) = \frac{\bar{d}J_M^{(\Delta\Theta)}(x,x_0)}{dx}$$
$$= -[\beta_1^5 \cosh(\beta_1(x-x_0))\gamma_1 + \beta_2^5 \cosh(\beta_2(x-x_0))\gamma_2] \cdot H(x-x_0) \tag{A.32}$$

Interestingly, notice that the particular integrals are all continuous through the whole domain, except for $x = x_0$ where appropriate, i.e.:

$$J_S^{(P)}(x_0^+,x_0) - J_S^{(P)}(x_0^-,x_0) = -1 \tag{A.33}$$

$$J_\Theta^{(\Delta\Theta)}(x_0^+,x_0) - J_\Theta^{(\Delta\Theta)}(x_0^-,x_0) = 1 \tag{A.34}$$

$$J_S^{(\Delta\Theta)}(x_0^+,x_0) - J_S^{(\Delta\Theta)}(x_0^-,x_0) = -\alpha \tag{A.35}$$

where $\beta_1 = \sqrt{(\alpha - \sqrt{\alpha^2+4\omega})/2}$, $\beta_2 = \sqrt{(\alpha + \sqrt{\alpha^2+4\omega})/2}$ and $\gamma_1 = (\beta_1\sqrt{\alpha^2+4\omega^2})^{-1}$.

Eq.(A.33) and Eq.(A.34) derive from Eq.(A.28) and Eq.(A.30), respectively, being $\beta_1^3 \cdot \gamma_1 + \beta_2^3 \cdot \gamma_2 = 1$, while Eq.(A.35) derives from Eq.(A.32) being $\beta_1^5 \cdot \gamma_1 + \beta_2^5 \cdot \gamma_2 = \alpha$ (for the shear-force discontinuity due to a rotation discontinuity, see for instance ref. [44]). Likewise, the particular integral $J_\Theta^{(P)}$ is continuous at $x = x_0$, being $\beta_1 \cdot \gamma_1 + \beta_2 \cdot \gamma_2 = 0$.

A.3 Beams with mono-symmetric cross section (warping effects neglected)

The key step to build the closed-form frequency response (3.143) is to derive closed-form expressions for matrix $\mathbf{\Omega}(y)$ from the solution to the homogeneous solution associated with Eqs.(3.128)-(3.129), for matrix $\mathbf{J}(y,y_j)$ from the particular integrals of Eqs.(3.128)-(3.129) related to a unit point

force $P = 1$, unit bending moment $Mf = 1$ and unit twisting moment $Mt = 1$ applied at arbitrary location y_j along the elastic axis; for $\mathbf{Y}^{(f)}(y)$ and $\mathbf{Y}^{(g)}(y)$ from particular integrals associated with the external load.

Eq.(3.138) is the basis to obtain closed-form expressions for all terms in Eq.(3.143), as follows.

Matrix $\mathbf{\Omega}(y)$in Eq.(3.134)

Since the homogeneous equations associated with Eqs.(3.128)-(3.129) are formally identical to that associated with Eq.(3.138), terms in matrix $\mathbf{\Omega}(y)$ can be derived from Eq.(3.140) and successive differentiation according to the equations of the elementary coupled bending-torsion theory (3.111)-(3.116) without Dirac's deltas. In addition, the relations between the different sets of integration constants for bending and torsional variables have to be taken into account [49]. For example terms in the 3-rd and 5-th row of matrix $\mathbf{\Omega}(y)$ are given as:

$$\begin{aligned}
&\Omega_{M1} = EI \cdot r_1 \cosh(\sqrt{r_1} y) \ ; \ \Omega_{M2} = EI \cdot r_1 \sinh(\sqrt{r_1} y) \\
&\Omega_{M3} = -EI \cdot r_2 \cos(\sqrt{r_2} y) \ ; \ \Omega_{M4} = -EI \cdot r_2 \sin(\sqrt{r_2} y) \\
&\Omega_{M5} = -EI \cdot r_3 \cos(\sqrt{r_3} y) \ ; \ \Omega_{M6} = -EI \cdot r_3 \sin(\sqrt{r_3} y)
\end{aligned} \tag{A.36}$$

$$\begin{aligned}
&\Omega_{\Psi 1} = k_a \cdot \cosh(\sqrt{r_1} y) \ ; \ \Omega_{\Psi 2} = k_a \cdot \sinh(\sqrt{r_1} y) \ ; \ \Omega_{\Psi 3} = k_b \cdot \cos(\sqrt{r_2} y) \ ; \\
&\Omega_{\Psi 4} = k_b \cdot \sin(\sqrt{r_2} y) \ ; \ \Omega_{\Psi 5} = k_c \cdot \cos(\sqrt{r_3} y) \ ; \ \Omega_{\Psi 6} = k_c \cdot \sin(\sqrt{r_3} y)
\end{aligned} \tag{A.37}$$

being

$$k_a = \frac{(m\omega^2 - EI \cdot r_1^2)}{m x_a \omega^2} \quad k_b = \frac{(m\omega^2 - EI \cdot r_2^2)}{m x_a \omega^2} \quad k_c = \frac{(m\omega^2 - EI \cdot r_3^2)}{m x_a \omega^2} \tag{A.38}$$

Matrix $\mathbf{J}(y, y_j)$ in Eq.(3.207)

Terms in matrix $\mathbf{J}(y, y_j)$ can be derived by successive differentiation of the particular integral J^*, and considering the equations of the elementary coupled bending-torsion theory (3.111)-(3.116). A few examples are given below.

In view of Eq.(3.138), Eq.(3.128) and Eq.(3.130), it is readily seen that $J_H^{(Mt)}$, i.e. the particular integral for H due to a unit twisting moment $Mt = 1$, is given as:

$$\begin{aligned} J_H^{(M_t)}(y, y_0) =& J^{(*)}(y, y_0) = D\,[\sinh(\sqrt{r_1}(y - y_0))\sqrt{r_2}\sqrt{r_3}(r_3 - r_2) \\ & - \sin(\sqrt{r_2}(y - y_0))\sqrt{r_1}\sqrt{r_3}(r_1 + r_3) + \sin(\sqrt{r_3}(y - y_0)) \\ & \sqrt{r_1}\sqrt{r_2}(r_1 + r_2)\,] \cdot U(y - y_0) \end{aligned} \tag{A.39}$$

Likewise, in view of Eq.(A.48) for $J_H^{(Mt)}$ and Eqs.(3.111)-(3.112)-(3.113), it is seen that $J_S^{(Mt)}$, i.e. the particular integral for S due to a unit twisting moment $Mt = 1$, can be obtained as:

$$\begin{aligned} J_S^{(Mt)}(y, y_0) =& - EI\frac{\bar{d}^3 J_H^{(Mt)}(y, y_0)}{dy^3} = -EI \cdot D\,[\cosh(\sqrt{r_1}(y - y_0))\sqrt{r_2}\sqrt{r_3}(r_3 - r_2) \\ & + \cos(\sqrt{r_2}(y - y_0))\sqrt{r_1}\sqrt{r_3}(r_1 + r_3) - \cos(\sqrt{r_3}(y - y_0)) \\ & \sqrt{r_1}\sqrt{r_2}(r_1 + r_2)\,] \cdot U(y - y_0) \end{aligned} \tag{A.40}$$

that is derived taking into account that $\delta(y - y_0) = \frac{\bar{d}H(y-y_0)}{dy}$. Also, in view of Eq.(3.138), Eq.(3.128) and Eq.(3.130), it is evident that $J_H^{(P)}$, i.e. the particular integral for H due to a unit force $P = 1$, can be derived by using

and differentiating the particular integral J^* of Eq.(3.138) in this way:

$$\begin{aligned} J_H^{(P)}(y,y_0) &= (\frac{I_\alpha}{mx_a} - x_0)J^*(y,y_0) + \frac{GJ}{mx_a\omega^2}\frac{\bar{d}^2 J^*(y,y_0)}{dy^2} = \\ &= (\frac{I_a}{mx_a} - x_0)\cdot D\,[\sinh(\sqrt{r_1}(y-y_0))\sqrt{r_2}\sqrt{r_3}(r_3-r_2) \\ &- \sin(\sqrt{r_2}(y-y_0))\sqrt{r_1}\sqrt{r_3}(r_1+r_3) + \sin(\sqrt{r_3}(y-y_0)) \\ &\sqrt{r_1}\sqrt{r_2}(r_1+r_2)\,]\cdot U(y-y_0) + \frac{GJ}{mx_a\omega^2}\cdot D\,[r_1\sinh(\sqrt{r_1}(y-y_0)) \\ &\sqrt{r_2}\sqrt{r_3}(r_3-r_2) - r_2\sin(\sqrt{r_2}(y-y_0))\sqrt{r_1}\sqrt{r_3}(r_1+r_3) \\ &+ r_3\sin(\sqrt{r_3}(y-y_0))\sqrt{r_1}\sqrt{r_2}(r_1+r_2)\,]\cdot U(y-y_0) \end{aligned} \tag{A.41}$$

All terms in matrix $\mathbf{J}(y,y_j)$ can be obtained in a similar manner, and are not reported for brevity.

Vectors $\mathbf{Y}^{(f)}(y)$ in Eq.(3.136) and $\mathbf{Y}^{(g)}(y)$ in Eq.(3.137)

In view of the analytical expressions of $\mathbf{J}^{(P)}$ and $\mathbf{J}^{(Mt)}$ in matrix $\mathbf{J}(y,y_j)$, see Eq.(3.207), every integral in Eqs.(3.136)-(3.137) can be written in the general form $\int_a^b \lambda(y_0)U(y-y_0)dy_0$, where $\lambda(y_0)$ will be given by the product of the loading function and certain trigonometric/hyperbolic functions. For example, in view of Eq.(A.48) for $J_H^{(Mt)}$, computing $\mathbf{Y}^{(g)}(y)$ will involve, among the others the integral:

$$\int_a^b J_H^{(Mt)}(y,\xi)g(\xi)d\xi = \int_a^b \lambda(\xi)U(y-\xi)d\xi \tag{A.42}$$

with

$$\begin{aligned} \lambda(\xi) =& g(\xi)[\sinh(\sqrt{r_1}(y-\xi))\sqrt{r_2}\sqrt{r_3}(r_2-r_3) \\ &- \sin(\sqrt{r_2}(y-\xi))\sqrt{r_1}\sqrt{r_3}(r_3-r_1) + \sin(\sqrt{r_3}(y-\xi))\sqrt{r_1}\sqrt{r_2}(r_2-r_1)] \end{aligned} \tag{A.43}$$

Using the theory of generalized functions, integrals $\int_a^b \lambda(\xi)U(y-\xi)d\xi$ can

be computed as:

$$\int_a^b \lambda(\xi)H(y-\xi) = [H(y-\xi)(\lambda_1(\xi)-\lambda_1(y))]_a^b = H(y-b)(\lambda_1(b)-\lambda_1(y)) - H(y-a)(\lambda_1(a)-\lambda_1(y)) \tag{A.44}$$

where λ_1 denotes the first-order primitive function of $\lambda(\xi)$. It is noticed that, for polynomial loads $g(y)$ typically encountered in engineering applications, this first order primitive λ_1 can be obtained in a symbolic form by any symbolic package [2].

A.4 Beams with mono-symmetric cross section (warping effects included)

Eq.(3.210) with its solution is the basis to obtain closed-form expressions for the frequency response in Eq.(3.222), as follows.

Matrix $\mathbf{\Omega}(y)$ in Eq.(3.206)

The homogeneous equations associated with Eqs.(3.200)-(3.201) are formally identical to that associated with Eq.(3.138), so that terms in matrix $\mathbf{\Omega}(y)$ can be derived from Eq.(3.212) and successive differentiation according to the equations of the coupled bending-torsion theory including warping effects (3.185)-(3.190), without Dirac's deltas. In addition, the relations between the different sets of integration constants for bending and torsional variables shall be taken into account [57]. For example, terms in the 3-rd and 5-th row of matrix $\mathbf{\Omega}(y)$ are given as:

$$\begin{aligned}
&\Omega_{M1} = -EIr_1\cos(\sqrt{r_1}y)\ ;\ \Omega_{M2} = -EIr_1\sin(\sqrt{r_1}y)\ ;\ \Omega_{M3} = -EIr_2\cos(\sqrt{r_2}y)\\
&\Omega_{M4} = -EIr_2\sin(\sqrt{r_2}y)\ ;\ \Omega_{M5} = EIr_3\cosh(\sqrt{r_3}y)\ ;\ \Omega_{M6} = EIr_3\sinh(\sqrt{r_3}y)\\
&\Omega_{M7} = EIr_4\cosh(\sqrt{r_4}y);\ \ \Omega_{M8} = EIr_4\sinh(\sqrt{r_4}y)
\end{aligned} \tag{A.45}$$

$$\Omega_{\Psi 1} = k_a \cos(\sqrt{r_1} y) \; ; \; \Omega_{\Psi 2} = k_a \sin(\sqrt{r_1} y) \; ; \; \Omega_{\Psi 3} = k_b \cos(\sqrt{r_2} y)$$
$$\Omega_{\Psi 4} = k_b \sin(\sqrt{r_2} y) \; ; \; \Omega_{\Psi 5} = k_c \cosh(\sqrt{r_3} y) \; ; \; \Omega_{\Psi 6} = k_c \sinh(\sqrt{r_3} y) \quad \text{(A.46)}$$
$$\Omega_{\Psi 7} = k_d \cosh(\sqrt{r_4} y); \; \Omega_{\Psi 8} = k_d \sinh(\sqrt{r_4} y)$$

being

$$k_a = \frac{m\omega^2 - EIr_1^2}{mx_a\omega^2}; \; k_b = \frac{m\omega^2 - EIr_2^2}{mx_a\omega^2}; \; k_c = \frac{m\omega^2 - EIr_3^2}{mx_a\omega^2}; \; k_d = \frac{m\omega^2 - EIr_4^2}{mx_a\omega^2} \quad \text{(A.47)}$$

Matrix $\mathbf{J}(y, y_j)$ in Eq.(3.207)

Terms in matrix $\mathbf{J}(y, y_j)$ can be derived by successive differentiation of the particular integral J^*, Eq.(3.213), and considering the equations of the coupled bending-torsion theory (3.185)-(3.190). A few examples are given below.

In view of Eq.(3.210), Eq.(3.200) and Eq.(3.202), it is readily seen that $J_H^{(Mt)}$, i.e. the particular integral for deflection H due to a unit twisting moment $Mt = 1$, is given as:

$$\begin{aligned} J_H^{(M_t)}(y, y_0) &= J^{(*)}(y, y_0) \\ &= \frac{2}{d}\Big[\sin(\sqrt{r_1}(y - y_0))\sqrt{r_2}\sqrt{r_3}\sqrt{r_4}(r_3 + r_2)(r_4 + r_2)(r_4 - r_3) + \\ &+ \sin(\sqrt{r_2}(y - y_0))\sqrt{r_1}\sqrt{r_3}\sqrt{r_4}(r_3 + r_1)(r_4 + r_1)(r_3 - r_4) + \\ &+ \sinh(\sqrt{r_3}(y - y_0))\sqrt{r_1}\sqrt{r_2}\sqrt{r_4}(r_4 + r_1)(r_4 + r_2)(r_1 - r_2) + \\ &+ \sinh(\sqrt{r_4}(y - y_0))\sqrt{r_1}\sqrt{r_2}\sqrt{r_3}(r_1 + r_3)(r_2 + r_3)(r_2 - r_1)]U(y - y_0) \end{aligned} \quad \text{(A.48)}$$

Likewise, in view of Eq.(A.48) for $J_H^{(Mt)}$ and Eqs.(3.185)-(3.186)-(3.187), it is seen that $J_S^{(Mt)}$, i.e. the particular integral for shear force S due to a unit

twisting moment $Mt = 1$, can be obtained as:

$$J_S^{(Mt)}(y, y_0) = -EI\frac{\bar{d}^3 J_H^{(Mt)}(y, y_0)}{dy^3} =$$
$$= -EI\frac{2}{d}\Big[-\cos(\sqrt{r_1}(y - y_0))r_1\sqrt{r_1}\sqrt{r_2}\sqrt{r_3}\sqrt{r_4}(r_3 + r_2)(r_4 + r_2)$$
$$(r_4 - r_3) - \cos(\sqrt{r_2}(y - y_0))\sqrt{r_1}r_2\sqrt{r_2}\sqrt{r_3}\sqrt{r_4}(r_3 + r_1)(r_4 + r_1)$$
$$(r_3 - r_4) + \cosh(\sqrt{r_3}(y - y_0))\sqrt{r_1}\sqrt{r_2}r_3\sqrt{r_3}\sqrt{r_4}(r_4 + r_1)(r_4 + r_2)$$
$$(r_1 - r_2) + \cosh(\sqrt{r_4}(y - y_0))\sqrt{r_1}\sqrt{r_2}\sqrt{r_3}r_4\sqrt{r_4}(r_1 + r_3)(r_2 + r_3)$$
$$(r_2 - r_1)]U(y - y_0) \tag{A.49}$$

that is derived taking into account that $\delta(y - y_0) = \frac{\bar{d}H(y-y_0)}{dy}$. Also, in view of Eq.(3.210), Eq.(3.200) and Eq.(3.202), it is evident that $J_H^{(P)}$, i.e. the particular integral for H due to a unit force $P = 1$, can be derived by using

and differentiating the particular integral J^* of Eq.(3.210) in this way:

$$
\begin{aligned}
J_H^{(P)}(y,y_0) &= (\frac{I_\alpha\omega^2}{mx_a\omega^2} - x_0)J^*(y,y_0) + \frac{GJ}{mx_a\omega^2}\frac{\bar{d}^2J^*(y,y_0)}{dy^2} - \frac{E\Gamma}{mx_a\omega^2}\frac{\bar{d}^4J^*(y,y_0)}{dy^4} \\
&= \frac{2}{d}\sin(\sqrt{r_1}(y-y_0))\sqrt{r_2}\sqrt{r_3}\sqrt{r_4}(r_3+r_2)(r_4+r_2)(r_4-r_3) \\
&\left[\frac{I_a\omega^2}{mx_a\omega^2} - x_0 - r_1\frac{GJ}{mx_a\omega^2} - \frac{E\Gamma}{mx_a\omega^2}r_1^2\right] + \\
&+ \frac{2}{d}\sin(\sqrt{r_2}(y-y_0))\sqrt{r_1}\sqrt{r_3}\sqrt{r_4}(r_3+r_1)(r_4+r_1)(r_3-r_4) \\
&\left[\frac{I_a\omega^2}{mx_a\omega^2} - x_0 - r_2\frac{GJ}{mx_a\omega^2} - \frac{E\Gamma}{mx_a\omega^2}r_2^2\right] + \\
&+ \frac{2}{d}\sinh(\sqrt{r_3}(y-y_0))\sqrt{r_1}\sqrt{r_2}\sqrt{r_4}(r_4+r_1)(r_4+r_2)(r_1-r_2) \\
&\left[\frac{I_a\omega^2}{mx_a\omega^2} - x_0 + r_3\frac{GJ}{mx_a\omega^2} - \frac{E\Gamma}{mx_a\omega^2}r_3^2\right] + \\
&+ \frac{2}{d}\sinh(\sqrt{r_4}(y-y_0))\sqrt{r_1}\sqrt{r_2}\sqrt{r_3}(r_1+r_3)(r_2+r_3)(r_2-r_1) \\
&\left[\frac{I_a\omega^2}{mx_a\omega^2} - x_0 + r_4\frac{GJ}{mx_a\omega^2} - \frac{E\Gamma}{mx_a\omega^2}r_4^2\right]
\end{aligned}
\tag{A.50}
$$

All terms in matrix $\mathbf{J}(y,y_j)$ can be obtained in a similar manner, and are not reported for brevity. The same approach has been followed for the previous cases.

Vectors $\mathbf{Y}^{(f)}(y)$ in Eq.(3.208), $\mathbf{Y}^{(g)}(y)$ in Eq.(3.209)

In view of the analytical expressions of $\mathbf{J}^{(P)}$ and $\mathbf{J}^{(Mt)}$ in matrix $\mathbf{J}(y,y_j)$, see Eq.(3.207), every integral in Eqs.(3.208)-(3.209) can be written in the general form $\int_a^b \lambda(y_0)U(y-y_0)dy_0$, where $\lambda(y_0)$ will be given by the product of the loading function and certain trigonometric/hyperbolic functions. For example, in view of Eq.(A.48) for $J_H^{(Mt)}$, computing $\mathbf{Y}^{(g)}(y)$ will involve, among the others the integral:

$$
\int_a^b J_H^{(Mt)}(y,\xi)g(\xi)d\xi = \int_a^b \lambda(\xi)U(y-\xi)d\xi \tag{A.51}
$$

with

$$\lambda(\xi) = g(\xi)\frac{2}{d}\left[\sin(\sqrt{r_1}(y-y_0))\sqrt{r_2}\sqrt{r_3}\sqrt{r_4}(r_3+r_2)(r_4+r_2)(r_4-r_3)+\right.$$
$$+\sin(\sqrt{r_2}(y-y_0))\sqrt{r_1}\sqrt{r_3}\sqrt{r_4}(r_3+r_1)(r_4+r_1)(r_3-r_4)+$$
$$+\sinh(\sqrt{r_3}(y-y_0))\sqrt{r_1}\sqrt{r_2}\sqrt{r_4}(r_4+r_1)(r_4+r_2)(r_1-r_2)+$$
$$\left.+\sinh(\sqrt{r_4}(y-y_0))\sqrt{r_1}\sqrt{r_2}\sqrt{r_3}(r_1+r_3)(r_2+r_3)(r_2-r_1)\right] \tag{A.52}$$

Using the theory of generalized functions, integrals $\int_a^b \lambda(\xi)U(y-\xi)d\xi$ can be computed as:

$$\int_a^b \lambda(\xi)H(y-\xi) = [H(y-\xi)(\lambda_1(\xi)-\lambda_1(y))]_a^b = H(y-b)(\lambda_1(b)-\lambda_1(y))$$
$$-H(y-a)(\lambda_1(a)-\lambda_1(y)) \tag{A.53}$$

where λ_1 denotes the first-order primitive function of $\lambda(\xi)$. It is noticed that, for polynomial loads $g(y)$ typically encountered in engineering applications, this first order primitive λ_1 can be obtained in a symbolic form by any symbolic package [2].

Appendix B

Symbolic inversion of 4×4 and 6×6 matrices

This appendix provides closed-form expressions for the symbolic inverse of the 4×4 matrix $\mathbf{B}$ in Eq.(3.57) and Eq.(3.103), and the symbolic inverse of the 6×6 matrix $\mathbf{\Gamma}$ in Eq.(4.3), matrix $\mathbf{B}$ in Eq.(3.151) and matrix $\mathbf{A}$ in Eq. (4.9). They can be obtained by Mathematica.

B.1 Symbolic inversion of 4×4 matrix

Denoting by B_{ij} the elements of the 4×4 matrix $\mathbf{B}$, by A_{ij} the elements of the inverse matrix $\mathbf{A} = \mathbf{B}^{-1}$, the following symbolic forms hold for A_{ij}:
First row:

$$A_{11} = D^{-1}[B_{24}(B_{32}B_{43} - B_{33}B_{42}) + B_{23}(B_{34}B_{42} - B_{32}B_{44}) + B_{22}(B_{33}B_{44} - B_{34}B_{43})] \quad \text{(B.1a)}$$

$$A_{12} = D^{-1}[B_{14}(B_{33}B_{42} - B_{32}B_{43}) + B_{13}(B_{32}B_{44} - B_{34}B_{42}) + B_{12}(B_{34}B_{43} - B_{33}B_{44})] \quad \text{(B.1b)}$$

$$A_{13} = D^{-1}[B_{14}(B_{22}B_{43} - B_{23}B_{42}) + B_{13}(B_{24}B_{42} - B_{22}B_{44}) + B_{12}(B_{23}B_{44} - B_{24}B_{43})] \quad \text{(B.1c)}$$

$$A_{14} = D^{-1}[B_{14}(B_{23}B_{32} - B_{22}B_{23}) + B_{13}(B_{22}B_{34} - B_{24}B_{32}) + B_{12}(B_{24}B_{33} - B_{23}B_{34})] \quad \text{(B.1d)}$$

Second row:

$$A_{21} = D^{-1}[B_{24}(B_{33}B_{41} - B_{31}B_{43}) + B_{23}(B_{31}B_{44} - B_{34}B_{41}) + B_{21}(B_{34}B_{43} - B_{33}B_{44})] \quad \text{(B.2a)}$$
$$A_{22} = D^{-1}[B_{14}(B_{31}B_{43} - B_{33}B_{41}) + B_{13}(B_{34}B_{41} - B_{31}B_{44}) + B_{11}(B_{33}B_{44} - B_{34}B_{43})] \quad \text{(B.2b)}$$
$$A_{23} = D^{-1}[B_{14}(B_{23}B_{41} - B_{21}B_{43}) + B_{13}(B_{21}B_{44} - B_{24}B_{41}) + B_{11}(B_{24}B_{43} - B_{23}B_{44})] \quad \text{(B.2c)}$$
$$A_{24} = D^{-1}[B_{14}(B_{21}B_{33} - B_{23}B_{31}) + B_{13}(B_{24}B_{31} - B_{21}B_{34}) + B_{11}(B_{23}B_{34} - B_{24}B_{33})] \quad \text{(B.2d)}$$

Third row:

$$A_{31} = D^{-1}[B_{24}(B_{31}B_{42} - B_{32}B_{41}) + B_{22}(B_{34}B_{41} - B_{31}B_{44}) + B_{21}(B_{32}B_{44} - B_{34}B_{42})] \quad \text{(B.3a)}$$
$$A_{32} = D^{-1}[B_{14}(B_{32}B_{41} - B_{31}B_{42}) + B_{12}(B_{31}B_{44} - B_{34}B_{41}) + B_{11}(B_{34}B_{42} - B_{32}B_{44})] \quad \text{(B.3b)}$$
$$A_{33} = D^{-1}[B_{14}(B_{21}B_{42} - B_{22}B_{41}) + B_{12}(B_{24}B_{41} - B_{21}B_{44}) + B_{11}(B_{22}B_{44} - B_{24}B_{42})] \quad \text{(B.3c)}$$
$$A_{34} = D^{-1}[B_{14}(B_{22}B_{31} - B_{21}B_{32}) + B_{12}(B_{21}B_{34} - B_{24}B_{31}) + B_{11}(B_{24}B_{32} - B_{22}B_{34})] \quad \text{(B.3d)}$$

Fourth row:

$$A_{41} = D^{-1}[B_{23}(B_{32}B_{41} - B_{31}B_{42}) + B_{22}(B_{31}B_{43} - B_{33}B_{41}) + B_{21}(B_{33}B_{42} - B_{32}B_{43})] \quad \text{(B.4a)}$$
$$A_{42} = D^{-1}[B_{13}(B_{31}B_{42} - B_{32}B_{41}) + B_{12}(B_{33}B_{41} - B_{31}B_{43}) + B_{11}(B_{32}B_{43} - B_{33}B_{42})] \quad \text{(B.4b)}$$
$$A_{43} = D^{-1}[B_{13}(B_{22}B_{41} - B_{21}B_{42}) + B_{12}(B_{21}B_{43} - B_{23}B_{41}) + B_{11}(B_{23}B_{42} - B_{22}B_{43})] \quad \text{(B.4c)}$$
$$A_{44} = D^{-1}[B_{13}(B_{21}B_{32} - B_{22}B_{31}) + B_{12}(B_{23}B_{31} - B_{21}B_{33}) + B_{11}(B_{22}B_{33} - B_{23}B_{32})] \quad \text{(B.4d)}$$

In Eq.(B.1a) through Eqs.(B.4d) symbol D denotes the determinant of matrix $\mathbf{B}$ given as:

$$D = \det\mathbf{B} = \sum_{i=1}^{24} d_i \quad \text{(B.5)}$$

$$d_1 = B_{14}B_{23}B_{32}B_{41} \quad d_2 = -B_{13}B_{24}B_{32}B_{41} \quad d_3 = -B_{14}B_{22}B_{33}B_{41} \quad d_4 = B_{12}B_{24}B_{33}B_{41} \quad \text{(B.6a-d)}$$
$$d_5 = B_{13}B_{22}B_{34}B_{41} \quad d_6 = -B_{12}B_{23}B_{34}B_{41} \quad d_7 = -B_{14}B_{23}B_{31}B_{42} \quad d_8 = B_{13}B_{24}B_{31}B_{42} \quad \text{(B.6e-h)}$$
$$d_9 = B_{14}B_{21}B_{33}B_{42} \quad d_{10} = -B_{11}B_{24}B_{33}B_{42} \quad d_{11} = -B_{13}B_{21}B_{34}B_{42} \quad d_{12} = B_{11}B_{23}B_{34}B_{42} \quad \text{(B.6i-l)}$$
$$d_{13} = B_{14}B_{22}B_{31}B_{43} \quad d_{14} = -B_{12}B_{24}B_{31}B_{43} \quad d_{15} = -B_{14}B_{21}B_{32}B_{43} \quad d_{16} = B_{11}B_{24}B_{32}B_{43} \quad \text{(B.6m-p)}$$
$$d_{17} = B_{12}B_{21}B_{34}B_{43} \quad d_{18} = -B_{11}B_{22}B_{34}B_{43} \quad d_{19} = -B_{13}B_{22}B_{31}B_{44} \quad d_{20} = B_{12}B_{23}B_{31}B_{44} \quad \text{(B.6q-t)}$$
$$d_{21} = B_{13}B_{21}B_{32}B_{44} \quad d_{22} = -B_{11}B_{23}B_{32}B_{44} \quad d_{23} = -B_{12}B_{21}B_{33}B_{44} \quad d_{24} = B_{11}B_{22}B_{33}B_{44} \quad \text{(B.6u-x)}$$

Eqs.(B.1a)-(B.4d) can be used to build the inverse matrix $\mathbf{B}^{-1}$ in a symbolic form, thus deriving closed-form expressions for the integration con-

stants.

B.2 Symbolic inversion of 6×6 matrix

For brevity, only three elements of the 6×6 inverse matrix $\mathbf{\Gamma} = \mathbf{Q}^{*(-1)}$ are reported below. Denote as Q^*_{ij} the element at i-th row and j-th column of matrix $\mathbf{Q}^*$ and $Q^*_{ijhk} = Q^*_{ij}Q^*_{hk} - Q^*_{ik}Q^*_{hj}$, while $\mathrm{Det}(\mathbf{Q}^*)$ is the determinant of 6×6 matrix $\mathbf{Q}^*$, obtained in a closed analytical form using the Laplace expansion along the i-th row of $\mathbf{Q}^*$ as follows:

$$\mathrm{Det}(\mathbf{Q}^*) = \sum_{j=1}^{5} Q^*_{ij}(-1)^{i+j} M^*_{ij} \tag{B.1}$$

with M^*_{ij} the determinant of the ij-th minor of $\mathbf{Q}^*$, i.e. the determinant of the 5×5 matrix that results by deleting the i-th row and the j-th column of $\mathbf{Q}^*$. A general expression of determinant of a 5×5 matrix $\mathbf{R}$ can be obtained in a closed form by using Mathematica [2] and is reported below where R_{ij} is the element at i-th row and j-th column of matrix $\mathbf{R}$ and $R_{ijhk} = R_{ij}R_{hk} - R_{ik}R_{hj}$.

$$\Gamma_{11} = \frac{1}{\mathrm{Det}(\mathbf{Q}^*)}\Big[Q^*_{24}Q^*_{53}Q^*_{3645} + Q^*_{23}Q^*_{54}Q^*_{3546} + Q^*_{24}Q^*_{55}Q^*_{3346} + Q^*_{23}Q^*_{55}Q^*_{3644} + Q^*_{26}(Q^*_{45}Q^*_{3354} + Q^*_{35}Q^*_{4453} + Q^*_{3443}Q^*_{55}) +$$
$$+ (Q^*_{24}Q^*_{3543} + Q^*_{23}Q^*_{3445})Q^*_{56} + Q^*_{25}(Q^*_{46}(Q^*_{3453} + Q^*_{36}Q^*_{4354} + Q^*_{3344}Q^*_{56})) - (Q^*_{24}Q^*_{52}Q^*_{3645} + Q^*_{22}Q^*_{54}Q^*_{3546} + Q^*_{24}Q^*_{55}Q^*_{3246} +$$
$$+ Q^*_{22}Q^*_{55}Q^*_{3644} + Q^*_{26}(Q^*_{45}Q^*_{3254} + Q^*_{35}Q^*_{4452} + Q^*_{3442}Q^*_{55}) + (Q^*_{24}Q^*_{3542} + Q^*_{22}Q^*_{3445})Q^*_{56} + Q^*_{25}(Q^*_{46}Q^*_{3452} +$$
$$+ Q^*_{36}(Q^*_{4254} + Q^*_{3244}Q^*_{56}))Q^*_{63} + (Q^*_{23}Q^*_{52}Q^*_{3645} + Q^*_{22}Q^*_{53}Q^*_{3546} + Q^*_{23}Q^*_{55}Q^*_{3246} + Q^*_{22}Q^*_{36}Q^*_{4355} + Q^*_{26}(Q^*_{45}Q^*_{3253} + Q^*_{35}Q^*_{4352} +$$
$$+ Q^*_{3342}Q^*_{55}) + (Q^*_{23}Q^*_{3542} + Q^*_{22}Q^*_{3345})Q^*_{56} + Q^*_{25}(Q^*_{46}Q^*_{3352} + Q^*_{36}Q^*_{4253} + Q^*_{3243}Q^*_{56}))Q^*_{64} - Q^*_{23}Q^*_{52}Q^*_{3644} + Q^*_{22}Q^*_{53}Q^*_{3446} +$$
$$+ Q^*_{23}Q^*_{54}Q^*_{3246} + Q^*_{22}Q^*_{53}Q^*_{3446} + Q^*_{26}(Q^*_{44}Q^*_{3253} + Q^*_{34}Q^*_{4352} + Q^*_{33}Q^*_{42}Q^*_{54}) + (Q^*_{23}Q^*_{3442} + Q^*_{22}Q^*_{3344})Q^*_{56} + Q^*_{24}(Q^*_{46}Q^*_{3352} +$$
$$+ Q^*_{36}Q^*_{4253} + Q^*_{3243}Q^*_{56}))Q^*_{65} + (Q^*_{23}Q^*_{52}Q^*_{3544} + Q^*_{22}Q^*_{53}Q^*_{3445} + Q^*_{23}Q^*_{54}Q^*_{3245} + Q^*_{22}Q^*_{54}Q^*_{3543} + Q^*_{25}(Q^*_{44}Q^*_{3253} + Q^*_{34}Q^*_{4352} +$$
$$+ Q^*_{3342}Q^*_{54}) + (Q^*_{23}Q^*_{3442} + Q^*_{22}Q^*_{3344})Q^*_{55} + Q^*_{24}(Q^*_{45}Q^*_{3352} + Q^*_{35}Q^*_{4253} + Q^*_{3243}Q^*_{55}))Q^*_{66}\Big] \tag{B.2}$$

$$\Gamma_{21} = \frac{1}{\mathrm{Det}(\mathbf{Q}^*)}\Big[(Q^*_{24}Q^*_{53}Q^*_{3546} + Q^*_{23}Q^*_{54}Q^*_{3645} + Q^*_{24}Q^*_{55}Q^*_{3643} + Q^*_{23}Q^*_{55}Q^*_{3446} + Q^*_{26}(Q^*_{45}Q^*_{3453} + Q^*_{35}Q^*_{4354} + Q^*_{44}Q^*_{33}Q^*_{55}) +$$
$$+ (Q^*_{24}Q^*_{4533} + Q^*_{23}Q^*_{3544})Q^*_{56} + Q^*_{25}(Q^*_{46}Q^*_{3354} + Q^*_{36}Q^*_{4453} + Q^*_{3443}Q^*_{56}))Q^*_{61} + (Q^*_{24}Q^*_{51}Q^*_{3645} + Q^*_{21}Q^*_{54}Q^*_{3546} + Q^*_{24}Q^*_{55}Q^*_{3146} +$$
$$+ Q^*_{21}Q^*_{55}Q^*_{3644} + Q^*_{26}(Q^*_{45}Q^*_{3154} + Q^*_{35}Q^*_{4451} + Q^*_{3441}Q^*_{55}) + (Q^*_{24}Q^*_{3541} + Q^*_{21}Q^*_{3445})Q^*_{56} + Q^*_{25}(Q^*_{46}Q^*_{3451} + Q^*_{36}Q^*_{4154} +$$
$$+ Q^*_{3144}Q^*_{56}))Q^*_{63} - (Q^*_{23}Q^*_{51}Q^*_{3645} + Q^*_{21}Q^*_{53}Q^*_{3546} + Q^*_{23}Q^*_{55}Q^*_{3146} + Q^*_{21}Q^*_{55}Q^*_{3643} + Q^*_{26}(Q^*_{45}Q^*_{3153} + Q^*_{35}Q^*_{4351} + Q^*_{3341}Q^*_{55})$$
$$+ (Q^*_{23}Q^*_{3541} + Q^*_{21}Q^*_{3345})Q^*_{56} + Q^*_{25}(Q^*_{46}Q^*_{3351} + Q^*_{36}Q^*_{4153} + Q^*_{3143}Q^*_{56}))Q^*_{64} + (Q^*_{23}Q^*_{51}Q^*_{3644} + Q^*_{21}Q^*_{53}Q^*_{3446} + Q^*_{23}Q^*_{54}Q^*_{3146} +$$
$$+ Q^*_{21}Q^*_{54}Q^*_{3643} + Q^*_{26}(Q^*_{44}Q^*_{3153} + Q^*_{34}Q^*_{4351} + Q^*_{3341}) + (Q^*_{23}Q^*_{3441} + Q^*_{21}Q^*_{3344})Q^*_{56} + Q^*_{24}(Q^*_{46}Q^*_{3351} + Q^*_{36}Q^*_{4153} +$$
$$+ Q^*_{3143}Q^*_{56}))Q^*_{65} - (Q^*_{23}Q^*_{51}Q^*_{3544} + Q^*_{21}Q^*_{53}Q^*_{3445} + Q^*_{23}Q^*_{54}Q^*_{31}Q^*_{45} + Q^*_{21}Q^*_{54}Q^*_{3543} + Q^*_{25}(Q^*_{44}Q^*_{3153} + Q^*_{34}Q^*_{4351} +$$
$$+ Q^*_{3341}Q^*_{54}) + (Q^*_{23}Q^*_{3441} + Q^*_{21}Q^*_{3344})Q^*_{55} + Q^*_{24}(Q^*_{45}Q^*_{3351} + Q^*_{35}Q^*_{4153}Q^*_{55}))Q^*_{66}\Big] \tag{B.3}$$

$$\Gamma_{31} = \frac{1}{\mathrm{Det}(\mathbf{Q}^*)}\Big[(Q^*_{24}Q^*_{52}Q^*_{3645} + Q^*_{22}Q^*_{54}Q^*_{3546} + Q^*_{24}Q^*_{55}Q^*_{3246} + Q^*_{22}Q^*_{46}Q^*_{3554} + Q^*_{26}(Q^*_{45}Q^*_{3254} + Q^*_{35}Q^*_{4452} + Q^*_{3442}Q^*_{55}) +$$
$$+ (Q^*_{24}Q^*_{3542} + Q^*_{22}Q^*_{3445})Q^*_{56} + Q^*_{25}(Q^*_{46}Q^*_{3452} + Q^*_{36}Q^*_{4254} + Q^*_{3244}Q^*_{56}))Q^*_{61} - (Q^*_{24}Q^*_{51}Q^*_{3645} + Q^*_{21}Q^*_{54}Q^*_{3546} + Q^*_{24}Q^*_{55}Q^*_{3146} +$$
$$+ Q^*_{21}Q^*_{55}Q^*_{3644} + Q^*_{26}(Q^*_{45}Q^*_{3154} + Q^*_{35}Q^*_{4451} + Q^*_{3441}Q^*_{55}) + (Q^*_{24}Q^*_{3541} + Q^*_{21}Q^*_{3445})Q^*_{56} + Q^*_{25}(Q^*_{46}Q^*_{3451} + Q^*_{36}Q^*_{4154} +$$
$$+ Q^*_{3144}Q^*_{56}))Q^*_{62} + (Q^*_{22}Q^*_{51}Q^*_{3645} + Q^*_{21}Q^*_{52}Q^*_{3546} + Q^*_{22}Q^*_{55}Q^*_{3146} + Q^*_{21}Q^*_{55}Q^*_{3642} + Q^*_{26}(Q^*_{45}Q^*_{3152} + Q^*_{35}Q^*_{4251} +$$
$$+ Q^*_{3241}Q^*_{55}) + (Q^*_{22}Q^*_{3541} + Q^*_{21}Q^*_{3245})Q^*_{56} + Q^*_{25}(Q^*_{46}Q^*_{3251} + Q^*_{36}Q^*_{4152} + Q^*_{3142}Q^*_{56}))Q^*_{64} - (Q^*_{22}Q^*_{51}Q^*_{3644} +$$
$$+ Q^*_{21}Q^*_{52}Q^*_{3446} + Q^*_{22}Q^*_{54}Q^*_{3146} + Q^*_{21}Q^*_{54}Q^*_{3642} + Q^*_{26}(Q^*_{44}Q^*_{3152} + Q^*_{34}Q^*_{4251} + Q^*_{3241}Q^*_{54}) + (Q^*_{22}Q^*_{3441} + Q^*_{21}Q^*_{3244})Q^*_{56} +$$
$$+ Q^*_{24}(Q^*_{46}Q^*_{3251} + Q^*_{36}Q^*_{4152} + Q^*_{3142}Q^*_{56}))Q^*_{65} + (Q^*_{22}Q^*_{51}Q^*_{3544} + Q^*_{21}Q^*_{52}Q^*_{3445} + Q^*_{22}Q^*_{54}Q^*_{3145} + Q^*_{25}(Q^*_{44}Q^*_{3152} +$$
$$+ Q^*_{34}Q^*_{4251} + Q^*_{3241}Q^*_{54}) + (Q^*_{22}Q^*_{3441} + Q^*_{21}Q^*_{3244})Q^*_{55} + Q^*_{24}(Q^*_{45}Q^*_{3251} + Q^*_{35}Q^*_{4152} + Q^*_{3142}))Q^*_{66}\Big] \tag{B.4}$$

$$\begin{aligned}\mathrm{Det}(\mathbf{R}) = {} & R_{13}R_{42}R_{2534} + R_{12}R_{43}R_{2435} + R_{25}R_{44}R_{3312} + R_{35}R_{44}R_{1322} + R_{15}(R_{34}R_{2243} + R_{24}R_{3342} + R_{2332}R_{44}) + (R_{13}R_{2432}+ \\ & + R_{12}R_{2334})R_{45} + R_{14}(R_{35}R_{2342} + R_{25}R_{3243} + R_{2233}R_{45}))R_{51} - (R_{13}R_{41}R_{2534} + R_{11}R_{43}R_{2435} + R_{1133}R_{25}R_{44}+ \\ & + R_{35}R_{44}R_{1321} + R_{15}(R_{34}R_{2143} + R_{24}R_{3341} + (R_{2331})R_{44}) + (R_{13}R_{2431} + R_{11}R_{2334})R_{45} + R_{14}(R_{35}R_{2341} + R_{25}R_{3143}+ \\ & + R_{2133}R_{45}))R_{52} + (R_{12}R_{41}R_{2534} + R_{11}R_{42}R_{2435} + R_{25}R_{44}R_{1132} + R_{35}R_{44}R_{1221} + R_{15}(R_{34}R_{2142} + R_{24}R_{3241}+ \\ & + (R_{2231})R_{44}) + (R_{12}R_{2431} + R_{11}R_{2234})R_{45} + R_{14}(R_{35}R_{2241} + R_{25}R_{3142} + R_{2132}R_{45}))R_{53} + (R_{12}R_{41}R_{2533} + R_{11}R_{42}R_{2335}+ \\ & + R_{25}R_{43}R_{3211} + R_{1221}R_{35}R_{43} + R_{15}(R_{33}R_{2142} + R_{23}R_{3241} + R_{2231}R_{43}) + (R_{12}R_{2331} + R_{11}R_{2233})R_{45} + R_{13}(R_{35}R_{2241}+ \\ & + R_{25}R_{3142} + R_{2132}R_{45}))R_{54} + (R_{12}R_{41}R_{2433} + R_{11}R_{2334}R_{42} + R_{1132}R_{24}R_{43} + R_{34}R_{43}R_{1221} + R_{14}(R_{33}R_{2142} + R_{23}(R_{3241})+ \\ & + R_{2231}R_{43}) + (R_{12}R_{2331} + R_{11}R_{2233})R_{44} + R_{13}(R_{34}R_{2241} + R_{24}R_{3142} + R_{2132}R_{44}))R_{55}\end{aligned} \tag{B.5}$$

Appendix C

Other useful closed-form expressions

This Appendix provides closed-form expressions for $\mathbf{c}$, $\mathbf{c}^{(d,y_0)}$ and $\mathbf{c}^{(fg)}$ in Eqs.(3.226)-(4.15)-(4.22), here rewritten for convenience:

$$\mathbf{c} = \mathbf{B}^{-1}\mathbf{r} \tag{C.1}$$

$$\mathbf{c}^{(d,y_0)} = \mathbf{A}^{-1}\mathbf{e}^{(d,y_0)} \tag{C.2}$$

$$\mathbf{c}^{(fg)} = \mathbf{A}^{-1}\mathbf{e}^{(fg)} \tag{C.3}$$

A general procedure will be shown, to be applied for obtaining in a closed form vectors $\mathbf{c}$ in Eqs.(C.1), $\mathbf{c}^{(d,y_0)}$ in Eq.(C.2) and $\mathbf{c}^{(fg)}$ in Eq.(C.3), as explained in the following.

Consider the generic system:

$$\mathbf{Q}\mathbf{d} = \mathbf{s} \tag{C.4}$$

where $\mathbf{Q}$ is a 8×8 full matrix, i.e. does not contain elements equal to zero, $\mathbf{d} = \begin{bmatrix} d_1 & d_2 & d_3 & d_4 & d_5 & d_6 & d_7 & d_8 \end{bmatrix}$ is a vector of unknown constants

and $\mathbf{s} = \begin{bmatrix} s_1 & s_2 & s_3 & s_4 & s_5 & s_6 & s_7 & s_8 \end{bmatrix}$. It is possible to express the first two constants d_1, d_2 as functions of the other constants d_3, d_4, d_5, d_6, d_7, d_8 and the first two elements of the vector $\mathbf{s}$, i.e. s_1 and s_2, in the following way:

$$\begin{aligned} d_1 = {} & d_3\left[-\frac{Q_{12}}{Q_{11}}\Big(\frac{Q_{21}Q_{13}}{Q_{11}} - Q_{23}\Big)/D - \frac{Q_{13}}{Q_{11}}\right] + d_4\left[-\frac{Q_{12}}{Q_{11}}\Big(\frac{Q_{21}Q_{14}}{Q_{11}} - Q_{24}\Big)/D - \frac{Q_{14}}{Q_{11}}\right] + \\ & + d_5\left[-\frac{Q_{12}}{Q_{11}}\Big(\frac{Q_{21}Q_{15}}{Q_{11}} - Q_{25}\Big)/D - \frac{Q_{13}}{Q_{11}}\right] + d_6\left[-\frac{Q_{12}}{Q_{11}}\Big(\frac{Q_{21}Q_{16}}{Q_{11}} - Q_{26}\Big)/D - \frac{Q_{13}}{Q_{11}}\right] + \\ & + d_7\left[-\frac{Q_{12}}{Q_{11}}\Big(\frac{Q_{21}Q_{13}}{Q_{11}} - B_{27}\Big)/D - \frac{Q_{17}}{Q_{11}}\right] + d_8\left[-\frac{Q_{12}}{Q_{11}}\Big(\frac{Q_{21}Q_{18}}{Q_{11}} - Q_{28}\Big)/D - \frac{Q_{18}}{Q_{11}}\right] + \\ & + s_1\left[\frac{Q_{12}}{Q_{11}}\frac{Q_{21}}{Q_{11}}/D + \frac{1}{Q_{11}}\right] + s_2\left[-\frac{Q_{12}}{Q_{11}}/D\right] \end{aligned} \tag{C.5}$$

$$\begin{aligned} d_2 = {} & \left[d_3\left(\frac{Q_{21}Q_{13}}{Q_{11}} - Q_{23}\right) + d_4\left(\frac{Q_{21}Q_{14}}{Q_{11}} - Q_{24}\right) + d_5\left(\frac{Q_{21}Q_{15}}{Q_{11}} - Q_{25}\right)\right. \\ & \left. + d_6\left(\frac{Q_{21}Q_{16}}{Q_{11}} - Q_{26}\right) + d_7\left(\frac{Q_{21}Q_{17}}{Q_{11}} - Q_{27}\right) + d_8\left(\frac{Q_{21}Q_{18}}{Q_{11}} - Q_{28}\right)\right]/D \\ & - s_1\frac{Q_{21}}{Q_{11}}/D + s_2/D \end{aligned} \tag{C.6}$$

being $D = \left[Q_{22} - \dfrac{Q_{21}Q_{12}}{Q_{11}}\right]$.

Substituting the expressions of d_1 and d_2 in the remaining six equations of the system $\mathbf{Qd} = \mathbf{s}$, leads to the following reduced system:

$$\mathbf{Q}^*\mathbf{d}^* = \mathbf{s}^* \tag{C.7}$$

where $\mathbf{d}^{*\mathrm{T}} = [\mathrm{d}_3 \;\; \mathrm{d}_4 \;\; \mathrm{d}_5 \;\; \mathrm{d}_6 \;\; \mathrm{d}_7 \;\; \mathrm{d}_8]$, while $\mathbf{s}^*$ and $\mathbf{Q}^*$ are 6×1 vector and 6×6 matrix respectively, whose generic elements s^*_{j-2} and $Q^*_{j-2,i-2}$ are given

as follows:

$$\begin{aligned}\mathbf{s}^*_{j-2} = s_j &- \left[Q_{j1}\left(\frac{Q_{12}Q_{21}}{Q_{11}^2}/D + \frac{1}{Q_{11}}\right) - Q_{j2}\frac{Q_{21}}{Q_{11}}/D\right]s_1 \\ &- \left[-Q_{j1}\frac{Q_{12}}{Q_{11}}/D + Q_{j2}/D\right]s_2\end{aligned} \tag{C.8}$$

$$\begin{aligned}Q^*_{i-2,j-2} = &\left[\left(-\frac{Q_{12}}{Q_{11}}\left(\frac{Q_{21}}{Q_{11}}Q_{1j} - Q_{2j}\right)/D - \frac{Q_{1j}}{Q_{11}}\right)Q_{i1}\right. \\ &\left. + \left(\frac{Q_{21}}{Q_{11}}Q_{1j} - Q_{2j}\right)Q_{i2}/D + Q_{ij}\right]\end{aligned} \tag{C.9}$$

denoting with s_j the j-th element of vector $\mathbf{s}$ and Q_{ji} the element in the i-th row and j-th column of matrix $\mathbf{Q}$, with $3 \leq i, j \leq 8$.

Vector $\mathbf{d}$ can be simply built in closed analytical form by inverting the 6×6 matrix $\mathbf{Q}^*$ to obtain $\mathbf{d}^*$ from Eq.(C.7), and then substituing in (C.5) and (C.6) to obtain d_1 and d_2; the symbolic inverse of an arbitrary 6×6 matrix is readily obtained by Mathematica [2] (see the previous Section).

The general procedure previously shown to determine a closed-form expression for $\mathbf{d}$ in Eqs.(C.4) can be used to derive $\mathbf{c}$ in Eq.(C.1), $\mathbf{c}^{(d,y_0)}$ in Eq.(C.2) and $\mathbf{c}^{(fg)}$ in Eq.(C.3), on replacing matrix $\mathbf{Q}$ by matrices $\mathbf{A}$ or $\mathbf{B}$, and vector $\mathbf{s}$ by vectors $\mathbf{r}$, $\mathbf{e}^{(d,y_0)}$, $\mathbf{e}^{(fg)}$.